



National Library
of Canada

Bibliothèque nationale
du Canada

Canadian Theses Service

Service des thèses canadiennes

Ottawa, Canada
K1A 0N4

NOTICE

The quality of this microform is heavily dependent upon the quality of the original thesis submitted for microfilming. Every effort has been made to ensure the highest quality of reproduction possible.

If pages are missing, contact the university which granted the degree.

Some pages may have indistinct print especially if the original pages were typed with a poor typewriter ribbon or if the university sent us an inferior photocopy.

Reproduction in full or in part of this microform is governed by the Canadian Copyright Act, R.S.C. 1970, c. C-30, and subsequent amendments.

AVIS

La qualité de cette microforme dépend grandement de la qualité de la thèse soumise au microfilmage. Nous avons tout fait pour assurer une qualité supérieure de reproduction.

S'il manque des pages, veuillez communiquer avec l'université qui a conféré le grade.

La qualité d'impression de certaines pages peut laisser à désirer, surtout si les pages originales ont été dactylographiées à l'aide d'un ruban usé ou si l'université nous a fait parvenir une photocopie de qualité inférieure.

La reproduction, même partielle, de cette microforme est soumise à la Loi canadienne sur le droit d'auteur, SRC 1970, c. C-30, et ses amendements subséquents.

THE UNIVERSITY OF ALBERTA

ASPECTS OF SPATIAL SCALE IN PROCESS GEOMORPHOLOGY

by

DIRK H. DE BOER

A THESIS

SUBMITTED TO THE FACULTY OF GRADUATE STUDIES AND RESEARCH
IN PARTIAL FULFILMENT OF THE REQUIREMENTS FOR THE DEGREE
OF DOCTOR OF PHILOSOPHY

DEPARTMENT OF GEOGRAPHY

EDMONTON, ALBERTA



National Library
of Canada

Bibliothèque nationale
du Canada

Canadian Theses Service

Service des thèses canadiennes

Ottawa, Canada
K1A 0N4

NOTICE

The quality of this microform is heavily dependent upon the quality of the original thesis submitted for microfilming. Every effort has been made to ensure the highest quality of reproduction possible.

If pages are missing, contact the university which granted the degree.

Some pages may have indistinct print especially if the original pages were typed with a poor typewriter ribbon or if the university sent us an inferior photocopy.

Reproduction in full or in part of this microform is governed by the Canadian Copyright Act, R.S.C. 1970, c. C-30, and subsequent amendments.

AVIS

La qualité de cette microforme dépend grandement de la qualité de la thèse soumise au microfilmage. Nous avons tout fait pour assurer une qualité supérieure de reproduction.

S'il manque des pages, veuillez communiquer avec l'université qui a conféré le grade.

La qualité d'impression de certaines pages peut laisser à désirer, surtout si les pages originales ont été dactylographiées à l'aide d'un ruban usé ou si l'université nous a fait parvenir une photocopie de qualité inférieure.

La reproduction, même partielle, de cette microforme est soumise à la Loi canadienne sur le droit d'auteur, SRC 1970, c. C-30, et ses amendements subséquents.

ISBN 0-315-60381-X

THE UNIVERSITY OF ALBERTA
RELEASE FORM

NAME OF AUTHOR DIRK H. DE BOER
TITLE OF THESIS ASPECTS OF SPATIAL SCALE IN PROCESS
 GEOMORPHOLOGY
DEGREE FOR WHICH THESIS WAS PRESENT DOCTOR OF PHILOSOPHY
YEAR THIS DEGREE GRANTED 1990

Permission is hereby granted to THE UNIVERSITY OF ALBERTA LIBRARY to reproduce single copies of this thesis and to lend or sell such copies for private, scholarly or scientific research purposes only.

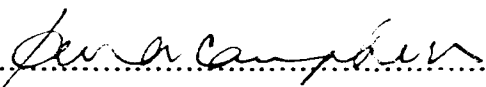
The author reserves other publication rights, and neither the thesis nor extensive extracts from it may be printed or otherwise reproduced without the author's written permission.

(SIGNED) *Dirk H. de Boer*

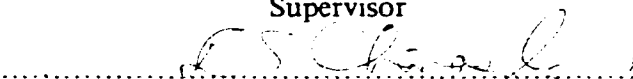
PERMANENT ADDRESS:
..... *Department of Geography*
..... *University of Alberta*
..... *Edmonton, Alberta*

THE UNIVERSITY OF ALBERTA
FACULTY OF GRADUATE STUDIES AND RESEARCH

The undersigned certify that they have read, and recommend to the Faculty of Graduate Studies and Research, for acceptance, a thesis entitled ASPECTS OF SPATIAL SCALE IN PROCESS GEOMORPHOLOGY submitted by DIRK H. DE BOER in partial fulfilment of the requirements for the degree of DOCTOR OF PHILOSOPHY.

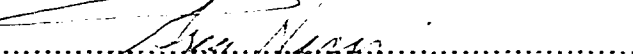
I.A. Campbell 

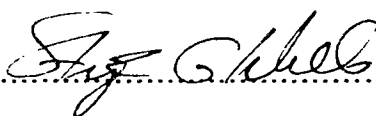
Supervisor

D. Chanasyk 

R. Gerard 

M.J. Hodgson 

G.H. Henry 

S.G. Wells 

External Examiner

Date... 6 Oct 1989

ABSTRACT

Geomorphic systems possess a hierarchical structure. Every geomorphic system consists of smaller, lower-level systems, and is at the same time part of larger, higher-level systems. Insight into the aspects of spatial scale transference aids in focussing on those hierarchical levels dominating behaviour of the geomorphic system of interest.

A literature review led to the formulation of a series of propositions concerning spatial scale transference in process geomorphology. Results of a field study of the effect of spatial scale on the rainfall-runoff relationship and sediment and solute dynamics in a series of semi-arid, ephemeral, badland drainage basins were used to test these propositions, and to deduce new ones. For the field study, the timescale of interest was that relevant to basin response to a single rainstorm.

Results from the field study indicated that spatial scale transference between geomorphic systems of differing scales is restricted by morphological and functional constraints. Morphological constraints are caused by morphological elements existing in large-scale systems, but not at smaller scales. Functional constraints follow from the characteristics of the matter and energy flows in the systems of interest. The boundaries imposed upon spatial scale transference by morphological and functional constraints are fuzzy rather than sharp in character. Thus, the greater the scale difference between two geomorphic systems, the smaller the amount of information that can be extrapolated from the one to the other. From the viewpoint of a geomorphic system, when a system 'looks' at systems of smaller and larger scales, the amount of detail and information the system 'sees' decreases with distance. Nevertheless, certain prominent features may continue to

PREFACE

An important part of geomorphology is concerned with the study of geomorphological processes, and studies the flows of matter and energy in the landscape. Direct observations form a crucial part of process research. These observations usually are of limited spatial and temporal extent. For instance, the steady-state infiltration rate is often determined with an infiltrometer ring covering only a fraction of the area of interest. Smettem and CollinsGeorge (1985) demonstrated that on a soil containing macropores, ring size has a considerable effect on the measured infiltration rates. A smaller ring has a larger chance of being installed at a site which is not representative of the soil, and hence will give a poor representation of the actual field conditions.

Logistical and financial constraints place severe limits on long-term studies, and comparatively few geomorphologic investigations of processes extend over more than a decade. Lewin (1980), for example, used the example of process observations which are restricted to a few years of 'Ph.D. time'.

Problems occur when attempts are made to extrapolate, either in space or in time, the information obtained in the field from studies of small areas or investigations of short duration. These problems arise from the fact that increases in scale do not merely involve increases in the spatial and temporal dimensions, and the number of components of a system, but instead result in new variables, new relationships, and as a rule lead to the identification of new problems (Haggett et al., 1965).

An awareness of scale effects has a significance beyond the problems of spatial and temporal extrapolation of process observations. Sugden and Hamilton (1971) argued that

linking process and form on different temporal and spatial scales as equivalent to establishing geomorphological theory. Mark (1980) argued that recognizing the scale-based dichotomy of small-scale processes and large-scale landforms is essential to further advances in linking process and form. Roswall et al. (1988) viewed an appreciation of scale effects as essential to overcome the disparities in spatial and temporal scales used in the different disciplines concerned with global environmental change.

The transfer of information between systems of differing scales, hereafter referred to as scale transference, has both temporal and spatial aspects. Schumm and Lichty (1965) explored the geomorphological implications of temporal scale transference in their classic paper 'Time, space, and causality in geomorphology'. Since then, temporal scale has been the subject of a number of papers (e.g. Wolman and Gerson, 1978; Brunsten and Thornes, 1979; Church, 1980). In 1978 a Symposium was held by the British Geomorphological Research Group with the aim of bringing together geomorphologists investigating different timescales, and to examine how results from one timescale could be extrapolated to another (Cullingford et al., 1980).

Spatial scale transference, however, has received considerably less attention. There is especially a scarcity of studies under controlled experimental conditions of the effects of changes in spatial scale on geomorphic processes.

The objective of this study is twofold: first, to review earlier work relevant to spatial scale transference in process geomorphology; second, to investigate the effect of spatial scale on the rainfall-runoff relationship and solute and sediment dynamics in semi-arid badland basins drained by ephemeral streams.

The field area is located in the Dinosaur Provincial Park badlands in the semi-arid

choosing the field area. Badlands have special advantages for this type of study as they are areas in which many of the varied effects of geomorphic processes can be easily discerned and measured. Even at the smallest scale, drainage basins are readily defined in badlands. Furthermore, the lack of a soil and vegetation cover facilitates detailed investigation of, for example, the relationship between rainfall, lithology, and drainage basin response at all levels of scale.

The field study was carried out at three scale levels: (1) the microscale of the experimental plot, typically concerned with an area of less than 1 m²; (2) the subbasin scale, concerned with two subbasins of ca. 2000 m²; and (3) the mesoscale, concerned with two basins of 79,230 and 202,260 m², respectively. The basins were nested, so that each mesoscale basin contained one subbasin which, in turn, contained a number of microscale basins. The timescale of interest for the field study concerned basin response to a single rainstorm. The timescale was kept constant for all three spatial scale levels to avoid confusion arising from the interaction of temporal and spatial scales. An additional reason for the choice of timescale is that in semi-arid regions the considerable variability in rainfall from year to year limits the validity of estimating long-term geomorphic conditions from short-term observations. Hence, extrapolating data from short-term experiments to longer periods should be avoided. Drainage basins are well suited to spatial scale research because they exist in a wide range of sizes, and are relatively easy to delineate. In addition, as drainage basins are fundamental geomorphologic units their use is particularly appropriate for geomorphological research.

Research was first directed towards the development of a series of propositions that would be generally applicable to the problems of spatial scale in process

reviews previous research on geomorphic processes in Dinosaur Provincial Park. The results of the field study at the three scale levels are presented in Chapter 3 (microscale), Chapter 4 (subbasin scale), and Chapter 5 (mesoscale). In Chapter 6 the relationship between the results obtained at the different scales in the field is analyzed, and some of the propositions derived in Chapter 1 are applied to these results. Finally, in Chapter 7 the conclusions from the field study are presented. Three new propositions, derived from the field study, concern the constraints on spatial scale transference between geomorphic systems, and characterize the boundaries across which spatial scale transference cannot take place without extensive revision of the concepts and models involved.

ACKNOWLEDGEMENTS

The very first time I visited Dinosaur Provincial Park was in August 1985 with Ian Campbell and Sarah O'Hara. While we were in the field it started to rain, and we got thoroughly wet, cold, and muddy running around looking at the processes on the various surface units, and following the leading edge of the flow down the arroyo. Since then I have been wet, cold, and muddy many more times, but that first time still stands out. I would like to thank Ian Campbell, my supervisor, for this cleverly arranged introduction to process geomorphology in Dinosaur Provincial Park, and for his continuing encouragement and guidance, without which this thesis would not be the same. Thanks also to my committee members: D. Chanasyk, R. Gerard, G.H. Henry, M.J. Hodgson, and S.G. Wells.

Sarah O'Hara, Jo-Anne Bund, Darin Peters, and Lorne Dmitruk assisted with with the fieldwork, and got wet, cold and muddy too (although some more so than others). Laury Davis provided hours of entertainment with the floating bedload trap and his special version of 'Oh, Canada'. My Arctic colleagues David 'Evs' Evans, Tom Morris, Don Lemmen, Hector Beaudet, Val Sloan, and Trevor Bell took my mind of process geomorphology with endless discussions about marine limits and all those other glacial things. My office mates, Don Lemmen and Gesche Schmid-McGibbon, generously let me have the lighttable so my desk could be used for piling stuff on. Many thanks also to the Englands for hours of skiing on the Rolling Hills, throwing sticks, and, in general, providing a home away from home.

Research in Dinosaur Provincial Park was made possible by permission from

Finally, the person who contributed the most to the successful outcome of my Ph.D. endeavour was Francien, and I would like to thank her for all her support.

TABLE OF CONTENTS

Chapter	Page
CHAPTER 1	
1.1 General principles of hierarchy theory	i
1.2 Hierarchy theory in geomorphology	6
1.3 Previous research on scale transference in geomorphology	9
1.3.1 Time	10
1.3.2 Space and time	14
1.3.3 Process and form	22
1.3.4 Catastrophic events	29
1.3.5 Input-output relationships	32
1.4 Overview	40
CHAPTER 2	
2.1 General description of the study area	44
2.2 Climate and rainfall characteristics	48
2.3 Lithology	58
2.3.1 Sandstones	58
2.3.2 Shales	59
2.4 Regolith chemistry	60

2.7.3 Sandstone surfaces	67
2.7.4 Shale surfaces	68
2.8 Mesoscale drainage basins	70
2.9 Design of the present study	72

CHAPTER 3

3.1 Microscale plot studies	74
3.2 Direct-runoff tests	74
3.2.1 Experimental design	74
3.2.2 Results	77
3.2.2.1 Pediment surfaces	77
3.2.2.2 Sandstone surfaces	88
3.2.2.3 Shale surfaces	94
3.2.3 Discussion	101
3.3 Rainfall simulation tests	109
3.3.1. Experimental design	109
3.3.2 Results	117
3.3.2.1 Pediment surfaces	117
3.3.2.2 Sandstone surfaces	123
3.3.2.3 Shale surfaces	129
3.3.3 Discussion	135
3.4 Relating direct-runoff tests and rainfall simulations	143
3.5 Summary	144

4.3 Instrumentation	151
4.4 Rainfall characteristics	157
4.5 Subbasin A	162
4.5.1 Runoff characteristics	162
4.5.2 Sediment and solute dynamics	164
4.6 Subbasin B	169
4.6.1 Runoff characteristics	169
4.6.1.1 Runoff coefficients	173
4.6.1.2 Hydrograph characteristics	179
4.6.2 Sediment and solute dynamics	184
4.7 Contrasts between Subbasins A and B	186
4.8 Summary	188

CHAPTER 5

5.1 Mesoscale drainage basin studies	190
5.2 Basin instrumentation	190
5.3 Laboratory procedures	194
5.4 The rainfall-runoff relationship	196
5.4.1 Runoff coefficients	198
5.4.2 Hydrograph characteristics	206
5.5 Sediment dynamics	
5.5.1 Sediment yields	215
5.5.2 Effect of storm type	219

5.6.2.1 Cations	245
5.6.2.2 Anions	248

CHAPTER 6

6.1 Spatial scale transference in semi-arid drainage basins	255
6.2 Rainfall-runoff relationship	255
6.2.1 Hydrological rainfall and complexity of basin topography	255
6.2.2 Hydrological versus meteorological rainfall	257
6.2.3 Thresholds of runoff generation and thresholds of flow	259
6.2.4 Runoff coefficients	260
6.2.5 Hydrograph characteristics	265
6.3 Sediment dynamics	269
6.3.1 Sediment concentration/discharge relationships and sediment yields ...	269
6.3.2 Tunnel systems	272
6.4 Morphological and functional constraints on spatial scale transference	276

CHAPTER 7

7.1 Conclusions	278
-----------------------	-----

BIBLIOGRAPHY	282
---------------------------	------------

APPENDIX A - Data for representative microscale plots	295
--	------------

LIST OF TABLES

Table	Page
1.1 Status of drainage basin variables as a function of time.....	13
2.1 Information on Atmospheric Environment Service weather stations	49
2.2 Long-term precipitation and temperature records for Brooks AHRC.....	50
3.1 Characteristics of direct-runoff plots	80
3.2 Overview of results of direct-runoff tests	81
3.3 Summary of results of direct-runoff tests	103
3.4 Characteristics of rainfall simulation plots	114
3.5 Overview of results of rainfall simulations	115
3.6 Summary of results of rainfall simulations	136
4.1 Percentage of basin area taken up by different surface units	149
4.2 Characteristics of tilted raingauges in Subbasins A and B	153
4.3 Overview of data collected in Subbasin A and B during 1986 and 1987	155
4.4 Hydrological rainfalls in Subbasins A and B for entire observation period and for selected storms	161
4.5 Rainfall and runoff of Subbasin B	174
5.1 Percentage of basin area taken up by different surface units	193
5.2 Overview of rainfall and runoff data collected during 1986 and 1987.....	197
5.3 Rainfall, runoff, and sediment yields of the Rimco Basin for 1986 and 1987.....	200
5.4 Rainfall, runoff, and sediment yields of the New Basin for 1986 and 1987	201

LIST OF FIGURES

Figure	Page
<p>1.1 Filtering of signals by a holon. The holon, represented by the rectangle, decreases the frequency of the signals it receives from its lower holons (bottom). Signals having a frequency characteristic of the holon (middle) and low-frequency signals from the holon's environment (top) are not filtered, and retain their frequency. (Modified after O'Neill et al., 1986)</p>	4
<p>1.2 System type as a function of randomness and complexity. See text for explanation. (Modified after Weinberg, 1975)</p>	7
<p>1.3 Types of equilibrium: static equilibrium - no change over time; steady state equilibrium - short term fluctuations around a constant long-term average; dynamic equilibrium - short term fluctuations around a declining long-term average.....</p>	11
<p>1.4 Reaction and relaxation times of a geomorphic system. The horizontal axis represents time; the vertical axis, a typical system variable such as a process rate or a morphological parameter. See text for explanation</p>	15
<p>1.5 Top: Nested hierarchy of geomorphic systems. The nested negative feedback loops allow the different levels to mutually adjust each other. Bottom: Reaction and relaxation times (Fig. 1.4) increase from the lowest (alluvial channels) to the highest level (divides). Thus, the morphology of the alluvial channels will show a rapid response to new conditions, whereas the divides will only be adjusted after a much longer timespan. (Modified after Chorley et al., 1984)</p>	16

slope caused by events of differing magnitude. At time A, a flood of relatively high magnitude causes the valley floor slope to exceed the threshold slope of incision. Valley floor incision, however, would have occurred at time B regardless of the magnitude of the flood at that time. (Modified after Schumm, 1977)23

1.8 Contrasts in annual sediment yield regime between small-scale (0.5-1 ha) basins and a large-scale (15 500 km²) basin. See text for explanation. (Modified after McGuinness et al., 1971)36

1.9 Downstream attenuation of a flood wave resulting from rainfall in the headwaters of the Savannah River, South Carolina and Georgia. (Data from Hoyt and Langbein, 1955; Modified after Strahler (1975) and Bennett and Chorley, 1978)37

1.10 Longitudinal dispersion, causing downstream changes in the shape of the concentration vs. time curve for a slug injection of NaCl into a stream. See text for explanation. (Modified after Day, 1975)38

1.11 Overview of propositions concerning the problem of spatial scale transference, derived from a survey of the geomorphological literature41

2.1 Location of Dinosaur Provincial Park, Alberta. Also shown are the locations of the experimental basins, and of the AES weather stations in the area45

2.2 Map of Dinosaur Provincial Park, showing the location of the experimental basins ..46

2.3 Typical badland morphology in Dinosaur Provincial Park, consisting of straight, densely-rilled sandstone slopes, and convex, gentle shale slopes. Ironstone bands cause prominent ledges. Locally, ironstone debris covers large portions of the slopes. Vegetation occupies much of the low-lying alluvial and aeolian surface units47

2.4 Monthly precipitation for Dinosaur Provincial Park and nearby AES weather stations

May to August, 1987	56
2.7 Pediment, separated from the overlying shale slope by a sharp slope break	66
3.1 Experimental set-up during direct-runoff test on plot A3. Runoff rapidly concentrates in distinct flowpaths, precluding conversion of the data to areal values	75
3.2 Surface units and locations of microscale experimental plots in Subbasin A	78
3.3 Surface units and locations of microscale experimental plots in Subbasin B	79
3.4 Test results for a representative pediment plot (A4), showing flushing of solute-rich runoff; decrease of \underline{EC}_p and \underline{SC}_p for the wet run; and reduced lag in start of flow and steeper rise in discharge for the wet run. The decrease of \underline{EC}_s for the wet run lies within the range of precision of the EC meter	83
3.5 Contrasting sediment concentration/discharge relationships for plots A2 and A3 (pediment). During the dry run, plot A3 exhibits initial flushing, whereas plot A2 does not. Subsequent variations in sediment concentration are partially independent of discharge, and may reflect collapse of microfeatures or episodic migration of headcuts. During the wet run, sediment concentrations on plot A2 generally increase with decreasing discharge, whereas plot A3 displays a general decrease in sediment concentrations at a relatively constant discharge	86
3.6 Moisture profiles before the dry, and after the wet run on a representative pediment plot (A4). The stepped curve reflects the sampling of the regolith in layers	89
3.7 Test results for a representative sandstone plot (A10), showing flushing of solute-rich runoff; decrease of \underline{EC}_p and \underline{SC}_p for the wet run; and reduced lag in start of flow and steeper rise in discharge for the wet run	90
3.8 Contrasting sediment concentration/discharge relationships for plots A2 and A3 (sandstone). During the dry run, plot A3 exhibits initial flushing, whereas plot A2 does not. Subsequent variations in sediment concentration are partially independent of discharge, and may reflect collapse of microfeatures or episodic migration of headcuts. During the wet run, sediment concentrations on plot A2 generally increase with decreasing discharge, whereas plot A3 displays a general decrease in sediment concentrations at a relatively constant discharge	96

plot (A10). Samples were taken within the central rill	95
3.10 Test results for a representative shale plot (B7), showing flushing of solute-rich runoff; rising \underline{EC} 's and sediment concentrations at the end of the wet run; decrease of \underline{EC}_p and \underline{SC}_p for the wet run; and reduced lag in start of flow for the wet run	96
3.11 Sediment concentration/discharge relationships of plot A6, showing an initial decrease in sediment supply, followed by slight variations, during the the dry run; and showing a steady increase, independent of discharge, during the wet run	99
3.12 Sediment concentration/discharge relationships of plot B7, indicating a decreasing sediment availability during the dry run; and showing irregular variations in sediment concentration, independent of discharge, during the wet run	100
3.13 Moisture profiles before the dry, and after the wet run on a representative shale plot (A8)	102
3.14 Sediment concentration/discharge data for the dry runs of the direct runoff tests, showing the contrasts in sediment yields between the pediments, sandstones, and shales	105
3.15 Variables measured during direct-runoff tests, and the processes whereby they interact	108
3.16 Experimental set-up during rainfall simulation on plot BR3. The sample is taken at the plot outlet, where a funnel made of thin aluminum is installed. The windscreen wrapped around the frame minimizes disturbance of the rainfall by wind	110
3.17 Detailed view of the rainfall simulator. The plexiglas box is fed from the blue jerrycans acting as constant-head devices. The vertical tubes are open to the atmosphere, and allow expulsion of air from the box during filling. The water level in	

flow for the wet run; exponential decrease of <u>EC</u> ; and relatively constant but low sediment concentrations	119
3.19 Sediment concentration/discharge relationship for the dry run on plots AR2 and BR3. On plot AR2, sediment concentrations remain relatively constant throughout most of the test, notwithstanding an increase in discharge from 0.4 to 13.7 ml s ⁻¹ . Plot BR3 shows evidence of initial flushing, followed by a slight increase in sediment concentration as discharge increases. The curve of plot BR3 possesses clockwise hysteresis, indicating a decreasing sediment supply	121
3.20 Contrasts between the moisture profiles before the dry, and after the wet run on plots BR2 (top), a sandstone pediment, and AR2 (bottom), a shale pediment	124
3.21 Test results for a representative sandstone plot (BR8), showing reduced lag in start of flow for the wet run; exponential decrease of <u>EC</u> during both runs; and variations in sediment concentration independently from the discharge, caused by microscale slumps and mudflows	125
3.22 Contrasting sediment concentration/discharge relationships for the dry runs on plots BR6 and BR8. Plot BR6 shows exhaustion of the sediment supply, whereas plot BR8 displays an increase in sediment concentration at a relatively constant discharge ...	128
3.23 Moisture profiles before the dry, and after the wet run on a representative sandstone plot (BR8)	130
3.24 Test results for a representative shale plot (BR12), showing a large lag between the beginning of the test and the start of runoff; high, and exponentially decreasing <u>EC</u> 's; and high, and generally increasing sediment concentrations	131

(BR12)	137
3.27 Sediment concentration/discharge data for the dry runs of the rainfall simulations, showing the contrasts in sediment yields between the pediments, sandstones, and shales. Data for the wet runs on the pediments and the sandstones display a similar pattern	138
3.28 Variables measured during rainfall simulations, and the processes whereby they interact	139
4.1 Locations of Subbasins A and B in the Rimco Basin and the New Basin	146
4.2 Map of Subbasin A, showing topography and locations of tilted raingauges	147
4.3 Map of Subbasin B, showing topography and locations of tilted raingauges	148
4.4 Overview of Subbasin A, showing topography and arrangement of surface units. Note that sandstone overlies shale on the steep slope sections, causing the formation of tunnel erosion features in shale, transmitting runoff generated on sandstone. Photograph by I.A. Campbell	150
4.5 Overview of Subbasin B, showing topography and arrangement of surface units. Because, in contrast to the situation in Subbasin A, shale overlies sandstone on the steep slopes, tunnel erosion features are limited to microscale features on the shale. The basin outlet is located to the left, just outside the picture. Photograph by I.A. Campbell	152
4.6 Instrumentation at the outlet of Subbasin B. Runoff is collected in a 65 l barrel into which a V-shaped opening is cut to allow controlled overflow. Stage in the barrel is measured with a Stevens stage recorder. The inlet for the ISCO water sampler is	

4.8 Hydrograph, hyetograph (Rimco recording raingauge), sediment concentration, and EC of Subbasin A on July 18, 1987 (I). The Rimco recording raingauge is located ca. 230 m WNW of Subbasin A. Because of the limited basin size the hydrograph of Subbasin A is extremely sensitive to rainfall intensity variations	163
4.9 Hydrograph, hyetograph (Rimco recording raingauge), sediment concentration, and EC of Subbasin A on May 26, 1987 (I)	165
4.10 Sediment concentration/discharge relationship for Subbasin A	166
4.11 Contrasting sediment concentration/discharge relationships for Subbasin A. On May 26, 1987 (I), sediment sources were confined to the supply limited sandstones and pediments, resulting in clockwise hysteresis (top). On August 14, 1987, sediment concentrations increased with time as shales and tunnel systems contributed sediment-rich runoff, resulting in counterclockwise hysteresis (bottom)	167
4.12 EC/discharge relationship for Subbasin A	170
4.13 Antecedent Precipitation Index plotted against total rainfall for the Rimco Basin and the New Basin. Indicated is whether or not runoff from Subbasin B occurred	171
4.14 Relationship between total rainfall and total discharge, and the effect of antecedent moisture conditions, in Subbasin B. The lines indicate the value of the runoff coefficient	175
4.15 Hydrological rainfall on July 18-19, 1987, corrected for differing tilts, and expressed as a fraction of the average rainfall for the Rimco Basin and the New Basin on the same day	177
4.16 Hydrological rainfall on August 14, 1987, corrected for differing tilts, and expressed as a fraction of the average rainfall for the Rimco Basin and the New Basin on the same day	177

4.18 Hydrograph and hyetograph (Rimco recording raingauge) for Subbasin B on July 3-4, 1987, showing isolated periods of flow separated by short, dry intervals 181

4.19 Hydrograph and hyetograph (Rimco recording raingauge) for Subbasin B on July 5, 1987, showing the effect of low-intensity rainfall during the falling stage of the hydrograph. The sediment concentration does not show evidence of initial flushing, and is low and fairly constant throughout the runoff event. The EC shows some evidence of initial flushing, reaches a trough during peak flow, and increases sharply during the falling stage 182

4.20 Hydrograph and hyetograph (Rimco recording raingauge) for Subbasin B on July 18, 1987 (I), showing the hydrograph of a low-intensity, long-duration, frontal rainstorm. Also shown is the hydrograph of Subbasin A. The smaller discharges in the latter subbasin are caused by a greater thickness and extent of sheetwash deposits, and by the fact that a portion of the pediment is underlain by shale instead of by sandstone as in Subbasin B 183

4.21 Hydrograph, hyetograph (Rimco recording raingauge), sediment concentration, and EC of Subbasin B on May 26, 1987 (I). Peak discharge exceeded the maximum measurable discharge. Sediment concentrations indicate initial flushing, and reach high values during peak flow. EC's show evidence of initial flushing also, reach minimum values during peak flow, and increase again during the falling stage 185

4.22 Hydrograph, hyetograph (Rimco recording raingauge), and EC for Subbasin B on August 14, 1987. The EC varies inversely with discharge, and increases to high values towards the end of the runoff event 187

5.1 Mesoscale basin configuration and instrumentation 191

5.2 Surface units of the Rimco Basin and the New Basin (Modified after Bryan and Campbell, 1986) 192

5.3 Upstream view of the outlets of the New Basin (left) and the Rimco Basin (right) with the associated instrumentation. The Aquatot sonic-echo flowgauge can be seen

suspended above the 1.5 foot wide Parshall flume of the New Basin. The instrument stand between the channels contains batteries, a solar panel for recharging, and the chart recorder for the Aquatot flow gauge. Note the typical light brown colour of the runoff, indicative of the high sediment concentrations 195

5.4 Antecedent Precipitation Index plotted against total rainfall for each storm for the Rimco Basin and the New Basin 199

5.5 Relationship between total rainfall and total discharge for the Rimco Basin and the New Basin 203

5.6 Ratio of runoff coefficients of the Rimco Basin and the New Basin (runoff coefficient Rimco Basin divided by runoff coefficient New Basin) plotted against total rainfall 205

5.7 Total rainfall distribution on July 9, 1986 207

5.8 Hydrographs and hyetograph (Rimco recording raingauge) for July 9, 1986. The second peak in the hydrograph of the Rimco Basin is caused by localized rainfall in the upstream parts of the basin. This rainfall, however, has no significant effect on the hydrograph of the New Basin 208

5.9 Total rainfall distribution on July 26, 1986 210

5.10 Hydrographs and hyetograph (Rimco recording raingauge) for July 26, 1986, showing typical basin response to a convectional thunderstorm 211

5.11 Total rainfall distribution on July 18, 1987 213

5.12 Hydrographs and hyetograph (Rimco recording raingauge) for July 18, 1987, showing typical basin response to frontal rainfall 214

5.13 Relationship between total rainfall and sediment yield per unit area, and the effect of antecedent moisture conditions (API) 216

5.14 Ratio of sediment yield per unit area of the Rimco Basin and the New Basin (sediment yield Rimco Basin divided by sediment yield New Basin) plotted against total rainfall 217

5.15 Sediment concentration/discharge relationship for the Rimco Basin 222

5.16 Sediment concentration/discharge relationship for the New Basin 223

5.17 Relationship between antecedent moisture conditions and total rainfall at the time of increasing sediment concentration. The latter variable is interpreted as the threshold of tunnel flow initiation, exceedance of which causes a change from clockwise to counterclockwise hysteresis 227

5.18 Sediment concentration/discharge relationship for the New Basin on August 14, 1987, showing an increasing sediment supply as deep tunnel systems and shale surfaces contribute sediment 228

5.19 Sediment concentration/discharge relationship for the Rimco Basin on May 27, 1987, showing exhaustion of the sediment supply as sediment accumulated on the sandstone and pediment surfaces is flushed away during the rising stage 231

5.20 Sediment concentration/discharge relationship on June 20, 1987, compared to other data for the New Basin. The flushing away of sediment accumulated on the sandstone and pediment surfaces causes exceptionally high sediment concentrations on the rising stage, disguising the counterclockwise hysteresis expected during this event 233

5.21 Hydrograph, hyetograph (Rimco recording raingauge), and EC for the New Basin on May 26, 1987 (I), showing steep decrease in EC during initial flushing, followed by a gradual increase during the falling stage 235

5.22 EC/discharge relationship for the New Basin 237

5.23 EC/discharge relationship for the Rimco Basin 238

5.24 Contrasting EC/discharge relationships for the New Basin. On June 20, 1987, the peak discharge lagged after the EC trough, resulting in counterclockwise hysteresis. On August 14, 1987, the peak discharge preceded the EC trough a number of times, resulting in a series of clockwise loops. On both days, however, the highest EC's occurred during the final stages of flow 240

5.25 Contrast between EC/discharge relationship of the Rimco Basin and the New Basin. In the Rimco Basin, the discharge peak precedes (or coincides with) the EC trough,

whereas in the New Basin it lags after the EC trough on two occasions. The difference is possibly caused by more rapid flushing of solute-rich water and, more importantly, by an earlier contribution to the EC by dissolving suspended sediment in the New Basin 242

5.26 Change in EC/discharge relationship of the New Basin during low-intensity rainstorms. The wetness of the basin at the time of runoff generation causes higher solute export and increases the EC during the rising stage and the flow peak, causing the EC trough to lag after the peak discharge. The same mechanism also operates during secondary and later flow peaks 243

5.27 Comparison of the EC at the time of sampling (EC) and after centrifuging (EC2) 244

5.28 Hydrographs, hyetograph (Rimco recording raingauge), and chemographs (Na, K, Ca, Mg, Al, and SO₄) for the New Basin on July 26, 1986. All solute concentrations are in mg l⁻¹ 246

5.29 Relationship between EC and SO₄ concentration 250

5.30 SO₄/EC relationship for the New Basin on June 20, 1987, and July 18, 1987. See text for explanation 251

5.31 SO₄/EC relationship for the Rimco Basin on July 19, 1987 (I). See text for explanation 253

6.1 Hyetograph (Rimco recording raingauge) and dimensionless hydrographs of Subbasin B and the Rimco Basin on July 18, 1987 (I). See text for explanation 266

6.2 Hyetograph (Rimco recording raingauge) and dimensionless hydrographs of Subbasin A and the New Basin on May 26, 1987 (I). See text for explanation 267

6.3 Percentage of basins having a deep tunnel system plotted against spatial scale. See text for explanation 275

CHAPTER 1

1.1 GENERAL PRINCIPLES OF HIERARCHY THEORY

At present there is no widely accepted theoretical framework within which the problems of spatial scale transference can be investigated. This indispensable framework may be provided by hierarchy theory (Haigh, 1987).

A geomorphic system is defined by Chorley et al. (1984, p. 5) as 'a structure of interacting processes and landforms that function individually and jointly to form a landscape complex'. The term system is used here to refer to an open system, i.e. one with boundaries open to the import and export of matter and energy from its environment. Closed systems, with boundaries across which no import or export of matter and energy occurs, have limited use in geomorphology (Graf, 1988) and will be ignored in this study. Any geomorphic system, such as a drainage basin, can be viewed as a nested hierarchy of systems. In this approach, every system consists of smaller subsystems, and is in itself a subsystem of a larger system. Koestler (1967) introduced the term 'holon' for such a system in a hierarchy in a biological context. The meaning of the term 'holon' was subsequently generalized by Allen and Starr (1982) to include systems of any type. A geomorphic system can therefore be considered to be a holon. To illustrate the concept of holons, Koestler (1967) uses the image of the Roman god Janus, who has two faces looking in opposite directions: one face looks inward at the subordinate parts, and is that of a self-contained whole; the other face looks outward, and is that of a dependent part. This duality of being both a self-contained whole and a dependent part, or the 'Janus-effect' (Koestler, 1967), is a fundamental characteristic of all holons. A hierarchy consisting of holons was termed a holarchy by Koestler (1967).

The structure and functioning of a holon are governed by a set of fixed rules, which Koestler (1967) calls its 'canon'. The canon of a holon describes its fixed properties

and the laws governing its structure and functioning. Within the constraints imposed by the canon the holon has a wealth of options, or strategies, for responding to changes in its environment. Koestler (1978, p. 38) illustrates this idea with the example of the game of chess: the canon consists of the rules defining the permissible moves, but the actual moves are determined by the players whose strategy is based on the environment, i.e. the positions of the pieces on the board.

In a hierarchy, a higher and a lower holon are linked by an exchange of information, matter, or energy. Allen and Starr (1982) distinguish two cases in which such a link is not present. The first, somewhat trivial case, occurs when the lower and the higher holon are in different stems of the hierarchy. The second case occurs when the vertical distance between the holons is too large. Allen and Starr (1982, p. 13) define a holon's environment as 'being made up of all things with slower behavior with which it interacts'. The holon in its turn forms the environment for 'all faster behaving holons with which it interacts' (Allen and Starr, 1982, p. 13). There is no link between the two holons when the ratio of cycle times, or frequencies or rates of behaviour of two holons becomes too large. From the viewpoint of the higher holon, the lower holon behaves so rapidly that it appears to quickly attain static or, in some cases, dynamic, equilibrium (Schumm, 1977). From the viewpoint of the lower holon, the higher holon behaves at an imperceptually slow rate, and essentially provides a constant background. In this manner, when the vertical distance between two holons is large, they may become part of each others' canon. Similarly, links between a higher and a lower holon will not exist when the lower holon has a lifespan which is too short, has too short a memory, or exerts too little influence to establish a direct link with the higher holon (Allen and Starr, 1982). This point implies that the search for a fundamental level at which all higher level phenomena can be explained will prove to be inefficient if not ineffective (O'Neill, 1988).

The concept of 'emergent properties' is of considerable importance in hierarchy theory (Allen and Starr, 1982). This concept concerns the properties of high-level holons

which cannot be predicted from the properties of the lower levels. The existence of such properties limits the usefulness of the reductionist approach because to understand the whole it becomes necessary to understand more than just the parts.

O'Neill et al. (1986) illustrate the difference in process rates at different levels in a hierarchy with the example of a holon which acts as a filter for its lower holons. The high-frequency signal from the lower holons is transformed into a signal having a lower frequency, characteristic of the upper holon (Fig. 1.1). The upper holon is thus not sensitive to every variation at the lower level, but only to the overall, filtered state. Signals from the upper holon's environment, which have a lower frequency, are not filtered by the upper holon. The upper holon thus has no control over the signals it receives from its environment, and must respond to these signals without being able to modify them.

When used in an every-day context the term 'hierarchy' connotes a system of rank in which the higher levels constrain the lower levels. In hierarchy theory, however, this is not necessarily the case. Although not sensitive to every little change at the lower levels, the characteristics of the higher holons are partly determined by those of the lower holons, which therefore are essential to the functioning at the higher level. At the same time the lower holons are constrained by the higher level assemblage of which they are part. Grene (1969) describes this situation as a double asymmetry. The link between two holons is called symmetrical when two holons which are at the same level constrain each other to a similar extent, in a similar manner. The other type of link, asymmetrical, occurs between holons at different levels when one of the holons has a greater influence over the other (Allen and Starr, 1982). Double asymmetry as used by Grene (1969) indicates that holons at different levels mutually constrain each other, but that the manner of constraint differs.

An important property of a hierarchy is its 'near-decomposibility'. This concept was introduced by Simon (1962) who used the term to refer to systems consisting of subsystems. In a nearly decomposable system, interaction within the subsystems is relatively strong, whereas interaction between the subsystems is relatively weak, although

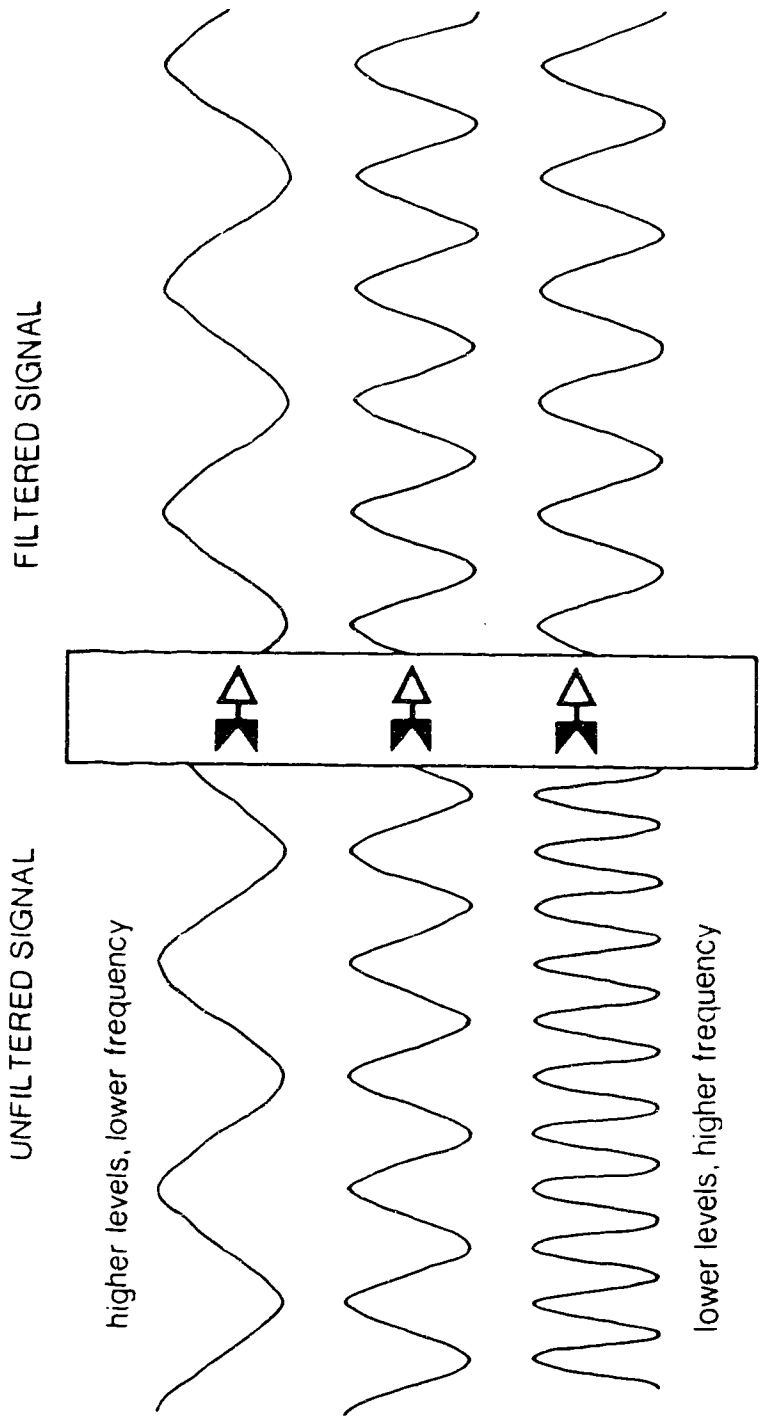


Fig. 1.1 Filtering of signals by a holon. The holon, represented by the rectangle, decreases the frequency of the signals it receives from its lower holons (bottom). Signals having a frequency characteristic of the holon (middle) and low-frequency signals from the holon's environment (top) are not filtered, and retain their frequency. (Modified after O'Neill et al., 1986).

not negligible (Platt, 1969). Components of a subsystem interact directly with each other, but only indirectly, through the higher level, with components of other subsystems. The strength of the interaction between subsystems may thus provide clues for locating the system boundaries.

Allen and Starr (1982) argue that the composition and boundaries of a holon are essentially arbitrary. They recognize, however, that for a certain purpose some holons may be more useful than others. Klemes (1983) calls such holons 'nodes', and suggests that the distinction of these few, but important, levels provides a firm basis for the development of concepts, and promotes a rapid development of science. In biology, for instance, the following nodes can be distinguished: molecule, cell, organism, species, population, community, ecosystem, biosphere. According to Klemes (1983), in disciplines such as hydrology where nodes are absent, or perhaps it is better to say ill-defined, progress is significantly slower. O'Neill (1988) uses the term 'coherent level' to describe a level that 'makes sense' as an isolated object of study.

The observer's decision of the location and nature of the boundary has far-reaching effects on the results obtained from studying the holon. Allen and Starr (1982) propose that all boundaries are in essence functional: the holon is separated from its environment by the relatively more rapid intrinsic process rates, and may be functionally isolated while being spatially interwoven with its environment. A special class of functional boundaries is formed by structural boundaries, which involve a physical surface separating the systems on either side. An example of a structural boundary is a cell membrane isolating the inside of the cell by impeding or slowing down intrusion from the cell's environment. An extensive discussion of the properties of boundaries in hierarchical systems may be found in Platt (1969).

1.2 HIERARCHY THEORY IN GEOMORPHOLOGY

The characteristics of a system are to a large extent determined by its complexity and its randomness (Weinberg, 1975). Both concepts are hard to define. For the purpose of this discussion randomness may be thought of as representing unpredictability, in the sense that when a die is thrown the outcome is unpredictable within certain bounds. Complexity is equally hard to describe, but may be thought of as a measure of the number of interactions between the components of a system. Weinberg (1975) distinguishes three classes of systems having differing degrees of randomness and complexity (Fig. 1.2). Systems in class I exhibit 'organized simplicity'. Such systems have a low degree of randomness, possess few components, and may be successfully treated in a deterministic manner, for instance with differential equations. Many systems in engineering are examples of class I systems.

Systems in class II are characterized by the term 'unorganized complexity'. These systems possess a large degree of randomness, allowing a statistical approach in which the exact behaviour of each component is ignored in favour of the calculation of averages. An example of a class II system having a large degree of randomness and complexity is a cylinder filled with gas. The relationship between the temperature, pressure, and density of the gas is described by the gas laws derived from statistical considerations of the large number of molecules in the cylinder. The behaviour of each individual molecule is ignored because in any practical problem the large number of molecules would make the resulting system of equations totally intractable.

Systems in between these two extremes are in class III, and possess 'organized complexity'. Systems in this last class are too complex, and their degree of randomness is too high, to be analyzed by the methods which are successful for class I systems. At the same time, their degree of randomness is too low for a purely statistical approach. Methods successful for class I and II systems can be applied to systems of class III, but

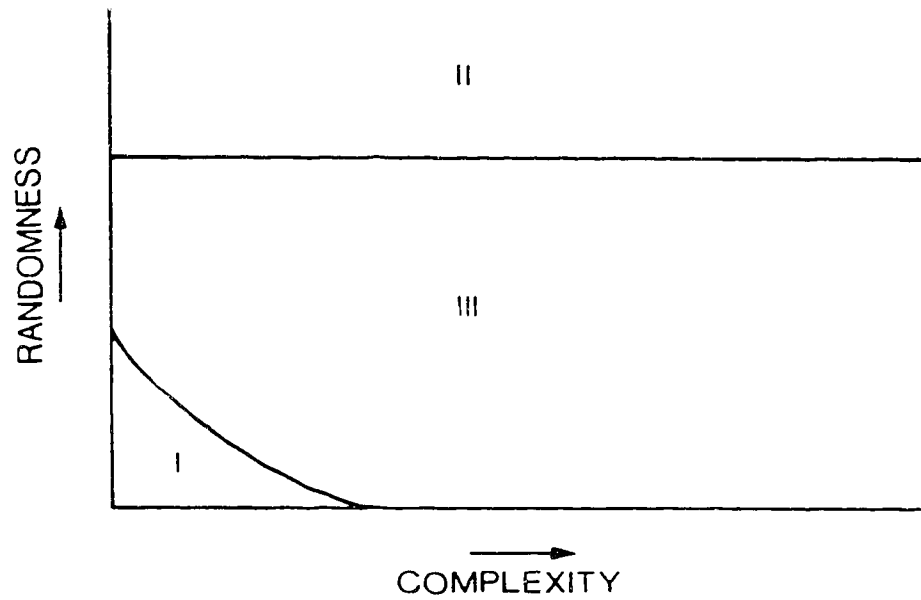


Fig. 1.2 System type as a function of randomness and complexity. See text for explanation. (Modified after Weinberg, 1975).

usually only with very limited success because very often the limit of the methods is reached. Weinberg (1975) calls systems in class III medium-number systems, which thus contrast with low-number systems (class I) and large-number systems (class II).

Medium-number systems cover the middle ground where the large number of components bring about a complexity which precludes the use of the mathematical techniques developed for dealing with small-number systems. At the same time, medium-number systems are small enough that the behaviour of each component will affect the system.

Klemes (1978) expresses a similar idea, and states that randomness can be of considerable importance in an aggregate where the number of components is large, but not large enough to suppress the influence of the individual components on the behaviour of the aggregate. With an increase in aggregate size the effect of the individual components weakens, and the behaviour of the aggregate may become more susceptible to a deterministic analysis. Klemes (1978) hence relates the change from random to deterministic behaviour to an increase in spatial scale.

Hierarchies have been recognized in many diverse branches of science ranging from cosmology to crystallography. In geomorphology, (hypothetical) examples of hierarchies have been given by Chorley and Kennedy (1971) and Chorley et al. (1984). Hierarchies are so common that their existence is often overlooked (Pattee, 1973). Allen and Starr (1982) avoid the question whether reality is hierarchically structured or not. Rather, they view hierarchies as coming into the picture when humans try to understand the world they live in. This outlook coincides with that of Simon (1962, p. 477) who suggests that

'If there are important systems in the world that are complex without being hierarchic, they may to a considerable extent escape our observation and our understanding. Analysis of their behaviour would involve such detailed knowledge and calculation of the interactions of their elementary parts that it would be beyond our capacities of memory or computation.'

This view of hierarchies does not in any way lessen their importance because at we st it means that hierarchies are abstractions conceived by the researcher for conceptualization and investigation. Similar views have been expressed regarding systems (Haigh, 1985), and the systems approach has proved to be extremely fruitful in geomorphological research.

Allen and Starr's (1982) interest in applying hierarchy theory to ecology arises from the fact that the majority of ecological systems are medium-number systems. In this respect geomorphic and ecologic systems are similar (Graf, 1988). Allen and Starr (1982) suggest that to deal with these complex systems, models will almost of necessity have to be hierarchical. O'Neill et al. (1986) and Risser (1987) see hierarchy theory as a promising framework with which to approach the problems of spatial and temporal scale transference in ecology. In a nested hierarchy of geomorphic systems the scale of holons increases from small at the bottom, to large at the top. The concept of scale hence permeates hierarchy theory, which may thus provide concepts, a philosophical basis, and a neutral terminology to deal with the problems of spatial scale transference in geomorphology.

1.3 PREVIOUS RESEARCH ON SCALE TRANSFERENCE IN GEOMORPHOLOGY

Haigh (1987) wrote the first and, at present, the only paper in the geomorphological literature in which hierarchy theory is explicitly used. Prior to Haigh's paper, however, a small number of other papers appeared in which hierarchies were implied. Haigh (1987) distinguishes three areas in geomorphology where hierarchies have been employed. First, hierarchies have been used in landscape classification and terrain synthesis (e.g. Isachenko, 1973). Second, hierarchy theory has been applied to drainage networks, leading to the different methods of stream ordering (Horton, 1945; Jarvis, 1976). In both of these areas the systems being studied are treated as static objects. The third area of application of hierarchy theory in geomorphology deals with dynamic

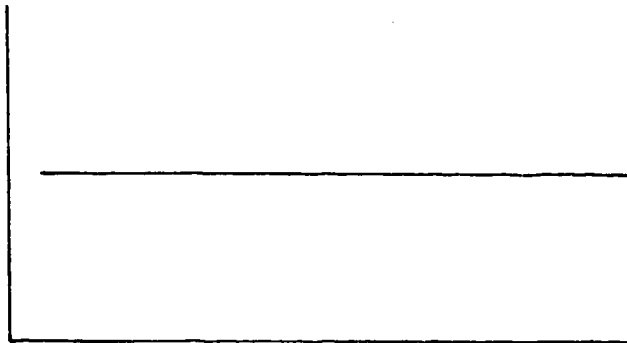
systems, and allows system evolution and changes in the hierarchy. This last area is the most significant from the viewpoint of process geomorphology.

In the following review certain papers in this third area will be discussed, in addition to papers having relevance to the problems of spatial scale transference in geomorphology but not directly concerned with hierarchy theory. It will be attempted to deduce, from the specific evidence presented, propositions that have a wider, more general application to the problems of scale transference in geomorphology. Some of these principles will be old truths in new words, the terminology of hierarchy theory; others will sound more fresh. In the following sections geomorphic systems will be viewed as holons, but to emphasize that not all holons are geomorphic systems the term holon will not be used.

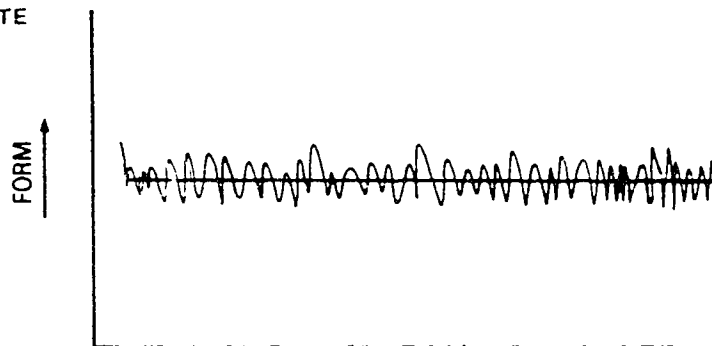
1.3.1 TIME

In the 1960's the focus of geomorphology shifted from long-term landform evolution to short-term process observation. In a successful attempt to unify the different viewpoints, Schumm and Lichty (1965) evaluated the connections between the three approaches to geomorphology current at that time and proposed a hierarchical classification of timespans. At the highest level of 'cyclic time', periods are up to several millions of years in length. During cyclic time a fluvial system progresses through a cycle of erosion (Davis, 1899). At the middle level of 'graded time', periods vary in length from a few hundreds to a few thousands of years. This timespan corresponds to the period during which the system variables are in a steady state equilibrium (Fig. 1.3), so that a fluvial system may be characterized as being in a graded condition (Mackin, 1948; Chorley et al., 1984). The lowest level of 'steady time' concerns the relatively short periods during which the system variables do not change with time, i.e. are in static equilibrium (Fig.

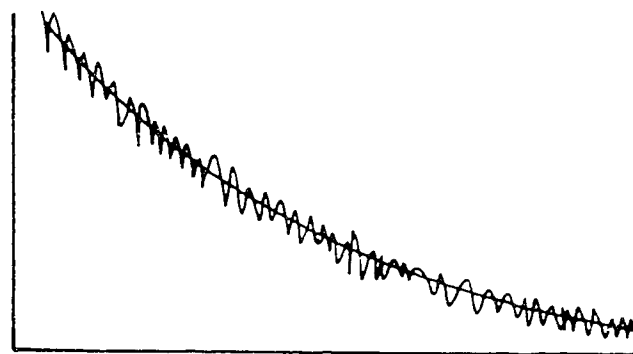
STATIC
EQUILIBRIUM



STEADY STATE
EQUILIBRIUM



DYNAMIC
EQUILIBRIUM



TIME →

Fig. 1.3 Types of equilibrium: static equilibrium - no change over time; steady state equilibrium - short term fluctuations around a constant long-term average; dynamic equilibrium - short term fluctuations around a declining long-term average.

1.3).

Schumm and Lichty (1965) divide the variables describing the state of a drainage basin during each of the three timespans into three categories: not relevant, independent, and dependent (Table 1.1). In the terms of hierarchy theory the independent variables establish the canon of the drainage basin during each timespan (Haigh, 1987). The independent variables can be considered to be constant during a timespan (i.e. vary at a frequency too low to detect variations over the timespan of interest), and hence pose certain constraints on drainage basin behaviour during that timespan. The dependent variables provide the options of the drainage basin. These variables are allowed to vary in response to changes in the environment of the drainage basin, or to internally adjust the system within the constraints imposed by the canon. These ideas are expressed in the following propositions:

I - The canon and options of a geomorphic system vary with the timescale of interest. With a change in timescale certain options may become part of the canon, or parts of the canon may become options, depending on the direction of scale change.

II - The model of evolution of a geomorphic system varies with the timescale of interest.

A geomorphic system may thus be viewed as being in static, steady state, or dynamic equilibrium, depending on the timescale of interest.

Table 1.1 Status of drainage basin variables as a function of time

Drainage basin variables	Status of variable during indicated timespan		
	Cyclic	Graded	Steady
1 Time	Independent	Not relevant	Not relevant
2 Initial relief	Independent	Not relevant	Not relevant
3 Geology (lithology, structure)	Independent	Independent	Independent
4 Climate	Independent	Independent	Independent
5 Vegetation (type and density)	Dependent	Independent	Independent
6 Relief	Dependent	Independent	Independent
7 Hydrology (runoff and sediment yield per unit area within system)	Dependent	Independent	Independent
8 Drainage network morphology	Dependent	Dependent	Independent
9 Hillslope morphology	Dependent	Dependent	Independent
10 Hydrology (discharge of water and sediment from system)	Dependent	Dependent	Dependent

(After Schumm and Lichty, 1965)

1.3.2 SPACE AND TIME

Schumm and Lichty's (1965) approach may be extended to include spatial scale (Schwartz, 1968; Sugden and Hamilton, 1971; Chorley et al., 1984; Haigh, 1987; Graf, 1988). Both Haigh (1987) and Graf (1988) provide tables showing the combinations of temporal and spatial scales thought to be most suitable for the analysis of geomorphological systems.

The response of a geomorphic system can be characterized by two time periods describing change in system variables (Fig. 1.4). The reaction time is the timespan between a disturbance causing a change in process rate or type, and the beginning of observable morphological change. The relaxation time is the timespan between the onset of morphological change, and attainment of a (steady state) equilibrium corresponding to the new process conditions. Smaller spatial units can be analysed over short timescales because their short reaction and relaxation times will allow them to respond rapidly to changes in their environment. Such small systems are therefore more likely to be in an equilibrium state reflecting the system's environment. Large scale landscape features require a long timespan for analysis, for reaction and relaxation times increase with increasing spatial scale or, in certain cases, when the type of process and process rates are equal, with an increase in the amount of material that has to be transformed or transported to adjust a landscape feature to new conditions. Chorley et al. (1984) give an example of a hypothetical, hierarchical geomorphic system in which reaction and relaxation times increase from the lowest level (alluvial channel) to the highest level (divides) (Fig. 1.5).

The hierarchical structure of the landscape, comprised of micro-, meso-, and macroscale forms with differing reaction and relaxation times, cause the landscape to be polygenetic (Trudgill, 1976; Brunsdon and Thornes, 1979). For instance, the small-scale rock features adjust most rapidly to the conditions of rock weathering induced by the present climate. Macroscale forms may owe aspects of their morphology to earlier,

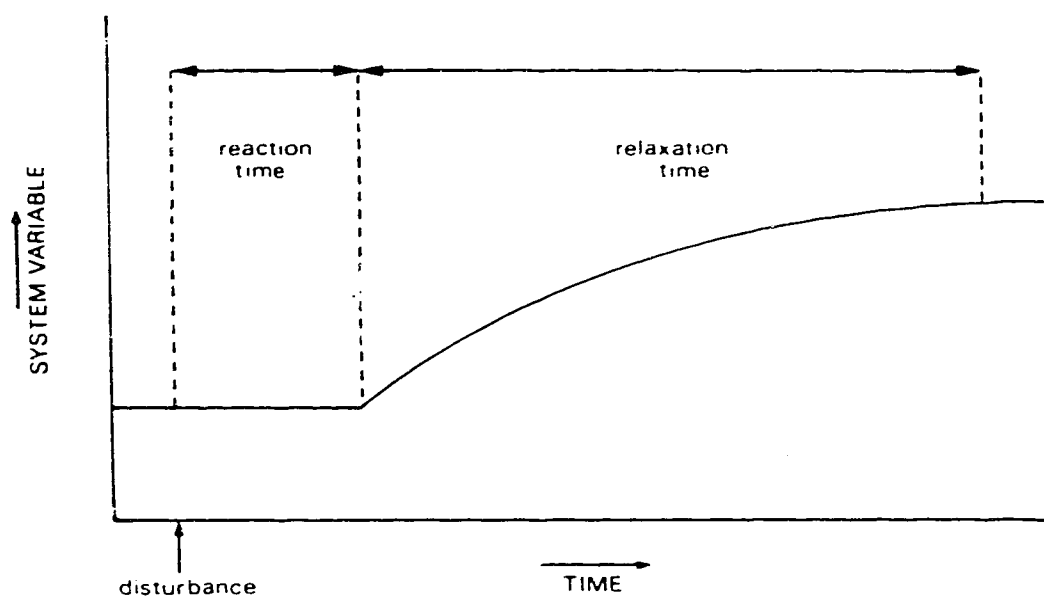


Fig. 1.4 Reaction and relaxation times of a geomorphic system. The horizontal axis represents time; the vertical axis, a typical system variable such as a process rate or a morphological parameter. See text for explanation.

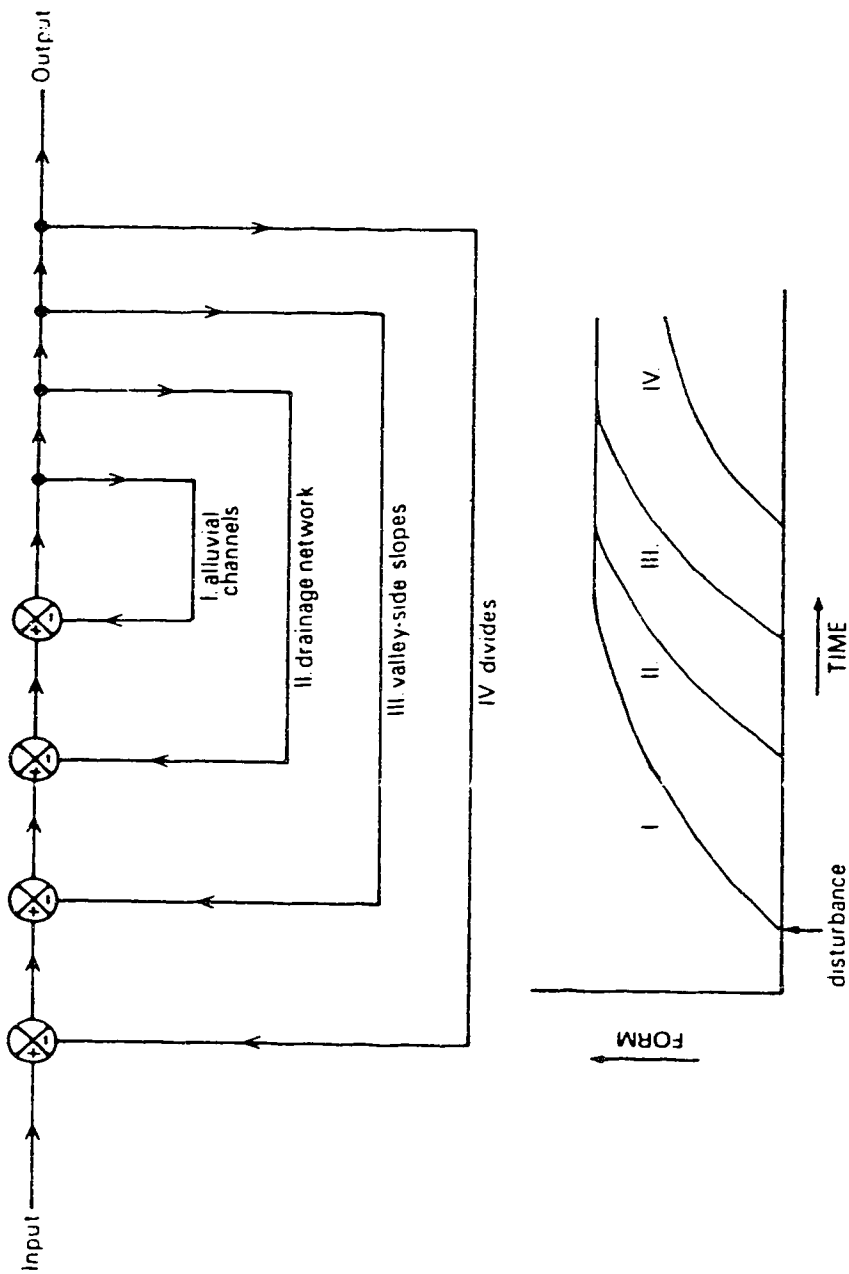


Fig. 1.5 Top: Nested hierarchy of geomorphic systems. The nested negative feedback loops allow the different levels to mutually adjust each other. Bottom: Reaction and relaxation times (Fig. 1.4) increase from the lowest (alluvial channels) to the highest level (divides). Thus, the morphology of the alluvial channels will show a rapid response to new conditions, whereas the divides will only be adjusted after a much longer timespan. (Modified after Chorley et al., 1984).

different climatic conditions, unless the climate has been stable over a timespan longer than the reaction and relaxation times of the form. This leads to the following proposition:

III - The hierarchical structure of the landscape gives rise to its polygenetic character.

The magnitude of reaction and relaxation times is not just a function of spatial scale. Trudgill (1976) introduces the concept of lability of geomorphic systems, and distinguishes sluggish and labile systems. A labile system, for instance a shale badland slope, may show adjustments in morphology to a high-magnitude rainstorm; a sluggish system, for instance a slope of similar scale developed in granite, will not. Figure 1.6 illustrates the relationship between temporal scale, spatial scale, and lability of a geomorphic system. Similarly, Brunson and Thornes (1979) distinguish sensitive and insensitive landforms (and all the gradations in between) and define the sensitivity of a landform as the ratio of the mean relaxation time to the mean recurrence time of events controlling the morphology.

Several field studies have illustrated the relationship between temporal and spatial scales. Slaymaker (1972) undertook an analysis of the production, transport, and deposition of sediment at the micro-, meso-, and macroscale in order to clarify the effect of present-day processes on fluvial landforms of different spatial scales. Sediment dynamics at the two smallest scales, of the individual site and the slope or stream reach, could be explained in terms of present-day geomorphological processes. At the macroscale of the second- and third-order basin, however, several examples of severe disequilibrium with respect to sediment supply and removal were found over the 4 yr observation period. It should be noted that if the observation period were longer it might well have been found that at the macroscale a steady state equilibrium had been reached. Slaymaker's (1972) study stresses that the length of the observation period should be in accordance with the

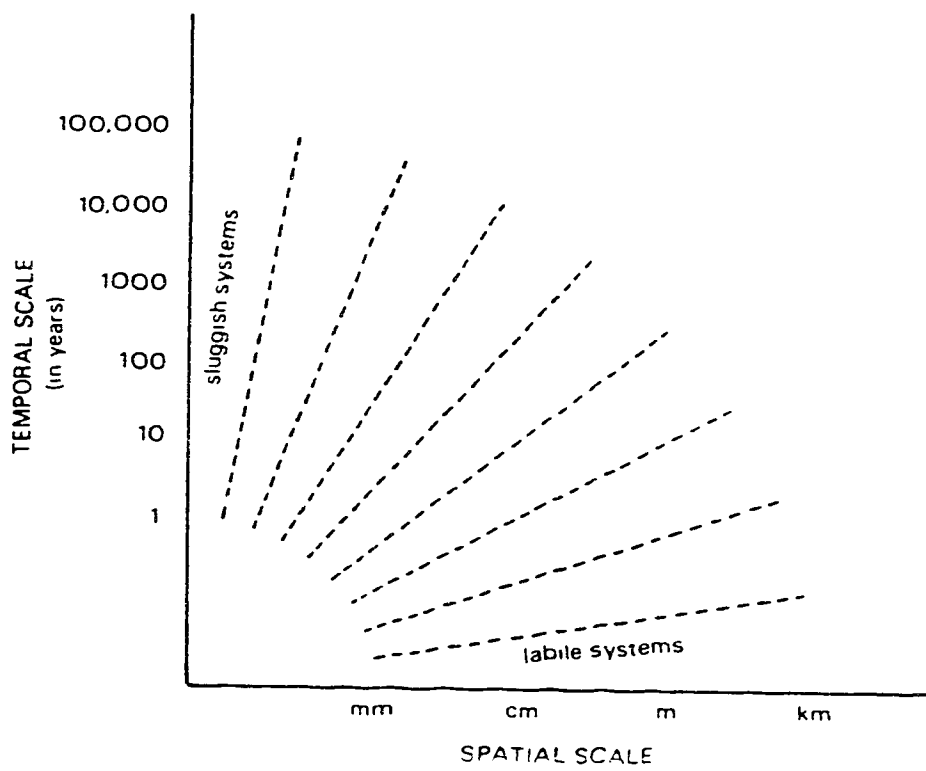


Fig. 1.6 Relationship between temporal scale, spatial scale, and lability of geomorphic systems. See text for explanation. (Modified after Trudgill, 1976).

spatial scale of the system of interest.

Jackson (1975) directly correlates bedform life, or time span of existence, and bedform size in a hierarchical, unifying model of bedforms. Bedforms generated by the flow of a fluid over a cohesionless, granular material range in size from a small-scale ripple to, in a meandering stream, a pointbar, or, in an area of aeolian sands, a dune (Jackson, 1975). The smallest bedforms, or microforms, form in response to the local, non-uniform, unsteady fluid-dynamic regime, and require detailed, small-scale measurements of local flow conditions. When bedform size increases, local flow conditions become less important until, at the macroscale, the 'geomorphological regime' controls bedform development (e.g. in the case of a point bar). With this latter term Jackson (1975) denotes factors such as geological control of channel plan-form, and the location of sources of coarse sediment. To describe the development of bedforms at the macroscale, process observations do not have to be as closely spaced in time (and space) as for microforms.

The relationship between temporal and spatial scales is featured prominently in a paper by Brunnsden and Jones (1980) who studied the development of coastal landslide systems in southern England over a 100 yr period. Within the landslide systems three zones were distinguished: Zone 1 is the zone of large-scale landslides, and extends seaward from the cliff top to the furthest extent of these large slides; Zone 2 may be viewed as the zone of transmission, where the large landslide blocks from Zone 1 are broken up by small-scale landslides, mudslides, and gully erosion; and Zone 3 consists of the near-vertical sea cliffs, where retreat occurs through toppling failures, sagging failures, and rock falls. Observations indicated that over the observation period the whole system was in a state of dynamic equilibrium: the overall landform assemblage appeared to be diagnostic of the processes operating in the area, even though the individual landforms were continually changing.

Zone 1 and Zone 3 represent different geomorphic systems at the same hierarchical level. The cliffs in both zones retreated at similar rates over the observation period. The processes responsible for cliff retreat, however, were markedly different. In Zone 1 cliff retreat occurred through high-magnitude, infrequent landslides, whereas in Zone 3 low-magnitude, high-frequency failures and rockfalls were responsible. Brunsden and Jones (1980) draw attention to the importance of a sufficiently long observation period, necessitated by the considerable length of time between large-scale landslides in Zone 1. Observation over a shorter period might lead to the conclusion that cliff retreat in Zone 1 and Zone 3 occurred at dissimilar rates, which would indicate an increase or decrease in the areal extent of the landslide system and a state of disequilibrium (compare Slaymaker, 1972). Brunsden and Jones (1980) also call attention to the connection between the three zones. Storage in the form of a landslide block at the base of a landslide scar protects the scar from further erosion, and thus slows down the rate of retreat. The subsequent breaking-up of the landslide block by more frequent, low-magnitude processes causes unloading of the slope, and provides the conditions for a repeated occurrence of a high-magnitude, low-frequency, large-scale landslide. As Brunsden and Jones (1980, p. 16) state: 'Thus the persistent and more even erosion of the sea cliffs is translated into large event failures in other parts of the system'.

The following proposition indicates the connection between temporal and spatial scales:

IV - Because of the slow response to changes in the environment, or inertia, the morphology, functioning, and evolution of high-level, large-scale geomorphic systems are best, and frequently can only be, analyzed over long timespans. Lower-level, small-scale geomorphic systems equilibrate much more rapidly with the environment, enabling analysis over shorter timespans.

Brunsdon and Jones (1980) introduce the concept of 'formative events', which are those events that produce the dominant or diagnostic features of a landscape. They suggest that in a situation as in Zone 1, where the average erosion rate is low but variations around the mean large, the formative events are likely to be of a high magnitude and low frequency, shaping a landscape with abrupt variations in relief. Conversely, in Zone 3, where the average erosion rate is equally low but with small variations around the mean, the formative events are events of a lower magnitude and higher frequency, and the resulting landscape is more regular. The same idea was expressed by Brunsdon and Thornes (1979) in a review of the concepts of magnitude and frequency in geomorphology. Brunsdon and Jones (1980) add that it remains to be seen whether the relationship between magnitude and frequency of formative events and irregularity of the landscape is a general geomorphological principle, applicable to other areas within geomorphology.

The following proposition is derived from Brunsdon and Jones' (1980) hypothesis:

V - High-frequency, low-magnitude processes produce a smoother, more regular morphology (i.e. with irregularities of a relatively small scale) which can be studied at a relatively small scale. Low-frequency, high-magnitude processes produce an irregular morphology with considerable variations in relief. Such a morphology should be studied at a relatively large scale.

The following proposition calls attention to the relationship between large-scale and small-scale events at the same hierarchical level, and describes the cumulative effect of small-scale thresholds:

VI - Low-magnitude, high-frequency processes operating on a small scale in a geomorphic system may, given sufficient time, provide the conditions for the occurrence of a high-magnitude, low-frequency event, operating on a much larger scale at the same

hierarchical level.

The temporal and spatial resolution of a study of high-magnitude, low-frequency processes and the landforms resulting thereof should be high enough to take into account such a seeming discrepancy in scale. The basic idea behind this principle has also been expressed by Schumm (1977) who gives an example in which a high-magnitude, low-frequency flood is only the most apparent cause of valley-floor incision (Fig. 1.7). Floods of a lower magnitude and higher frequency have caused a gradual increase in the valley-floor slope, and hence play a crucial role in preparing the conditions in which incision of the valley-floor by a high-magnitude, low-frequency flood can occur. In Schumm's (1977) example a high-magnitude, low-frequency flood not preceded by a period of low-magnitude, high-frequency floods may only have a minor effect on the landscape. It is, however, important to note that not all high-magnitude floods need to be preceded by a series of low-magnitude events to strongly affect landscape evolution.

1.3.3 PROCESS AND FORM

In a study of the factors influencing the slope of stream channels Penning-Rowse and Townshend (1978) found that a change in spatial scale caused a change in the relative importance of the different factors. At their largest scale, channel slope was measured over a stream reach of approximately one kilometer in length. It was found that channel slope was mainly determined by the discharge through the reach, and to a lesser extent by bed material size along the reach. At the intermediate, or 'local' level, channel slope was measured over a distance of ca. 6.1 m. Bed material size was found to be the dominant factor controlling channel slope at this scale, whereas discharge was relatively unimportant. At the smallest scale, the variations of channel slope along a single reach were analyzed,

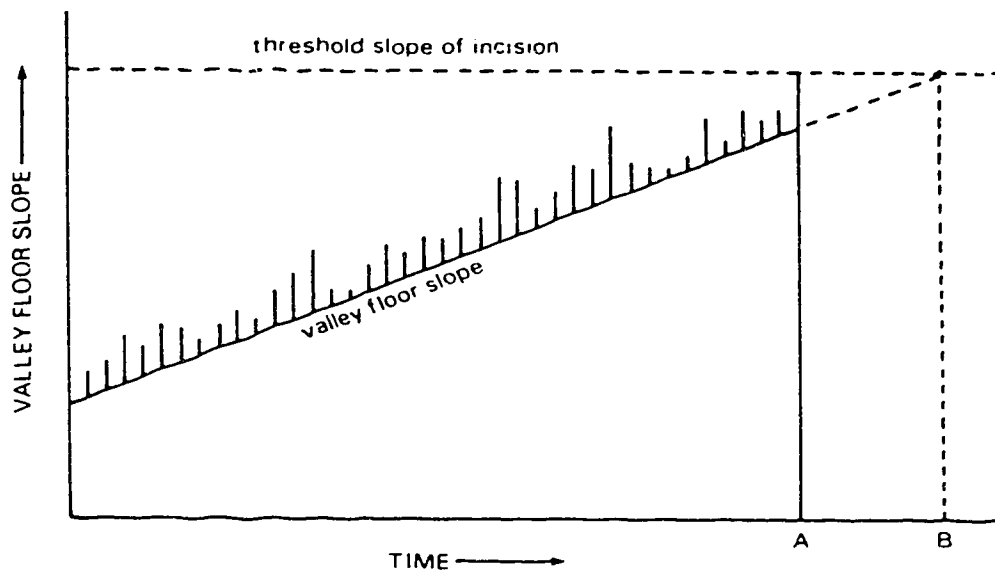


Fig. 1.7 Increasing valley floor slope through time, causing valley floor incision. The line segments superimposed on the gradually rising curve indicate variations in valley floor slope caused by events of differing magnitude. At time A, a flood of relatively high magnitude causes the valley floor slope to exceed the threshold slope of incision. Valley floor incision, however, would have occurred at time B regardless of the magnitude of the flood at that time. (Modified after Schumm, 1977).

and channel shape turned out to be the dominant variable. Penning-RowSELL and Townshend (1978) note that with a decrease in spatial scale there appears to be a shift in the importance of variables, from those variables showing systematic variations over long distances, to those displaying rapid variations over shorter distances. They add that their results may be interpreted in two ways: first, the observations indicate a real change in dominant variables with variations in spatial scale; second, there may not be a real change, but instead the variables chosen to describe the system may not be equally appropriate at all scales. Penning-RowSELL and Townshend (1978) also draw attention to the interaction between spatial and temporal scales, and remark that the frequency of discharge events determining channel slope at the local scale may be different from those controlling slope over a longer reach.

If it is accepted that the results obtained by Penning-RowSELL and Townshend (1978) indicate a real change in dominant variables with a change in spatial scale, the following proposition may be deduced from their work:

VII - Differences in morphology, functioning, and evolution between geomorphic systems at the same level in a hierarchy are controlled by variables showing systematic variations over distances equal to, or shorter than, the distance between the geomorphic systems, but equal to, or longer than, the spatial dimensions of the geomorphic systems.

A variable showing systematic variations over distances longer than the distance between the geomorphic systems will have the same value in the geomorphic systems, and hence can not explain a difference in morphology. Furthermore, a variable showing systematic variations over distances shorter than the spatial dimensions of the geomorphic system will be hard to characterize because of the variation within the geomorphic system. This will limit the usefulness of this variable for understanding differences between geomorphic systems. A transformation of this variable, for instance in a simple case by

calculating an average value for each geomorphic system, may lead to a transformed variable for each geomorphic system which may account for differences between the geomorphic systems.

Morgan (1973) provides an illustration of the last principle from the field of climatic geomorphology. An analysis of the effect of climatic factors on drainage density at different scale levels indicated that at the macroscale (160 000 km²), the variation in drainage density could be explained by climatic factors such as the return period of 100 mm daily rainfall, mean annual and mean monthly precipitation, and rainfall seasonality. At the mesoscale (1600 km²), climate was relatively uniform, both temporally and spatially, and climatic factors were replaced by relief factors in the explanation of drainage density variations. Morgan (1973) also investigated the factors controlling drainage density at the microscale of a 0.09 km² basin, and found that the extension of the drainage network during a storm is dominated by two climatic factors: the amount of rainfall in the previous two hours, and the return period of 50 mm daily rainfall. However, comparison to the results obtained at the various scales is difficult. A distinction should be made between the dynamics of a drainage network during a storm, as measured at the microscale, and the adjustment of the drainage network to climatic variables over a longer timescale, as measured at the meso- and macroscale. Morgan (1973) infers that when going from the micro- to the macroscale the significance of events of moderate magnitude decreases, whereas the significance of high-magnitude events increases. However, failure to recognize the effect of temporal scale makes this conclusion somewhat suspect. In addition, at the microscale a high magnitude event may well result in a permanent extension of the drainage network (see for example Gerson, 1974).

Another illustration of principle VII may be found in the work of Arnett (1979), who studied the factors controlling denudation rates at different scales of investigation. The study was carried out at three different levels of spatial scale. At the largest scale, 16 drainage basins were used, all lying within the same climatic regime and ranging in size

from 10 to 300 km². Statistical analysis indicated that at this scale annual sediment yield was closely related to lithology and land use factors, with relief, slope, and drainage density being of secondary importance. Lithology and land use are essentially concerned with the same factor, as the variations in denudation rate were explained by the presence or absence of agriculturally utilized boulder clays. At the medium scale, 93 subcatchments, with a surface area ranging from 0.9 to 50 km², were selected from within the 16 large-scale drainage basins. Because the large number of drainage basins at the medium scale precluded the establishment of annual sediment yields, Arnett (1979) used the concentrations of suspended and dissolved sediment during the falling stage as a measure of denudation rate. Relief and drainage density were found to control denudation rates at this scale. Distinct anomalies, however, were caused by lithology and land use, confirming their importance as controlling factors. At the smallest scale, three experimental plots, similar in slope, lithology, and aspect, were selected from within the drainage basins. The plots varied in their vegetation development, which ranged from recently burnt, through pioneer, to dense and mature. Not surprisingly, annual sediment yield was strongly controlled by vegetation development, the largest yields occurring at the freshly burnt plot, whereas the mature plot yielded the least sediment. The increase in destruction of the vegetation cover was accompanied by a reduction of the amount of precipitation needed to cause erosion. On freshly burnt plots, erosion was therefore more continuous in time, whereas on vegetated plots erosion only occurred during events of a higher magnitude, but lower frequency.

Arnett's (1979) study shows that measurements of sediment yield at the outlet of a drainage basin mask considerable variations within the basin. At the microscale these variations are caused by topographical, pedological, and land-use factors, at the medium scale by slope and drainage density, and at the largest scale by the combination of lithology and land use. The factors controlling denudation rates all exhibit spatial variability. Those causing variations at the microscale vary most rapidly, and with increasing scale there is a

change in dominant factors to those varying over longer distances.

A direct consequence of proposition VII is that the morphology of geomorphic systems at different levels in a hierarchy will be controlled by different factors (Harvey, 1968). An example of a change in spatial scale accompanied by a change in the factors controlling processes and morphology is given by Jackson (1975). At the scale of the microforms, morphology is controlled by the conditions in the inner zone of the turbulent boundary layer (Jackson, 1975). At the scale of the macroforms, however, geomorphological conditions control the morphology of the bedforms.

A similar idea has been expressed by Stoddart (1969) who notes that climatic geomorphology and structural geomorphology deal with landforms of different scales: structural geomorphology is concerned with the large-scale landscape features associated with geological structures; climatic geomorphology deals with the 'superficial' modifications of these features. At the local scale, lithology becomes important again, and may rank equally with climate. Stoddart (1969) remarks that it is probably significant that most successful studies in climatic geomorphology have been carried out at the medium, or regional, scale and at the microscale. The effect of spatial scale on the balance between climatic and structural influences has also been observed by Tricart and Cailleux (1972) and Morgan (1973).

Douglas (1976) distinguishes three aspects of geology controlling the morphology of landforms at different levels of scale. On the largest scale, major tectonic units dominate landscape evolution. On the small scale of the single hillslope (less than 1 km in length) the structure and lithology of the bedrock determine slope form. Folded and faulted structures control geomorphology at intermediate scales.

An example of variations in dominant process with changing spatial scale from drainage basin geomorphology is provided by Yair and Lavee (1985) who describe four mechanisms causing spatial variability in rainfall rates over a basin, three of which are scale-dependent. Non-uniformity of the synoptic conditions within the area covered by

rain, leads to a spatial variability in rainfall which is totally independent of the topography, and also independent of scale. The variations in rainfall induced by topography, however, show spatial scale dependence:

- (1) At the macroscale, non-uniformity of rainfall is caused by orographic effects.
- (2) At the mesoscale, non-uniformity of rainfall is caused by the carry-over effect. This applies to small watersheds (over 0.5 km^2) in which the upper slopes generally receive less rainfall than the slope base. The carry-over theory states that the higher wind velocities at the upper part of the slope cause drops to drift away in a downwind direction before being deposited in more protected areas on the leeward parts of the slope.
- (3) At the microscale, non-uniformity of rainfall is caused by the direction and inclination of the incoming rainfall in relation to the aspect and inclination of the slope. This causes large variations in the actual amount of effective hydrological rainfall reaching the ground surface.

The combined effect of these sources of non-uniformity of rainfall is that runoff generation will be non-uniform, even over very small areas. Variability at a certain scale may (partially) cancel out at larger scales. The network for the measurement of precipitation should be adjusted to the size of the area under investigation. In general, the possibility of extrapolating precipitation data collected in small areas to larger areas, or vice versa, is limited.

Hamlin (1983) suggests that the spatial scales of the precipitation measurement network and of the drainage basin of interest should be compatible. For smaller catchments precise knowledge of the spatial and temporal characteristics of the precipitation input may be essential. For instance, in a small drainage basin in which a partial area model of runoff generation is thought to operate, knowledge of the rainfall intensities over the partial areas is more important than the average intensity over the

whole basin. On the other hand, for large basins of say 40,000 km² monthly rainfall data may suffice to gain insight in the response of the basin (Hamlin, 1983).

In general, however, as Harvey (1968, p. 72) argues: 'we have no measure of the scale at which a particular process has most to contribute to the formation of a spatial pattern and our notions regarding the scale problem remain intuitively rather than empirically based'.

The following proposition describes the effect of spatial scale on the factors controlling processes and forms in geomorphic systems:

VIII - There is a close similarity, or balance, between the spatial and temporal dimensions of a geomorphic system, and the characteristic dimensions of the dominant processes controlling its morphology, functioning, and evolution. The ratio between these two measures is therefore near unity.

The characteristic dimensions of a geomorphological process are a measure of the total volume of material involved, the distance over which this material is moved, and the timespan characterizing the process.

1.3.4 CATASTROPHIC EVENTS

In a study of coastal cliff erosion systems, Cambers (1976) found that the relative importance of high-magnitude, low-frequency (or catastrophic) events and events of a moderate magnitude and frequency is to some extent a function of the spatial and temporal scale of investigation. At the largest scale of investigation, cliff retreat rates for three cliff systems 30 to 60 km in length were determined over a 70 to 100 yr timespan. At this scale Cambers (1976) found that moderate, frequent storms accomplished more work

than high-magnitude, infrequent storm surges that are catastrophic when coinciding with high spring tide, thus providing support for Wolman and Miller's (1960) magnitude-frequency hypothesis.

At the smaller scale, Cambers (1976) examined cliff systems 1 km in length over a period of 1 yr. The catastrophic event at this scale was found to be the landslide, whereas moderate, frequent events were water and wind erosion, and mudflows. A comparison of the volume of material removed by each of these processes showed that landslides accounted for the bulk of the material transported so that, at this smaller scale, the catastrophic event accomplished most of the geomorphological work.

However, Cambers (1976) observed that at the smaller scale the highest rates of cliff retreat occurred where the frequency of high-tide marks reaching the cliff base was greatest. The removal of debris from the cliff base by wave action maintained the cliffs at a high, unstable angle, and provided the conditions for the occurrence of landslides. This means that the moderate storms of the large scale systems and the landslides of the small scale systems are essentially concerned with the same process. At the smallest scale, with a period of observation of 1 yr, these storm-induced landslides accomplish most of the work and are classified as catastrophic. If the 1 km cliff systems had been observed over a period of 70 to 100 yr it would in all likelihood be found that the landslides still accomplish most of the work. However, because of the occurrence of catastrophic surges with a higher magnitude and lower frequency, the landslides would not be classified as catastrophic at this timescale. Over a period of observation of 1 yr, a catastrophic surge would probably not occur so that its relevance to cliff retreat over this period would be undefined.

Cambers' (1976) study shows that when the observation period is short, certain events may be classified as catastrophic, which they would not be on a longer timescale. The term catastrophic as used by Cambers (1976) indicates a high magnitude, low-frequency event. Whether or not an event is classified as catastrophic thus depends on

the length of the observation period, and on the magnitude and frequency of the events occurring during this period.

A better use of the term catastrophic would be to call an event catastrophic for a geomorphic system if it leads to the breakdown of that system into lower-level geomorphic systems. A catastrophic event for a low-level geomorphic system may have little or no effect at a higher level. However, a catastrophic event for a high-level geomorphic system must have considerable effect at lower levels. Whether or not an event is classified as catastrophic hence depends on the level of interest, but is independent of the period of observation.

Cambers' (1976) conclusion that the relative importance of catastrophic and moderate events, in terms of geomorphic work done, is to some extent a function of scale should thus, because of his particular use of the term catastrophic, be viewed with caution. If during the 1 yr, small-scale observation period a storm surge had occurred, the landslides would probably still do most of the work, but would no longer be classified as catastrophic.

The following propositions describes the scale dependence of catastrophic events:

IX - A catastrophic event is an event causing the breakdown of a geomorphic system into lower-level components. Whether or not an event is catastrophic depends on the hierarchical level of interest. A catastrophic event will only affect geomorphic systems at lower hierarchical levels, and not those at higher levels.

1.3.5 INPUT-OUTPUT RELATIONSHIPS

Chorley and Kennedy (1971, p. 5) describe cascading systems as 'composed of a chain of subsystems, often characterized by thresholds, having both spatial magnitude and geographical location, which are dynamically linked by a cascade of mass or energy'. A cascading system thus consists of the flows of matter and energy through a part of the landscape, for instance through a drainage basin. Several studies have investigated the effect of spatial scale of a cascading or geomorphic system on the relationship between input and output of matter and energy. These studies were focussed on drainage basins, a specific class of geomorphic systems, because for drainage basins input and output are concepts that are relatively easy to understand.

Generally, a spatial scale increase of a geomorphic system results in an increased average path length between the points of input and output. As a consequence, travel times through the system tend to increase because flow rates remain relatively constant with increasing spatial scale. Processes that operate on the material in transit through the system therefore have the opportunity to progress to a further stage in larger systems. These processes can be divided into two groups. The first group consists of those processes that are time-dependent, for instance solution and weathering. The second group consists of processes that are distance-dependent, such as sorting and attrition. The time-dependent processes continue to operate when the transported material is temporarily stored, for instance, in the case of fluvially transported gravels, in a channel bar. The distance-dependent processes only operate when the material is in motion. This distinction is useful because when two samples of material need different periods of time to travel the same distance, the samples will be similar in those characteristics caused by the distance-dependent processes, but dissimilar in those characteristics caused by the time-dependent processes. In practice the effect of both groups of processes is usually hard to separate because of their interaction. For instance, a fluvially transported boulder will

diminish in size more rapidly if it is in a weathered state.

Fluvially transported material generally shows a downstream change in size, sorting, shape, and composition. In many cases the downstream decrease in particle size follows the Sternberg Law of the form $W = W_0 \exp(-kx)$, where W is the weight of an individual boulder or particle, W_0 its original weight, x the distance travelled, and k a constant depending on the lithology of the sediment (Gregory and Walling, 1973). When flow conditions promote sorting, the degree of sorting generally increases with the travelled distance.

The direction of the downstream change of shape depends on rock type and local conditions. Generally roundness increases downstream, but in some cases a decrease in roundness has been observed downstream of a high energy channel reach (Pittman and Overshine, 1968). Downstream decreases in roundness have also been attributed to the breakup of boulders along intersecting sets of fracture planes (Dawson, 1982).

Downstream changes in sediment composition occur because of the variation in resistance to breakup of the different lithologies. Gregory and Walling (1973, p. 281) present a table of the resistance of pebbles of different rock types. Length of transport before complete disaggregation varies from virtually zero for a poorly consolidated sandstone, to hundreds of kilometers for granites or quartzites. Because of the downstream changes, bedload lithology may be a poor indicator of basin lithology. For instance, Dietrich and Dunne (1978) found that in a basin which was for approximately 80 per cent underlain by porphyritic basalt, 50 per cent of the gravel in the fourth order channel consisted of hard aphanitic basalt.

A number of other effects of increased travel distances within a geomorphic system can be grouped under the heading 'dispersion'. This term is used here to describe an effect analogous to the dispersion occurring during the flow of water carrying a tracer through a soil. Within the soil, spatial variations in pore size occur which, because of the relationship between pore diameter and flow velocity, translate into variations in flow velocity.

Consequently, when a stepwise change in the tracer concentration occurs at the input, the differences in flow velocity in pores of different diameter cause the change in tracer concentration to become less sharp at the outlet. This effect becomes more pronounced with distance travelled. Dispersion hence has a smoothing effect. Variations in the input characteristics are smoothed out in the output, and the larger the system, the larger the degree of smoothing. Bennett and Chorley (1978, p. 363) describe a similar situation known as a 'confined spatial cascade', in which an impulse cascading through a series of first-order, linear systems results in progressively dampened outputs for each of these systems.

There are two factors which affect the relationship between dispersion and spatial scale in a geomorphic system: first, a larger system generally possesses a larger variety of possible pathways between the input and output, so that dispersion is increased; second, path length through a larger geomorphic system is longer, which also enhances the effect of dispersion.

Dispersion occurs in geomorphologic systems because travel times from the input to the output vary from very short, for matter (e.g. water or suspended sediment) experiencing no delay, to very long or even infinitely long, for matter undergoing storage within the system for a certain period of time. For example, a portion of rainfall may cause direct-runoff or storm flow, but another portion will infiltrate, contribute to throughflow, and leave the basin during subsequent storms (e.g. Sklash et al., 1986). Suspended sediment may be exported from the basin during a storm, but alternatively can be stored in bars, debris fans, and floodplains for a longer or shorter period of time (e.g. Dietrich and Dunne, 1978). For small systems there is a close relationship between input and output. The relationship becomes more and more vague with increasing system size. This has been illustrated in a number of studies, a few of which will be discussed in the following paragraphs.

McGuinness et al. (1971) provide an example of the dispersion effect from the perspective of sediment dynamics. They compared the annual sediment yield regime of small-scale (0.5-1 ha) basins at the North Appalachian Experimental Watershed research station with the regime of the large-scale (15 500 km²) basin of the Muskingum River. The former represented the pattern of sediment movement from the fields to the first-order channels, and closely reflected the annual distribution of the product of rainfall energy and cover factor terms in the USLE; the latter mirrored the annual runoff regime (Fig. 1.8) which shows a peak during the spring snowmelt causing sediment stored in the channels earlier to be flushed out of the basin.

Another example of the dispersion effect may be found in the work of Trimble (1981, 1983), who studied culturally accelerated erosion in the 360 km² Coon Creek basin in Wisconsin. Trimble demonstrated that most sediment eroded during a period of severe soil erosion in the latter part of the nineteenth century and the early twentieth century accumulated as alluvium in the valley system. The introduction of improved land-use practices did not reduce sediment yield to the extent that might have been expected because of the remobilization of these alluvial deposits and the subsequent export of sediment from the basin. Erosion in, and sediment yield of the Coon Creek basin are thus out of phase due to the dispersion occurring in the system. Dickinson and Wall (1978) refer to this temporal attenuation within the sediment delivery process resulting from storage and remobilization as the temporal paradox.

An example from a slightly different field is provided by the routing of flood waves through a river channel. Temporary storage in the channel causes a downstream attenuation of the hydrograph (Leopold and Maddock, 1954; Wilson, 1974; Linsley et al., 1982) (Fig. 1.9). The degree of attenuation depends on channel characteristics.

A similar effect, called longitudinal dispersion, occurs during the downstream transport of solutes and pollutants in river channels (Fig. 1.10). The effect of longitudinal dispersion is that a step-wise change in solute concentration becomes progressively less

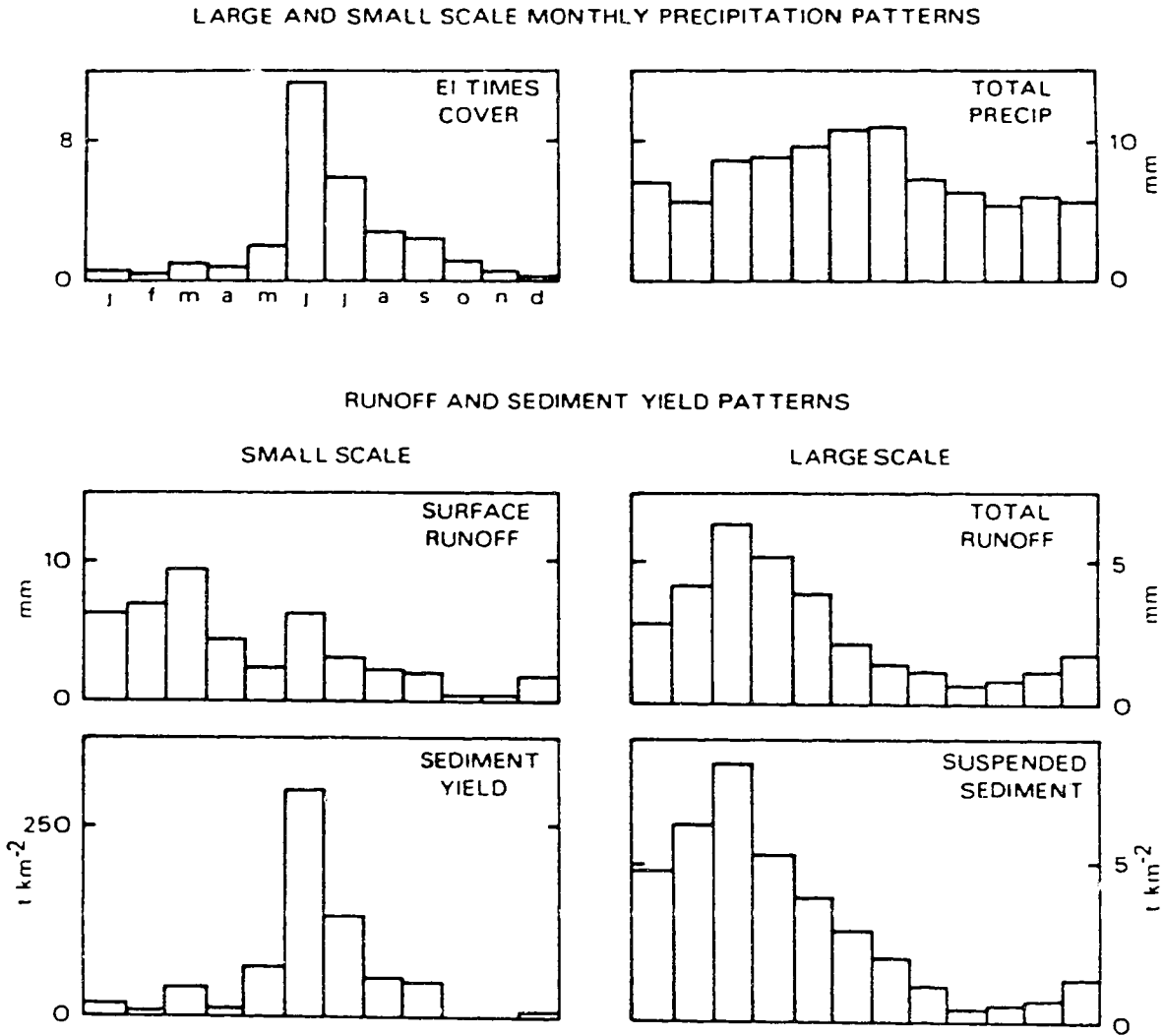


Fig. 1.8 Contrasts in annual sediment yield regime between small-scale (0.5-1 ha) basins and a large-scale (15 500 km²) basin. See text for explanation. (Modified after McGuinness et al., 1971).

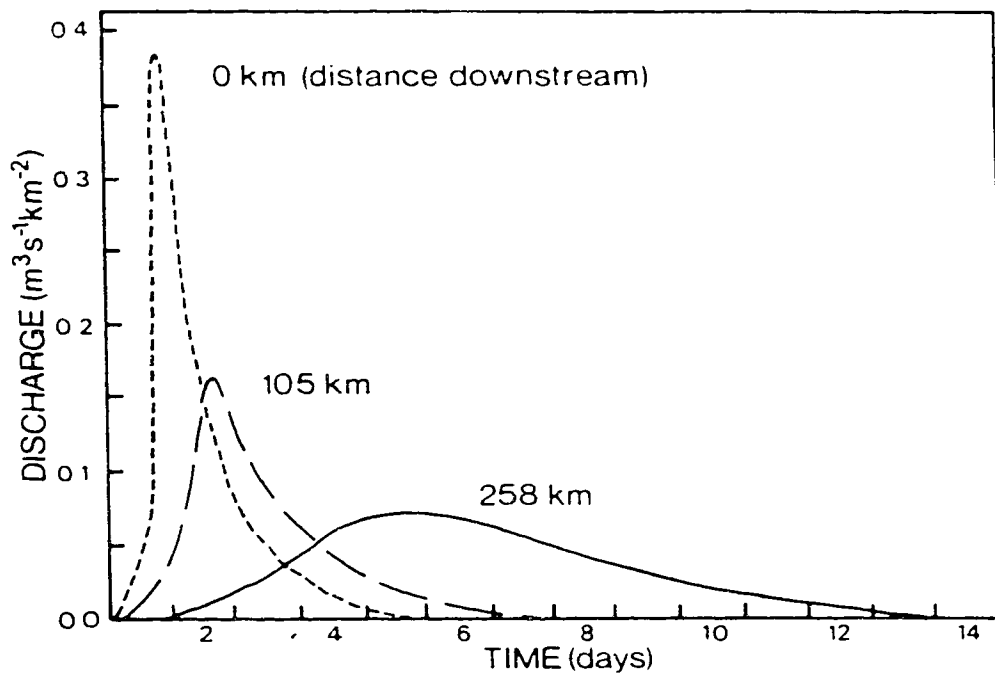


Fig. 1.9 Downstream attenuation of a flood wave resulting from rainfall in the headwaters of the Savannah River, South Carolina and Georgia. (Data from Hoyt and Langbein, 1955; Modified after Strahler (1975) and Bennett and Chorley, 1978).

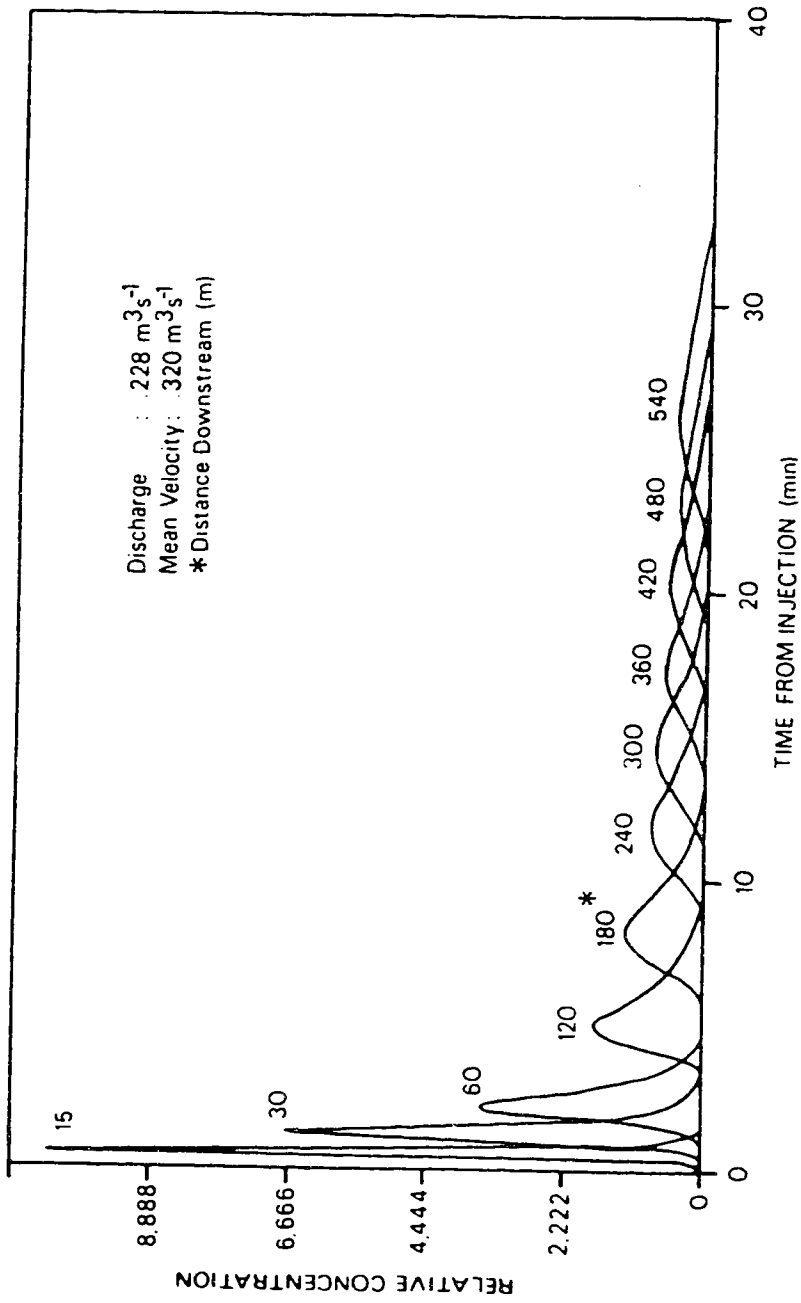


Fig. 1.10 Longitudinal dispersion, causing downstream changes in the shape of the concentration vs. time curve for a slug injection of NaCl into a stream. See text for explanation. (Modified after Day, 1975).

pronounced in a downstream direction (e.g. Day, 1975). Longitudinal dispersion is primarily caused by velocity gradients across the channel (Brady and Johnson, 1981). These gradients are largest when so-called 'dead-zones' are present along the channel bed and banks. These zones of stationary and slowly moving water may entrap and slowly release the substance of interest, and strongly affect the magnitude of longitudinal dispersion (Day, 1975). A secondary cause is Fickian diffusion under the influence of a concentration gradient (Beer and Young, 1983). Longitudinal dispersion is strongly affected by channel characteristics. Brady and Johnson (1981) found that longitudinal dispersion was most pronounced in shallow and fast flowing reaches, where significant velocity variations in the stream cross-section occurred.

The following proposition concerns the effects of dispersion in geomorphic systems:

X - Differences between the temporal patterns of input and output of a geomorphic system increase with spatial scale, due to the increased possibilities for temporary, internal storage of matter and energy.

As illustrated in the previous paragraphs, these differences range from a simple attenuation in the case of a flood wave, to the more complex changes involving long-term storage in the case of sediment.

A direct consequence of this proposition is that for larger geomorphic systems, the temporal and spatial resolution of input observations can be lower than for smaller geomorphic systems. This has also been suggested by Hamlin (1983) who proposed that the spatial scale of a precipitation measurement network should be adjusted to that of the drainage basin so that the same number of raingauges would suffice in both small and large basins (Section 1.4.3).

1.4 OVERVIEW

Figure 1.11 depicts a synthesis of the propositions derived from a survey of the geomorphological literature concerning the problems of scale transference. The propositions are arranged so as to indicate how they relate to each other, not to suggest a logical progression in which they could be logically deduced from a few premises. For the majority of propositions one or more references having special relevance have been given. However, in a number of cases, many relevant references exist.

Central to the problem of scale transference in geomorphology is that geomorphic systems are hierarchically structured. Every geomorphic system consists of a hierarchy of lower-level geomorphic systems, and is in its turn part of higher-level systems. Every geomorphic system should therefore be viewed in its complex, spatiotemporal context.

Geomorphic systems consist of a cascading component, concerning the aspects of process, and a morphologic component, concerning the aspects of form. Generally, in a geomorphic system there exists a similarity between the scales of process and form, so that both aspects should be investigated at close, compatible scales. Furthermore, within a geomorphic system there is a similarity between spatial and temporal scale so that the timespan relevant to present system behaviour and morphology increases with system size.

In a geomorphic system, differences occur in sensitivity of morphology to changing process conditions. Depending on the time elapsed since a change in process conditions, morphology in a geomorphic system may be either polygenetic, when only partial adjustment of the morphology has occurred, or characteristic of the process domain, when all aspects of morphology are adjusted to present process conditions. In the latter case, dominance of landscape evolution by high-frequency, low-magnitude processes results in a smooth landscape having small-scale irregularities, whereas dominance by low-frequency, high-magnitude processes produces an irregular landscape having large-scale irregularities.

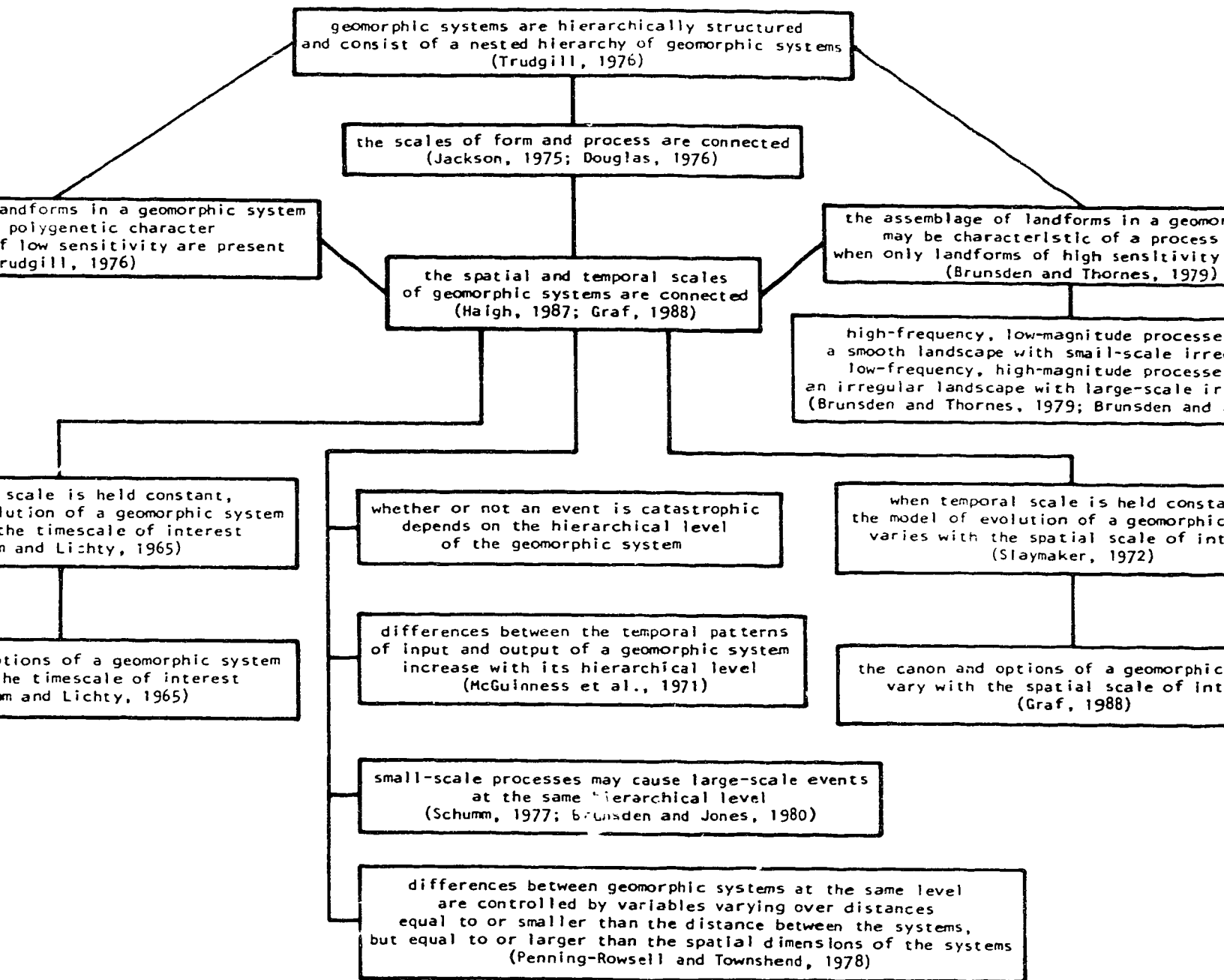


Fig. 1.11 Overview of propositions concerning the problem of spatial scale transference, derived from a survey of the geomorphological literature.

Severing the linkage between spatial and temporal scales, either intentionally or, more often, unintentionally, produces the following results. When spatial scale is held constant, the model of evolution of a geomorphic system varies with the timescale of interest. Conversely, when temporal scale is held constant, the model of evolution varies with the spatial scale of interest. In both cases, the canon and options of a geomorphic system vary with scale, temporal or spatial, of interest. This implies that a factor which varies when viewed at a large scale becomes part of the constant background when the scale of interest decreases. In addition, systems at very much lower hierarchical levels fluctuate too rapidly to affect the level of interest. Thus, there exist both upper and lower limits for scales relevant to explaining system behaviour.

The linkages between the spatial and temporal scales and between the scales of form and process of geomorphic systems lead to four additional points. First, whether or not an event is catastrophic depends on the hierarchical level of the geomorphic system. An event which is catastrophic at a low level will have little impact on a higher level. Second, because of increased travel time and a larger variety of possible pathways, differences between the temporal patterns of input and output increase with the hierarchical level and scale of a geomorphic system. Third, frequent, small-scale processes may cause infrequent, large-scale events when viewed at the same hierarchical level. This point illustrates that frequent, small-scale processes at a low hierarchical level can be aggregated to interact as a system with other systems at the higher level. Fourth and last, differences between geomorphic systems at the same level are controlled by variables varying over distances equal to or smaller than the distance between the systems, but equal to or larger than the spatial dimensions of the systems. This last point concerns the factors determining differences between geomorphic systems, and the observed variations in dominance of these factors with spatial scale.

An awareness of a geomorphic system's specific spatial and temporal scale, and of the principles of scale transference established here, allows evaluating which levels should

be taken into account to explain system behaviour. Propositions VII, VIII, and X derived in this chapter will be applied in the following chapters to the results of the field study, and the effect of spatial scale on the rainfall-runoff relationship and solute and sediment dynamics in semi-arid badland drainage basins will be shown. The remaining propositions, however, cannot be illustrated with the field study, and support for these propositions will have to await future research.

CHAPTER 2

2.1 GENERAL DESCRIPTION OF THE STUDY AREA

Dinosaur Provincial Park is an area of extensive badland development along the Red Deer River in the semi-arid prairie region of southern Alberta (Fig. 2.1). The initiation of badland development is associated with the incision of spillways during Wisconsin deglaciation (ca. 12.5 ka BP), which exposed the highly erodible Upper Cretaceous Judith River Formation (Bryan et al., 1987). This formation consists of a variety of often highly montmorillonitic shales, muddy sandstones, and coarse channel sandstones, interspersed with thin coal seams and resistant ironstone bands. The generic term shale is used here to describe all fine-grained argillaceous rocks (Potter et al., 1980). Aeolian sands and silts deposited ca. 5.5 ka BP (Bryan et al., 1987) and alluvium are also present.

Badland development has reached its greatest extent to the south of the Deadlodge Canyon section of the Red Deer River, where the distance between the river and the edge of the prairie surface is up to 4 km (Fig. 2.2). The study area is located in this portion of the badlands. Figure 2.3 shows an example of the morphology in the study area, consisting of straight, densely-rilled sandstone slopes, and convex, gentle shale slopes. Ironstone bands form prominent ledges and, locally, ironstone debris covers large portions of the slopes. Vegetation occupies much of the low-lying aeolian and alluvial surfaces. The study area lies ca. 1 km south of the Red Deer River, and is close to the 3.2 km loop road which originates at the Dinosaur Provincial Park campground along the Little Sandhill Creek (Fig. 2.2).

Research on the geomorphological processes in Dinosaur Provincial Park has been carried out since the late 1960's, and has yielded insight into erosion rates and response to rainfall of the different surface units. In 1981, a 336,810 m² research basin was

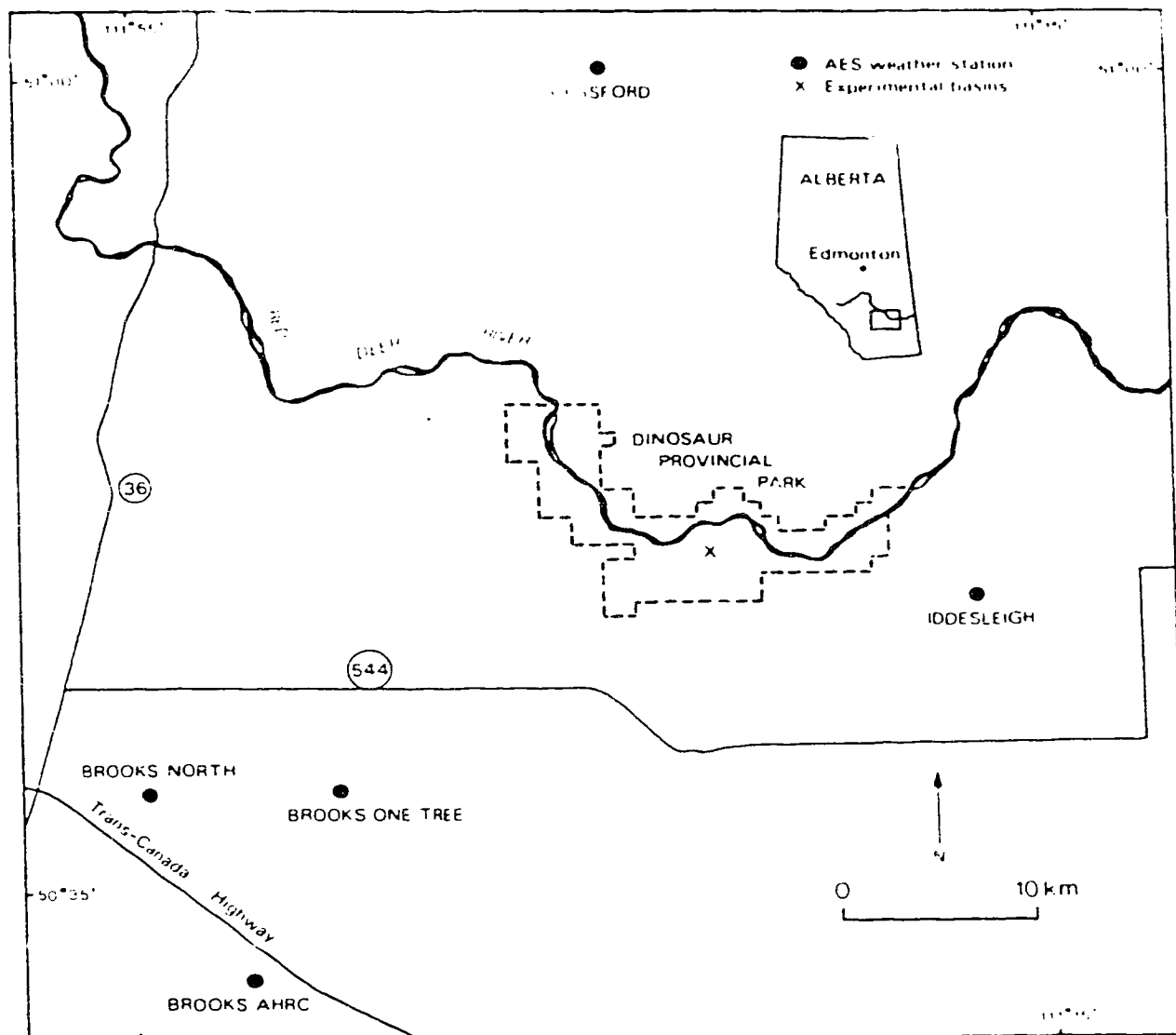


Fig. 2.1 Location of Dinosaur Provincial Park, Alberta. Also shown are the locations of the experimental basins, and of the AES weather stations in the area.

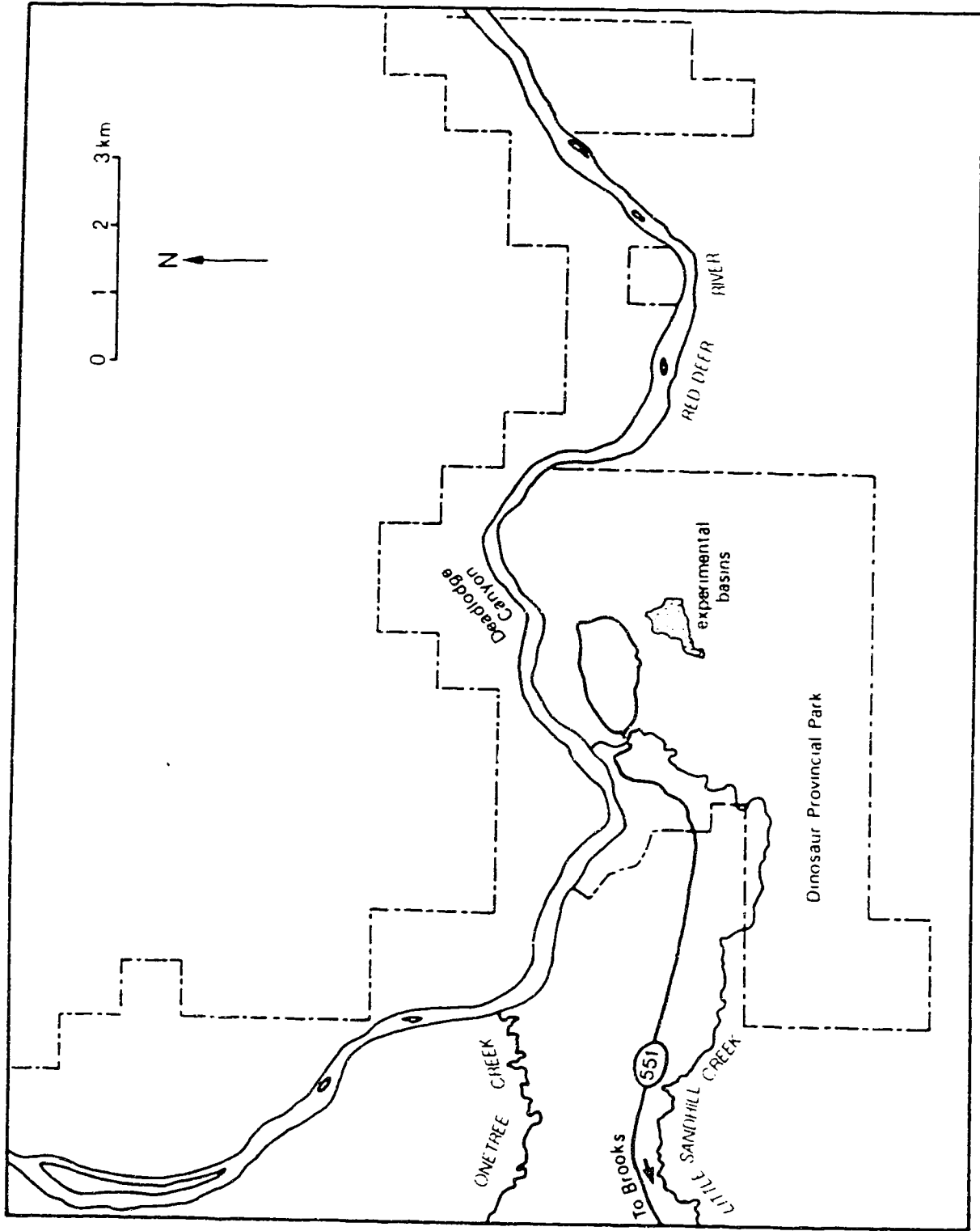


Fig. 2.2 Map of Dinosaur Provincial Park, showing the location of the experimental basins.

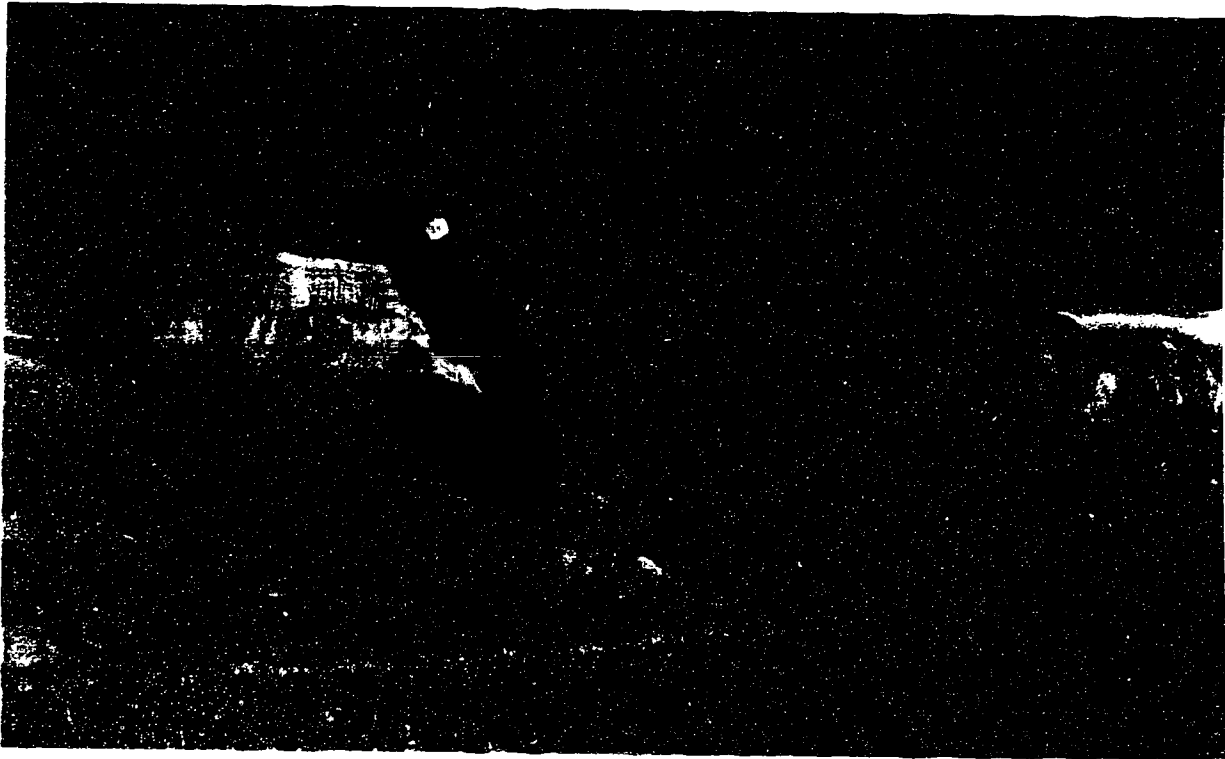


Fig. 2.5 Typical badland morphology in Dinosaur Provincial Park, consisting of straight, densely-rilled sandstone slopes, and convex, gentle shale slopes. Ironstone bands cause prominent ledges. Locally, ironstone debris covers large portions of the slopes. Vegetation occupies much of the low-lying alluvial and aeolian surface units.

instrumented. In this chapter an overview of previous research in the Dinosaur Provincial Park badlands is presented.

2.2 CLIMATE AND RAINFALL CHARACTERISTICS

Mean annual precipitation for the general area is between 300 and 360 mm (Longley, 1972a), approximately one-third of which falls as snow. About 40 per cent of the annual precipitation falls during the summer months (June, July, and August), and the maximum value of the mean monthly precipitation generally occurs in June. Daily temperatures may exceed 40°C during the summer. High winds and, during the summer, high temperatures give rise to an average annual potential evapotranspiration of 560 to 610 mm (Longley, 1972a).

Spring and early summer rainstorms are usually extensive in nature, of low intensity, and associated with the passage of frontal disturbances. Midsummer rainstorms, on the other hand, are often localized, of higher intensity, and associated with convectional disturbances caused by the high surface temperatures (Longley, 1972a, 1972b). This latter type of rainstorm may move for a considerable distance along a narrow track. These storm tracks tend to follow the dominantly westerly winds in the area. This dominant wind direction also coincides with the trend of the major river valleys (e.g. Red Deer River) in an easterly direction.

Figure 2.1 also shows the location of the Atmospheric Environment Service weather stations of Brooks AHRC (Alberta Horticultural Research Center), Brooks North, Brooks One Tree, Cessford, and Iddesleigh relative to Dinosaur Provincial Park. Table 2.1 gives the latitude, longitude, elevation, and the year observations started for each station. Table 2.2 displays long-term precipitation and temperature data for Brooks AHRC, the station with the longest record in the area (39 to 50 years, depending on the variable). All

Table 2.1 Information on Atmospheric Environment Service weather stations

station name	latitude	longitude	elevation (m)	year observations started
Brooks AHRC	50°33'	111°51'	758	1915
Brooks North	50°37'	111°53'	759	1970
Brooks One Tree	50°38'	111°47'	737	1960
Cessford	51°01'	111°33'	701	1982
Iddesleigh	50°45'	111°14'	770	1982

Table 2.2 Long-term precipitation and temperature records for Brooks AHRC

	J	F	M	A	M	J	J	A	S	O	N	D	year
Daily maximum temperature	-8.6	-3.8	1.7	11.3	18.4	22.5	26.2	24.9	19.2	13.6	2.9	-3.7	10.4
Daily minimum temperature	-19.6	-15.1	-9.8	-2.2	3.8	8.6	11.0	9.7	4.4	-1.0	-9.1	-15.1	-2.9
Daily temperature	-14.2	-9.5	-4.1	4.6	11.1	15.6	18.6	17.3	11.9	6.3	-3.1	-9.4	3.8
Rainfall	0.9	0.8	2.5	14.8	37.4	65.7	32.2	40.1	32.8	8.3	2.4	1.0	238.9
Snowfall	20.9	13.6	13.5	11.3	0.9	0.0	0.0	0.0	1.0	5.1	12.5	18.1	96.9
Total precipitation	21.9	14.4	16.0	26.0	38.3	65.7	32.2	40.1	33.8	13.4	14.9	18.7	335.4

Temperatures in °C, precipitation in mm.

Source: Atmospheric Environment Service, 1982.

five stations in Table 2.1 are situated on the prairie surface. A comparison of the monthly precipitation for May, June, July, and August, 1986 and 1987, for all stations indicates that even on the topographically uniform prairie surface considerable differences occur in monthly rainfall (Fig. 2.4). Even the three stations close together in and around Brooks show large differences in their monthly rainfall. For example, in June 1986 the monthly rainfall at Brooks North was 34.2 mm, whereas at Brooks One Tree it was only 18.6 mm, or 54 per cent of the monthly rainfall at Brooks North.

High variability in rainfall over the Canadian prairies has also been reported by Longley (1972b). Semi-arid and arid areas characteristically display high spatial and temporal variability of rainfall (e.g. Berndtsson and Niemczynowicz, 1986). Yair and Lavee (1985) attribute the high variability of rainfall in the Negev Desert to convective cell motion (at rates of 500 to 1600 m min⁻¹) and rapid variations in cell properties in the case of convective storms, and to non-uniform synoptic conditions, independent of the topography, in the case of frontal rainstorms. Typically, the diameter of convective cells varies from 3 to 10 km (Yair and Lavee, 1985).

Included in Fig. 2.4 are the monthly rainfall data in Dinosaur Provincial Park for June and July 1986, and for May, June, and July 1987, obtained by averaging the values for all the raingauges in the experimental basins. In most cases, monthly rainfall in Dinosaur Provincial Park is 30 to 70 per cent of that of the surrounding stations located on the prairie surface. Similar findings were reported by Longley (1973, 1975), who compared precipitation records of neighboring stations and found that the average precipitation in a valley cut into a widespread plain is 10 to 20 per cent below that on the surrounding plain. One of stations used in Longley's study was Drumheller, Alberta, located ca. 120 km eastnortheast of Dinosaur Provincial Park. The town is situated on the banks of the Red Deer River which has cut a narrow valley 120 to 150 m below the level of the surrounding plain. A comparison of the mean precipitation values for Drumheller and neighboring stations indicates that precipitation on the valley bottom is ca. 20 per cent below that on

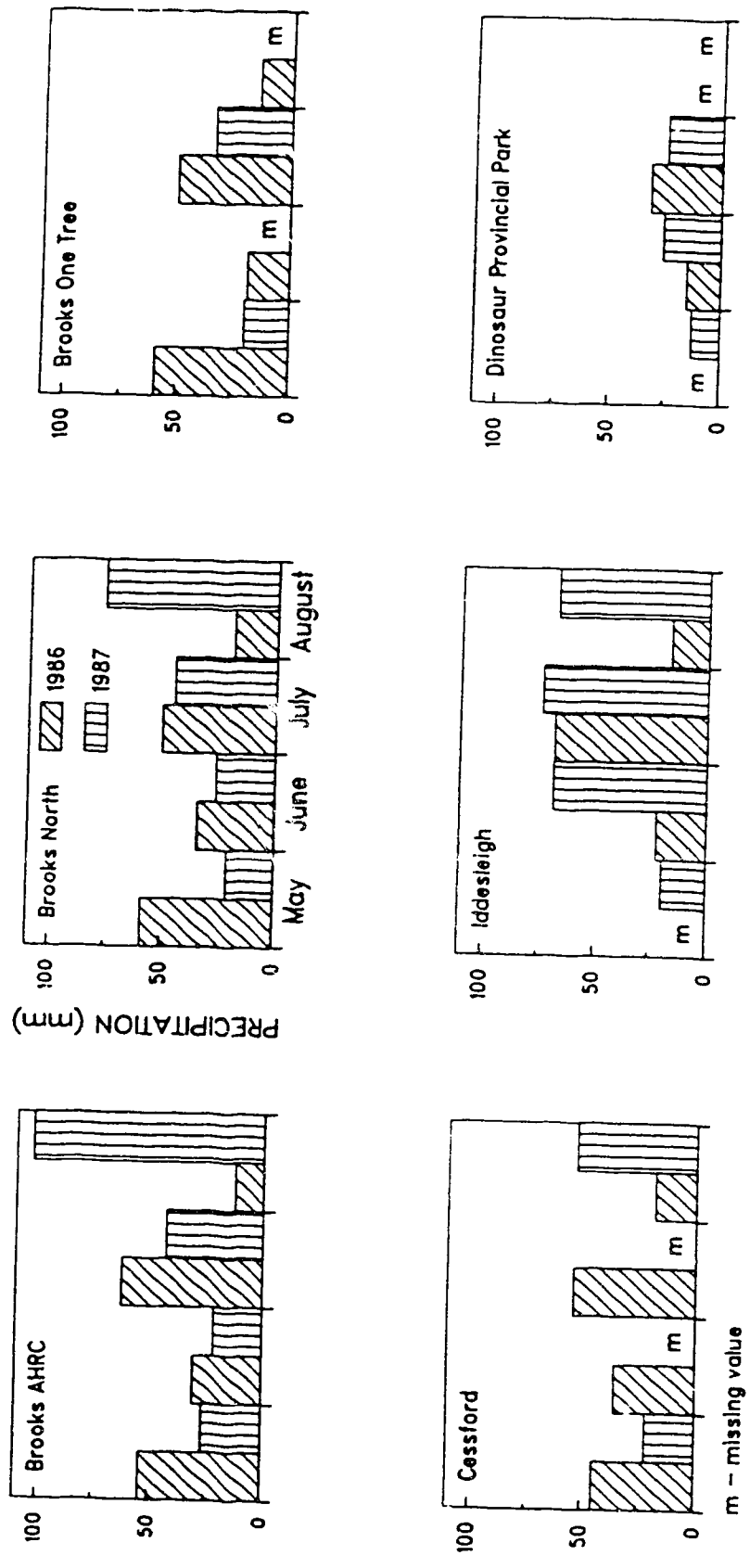


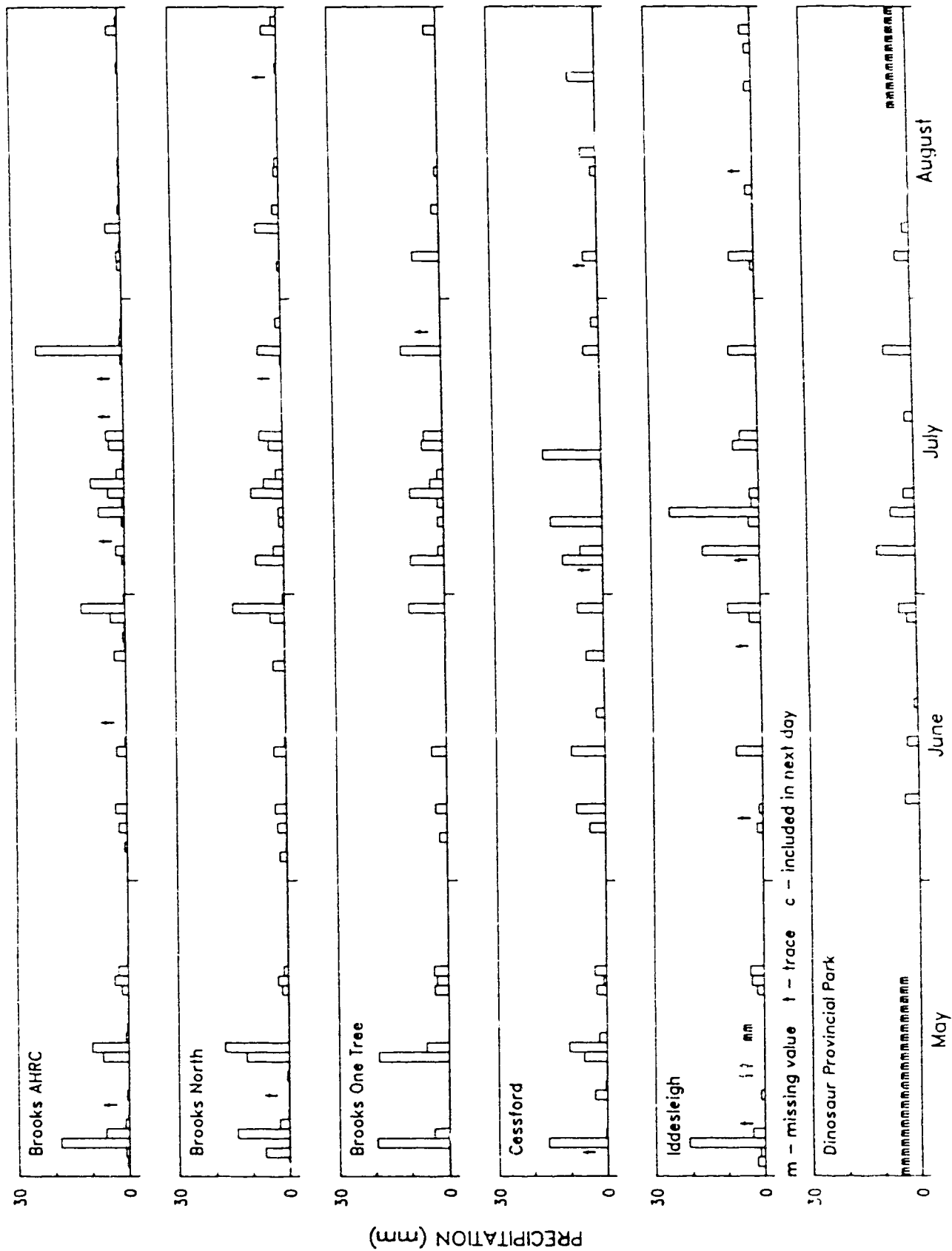
Fig. 2.4 Monthly precipitation for Dinosaur Provincial Park and nearby AFS weather stations for May to August, 1986 and 1987.

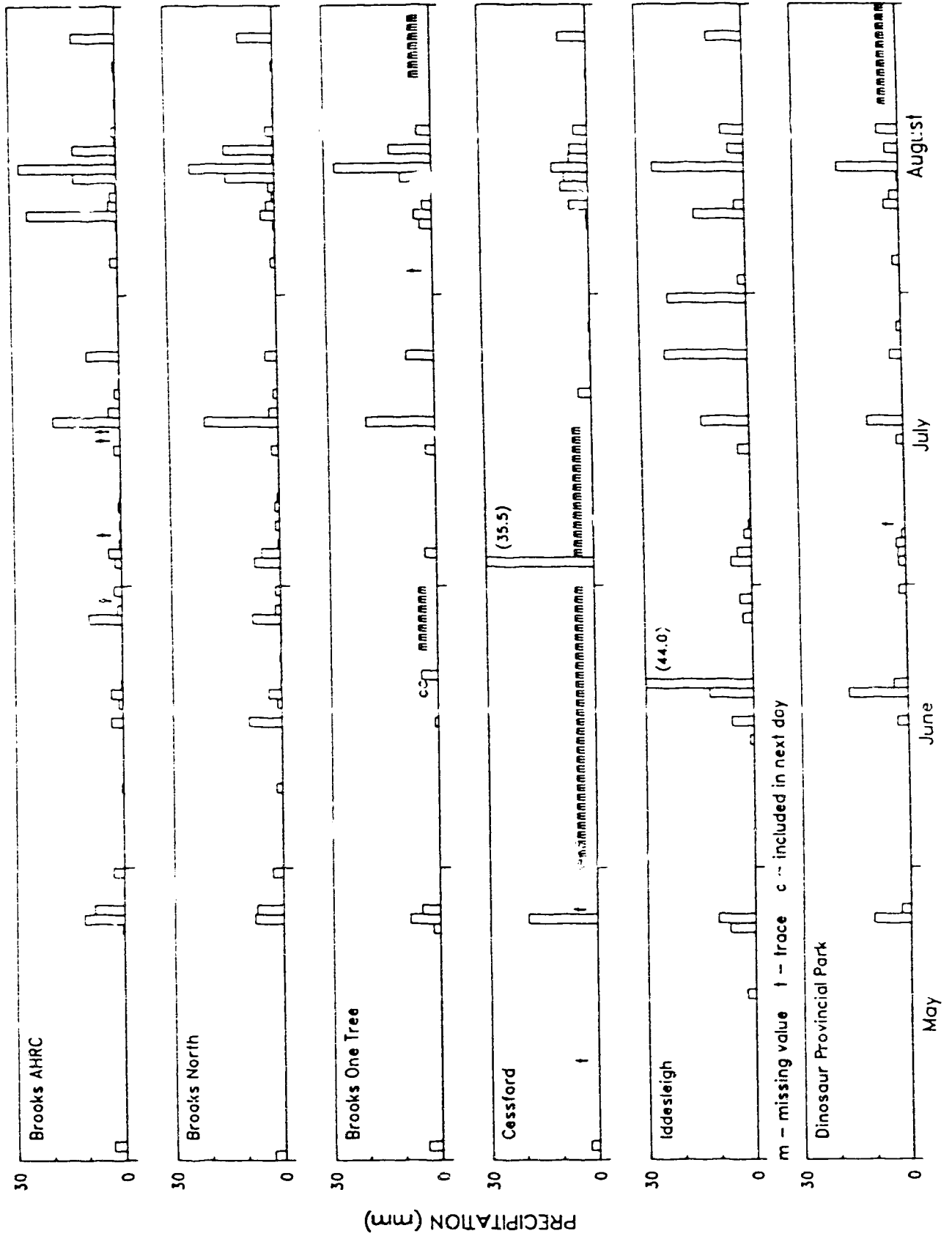
the plain on either side of the valley.

A similar situation occurs in Dinosaur Provincial Park, where in the Deadlodge Canyon the present floodplain of the Red Deer River lies ca. 100 m below the prairie surface. Precipitation can therefore be expected to be significantly lower than at neighboring stations on the plain. Only in June 1987 did the monthly rainfall in Dinosaur Provincial Park approach or even exceed that of some of the surrounding prairie stations. In this particular month rainfall in Dinosaur Provincial Park was 116 and 98 per cent of the monthly rainfall at Brooks AHRC and Brooks North, respectively. However, during that same month rainfall in Dinosaur Provincial Park was only 37 per cent of that in Iddesleigh. These differences emphasize the extreme variability of rainfall over the prairies.

Figures 2.5 and 2.6 show the daily precipitation data for the study period for Dinosaur Provincial Park and the five stations on the prairie surface. A minor part of the discrepancy between the data for Dinosaur Provincial Park and those for the other five stations occurs because rainfall in Dinosaur Provincial Park was recorded on an event basis. To translate these amounts to a daily basis is not always possible in the case of the standard non-recording raingauges, so that the daily record for Dinosaur Provincial Park must be viewed as an approximation.

The high variability of rainfall summarized by the monthly record is also present in the daily data. For example, on July 25, 1987, daily rainfall was 3.5 mm in Dinosaur Provincial Park, 9.0 mm at Brooks AHRC, 3.4 mm at Brooks North, 7.6 mm at Brooks One Tree, 0.3 mm in Cessford, and 23.2 mm at Iddesleigh. The large variability of rainfall for the stations on the prairie surface indicates a rainstorm of limited areal extent, likely of convective origin. In Dinosaur Provincial Park during that day, observations were made of extensive thunderclouds and lightning in southerly to easterly directions. Maximum intensity in Dinosaur Provincial Park for this rainstorm was 25 mmh^{-1} for a six minute period, so that 70 per cent of the daily rainfall fell during this period. Superimposed on the variability of rainfall on the prairie surface is the effect of the valley





of the Red Deer River, causing rainfall in Dinosaur Provincial Park to be lower than on the surrounding prairies.

An example of a more extensive rainstorm occurred over the three day period of May 25 to 27, 1987. Total rainfall was 13.0 mm for Dinosaur Provincial Park, 19.9 mm for Brooks AHRC, 15.2 mm for Brooks North, 15.9 mm for Brooks One Tree, 19.2 mm for Cessford, and 17.4 mm for Iddesleigh. In Dinosaur Provincial Park three separate runoff events occurred in the research basin, and the maximum intensity for a six minute period was 18 mm h^{-1} , which accounted for 14 per cent of the total rainfall during this three day period. The areal uniformity and the spatial extent of the rainfall, the long period of rainfall, and the relatively low intensities indicate that the rainfall was associated with the passage of a frontal disturbance.

2.3 LITHOLOGY

The Upper Cretaceous Judith River Formation consists of lagoonal, deltaic, or shallow water deposits (Koster, 1983). The formation shows considerable lateral and vertical variation, but two principal lithologic groups can be distinguished: (1) sandstone channel sequences; and (2) shale overbank sequences.

2.3.1 SANDSTONES

The sandstones are mostly fine-grained, and may contain up to 30 per cent clay ($<2\mu\text{m}$). Bryan et al (1984) report a particle size analysis of a sandstone and found no particles $>250\mu\text{m}$. The main cementing agent is calcium carbonate. The clays are dominantly montmorillonitic (Hodges and Bryan, 1982), but illite and small amounts of

kaolinite are also present (Campbell, 1987). Sandstone surfaces are covered with a weathering rind, varying in thickness from 2 to 3 mm on interrill areas, to 15 mm on rill bottoms (Hodges and Bryan, 1982). This weathering rind appears to form by dissolution and dispersion caused by wetting (Hodges and Bryan, 1982). Thickness of the weathering rind is greater in rills because rills often exploit fractures in the bedrock, which may increase infiltration. Furthermore, snow tends to accumulate in rills, so that during snowmelt rills receive more runoff than interrill areas (Harty, 1984).

Slopes developed in sandstone are typically densely rilled (Fig. 2.3). Bowyer-Bower and Bryan (1986) propose that the rills form when flow concentration of runoff occurs, for instance in overlying shale units. Such rills continue to exist even when the overlying shale is removed. Bowyer-Bower and Bryan's (1986) results suggest that rills will not develop in the absence of flow concentrations, as on a smooth sandstone slope lacking an overlying shale. Field observations indicate that runoff concentration by cracks in the sandstone may also cause rill formation.

2.3.2 SHALES

Clay contents of the shales vary considerably, and reported values range from 30 to 90 per cent (Bryan et al., 1984; Campbell, 1987). A significant portion of the clay fraction is very fine. Bryan et al. (1984) report that ca. 35 per cent of the clay fraction is finer than $0.3 \mu\text{m}$. The dominant clay mineral is montmorillonite, although some samples have been shown to contain up to 75 per cent illite and significant amounts of kaolinite (Campbell, 1987).

On gentle slopes the regolith profile on the shale typically consists of several distinct layers. The surface layer consists of a 4 to 5 cm thick 'popcorn' crust, made up of loose, puffy, popcorn-like aggregates. Underlying this is a 5 to 8 cm thick, dense, compact

subcrust, typically breaking up in large (up to 15 cm in cross-section) flat aggregates, which are usually oriented parallel to the local slope. Finally, there is a layer of shards (with a longest diameter of a few mm) consisting of shale which has not undergone any visible alteration due to subaerial weathering. The size of the shards rapidly increases with depth. The boundary between the dense subcrust and the shards sometimes has the character of a transitional zone, consisting of shards which are partially altered by hydration and are fused together in larger aggregates. On steeper slopes the layers are usually thinner, and the dense subcrust may be absent.

The morphology of the popcorn crust shows considerable variation over time. Observations of the changes in popcorn crust morphology over the summer of 1987 indicate that it is destroyed by large rainstorms, resulting in a platy crust morphology. Regeneration of the popcorn crust is caused by small, low-intensity rainstorms, a few of which suffice to eliminate all traces of the popcorn crust. The popcorn crust has the capacity to absorb large amounts of water, in some cases in excess of 200 per cent by weight. Hence, the presence of a popcorn crust greatly impedes runoff generation.

On certain shale units, especially on steeper slopes, popcorn crusts never form. Instead, a thin platy surface crust develops. The diameter of the thin platy aggregates is usually less than 3 cm. At present the factors determining whether a popcorn crust or a platy crust develops on a shale are unknown. Analyses of grain size, clay mineralogy, and exchangeable sodium percentage (ESP) have not indicated specific differences between shales showing different crusts (Hodges and Bryan, 1982).

2.4 REGOLITH CHEMISTRY

Chemical analysis of the shale and sandstone regolith has indicated strong similarities between these two lithologic groups. Hodges and Bryan's (1982) reports of a

cation adsorption analysis suggest that Ca and Na are dominant, while small amounts of Mg and K are present. However, in view of the difficulties of an accurate exchangeable Na determination (Bresler et al., 1982) these results should be viewed with some caution. Analyses of water-soluble salts in saturated extracts (U.S. Salinity Laboratory Staff, 1954) by Bryan et al. (1984) show that Na accounts for 80 to 95 per cent of the total cations in the saturated extract, while values of the Sodium Adsorption Ratio (SAR) range from 9 to 19. The dominance of Na creates conditions conducive to swelling and dispersion of the montmorillonitic clays, and is an important factor in explaining the morphology of the popcorn crust and the high erosion rates in the badlands.

The dominant anion is SO_4 , with smaller amounts of NO_3 and traces of Cl present (Bryan et al., 1984). pH values of the saturated extract range from 6.59 to 8.47 (Bryan et al., 1984), indicating that HCO_3 (bicarbonate) and small quantities of CO_3 (carbonate) are present. The EC of a solution is a measure of the ability of that solution to conduct an electric current, and is a function of the total dissolved solids in the solution. The EC is often used as an indicator of water quality because of its simplicity of measurement. The EC of the saturated extract was $1,643 \mu\text{S cm}^{-1}$ for sandstone, and ranged from 2,938 to $6,280 \mu\text{S cm}^{-1}$ for shale. Similar differences in EC were reported by Sutherland and Bryan (1988) who, in a 1:5 regolith-water paste, found an EC of $480 \mu\text{S cm}^{-1}$ for a sandstone weathering rind, and of 636 to $1,040 \mu\text{S cm}^{-1}$ for a shale. Both studies indicate the importance of the shales as a solute source in Dinosaur Provincial Park. The analyses of Sutherland and Bryan (1988) also suggest that the solute content of the dense subcrust is significantly higher than that of the overlying popcorn crust and of the underlying shards.

Gypsum ($\text{CaSO}_4 \cdot 2\text{H}_2\text{O}$) is present in considerable quantities in the Judith River Formation. It occurs in several forms, ranging from powdery or fibrous on fracture planes in the sandstone and between shale shards, to imperfect crystals lying on the surface of the popcorn crust.

2.5 PIPING AND TUNNEL EROSION

Piping and tunnel erosion are ubiquitous in semi-arid areas (e.g. Barendregt and Ongley, 1977; Yair et al., 1980; Drew, 1982; Harvey, 1982). Both pipes and tunnels are subsurface erosion features. A number of classification schemes based on morphology and genesis have been proposed (Jones, 1981). The terminology used here will follow Bryan and Harvey (1985) who reserve the term pipes for subsurface erosion features caused by steep hydraulic gradients in homogeneous materials, such as those present in earth-fill dams. Tunnels, on the other hand, result from the enlargement by flowing water of existing cavities, e.g. desiccation cracks and root channels (Bryan and Harvey, 1985). This may involve a steep hydraulic gradient, but this is not a prerequisite.

In Dinosaur Provincial Park tunnel erosion is widespread. Tunnel diameters vary from a few mm for microtunnels on the shales, to several meters for large collapse features. Bryan and Harvey (1985) distinguish two kinds of tunnel systems in Dinosaur Provincial Park. The first occurs on the shales, and is caused by swelling and shrinking of the montmorillonite-rich material (Hodges and Bryan, 1982). Runoff alternates between rills and the shallow micro-tunnels on its route downslope, and no hydrologic distinction can be made between tunnel flow and rill flow (Bryan et al., 1978). These micro-tunnels often develop at the top of the shard layer, directly beneath the dense subcrust which acts as a caprock. Rapid slaking and dispersion of the shards on wetting creates an impermeable surface causing lateral diversion of the infiltrating water (Bryan et al., 1978).

The second kind of tunnel system, consisting of larger features, may penetrate several meters below the surface and is not exclusively associated with the shales. Tunnels like these may transect basin divides. The genesis of the deep tunnel systems is uncertain, but may reflect wetter climatic conditions during various phases of the Holocene. Observations indicate that roof and wall collapse due to unloading control development to a considerable extent and are often responsible for valley forms. Two deep tunnel systems

were monitored by Bryan and Harvey (1985) who showed that flow through these larger features may contribute up to 10 per cent of the total basin discharge. Solute and sediment concentrations of tunnel flow are typically three to four times higher than normally found in channel flow, as runoff passing through the tunnels picks up solutes and sediment (Bryan and Harvey, 1985). This makes tunnel flow an important factor in the denudation budget. The deep tunnel systems form an integral and vital part of the drainage network, and may transfer runoff that was generated on sandstones and pediment surfaces.

2.6 EROSION AND DENUDATION RATES

Measurement of the changes in elevation on nine 1 m² plots over a period of 10 years have indicated an average erosion rate of 4 mm yr⁻¹ (Campbell, 1981) for shale, sandstone, and pediment plots combined. This average conceals considerable variation, both temporal and spatial, within and between plots. However, no evident correlation between erosion rate and slope angle or lithology was found (Campbell, 1982). Two plots located on pediment surfaces actually showed net aggradation at a rate of 1.8 and 4.3 mm yr⁻¹ over the ten years of measurement. Based on the sediment yield of 202,260 and 336,810 m³ drainage basins, Bryan and Campbell (1986) give an estimate of the erosion rate of 3 mm yr⁻¹, which is remarkably close to Campbell's (1982) value.

The regional erosion rate for the 43 000 km² Red Deer River basin has been estimated to be of the order of 0.021-0.040 mm yr⁻¹ (Slaymaker and McPherson, 1973) which is considerably lower than the estimate for the Dinosaur Provincial Park badlands. Campbell (1977a, 1977b) has shown that 80 to 90 per cent of the sediment load of the Red Deer River originates in the 800 km² of badlands fringing the river on the last 300 km of its course before it joins the South Saskatchewan River. The magnitude of this localized sediment input, derived from less than 2 per cent of the basin area, is sufficiently large to

produce a distinctive high point in the long profile of the Red Deer River. Campbell's (1977a, 1977b) results indicate that the concept of a regional erosion rate ignores the considerable variability within a basin, so that using this concept can produce misleading results.

2.7 THRESHOLDS OF RUNOFF GENERATION AND SOLUTE AND SEDIMENT ENTRAINMENT

The four major surface units in the Dinosaur Provincial Park badlands are vegetated surfaces, pediment surfaces, sandstone surfaces, and shale surfaces, each showing a distinct response to rainfall. The terms 'sandstone' and 'shale' are here not merely used in their lithological sense, but refer to areas with a distinct morphology, lithology, and response to rainfall.

2.7.1 VEGETATED SURFACES

The vegetation on the vegetated surfaces consists of different species of grasses, prickly pear (*Opuntia polycantha*) and barrel cactus (*Mammillaria vivipara*), and sage brush (*Artemisia spp.*) and greasewood (*Sarcobatus vermiculatus*). These surfaces can be fairly extensive in certain parts of the badlands, and are associated with aeolian and, locally, alluvial deposits with generally high infiltration capacities. No runoff was generated during rainfall simulations in which ca. 16 mm of rainfall was delivered to a vegetated plot at intensities of 38.0 and 43.5 mm h⁻¹ (Hodges and Bryan, 1982). Thus, except possibly during prolonged, high-intensity rainstorms or during rapid snowmelt when the subsurface is still frozen, the vegetated surfaces do not produce runoff or sediment.

2.7.2 PEDIMENT SURFACES

Pediments are gently sloping planation surfaces developed in bedrock, and are covered by a thinly laminated deposit of sheet-wash derived silts and sands of varying thickness (Fig. 2.7). The pediments are separated by a sharp break in slope from the much steeper, overlying sandstone and shale slopes. Hodges (1982) calls these badland features 'pseudo-pediments' to distinguish them from the large-scale pediments commonly found in arid regions.

The depth of wetting on the pediments is typically only 3 to 5 mm. Infiltration is impeded by thin vesicular layers in the sheetwash deposit. Such vesicular layers are quite common in arid and semi-arid soils (e.g. McFadden et al., 1986), and are also frequently found under irrigation furrows on highly silty soils (Miller, 1971). Formation of the vesicles appears to be caused by the entrapment of air by infiltrating water (Springer, 1958; Miller, 1971), aided by diurnal temperature fluctuations (Evenari et al., 1974) and, possibly, by the release of CO_2 during drying of a soil solution containing bicarbonate (Paletskaya et al., 1958). Campbell (1987) attributes the limited infiltration on the pediments to the presence of thin clay skins deposited during the falling flowstages of earlier events.

Because of their limited infiltration capacity, the pediments display rapid generation of infiltration-excess overland flow, and possess high runoff coefficients. During rainfall simulations at an average intensity of 29 mm h^{-1} , Hodges and Bryan (1982) and Bryan and Hodges (1984) found rapid runoff generation, often in less than one minute. Bryan et al. (1984) found a time to runoff of 6 min at an intensity of 13.6 mm h^{-1} , suggesting a threshold of runoff generation (mm of rainfall needed to produce runoff) of 1.4 mm. Bryan and Campbell (1980) report virtually instantaneous runoff generation from natural rainfall on a 1 m^2 pediment plot. Campbell (1987) uses 3 mm as an estimate of the maximum infiltration depth in an infiltration storage compensated model of runoff



Fig. 2.7 Pediment, separated from the overlying shale slope by a sharp slope break.

generation.

Compared to the sandstones and the shales, sediment and solute concentrations in runoff from the pediments are generally low. Bryan et al. (1984) report that EC's declined gradually during the tests to the level of the water used for the rainfall simulations. Evidence of initial flushing of solute-rich runoff seemed to be associated with the presence on the pediments of sediment derived from overlying shale slopes. In the absence of such deposits no clear evidence of initial flushing was found. Sediment concentrations varied irregularly, and appeared to be roughly, though not always significantly, correlated with discharge (Bryan et al., 1984).

2.7.3 SANDSTONE SURFACES

The depth of wetting on the sandstones coincides with the thickness of the weathering rind of a few mm (Bryan et al., 1978; Hodges and Bryan, 1982). Weakly-crystalline gels released by weathering of the dominantly montmorillonitic clay minerals act as a sealant reducing infiltration (Bryan et al., 1984). This leads to the rapid generation of infiltration-excess overland flow, and induces high runoff coefficients. Bryan et al. (1978) reported that runoff started 1 min after the start of simulated rainfall with an average intensity of 22 mm h⁻¹. Hodges and Bryan (1982), Bryan and Hodges (1984), and Bryan et al. (1984) found similarly rapid response. Campbell (1987) uses a value of 5 mm for the maximum infiltration depth on sandstones in an infiltration-storage-compensated model of runoff generation.

During rainfall simulations the average value of the EC on the sandstones is slightly higher than on the pediments, indicating a greater potential for solute release (Bryan et al., 1984). During the tests the EC quickly decreased to a more or less constant level. Sediment concentrations displayed a generally similar pattern, although the initial

peak concentration occurred after the initial peak of the EC (Bryan et al., 1984).

2.7.4 SHALE SURFACES

Considerable variability in material properties, surface microrelief, and antecedent moisture conditions on the shales cause a large variability in the response to rainfall. Additional complexity arises from the fact that runoff on the shales occurs as crack flow, rill flow, microtunnel flow, and as interflow at the top of the dense subcrust and at the dense subcrust/shards interface (Hodges and Bryan, 1982).

Hodges and Bryan (1982) distinguish six stages in the runoff generation on the shales, starting from the dry initial conditions of stage A. During stage B swelling of the clays partially seals off the surface. Locally, runoff generation may occur on silt pockets and silt stringers, which are lower areas, in some cases compacted (e.g. animal tracks), in which a thin, often discontinuous silt layer has been deposited. This leads to incipient rill flow, part of which may be diverted into microtunnels. During stage C the wetting front penetrates to the popcorn/dense subcrust interface, where local saturation may occur. Rill and tunnel flow are sustained, while secondary cracks start to disappear and primary cracks start to close from the base. During stage D effective crack flow in primary cracks starts, and popcorn interrill areas start to contribute runoff. By stage E primary cracks have closed, and true sheet flow begins. The wetting front now has penetrated through the dense subcrust, and at the top of the shards layer slaking and dispersion cause tunnel formation. Continuing rainfall leads to stage F, during which the complete surface contributes runoff while tunnel flow is at a maximum, both in the microtunnels in the popcorn crust and in the tunnels at the dense subcrust/shards interface. During the majority of rainstorms the higher stages will not be reached, and runoff will be confined to rills and cracks, especially to those in which a silt stringer has been deposited.

A number of experiments have illustrated the complexity of runoff generation on the shales, and have led to estimates of the total rainfall associated with the different stages. For instance, during a rainfall simulation at an average intensity of 28.5 mm h^{-1} on a 30 m^2 shale plot, Bryan et al. (1978) found that under dry antecedent moisture conditions rill flow on the upper shale unit started after 10 to 12 min. During the test the rill flow rate continued to increase, and rill flow on the upper shale unit became continuous after 15 min. In contrast, on the lower shale unit no runoff generation was observed. Runoff from the upper shale unit infiltrated at the boundary of the two units and reappeared downslope as tunnel flow. Although this example illustrates the mechanisms of runoff generation on the shales and indicates the order of magnitude of the total rainfall causing different types of runoff, the large spatial variability in rainfall intensity (from 12 to 42 mm h^{-1}) during the test precludes calculating thresholds of runoff generation, a problem plaguing all rainfall simulations on large plots (Bryan et al., 1978; Hodges and Bryan, 1982; Bryan and Hodges, 1984; Bryan et al., 1984).

Bryan and Campbell (1980), using natural rainfall on 1 m^2 runoff plots, found on some shale plots a threshold of runoff generation and sediment entrainment of close to 0 mm, indicating that even small rainfalls could cause some erosion. On these plots, however, secondary thresholds were observed, exceedance of which sharply increased erosion rates. The secondary thresholds may indicate runoff generation in plot areas other than the rills (e.g. a contribution from the interrill popcorn areas) or may be associated with a change in the characteristics of the overland flow at high discharges, causing localized scour. The value of the secondary thresholds ranged from 21 to 42 mm. Data from two of the shale plots did not indicate a secondary threshold, and the threshold rainfall of runoff generation and sediment entrainment on these plots was 11 and 44 mm. Campbell (1987) uses a value of 10 mm for the maximum infiltration depth on shales in an infiltration-storage-compensated model of runoff generation for the badlands. In general, runoff generation on the shales lags behind that on pediments and sandstones by a

sizeable margin.

EC's and sediment concentrations of runoff are considerably higher on the shales than on the pediments and sandstones, and the delayed contribution of solute- and sediment-rich runoff from the shales has been observed during a number of rainfall simulations. Bryan et al. (1984) found that EC's and sediment concentrations increased on some plots, whereas on other plots the EC's and sediment concentrations remained relatively constant or decreased. The latter situation is believed to be caused by the flushing out of fine sands and silts deposited in rills and cracks as silt stringers during flow recessions of earlier runoff events, and hence shows the effect of microtopography. The collapse of microtunnels and the occurrence of small-scale slumping and mudflows serve to sustain or increase EC's and sediment concentrations during the later stages of tests. Variations in properties and microtopography within shale areas affect sediment dynamics to a considerable extent. Generally, runoff generation on the shales occurs most rapidly in rills also serving as supply-limited sediment sources. The contribution from interrill popcorn areas occurs much later, but these areas are transport-limited sediment sources, thus causing sediment concentrations to remain relatively constant or increase during rainfall.

2.8 MESOSCALE DRAINAGE BASINS

In 1981 the 336,810 m² Aquatot Basin was instrumented to investigate how information obtained on microscale plots could be spatially extrapolated to help understand the behaviour of a typical mesoscale badlands drainage basin. Details of the instrumentation are given in Honsaker et al. (1984) and, for the Rimco Basin, in Section 5.1. Several factors influenced the decision to instrument this particular basin. First, the basin is located in the restricted access area of Dinosaur Provincial Park. This means that

disturbance of the basin is minimal, enabling study of the basin in its natural state.

Second, because of the restricted access, damage to expensive and delicate equipment by vandalism is avoided. Third, the basin is easily accessible. Sampling sites are located at a ten minutes walking distance from the nearest road, allowing rapid access so that when rainfall occurs observations and sampling can be carried out during even the earliest stages of flow.

Since the start of the project, observations have been made of the discharge and sediment and solute concentrations at the outlets of the Aquatot Basin and of the Rimco Basin, a 202,260 m² subbasin, and research on various geomorphological and hydrological subjects has been carried out in the basin. A review of the most important results is provided by Bryan and Campbell (1986).

Basin response was shown to be strongly controlled by rainstorm characteristics such as rainfall intensity and amount, storm duration, direction of travel of the storm cell, and distribution of rainfall relative to the location of the different surface units within the basin. For the Dinosaur Provincial Park badlands, a partial area model of runoff generation seems appropriate in which, in contrast to humid areas, the location of partial areas is not determined by antecedent moisture conditions, but instead by surface properties and rainfall characteristics. Basin hydrographs do not indicate a distinct contribution of channel flow, indicating that lag times of tunnel systems and channel systems are similar.

The runoff coefficients of the basins ranged between 17 and 68 per cent (Bryan and Campbell, 1986; Sutherland, 1983). This makes the basins highly efficient runoff generators, even more so because 31.7 per cent of the Aquatot Basin, and 35 per cent of the Rimco Basin, consists of vegetated, aeolian surfaces which even under extreme rainfall have not been observed to yield runoff.

The largest component of the stream load was found to be suspended sediment. During four storms in 1982 bedload accounted for 0.2 to 2.7 per cent of the total

streamload (Bryan and Campbell, 1986). These values are, because of the problems of estimating bedload transport rates, believed to be too low. In view of the lack of sources of abundant coarse material in the basin, however, the estimates are thought to give a good indication of the order of magnitude of bedload transport.

From data from 12 storms in 1982, Sutherland and Bryan (1988) estimated that 1.4 per cent of the streamload was transported as solutes. Sutherland (1983) derived the following regression equation for the relationship between total dissolved solids and the electrical conductivity of channel and tunnel flow in Dinosaur Provincial Park:

$$\text{TDS} = 19.51 + 0.68 \text{ EC} \quad [2.1]$$

($n=20$, $r^2=0.92$, $P<0.05$) where TDS is the total concentration of dissolved solids (mg l^{-1}), and EC is the electrical conductivity ($\mu\text{S cm}^{-1}$).

2.9 DESIGN OF THE PRESENT STUDY

Detailed information on the geomorphic processes in the Dinosaur Provincial Park badlands obtained since the late 1960's was an important factor in choosing the field area. Badlands are an ideal environment in which to conduct spatial scale studies as even at the smallest scale, drainage basins are readily defined. The lack of a soil and vegetation cover greatly facilitates investigating the relationship between, for instance, rainfall, lithology, and basin response at all levels of scale.

The three following chapters present the results from the field study at three spatial scale levels: (1) the microscale (Chapter 3); (2) the subbasin scale (Chapter 4); and (3) the mesoscale (Chapter 5). The basins were nested, so that each mesoscale basin contained one subbasin which, in turn, contained a number of microscale basins. The

timescale of interest for the field study concerned basin response to a single rainstorm. The timescale was kept constant for all three spatial scale levels to avoid confusion arising from the interaction of temporal and spatial scales. An additional reason for the choice of timescale is that in semi-arid regions the considerable variability in rainfall from year to year limits the validity of estimating long-term geomorphic conditions from short-term observations. Hence, extrapolating data from short-term experiments to longer periods should be avoided.

CHAPTER 3

3.1 MICROSCALE PLOT STUDIES

To investigate the release of solutes and sediment from the different surfaces at the microscale of the experimental plot, two types of runoff tests were carried out. The first involved direct application of runoff to the upslope end of the plot; the second, generation of runoff using a small rainfall simulator. The latter tests also yielded data on the infiltration characteristics of the surfaces.

3.2 DIRECT-RUNOFF TESTS

3.2.1 EXPERIMENTAL DESIGN

Water was applied to the plot using a 1 m long section of PVC gutter, installed with the longitudinal axis perfectly horizontal and parallel to the slope surface (Fig. 3.1). The gutter was tilted slightly downslope, allowing water to flow over the downslope edge of the gutter onto the plot. To avoid non-uniform wetting of the edge, caused by the high adhesive forces between the PVC and the water molecules, a narrow strip of aluminum foil was folded tightly over this edge. This ensured that water was applied uniformly across the plot. To dissipate the energy of the fall and to avoid excessive erosion at the upstream end of the plot, a thin sheet of plastic was spread out directly under the gutter, folded to follow the plot topography. The water flowed from this sheet onto the plot. Water was applied to the gutter using a constant head device to ensure a constant rate of application. Once the water reached the plot surface it concentrated rapidly into distinct flow paths. In the major flow path a funnel made of thin aluminum was installed to enable sampling of

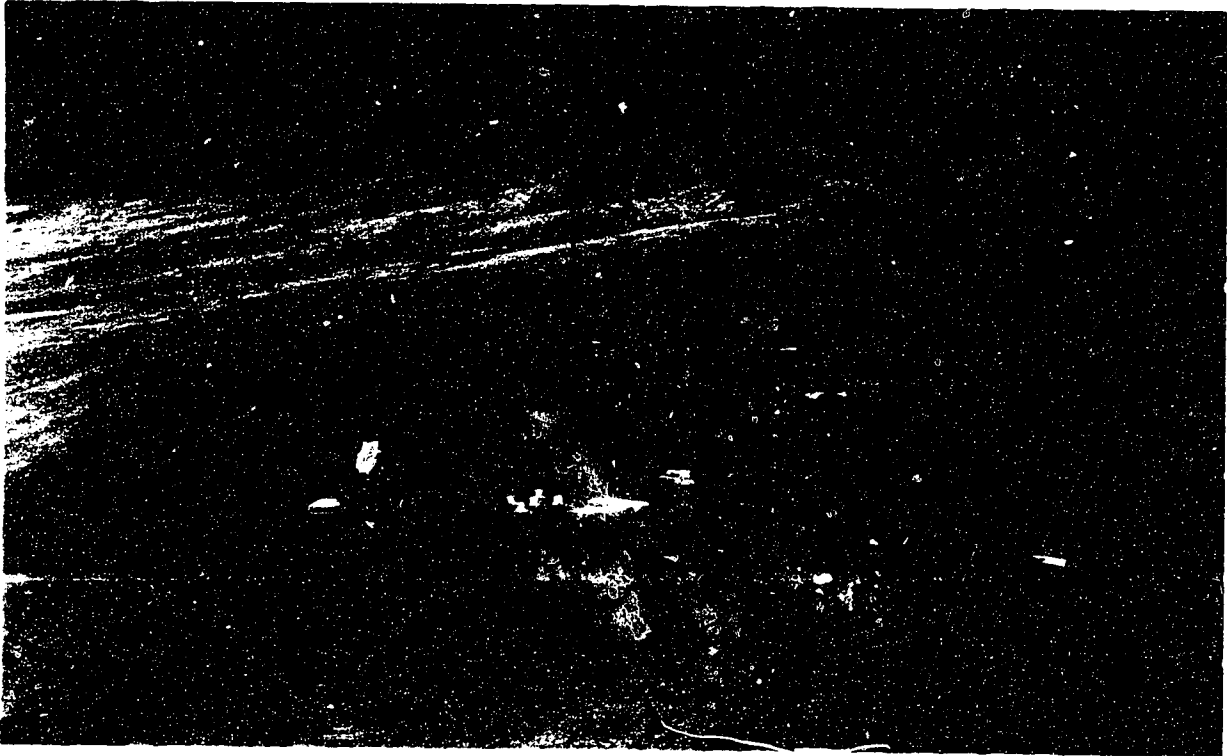


Fig. 3.1 Experimental set-up during direct-runoff test on plot A3. Runoff rapidly concentrates in distinct flowpaths, precluding conversion of the data to areal values.

the runoff. The shape of the funnel was adjusted to the microtopography of each plot, so that representative samples of the runoff could be taken. On smooth plots a broad (15 cm), flat funnel was used. On rough, steep plots the funnel was bent to conform with the cross-section of the rill or channel to be sampled.

A similar set-up was employed by Laronne, Shen, and co-workers who investigated solute release on the Mancos Shale in the Upper Colorado Basin (Shen et al., 1981; Laronne, 1982; Laronne and Shen, 1982). Inherent in the experimental technique are some limitations. For instance, the rapid concentration of runoff in flow paths precludes the estimation of areal values from the data. In addition, the concentration of runoff causes data on solute and sediment dynamics to refer to channel and rill flow rather than to sheet flow. Despite the limitations, the results indicated that direct-runoff tests are a simple way to rapidly compare sediment and solute release characteristics of contrasting areas (Laronne, 1982).

During the tests, discharge was estimated by measuring the volume of runoff collected in a sample bottle over a known period of time. The sediment concentration of the sample was determined in the laboratory by taking a known volume of sample and weighing the sediment remaining after evaporation of the water. Weakly crystalline gels in the water (Bryan et al., 1984) precluded separating solutes and suspended sediment by filtration. It was therefore decided to report sediment concentrations, which thus refer to the concentrations of solutes and suspended sediment combined. Sutherland and Bryan (1988) found that solutes accounted for approximately 1.4 per cent of the total streamload in the badlands. It can therefore be assumed that suspended sediment accounts for close to 100 per cent of the material exported from the plots.

Separate samples were taken to measure the EC (electrical conductivity) of the runoff. The first runoff sampled was always used to measure the EC. The EC was measured in the field directly after sampling, using a temperature compensating Lectro Mho-Meter (Lab-Line Instruments) with an accuracy, reported by the manufacturer, of 1

to 3% in the scale range used for this study. All reported EC's are corrected to 25°C. The sampling interval varied from 2 to 3 minutes. The water used for the test was taken from the Red Deer River, and had an EC_o varying from 550 $\mu\text{S cm}^{-1}$ at the beginning, to 465 $\mu\text{S cm}^{-1}$ at the end of the test period. To allow comparison between the plots, EC_o is subtracted from the EC's measured in the plot runoff. In the following sections, \underline{EC} , \underline{EC}_p , and \underline{EC}_s represent the corrected EC's and the corrected peak and steady value of the EC, respectively, whereas EC, EC_p , and EC_s indicate the uncorrected values.

On each plot the test was carried out at least twice. Firstly under dry antecedent moisture conditions ('dry run'), and, usually immediately following the dry run, under wet antecedent moisture conditions ('wet run'). Before the dry run and after the wet run, samples of the crust and the underlying materials were taken on each plot to determine the gravimetric moisture content. Table 3.1 gives the characteristics of each plot, Table 3.2 provides an overview of the results of each test.

3.2.2 RESULTS

3.2.2.1 PEDIMENT SURFACES

Values of \underline{EC}_p ranged from 40 to 110 $\mu\text{S cm}^{-1}$ during the dry run, and from 25 to 45 $\mu\text{S cm}^{-1}$ during the wet run. In all cases the peak value of the EC occurred during the first stages of flow, indicating a flushing away of solutes accumulated on the surface (Fig. 3.4, Appendix A). On some plots, this also caused a decrease of \underline{EC}_p for the wet run. Based on tests of a Mancos Shale-derived soil, Jurinak et al. (1977) speculate that the initial rapid dissolution is caused by the presence of finely divided, highly soluble salts (e.g. NaCl, Na_2SO_4). This phase is followed by a period of slower solute release controlled by the dissolution of $\text{CaSO}_4 \cdot 2\text{H}_2\text{O}$ (gypsum) and CaCO_3 . On all plots the EC

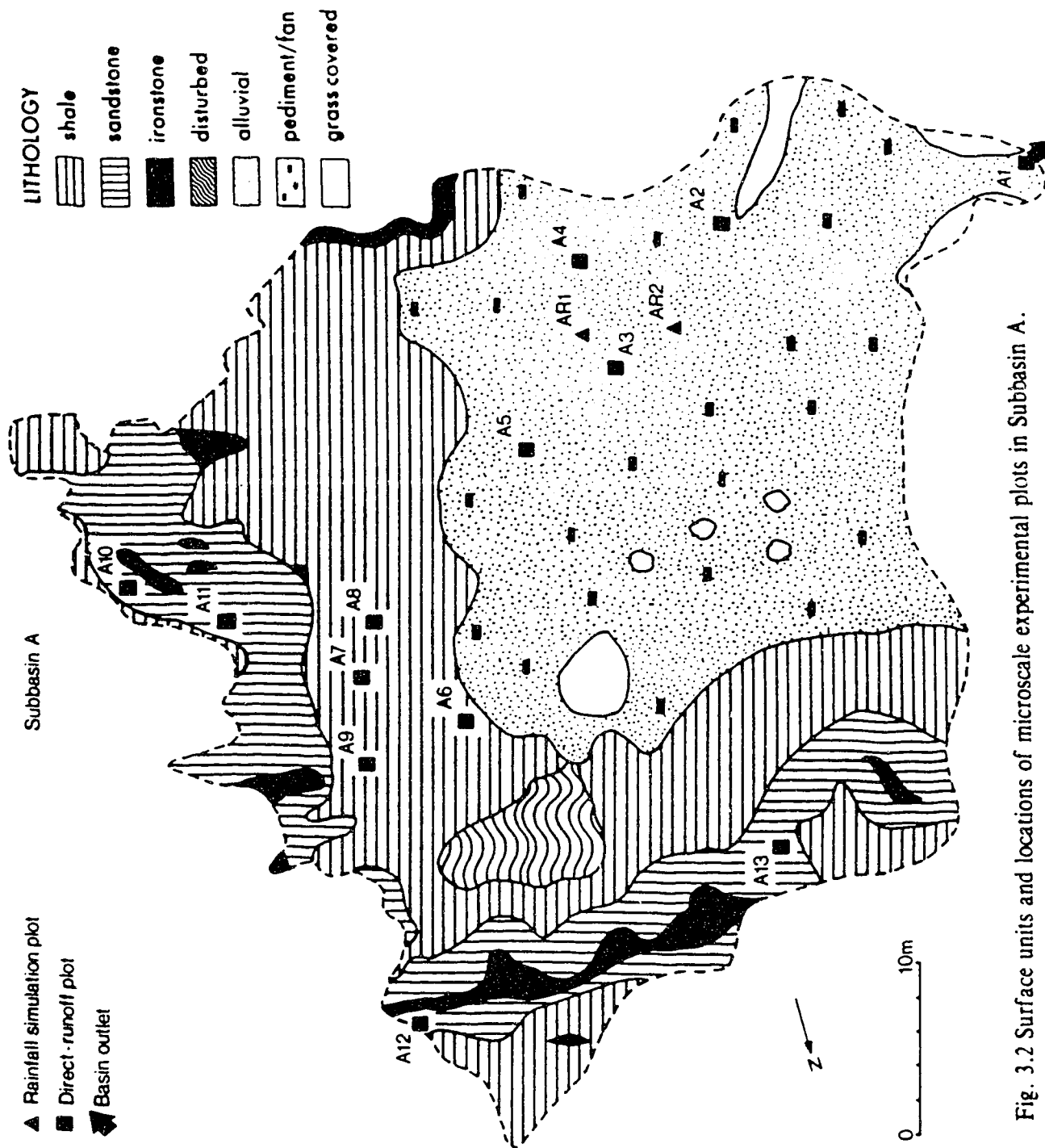


Fig. 3.2 Surface units and locations of microscale experimental plots in Subbasin A.

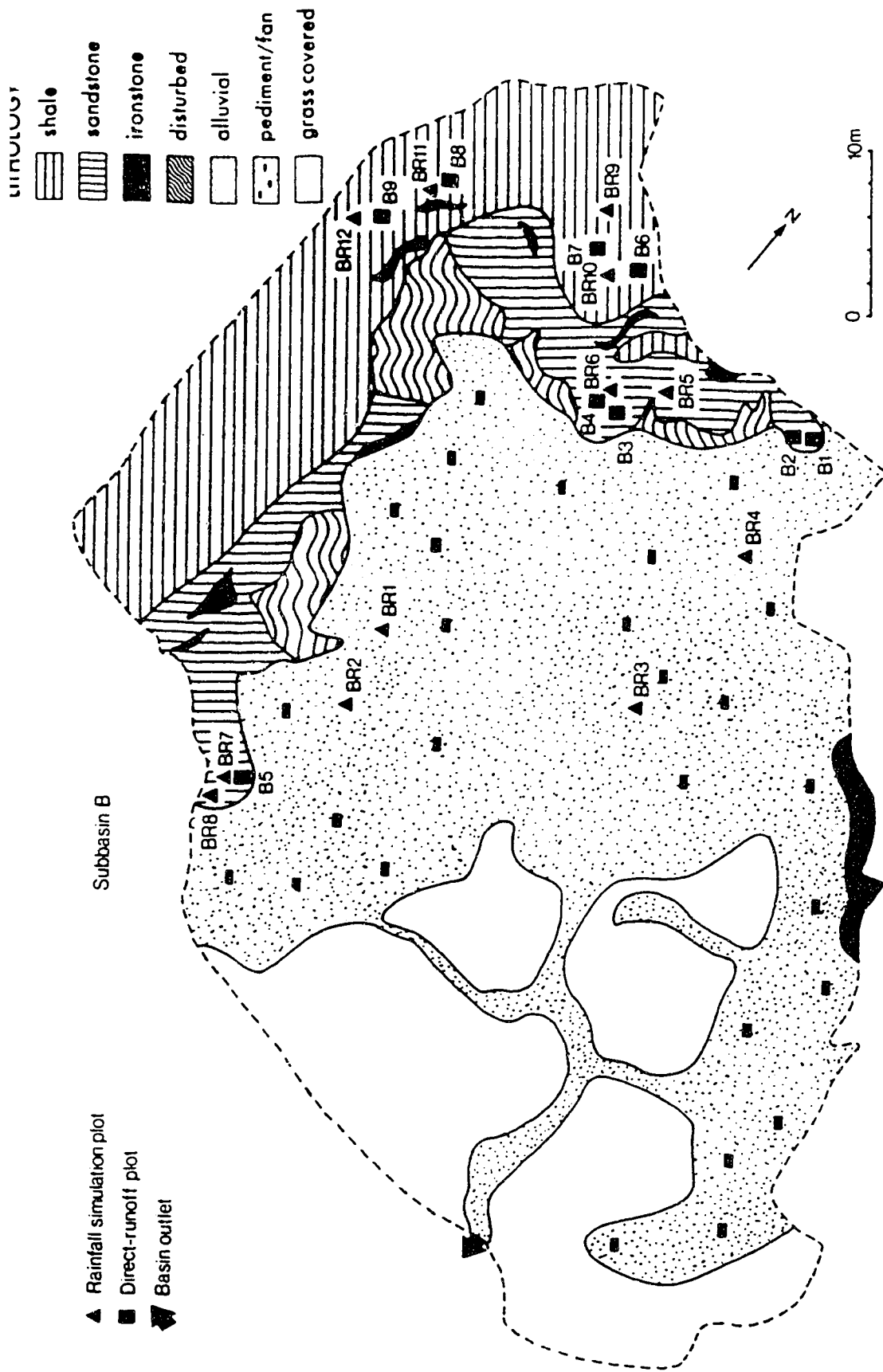


Fig. 3.3 Surface units and locations of microscale experimental plots in Subbasin B.

Table 3.1 Characteristics of direct-runoff plots

plot no.	surface unit†	slope‡ (°)	plot length (m)
B1	sst	42	0.70
B2	sst	38	0.90
B3	sst	34	2.00
B4	sst	32	2.30
B5	sst	28	1.60
B6	sh	29,59,39	1.90
B7	sh	21,45	3.10
B8	sh	15,29,43	3.00
B9	sh	12,45	2.70
A1	af	2	3.60
A2	ped/sh	5	2.20
A3	ped/sh	7	1.60
A4	ped/sst	4	1.80
A5	ped/sh	4	2.20
A6	sh	14,31,47	2.50
A7	sh	50	1.60
A8	sh	22,48	2.10
A9	sh	20,34	2.60
A10	sst	14,39,3	2.50
A11	sst	17,35	2.10
A12	sst	32,49,8	2.15
A13	sst	25	1.50

† sst - sandstone

sh - shale

af - alluvial fill

ped/sst - pediment in sandstone

ped/sh - pediment in shale

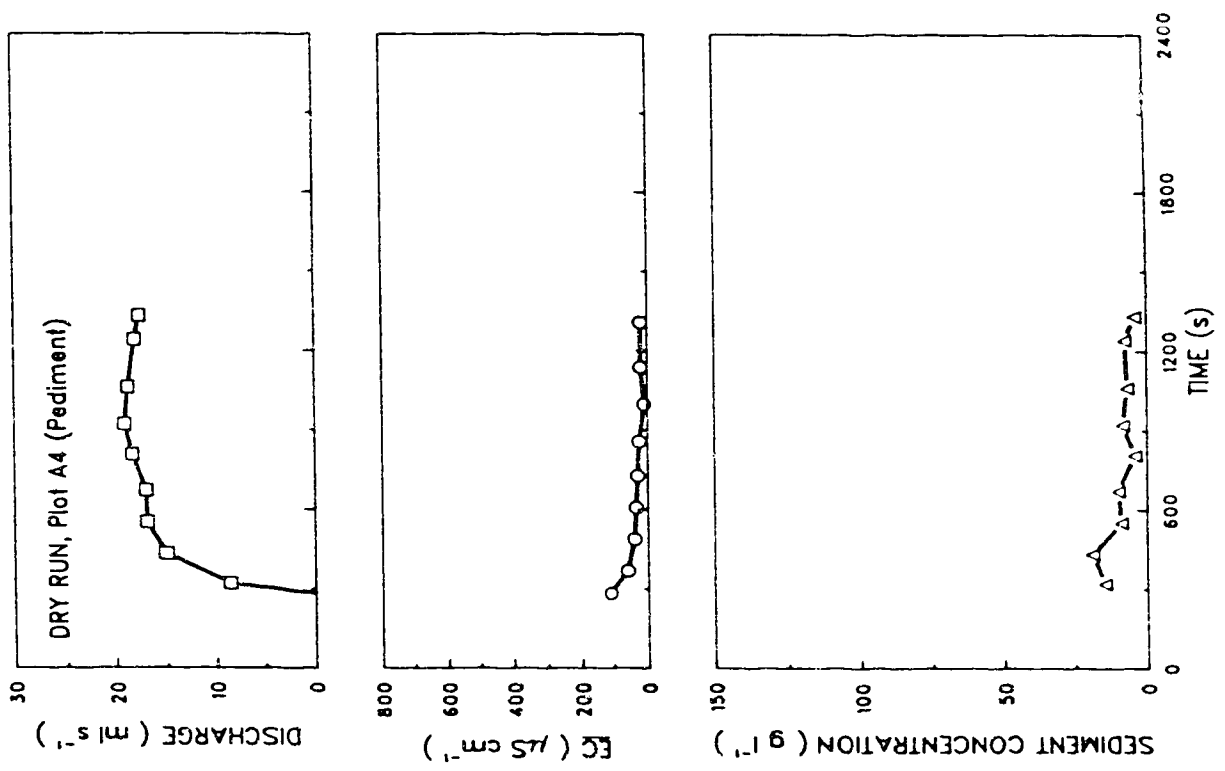
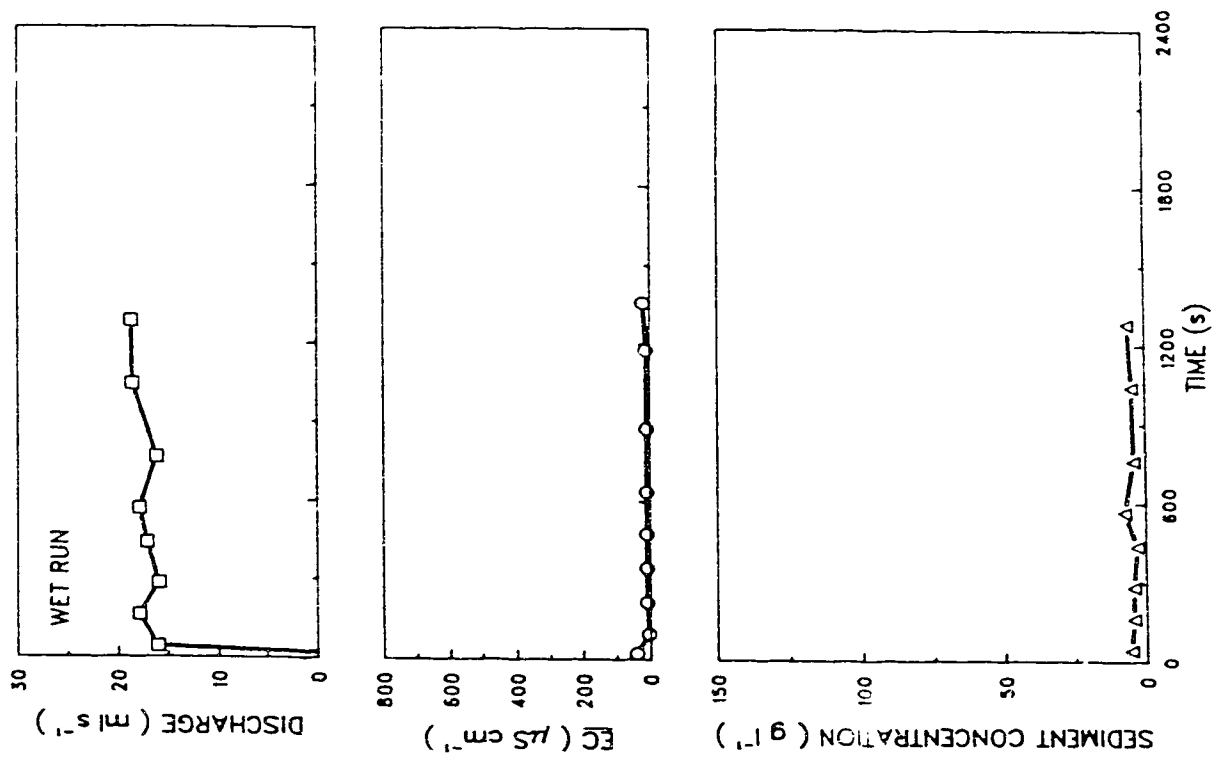
‡ multiple values indicate downslope changes in slope angle

Table 3.2 Overview of results of direct-runoff tests

plot no.	surface	unit	EC ₀ ($\mu\text{S cm}^{-1}$)	EC _p ($\mu\text{S cm}^{-1}$)	EC _p #	EC _s ($\mu\text{S cm}^{-1}$)	EC _s ††	EC _s ($\mu\text{S cm}^{-1}$)	EC _s ††	Q _p (mls ⁻¹)	Q _p pb	Q _s (mls ⁻¹)	Q _s #	pH	pH	SC _p (gl ⁻¹)	SC _p †††	SC _s (gl ⁻¹)	SC _s pbpb
B1		ss	1140/	/	/	/	/	/	/	/	/	/	/	8.32/	/	/	/	/	/
B2		ss	1150/	1160/	10/	1156/1190	6/40	6/40	6/40	/	/	/	/	8.36/8.31	/	/	/	/	/
B3		ss	545/	645/	100/	566/	21/	21/	21/	26.7/	24.0/	24.0/	24.0/	8.54/	/	/	/	/	/
B3		ss	545/	665/	120/	555/	10/	10/	10/	27.4/	27.4/	27.4/	27.4/	8.54/	6.6/	6.6/	6.6/	6.6/	1.6/
B4		ss	540/545	700/ 605	150/ 65	538/ 530	0/ 5	0/ 5	0/ 5	44.0/45.3	44.0/45.3	42.8/44.7	42.8/44.7	/	3.6 / 1.8*	3.6 / 1.8*	0.7/ 1.5	0.7/ 1.5	/ 0.8
B5		ss	530/540	675/ 630	125/ 90	540/ 508	0/ 8	0/ 8	0/ 8	43.0/43.3	43.0/43.3	/	/	/	5.6 / 1.4	5.6 / 1.4	/ 0.8	/ 0.8	/ 0.8
B6		sh	540/540	1140/ 825	600/285	773/	233/ 0	233/ 0	233/ 0	25.8/25.4	25.8/25.4	/	/	/	104.4 /56.0*	104.4 /56.0*	/26.9	/26.9	/26.9
B7		sh	530/530	1310/ 850	780/720	658/ 603	128/113	128/113	128/113	18.3/26.0	18.3/26.0	17.3/	17.3/	/	136.8 /22.6*	136.8 /22.6*	/21.8	/21.8	/21.8
B8		sh	540/540	885/ 785	345/245	635/ 606	95/ 66	95/ 66	95/ 66	12.1/13.7	12.1/13.7	10.5/11.8	10.5/11.8	/	55.6 /20.8	55.6 /20.8	/11.3	/11.3	/11.3
B9		sh	540/540	1210/1070	670/530	/ 689	/ 689	/ 689	/ 689	16.3/19.3	16.3/19.3	/	/	/	81.6 /28.6*	81.6 /28.6*	/	/	/
A1		af	545/550	615/ 590	70/ 40	560/ 561	15/ 11	15/ 11	15/ 11	11.3/14.9	11.3/14.9	/13.8	/13.8	/	1.6 / 0.6	1.6 / 0.6	0.5/ 0.4	0.5/ 0.4	0.5/ 0.4
A2		ped/sh	560/530	600/ 570	40/ 40	568/ 529	8/ 0	8/ 0	8/ 0	16.8/19.3	16.8/19.3	16.4/	16.4/	/	18.8*/12.6*	18.8*/12.6*	/	/	/
A3		ped/sh	510/510	555/ 555	45/ 45	523/ 516	13/ 6	13/ 6	13/ 6	21.7/21.0	21.7/21.0	20.5/19.7	20.5/19.7	/	19.0 / 7.0	19.0 / 7.0	/ 1.0	/ 1.0	/ 1.0
A4		ped/ss	520/530	630/ 570	110/ 40	539/ 541	19/ 11	19/ 11	19/ 11	19.1/18.7	19.1/18.7	18.3/17.3	18.3/17.3	/	19.2*/ 7.6*	19.2*/ 7.6*	/	/	/
A5		-d/sh	510/510	610/ 535	100/ 25	523/ 510	13/ 0	13/ 0	13/ 0	17.0/22.8	17.0/22.8	16.1/22.6	16.1/22.6	/	8.6 /10.8	8.6 /10.8	2.8/	2.8/	2.8/
A6		sh	505/500	1160/ 720*	655/220*	729/ 649	224/149	224/149	224/149	20.8/27.2	20.8/27.2	19.8/27.1	19.8/27.1	/	60.8 /20.0*	60.8 /20.0*	28.6/	28.6/	28.6/
A7		sh	495/495	1360/1015	865/520	777/ 645	282/150	282/150	282/150	17.4/27.0	17.4/27.0	/22.4	/22.4	/	93.8 /35.0*	93.8 /35.0*	/	/	/
A8		sh	500/500	1020/ 795*	520/295*	680/ 628	180/128	180/128	180/128	15.1/14.9	15.1/14.9	14.2/	14.2/	/	24.6*/35.2*	24.6*/35.2*	16.3/	16.3/	16.3/
A9		sh	470/470	840/ 830	370/360	/ 686	/ 686	/ 686	/ 686	1.3/22.7	1.3/22.7	1.3/21.5	1.3/21.5	/	47.6*/45.0*	47.6*/45.0*	46.7/	46.7/	46.7/
A10		ss	465/460	725/ 630	260/170	525/ 549	60/ 80	60/ 80	60/ 80	9.0/10.5	9.0/10.5	7.5/ 6.1	7.5/ 6.1	/	29.8*/ 4.6*	29.8*/ 4.6*	3.0/	3.0/	3.0/
A11		ss	470/470	960/ 620	490/150	537/ 519	67/ 49	67/ 49	67/ 49	22.5/27.0	22.5/27.0	/	/	/	27.2 / 4.4	27.2 / 4.4	4.8/ 1.9	4.8/ 1.9	4.8/ 1.9
A12		ss	475/470	860/ 570	385/100	511/ 495	36/ 25	36/ 25	36/ 25	17.6/16.9	17.6/16.9	/	/	/	24.0 / 7.4*	24.0 / 7.4*	6.2/ 2.8	6.2/ 2.8	6.2/ 2.8
A13		ss	465/465	850/ 705	385/240	471/ 479	6/ 14	6/ 14	6/ 14	29.1/28.8	29.1/28.8	28.3/28.5	28.3/28.5	/	18.0 /22.0	18.0 /22.0	1.6/ 1.5	1.6/ 1.5	1.6/ 1.5

Table 3.2 Supplementary notes

data are given as: dry run/wet run
 - no data available
 † sst - sandstone
 sh - shale
 af - alluvial fill
 ped/sst - pediment in sandstone
 ped/sh - pediment in shale
 ‡ EC of water used for the test
 † peak value of EC in runoff (• indicates that peak value did not occur during the first stage of flow.)
 # peak value of EC in runoff minus EC of water used for the test
 †† steady value of EC in runoff
 ††† steady value of EC in runoff minus EC of water used for the test
 ††† peak discharge
 # # steady value of discharge
 ††† measurement of pH was discontinued after plot B3
 ††† peak value of sediment concentration
 †††† steady value of sediment concentration



decreased and reached a relatively steady value \underline{EC}_s , varying from 8 to 19 $\mu\text{S cm}^{-1}$ for the dry run, and from 0 (indicating no solute export) to 11 $\mu\text{S cm}^{-1}$ for the wet run. For all plots, the change of \underline{EC}_s from the dry to the wet run was within the precision of the EC meter, but still indicative of a diminishing solute supply during the tests.

Contrary to expectations, the bedrock material in which the pediment had been developed appeared to have no effect on the EC as plot A4 (sandstone) showed similar EC's as plots A2, A3, and A5 (shale). On plots A2, A3, and A5 shale was exposed in both channel and interchannel areas. The regolith profile on these shale outcrops consisted of a thin platy crust (less than 5 mm), underlain by a dense subcrust which rapidly graded into platy shards at a maximum depth of 10 cm. Thickness of the sediment deposit varied from 0 to 4 mm in interchannel areas, and reached values of up to 35 mm in the channel areas. Vesicular layers were present in the sediment. On plot A4 the sandstone was relatively resistant. Some desiccation cracks had developed, but most were faint and narrow. The cracks had not developed into an integrated network. Thickness of the sediment deposit reached up to 3 mm in the channel at the downstream end of the plot, but was negligible on most of the plot surface. Differences in solute release characteristics between sandstone and shale surfaces (Bryan et al., 1984) led to the expectation that this would also affect solute release on pediment surfaces. The reason this was not observed is likely that due to rapid flow concentration during the direct-runoff tests, sediment and solute release characteristics reflect conditions in channels and rills where deposition of sediment has occurred, rather than conditions in the interrill areas.

The sediment concentrations displayed a much more irregular behaviour (Fig. 3.4). Plots A3 and A5 show evidence of initial flushing of sediment-rich runoff, whereas plots A2 and A4 do not (Fig. 3.5). This can possibly be explained by the fact that the first runoff sample was always used for the determination of the EC, and was discarded afterwards. In this manner, the high sediment concentrations associated with the initial flushing may have been missed. Except for plot A5, peak sediment concentrations are

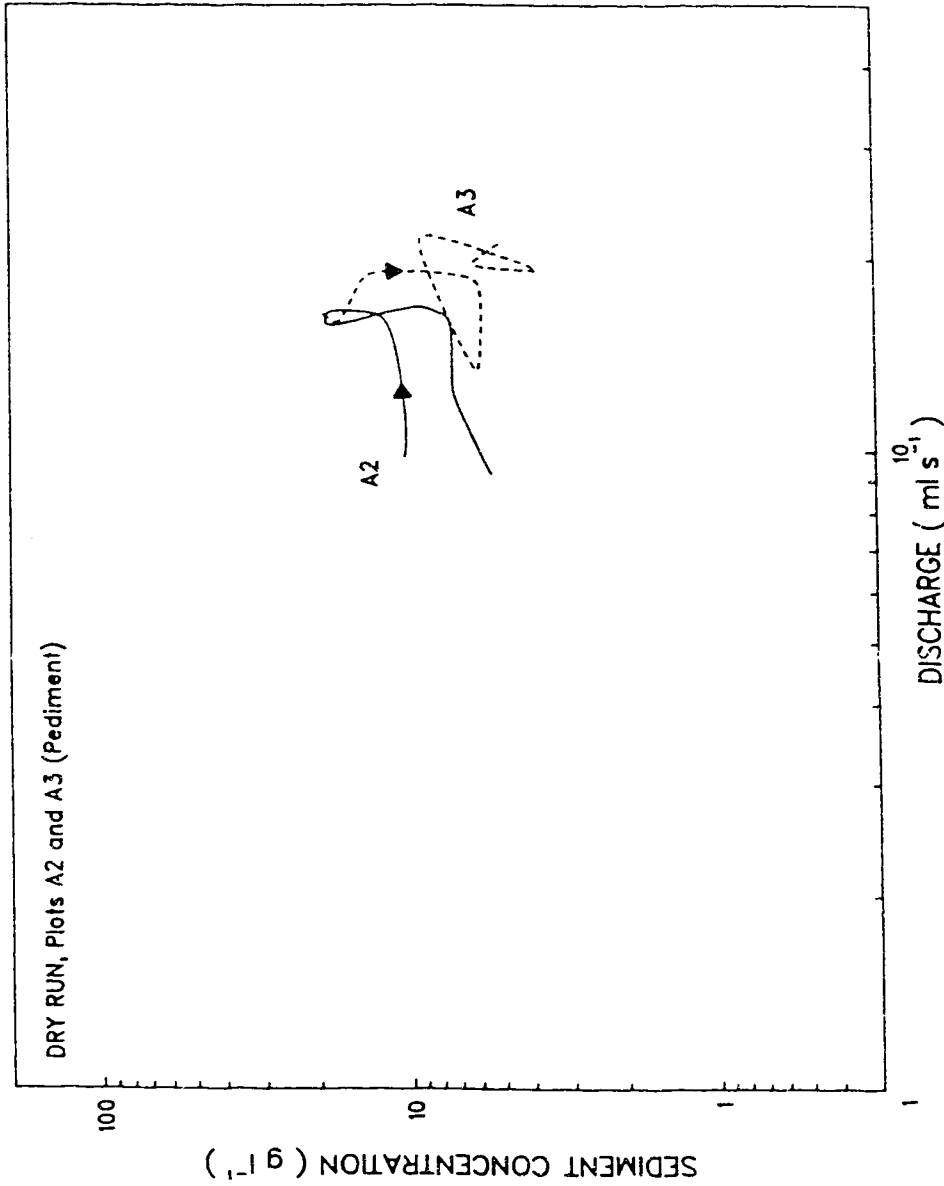
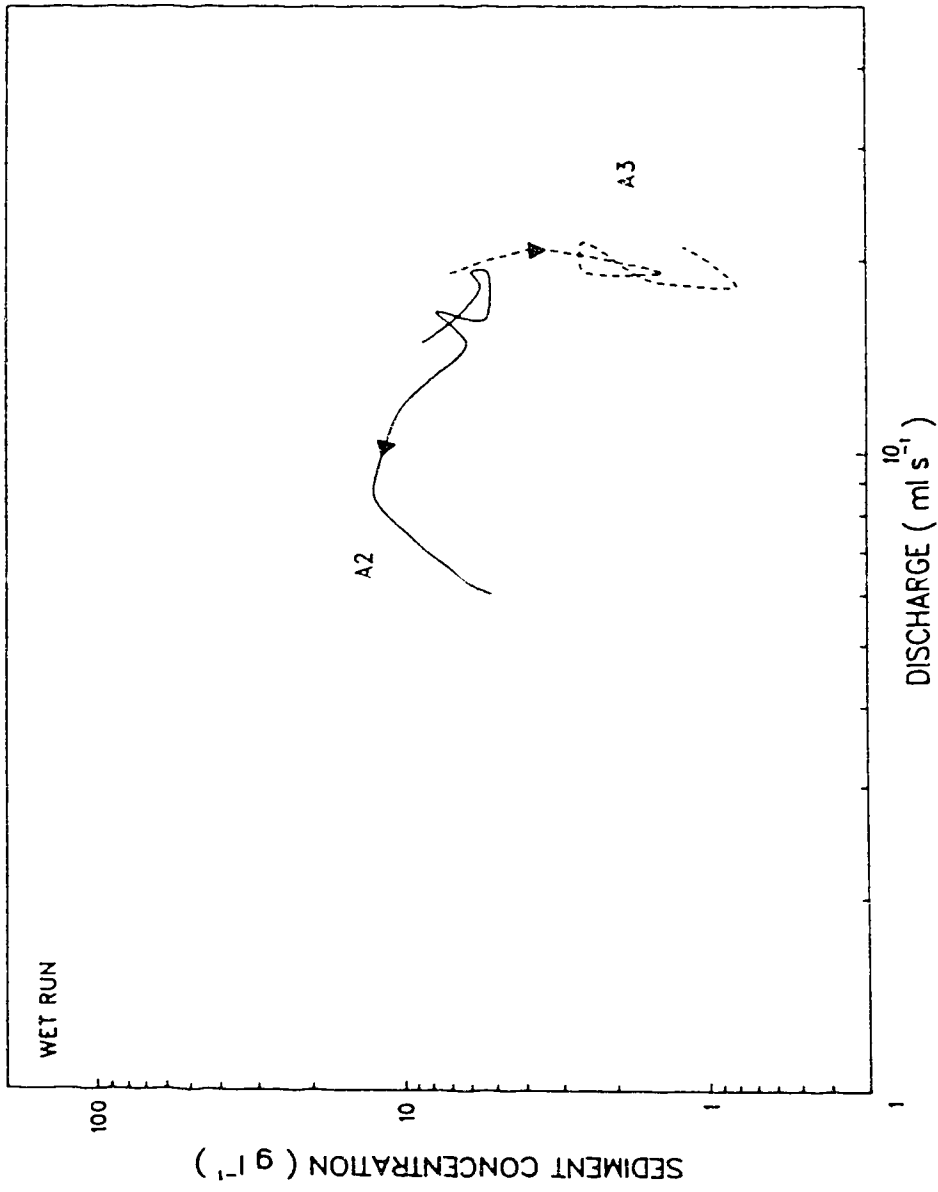


Fig. 3.5 Contrasting sediment concentration/discharge relationships for plots A2 and A3 (pediment). During the dry run, plot A3 exhibits initial flushing, whereas plot A2 does not. Subsequent variations in sediment concentration are partially independent of discharge, and may reflect collapse of microfeatures or episodic migration of headcuts. During the wet run, sediment concentrations on plot A2 generally increase with decreasing discharge, whereas plot A3 displays a general decrease in sediment concentrations at a relatively constant discharge.



lower for the wet run than for the dry run, indicating decreasing sediment supply. The irregular sediment concentrations generally precluded estimating a steady sediment concentration SC_s . Variations in sediment concentration generally did not follow variations in discharge. A possible reason for the irregularly varying sediment concentrations is the collapse of microfeatures or the episodic migration of microscale headcuts on the plot. As with the EC, differences in material underlying the plot appeared to have no effect on the characteristics of sediment removal.

The start of runoff ranged from 27 to 723 s for the dry run, and decreased strongly for the wet run, ranging from 9 to 22 s (Fig. 3.4). After the start of runoff discharge rapidly increased to a relatively steady level of 16.4 to 20.5 ml s⁻¹ for the dry run, and 17.3 to 22.6 ml s⁻¹ for the wet run. Steady discharge was generally attained 160 to 524 s after the start of runoff for the dry run, and 20 to 150 s after the start of runoff for the wet run. Comparison of the moisture profiles (variation of gravimetric moisture content with depth) before the dry run and after the wet run shows that the depth of moisture penetration was limited (Fig. 3.6).

3.2.2.2 SANDSTONE SURFACES

\underline{EC}_p occurred during the first stages of flow, and varied from 100 to 490 $\mu\text{S cm}^{-1}$ for the dry run, and from 65 to 240 $\mu\text{S cm}^{-1}$ for the wet run. On all plots, the EC decreased during the test and reached a relatively steady value \underline{EC}_s , varying from 0 (indicating no solute export) to 67 $\mu\text{S cm}^{-1}$ for the dry run, and from 5 to 80 $\mu\text{S cm}^{-1}$ for the wet run. \underline{EC}_p always occurred at the beginning of the test, and during the wet run, \underline{EC}_p was lower than during the dry run, both facts indicating exhaustion of the sediment supply (Fig. 3.7, Appendix A). On most plots the EC increased in the final stages of the test (Fig. 3.7). In some cases this can be attributed to a decreasing discharge causing a

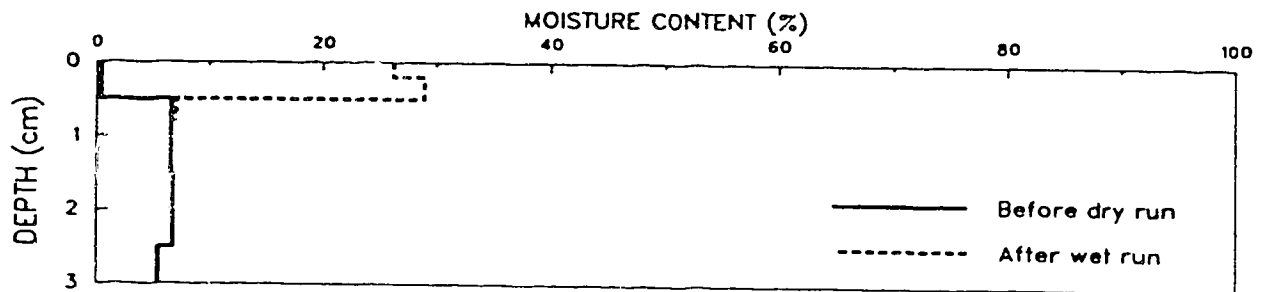
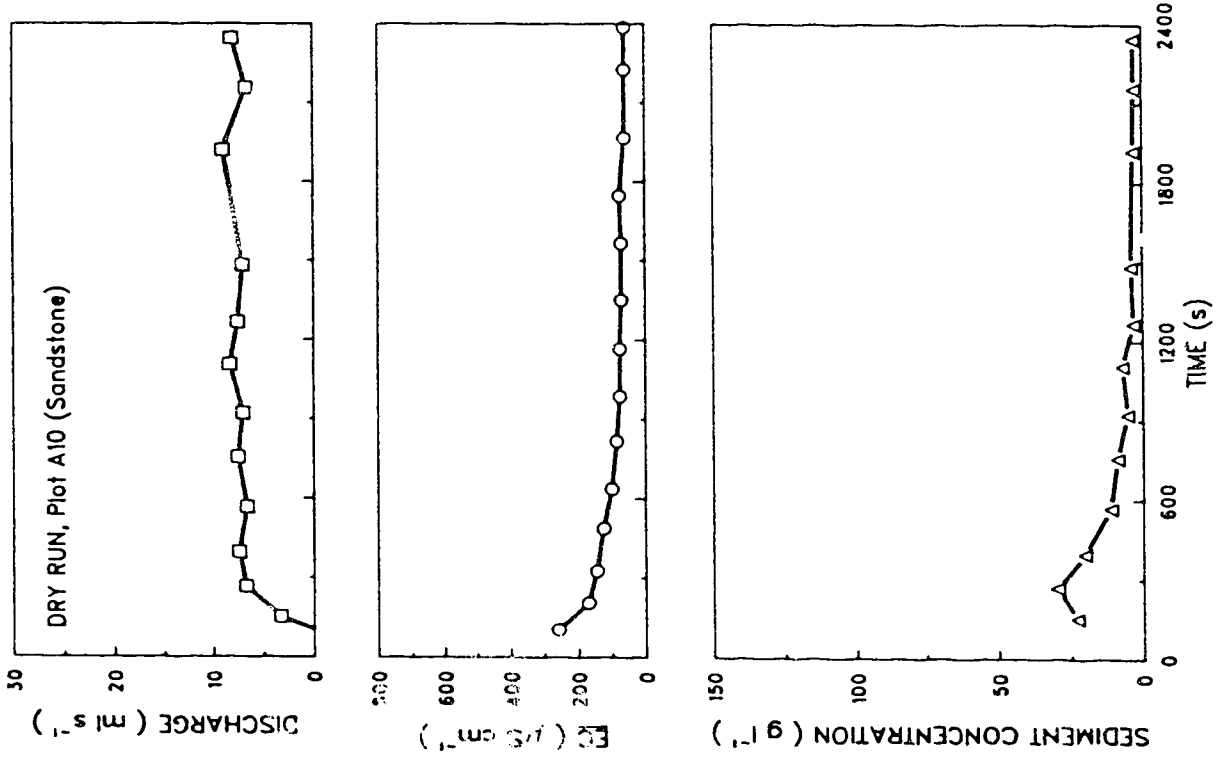
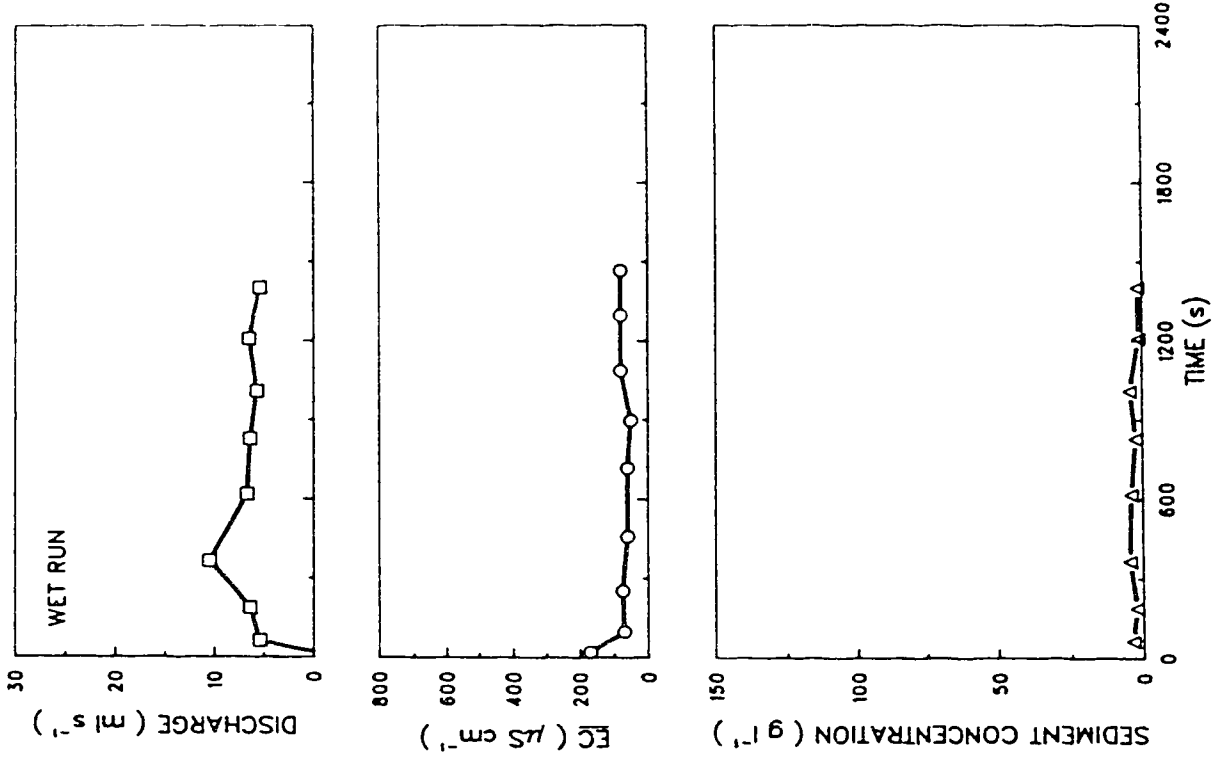


Fig. 3.6 Moisture profiles before the dry, and after the wet run on a representative pediment plot (A4). The stepped curve reflects the sampling of the regolith in layers.



decrease in dilution. In other cases the connection with decreasing discharge is not evident, and the increase in EC is likely caused by slugs of sediment becoming mobile because of the wetness, and the hence reduced strength, of the material (Fig. 3.7). Some plots showed that the increasing EC is accompanied by an increasing discharge and sediment concentration, so that increased flow capacity is likely to be an additional factor.

The sediment concentrations showed a more irregular behaviour than the EC. SC_p varied from 3.6 to 29.8 g l⁻¹ for the dry run, and from 1.4 to 22.0 g l⁻¹ for the wet run. In a few cases, SC_p did not occur during the initial runoff, but instead later during the test. The variability of the sediment concentrations precluded calculating SC_s on a number of plots. SC_s ranged from 0.7 to 6.2 g l⁻¹ for the dry run, and from 0.8 to 2.8 g l⁻¹ for the wet run.

Plot A12 differed from the other sandstone plots in that it did not consist of a simple, slightly convex or concave slope. Instead, plot A12 was formed by a convex, rilled slope with a slope angle of 32° (top) increasing to 49° (bottom), draining into a large rill with a bottomslope of 8-9°. The sampling point was located at the outlet of this rill. The rill did not contain a significant deposit of sediment. The thickness of the weathering rind in rills can be up to 5 times that on interrill areas, where thickness is usually around 3 mm (Hodges and Bryan, 1982). This makes the weathering rind within rills an additional and important source of sediment. This extra sediment did not cause an increase of SC_p . SC_s , however, during the dry run was 1.3 to 8.9 times larger, and during the wet run 1.4 to 3.5 times larger than on other sandstone plots. On plots where increases in discharge in the later stages of the test caused increases in sediment concentration. On other plots, however, similar increases in discharge had little or no effect on the sediment concentration (Fig. 3.8). It appears that the sediment stored in the thicker weathering rind in rills on the sandstone can become mobile under extremely wet conditions such as during later stages of a rainstorm. This, however, does not affect the EC.

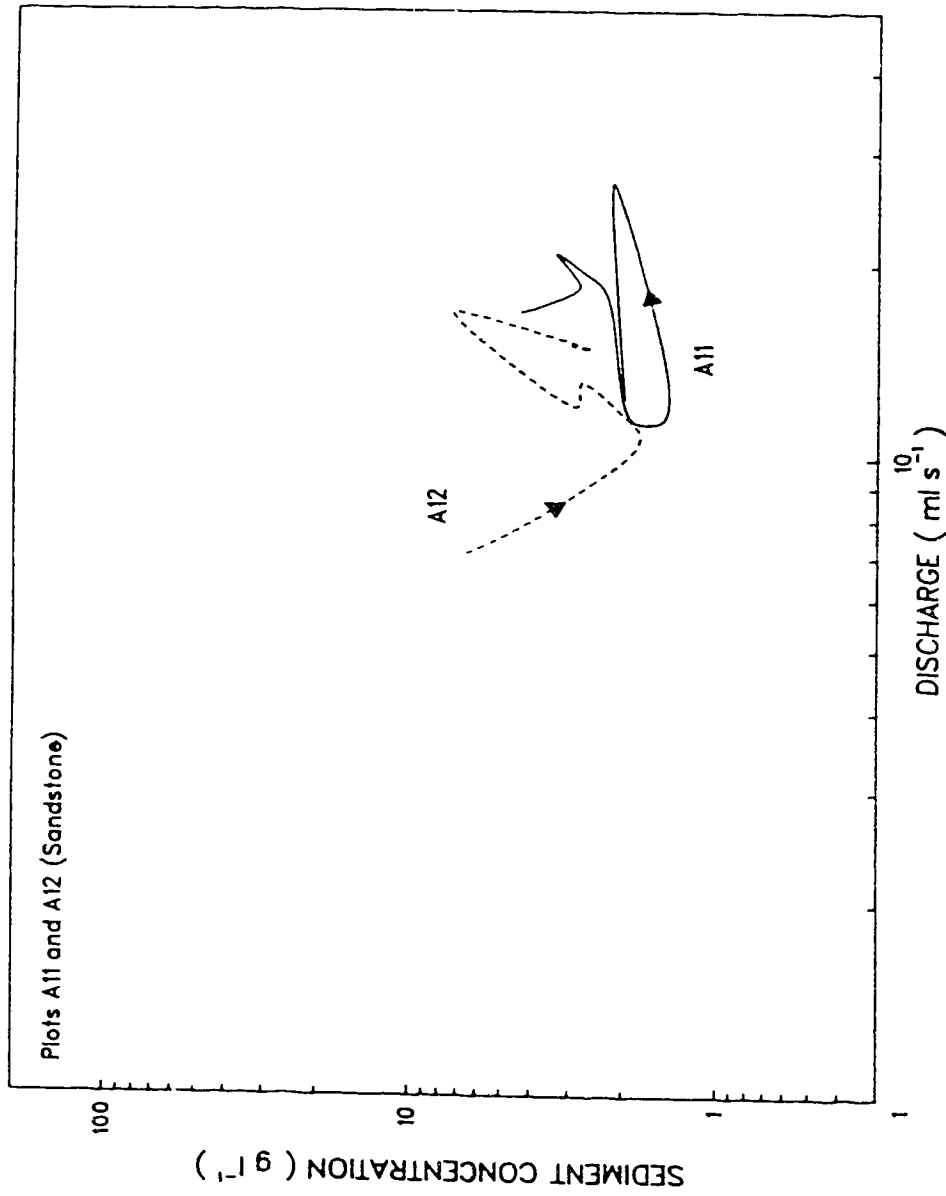


Fig. 3.8 Contrasting sediment concentration/discharge relationships for the wet run on plots A11 and A12. The large thickness of the weathering rind on plot A12 leads to a sharp increase in sediment concentration with discharge. On plot A11 a comparable increase in discharge has much less effect.

The start of runoff during the dry run varied from 7 to 194 s. For the wet run, the start of runoff decreased significantly, and varied from 6 to 20 s (Fig. 3.7). Discharge showed a varied behaviour from plot to plot. In some cases (e.g. plot B3, dry run) discharge increased slowly but steadily. Other plots showed a slow increase and a levelling-off at a relatively low discharge (Fig. 3.7, dry run, $Q_s = 7.5 \text{ ml s}^{-1}$), or a rapid increase and level off at a relatively high discharge (Table 3.2, plot A13, dry run, $Q_s = 28.3 \text{ ml s}^{-1}$). In general, the wet run showed a steeper increase in discharge than the dry run. It should be kept in mind, however, that a direct-runoff test is not suitable for determining infiltration characteristics of the plots. Figure 3.9 shows the moisture profiles before the dry run and after the wet run in the central rill on plot A10. Field observations indicated that the depth of moisture penetration is in excess of that observed on interrill areas, but nevertheless limited to a few cm.

3.2.2.3 SHALE SURFACES

\underline{EC}_p ranged from 345 to 865 $\mu\text{S cm}^{-1}$ for the dry run, and from 220 to 530 $\mu\text{S cm}^{-1}$ for the wet run (Table 3.2). During most tests the EC decreased exponentially, although not as smoothly as on the sandstone and pediment surfaces (Fig. 3.10, Appendix A). During the wet run on plots A6 and A8, \underline{EC}_p did not occur during the initial phase of runoff, but instead 180 s (plot A6) and 120 s (plot A8) after the start of runoff. These peak values were not clearly associated with variations in discharge or sediment concentration. Because of the irregular variations in the EC a steady value was not attained during the dry run on all plots. On those plots on which the EC did become steady, \underline{EC}_s ranged from 95 to 282 $\mu\text{S cm}^{-1}$ for the dry run, and from 66 to 216 $\mu\text{S cm}^{-1}$ for the wet run. On some plots, increases in the EC were caused by runoff from a section of the plots that had not previously contributed runoff to the outlet.

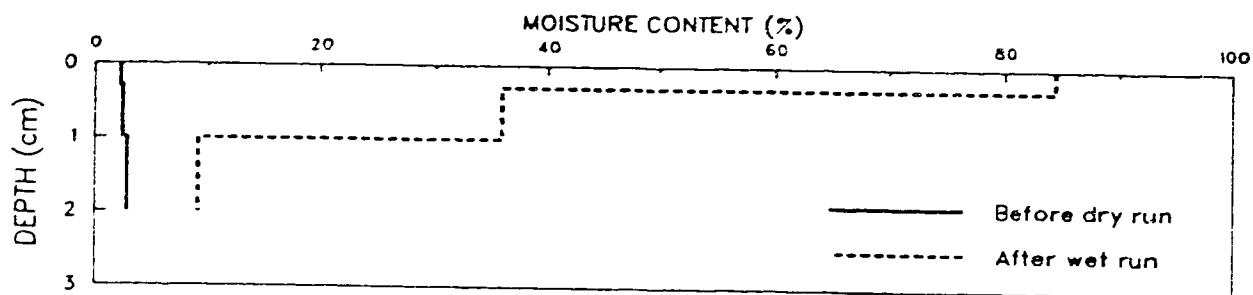
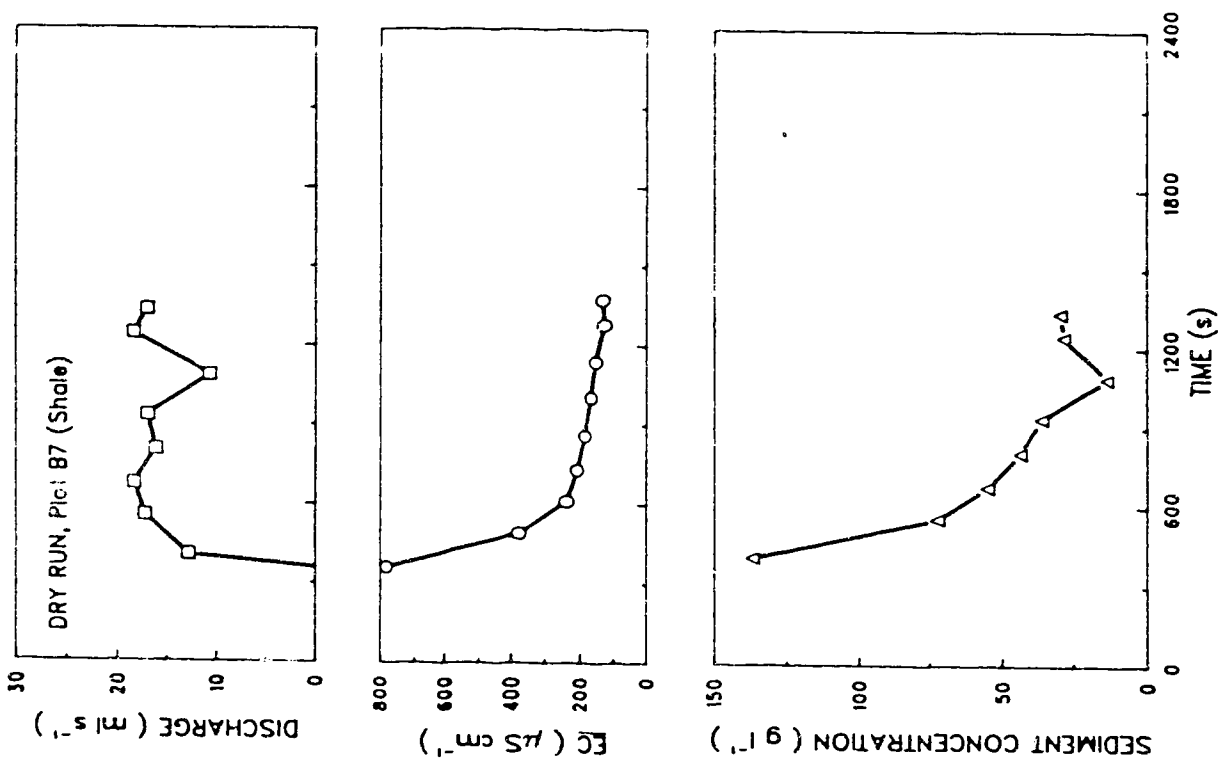
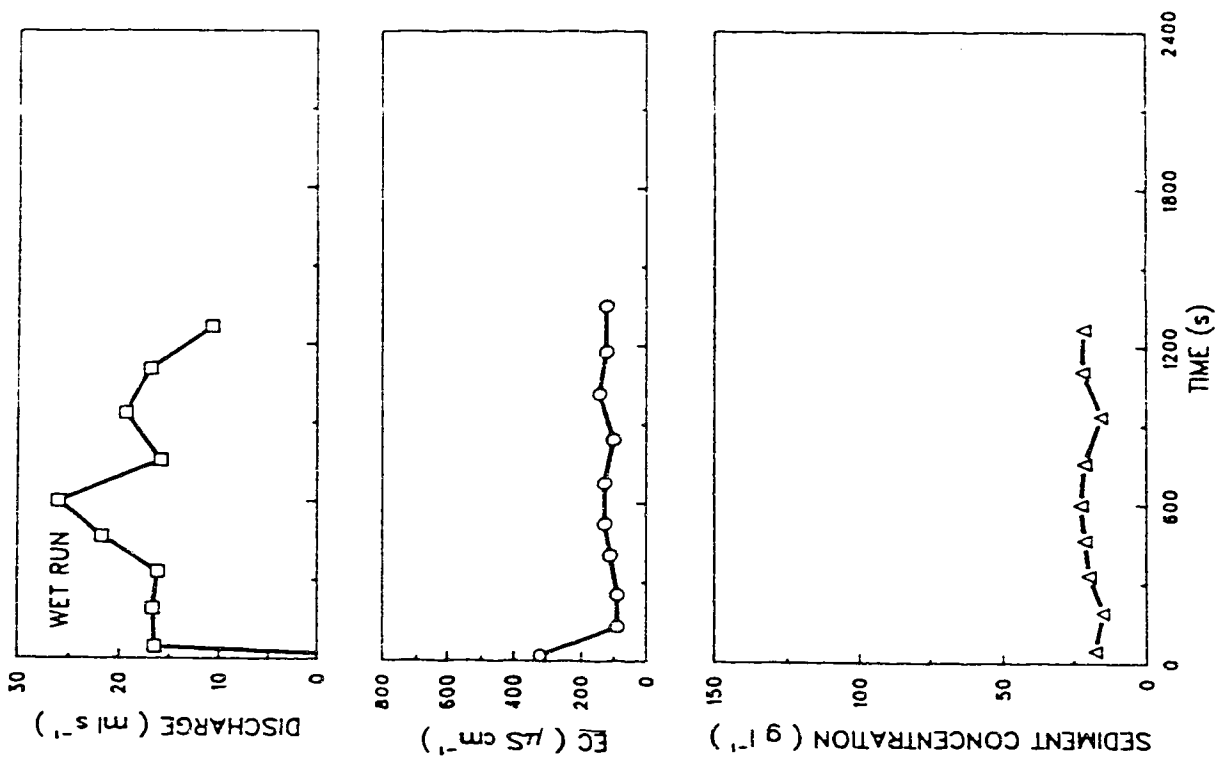


Fig. 3.9 Moisture profiles before the dry, and after the wet run on a representative sandstone plot (A10). Samples were taken within the central rill.



Variations in the sediment concentration were more irregular than on the sandstone and pediment surfaces. SC_p ranged from 24.6 to 136.8 g l⁻¹ for the dry run, and from 20.0 to 56.0 g l⁻¹ for the wet run. Six of the eight shale plots had the peak value of the sediment concentration at the beginning of runoff for the dry run, whereas this was the case on only one plot during the wet run. During the dry run, most plots displayed initial flushing of sediment, followed by an overall decline in sediment concentrations. During the wet run, sediment concentrations behaved much more irregularly (Fig. 3.10). The wet runs on plots A6 and A9 showed a gradual increase in sediment concentrations, with the peak value occurring in the final stages of the test. The wet run on other plots showed a sudden increase in sediment concentrations caused by a sharp increase in discharge (e.g. plot B6).

Two factors appeared to control sediment concentration on shale surfaces. First, wetting of the regolith reduced its strength, and caused microscale slumps and mudflows and the collapse of micropipes. This was especially important during the wet conditions of the wet run, and it caused variations in sediment concentration which were independent of discharge (Figs. 3.10, 3.11, 3.12). Second, variations in discharge, and therefore in flow capacity, caused variations in sediment concentration (Fig. 3.10). During the dry run, plot B7 showed evidence of initial flushing, followed by an exponential decline. This pattern was somewhat disturbed by a sudden decrease in discharge causing a drop in sediment concentration to 13.6 g l⁻¹, followed by an increase in discharge causing a rise in sediment concentration to 28.4 g l⁻¹. The sediment concentration/discharge relationship of the dry run on plot B7, however, is indicative of a decreasing availability of sediment (Fig. 3.12). During the wet run, the sediment concentration was relatively steady, and varied from 15.0 to 22.6 g l⁻¹ (Fig. 3.12). Variations in discharge did not cause variations in sediment concentration, and it appeared that sediment concentrations were controlled by a factor other than discharge. This factor could be the rate of slaking and dispersion of the surface aggregates, the latter being controlled by the solute concentration of the runoff.

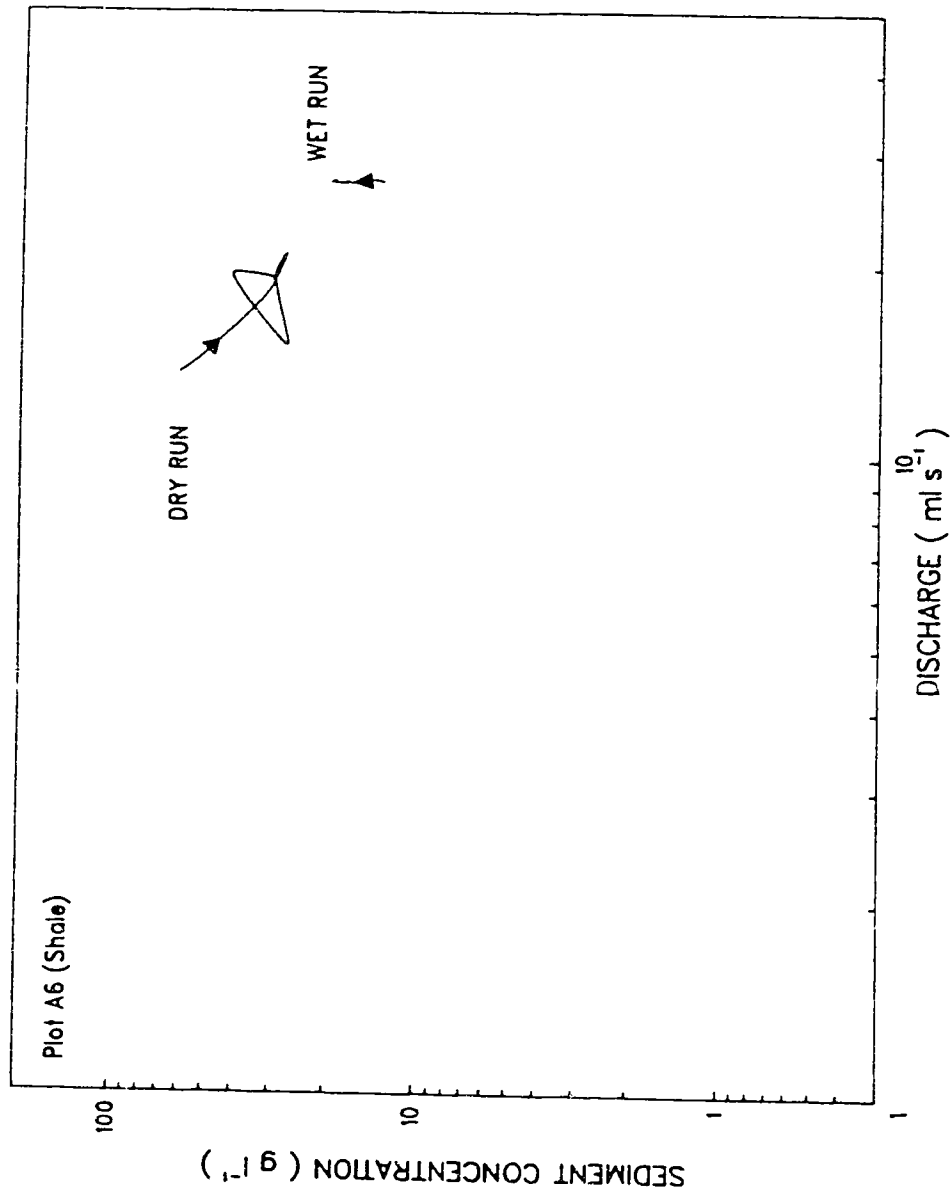


Fig. 3.11 Sediment concentration/discharge relationships of plot A6, showing an initial decrease in sediment supply, followed by slight variations, during the dry run; and showing a steady increase, independent of discharge, during the wet run.

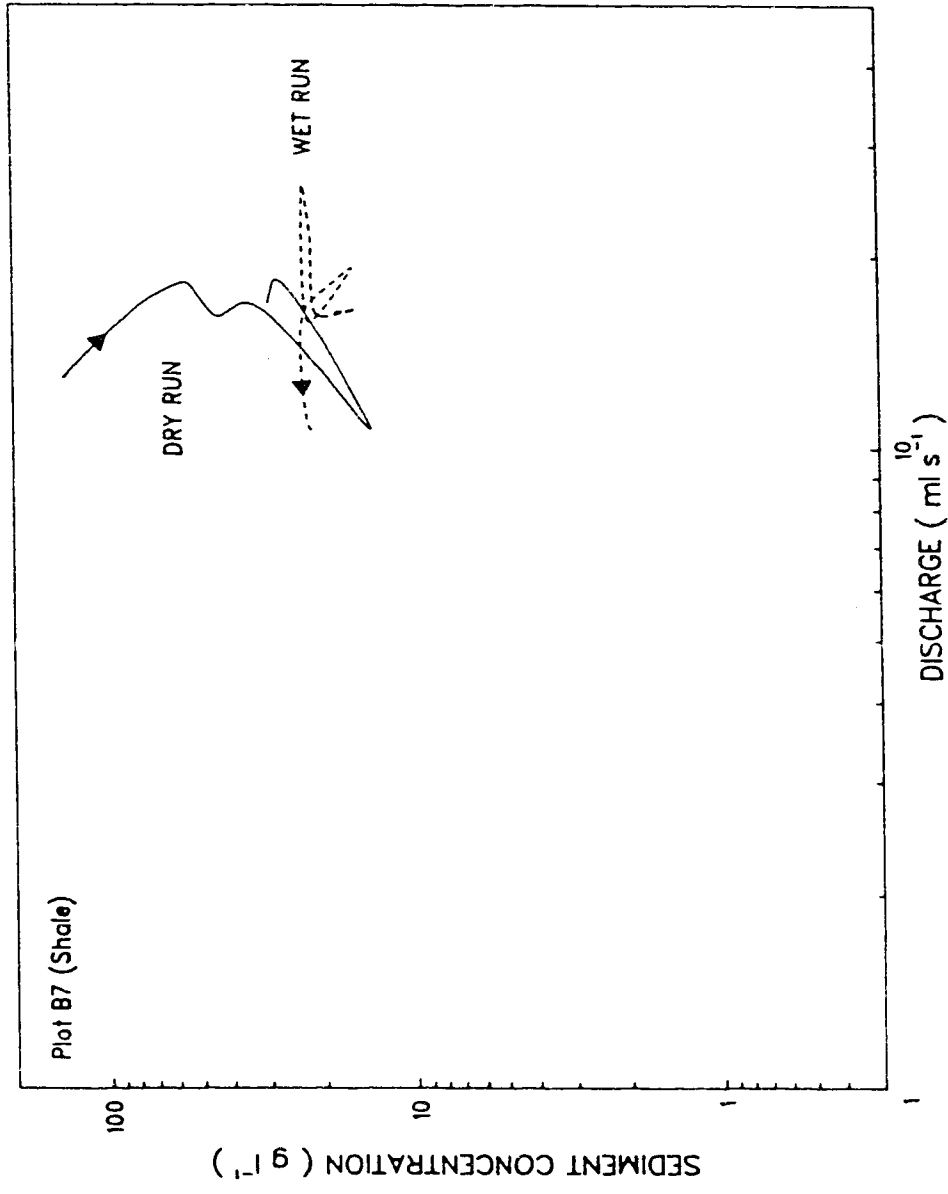


Fig. 3.12 Sediment concentration/discharge relationships of plot B7, indicating a decreasing sediment availability during the dry run; and showing irregular variations in sediment concentration, independent of discharge, during the wet run.

The start of runoff varied from 120 to 158 s for the dry run, and from 13 to 47 s for the wet run. Transmission losses were considerable during the dry run, as runoff flowed into cracks in the crust and subcrust. During the dry run, the advance of the leading edge of the flow was visible by the wetting of the popcorn aggregates from below. Overland flow on the shales occurred only over limited distances. A significant portion of the runoff took place over the dense subcrust as subsurface flow. Thus, solute and sediment levels in runoff from the shales may be controlled by the properties of the dense subcrust, rather than by those of the popcorn crust. The rills on plot B8 were lined with a silt deposit. Because of their limited permeability, these silt stringers acted as zones of rapid runoff generation during rainfall. The presence of silt stringers caused a significant lowering of the solute and sediment concentrations (Table 3.2), as the silt deposit has lost most of its solutes and is, because of its compactness, not as easily eroded as the shale itself.

As the shale swells on wetting the cracks seal, so that during the wet run transmission losses were strongly reduced. Q_s varied from 1.3 to 19.8 ml s⁻¹ for the dry run, and from 11.8 to 27.1 ml s⁻¹ for the wet run. During several tests, a steady value of the discharge was not attained. Figure 3.13 shows the moisture profiles for plot A8 before the dry run and after the wet run. Moisture penetration is deeper than on the sandstone and pediment surfaces.

3.2.3 DISCUSSION

During the direct-runoff tests, the three major surface units in the basin each showed a distinctive behaviour with regard to the release of solutes and sediment. Table 3.3 summarizes the more detailed data from Table 3.2. Pediments released the smallest amount of solutes. This is because the sheetwash-derived deposits have already lost most of the

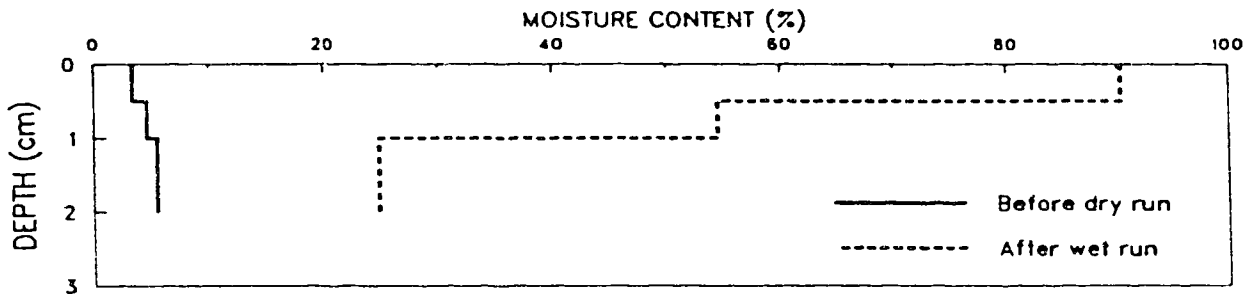


Fig. 3.13 Moisture profiles before the dry, and after the wet run on a representative shale plot (A8).

Table 3.3 Summary of results of direct-runoff tests

surface unit	\overline{EC}_p $\mu\text{S cm}^{-1}$ ‡	\overline{EC}_s $\mu\text{S cm}^{-1}$ b	SC_p (gl^{-1}) #	SC_s (gl^{-1}) ††	SC_m (gl^{-1}) ‡‡
ped	74/ 38	13/ 4	16.4/ 9.5	—/—	7.9/ 4.2
sst	252/136	23/ 32	16.4/ 6.9	3.3/ 1.7	6.7/ 2.8
sh	601/347	190/139	75.7/32.9	30.5/20.0	43.6/23.0

data are given as: dry run/wet run

† ped - pediment

sh - shale

sst - sandstone

‡ average peak value of EC in runoff minus EC of water used for the test

b average steady value of EC in runoff minus EC of water used for the test

average peak value of sediment concentration

†† average steady value of sediment concentration

‡‡ average sediment concentration

readily soluble material during transport. Data on the variation in specific conductance through the regolith profile (Sutherland and Bryan, 1988) indicate that the surface silt layer of pediment surfaces has a limited capacity for solute release. It appears that the underlying bedrock, sandstone or shale, did not affect solute concentrations. The reason for this is unclear. \underline{EC}_p was lower during the wet run than during the dry run, indicating exhaustion of the solute supply. \underline{EC}_s was similar for the wet and dry run. During the tests the EC fell exponentially and reached a steady level slightly higher or equal to the EC of the water used for the test.

The moisture profiles before and after the tests indicate that on that part of pediment surfaces covered with stable sheetwash deposits in which vesicular layers have developed water did not infiltrate deeper than ca. 5 mm. This is supported by visual observations of the typical depth of wetting. On areas with a thin or negligible cover of sheetwash deposits the infiltration of water increased significantly. The moisture profile on such a pediment underlain by shale was comparable to that on shale plots. However, EC's on these plots were similar to those on plots with a sheetwash deposit. Sediment concentrations on pediment plots were slightly higher or comparable to those on sandstone plots (Table 3.3). The lowest sediment concentrations were found on plot A1, which was located in a small channel where deposits had reached a thickness of 2.5 to 10 cm. The upper 2 mm of the deposit was compacted, reducing infiltration and, probably, erosion rates.

The rate of solute release on sandstone surfaces was initially higher than on the pediment surfaces, as the values of \underline{EC}_p indicate. However, \underline{EC}_s for the pediment and sandstone surfaces were similar. Thus, the initial solute supply on sandstone surfaces appears to be rapidly exhausted, and the rate of solute release becomes very low thereafter. Sediment concentrations on the sandstone surfaces were slightly lower or similar to those on pediment surfaces (Fig. 3.14), and for the majority of tests the sediment concentration/discharge relationship was indicative of an exhaustion of the sediment

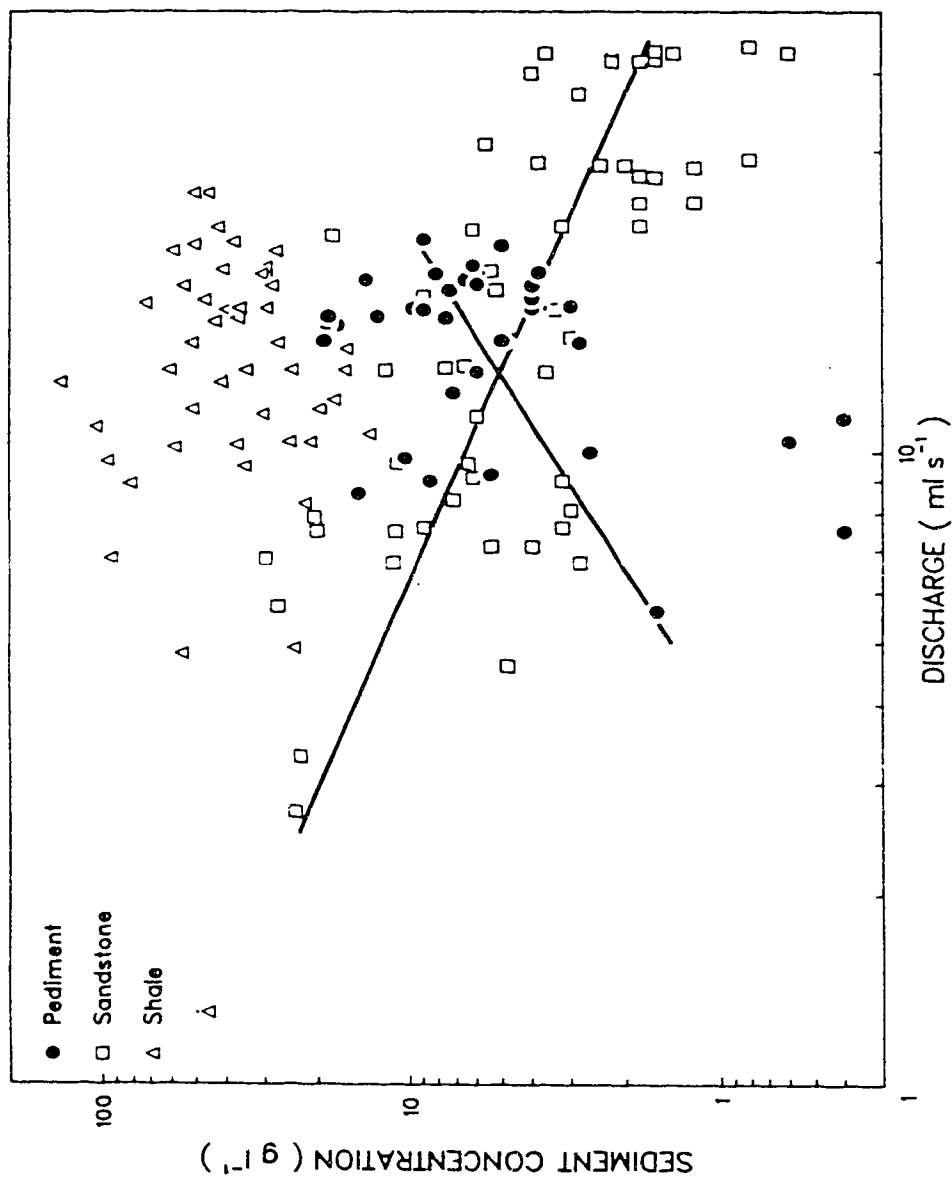


Fig. 3.14 Sediment concentration/discharge data for the dry runs of the direct runoff tests, showing the contrasts in sediment yields between the pediments, sandstones, and shales.

supply. Under wet conditions, the weathering rind acted as an additional sediment source, especially in rills where the thickness of the weathering rind is much greater than on the interrill areas. The sediment contributed by the weathering rind, however, did not affect solute concentrations. Sutherland and Bryan (1988) found that the EC of a 1:5 regolith/distilled water paste was $480 \mu\text{S cm}^{-1}$, which indicates that the weathering rind has a considerable potential for solute release. In the rills, the weathering rind likely loses most of its solutes during the early phases of a test, thus contributing to the initial high EC. In addition, the weathering rind in a rill may be supplemented by silty deposits derived from the interrill areas, which have lost most solutes during transport. Thus, when the deposit in the rills is eroded, solute levels are not affected.

In the rills on the plots, water infiltrated to depths in excess of 2 cm. Typically, the depth of water infiltration on the sandstones equals the thickness of the weathering rind (Bryan and Hodges, 1982). The greater depth of infiltration in the rills is associated with a greater thickness of the weathering rind. In addition, rills tend to exploit fractures in the bedrock which may serve as pathways for runoff and thus augment infiltration. Clay bands deposited along such planes support this idea.

The highest solute concentrations occurred on the shale surfaces, with both \underline{EC}_p and \underline{EC}_s being considerably higher than on the sandstone and pediment surfaces (Table 3.3). Generally, the EC decreased exponentially during the test, indicating a decrease in the supply of solutes. Values of \underline{EC}_s were quite high, indicating that shale surfaces can serve as an important source of solutes in the badlands. Sediment concentrations in runoff from the shale surfaces were also considerably higher than in that from the sandstone and pediment surfaces, especially under wet conditions, when the strength of the material was low.

Included in Fig. 3.14 are rating curves for the relationship between sediment concentration and discharge of the different surface units. The equation of the regression line is

$$SC = 0.18 Q^{1.29} \quad [3.1]$$

(n=37, r²=0.178, P<0.01) for the pediments, and

$$SC = 53.6 Q^{-0.91} \quad [3.2]$$

(n=56, r²=0.521, P<0.001) for the sandstones. For the shales, the correlation of sediment concentration and discharge is non-significant. Although the equations show general trends and testify to the differences between the surface units, the values of r² indicate that the scatter of the data around the rating curves is considerable.

Laronne (1982) and Laronne and Shen (1982) investigated the effect of slope length during direct-runoff tests, and found that sediment and solute concentrations increased downslope. This effect was most pronounced, however, with slope lengths exceeding those used in the present study by a considerable margin. Over shorter distances of up to 5 m the increases in sediment and solute concentrations were much smaller, if present at all. Data from the present study give no conclusive evidence for increasing sediment and solute concentrations with slope length, likely because of the small range of slope lengths used (Table 3.1), so that its effect was overshadowed by that of differences in plot characteristics.

Figure 3.15 shows the variables measured during the direct-runoff tests, and indicates how they interact. Discharge is the independent variable, externally controlled by application rate, that determines sediment concentration. Increasing the discharge results in increasing flow capacity, causing higher erosion rates and sediment concentrations. Increasing discharge may also result in more dilution, so that EC's decrease. On the other hand, increasing erosion rates and sediment concentrations may be accompanied by the exposure of fresh, readily soluble material, so that in this case an increasing discharge would cause a rise in EC. In addition, EC and sediment concentration interact because low

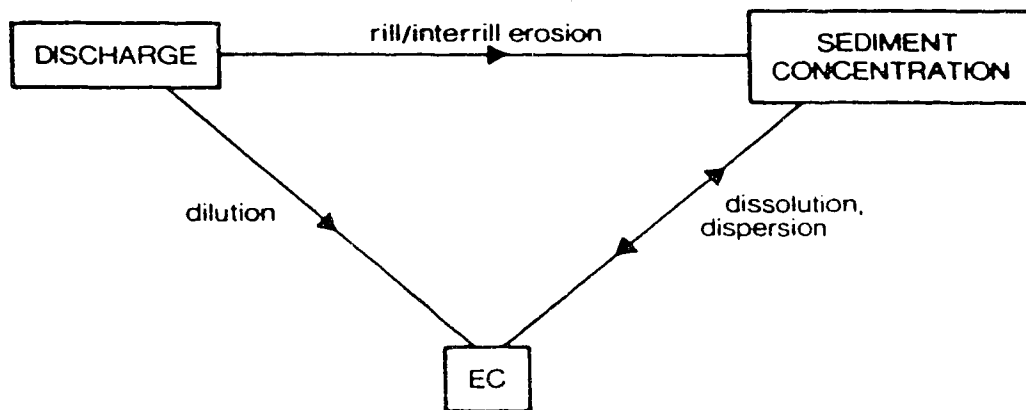


Fig. 3.15 Variables measured during direct-runoff tests, and the processes whereby they interact.

EC's and high Na concentrations are conducive to dispersion, which would cause an increase in sediment concentrations. Not included in Fig. 3.15 are the two outside factors of, first, supply-limited conditions controlling solute and sediment concentrations in the later stages of tests; second, microscale slumps and mudflows occurring independently of discharge.

3.3 RAINFALL SIMULATION TESTS

3.3.1. EXPERIMENTAL DESIGN

Artificial rainfall was applied to experimental plots with a portable rainfall simulator built following the design of Riezebos and Seyhan (1977) (Fig. 3.16 and 3.17). For practical reasons, this design was modified on several minor points. The dimensions of the plexiglas box were increased so that the wetted area measured ca. 80 X 80 cm. The drop-forming devices were made of Tygon tubing with an internal diameter of 0.79 mm (1/32 inch). In order to improve the capillary action and to lower the rainfall intensity, a section of monofilament nylon 18.0 kg (40 LB) fishing line with a diameter of 0.6 mm was inserted into each drop-forming tube. Water was supplied to the box from a jerrycan modified to function as a constant-head device according to the Mariotte principle. The rainfall intensity was controlled by varying the flowrate to the box. The hydrostatic pressure in the box, visible by the height of rise of a column of water open to the atmosphere, served as an indicator of rainfall intensity (Fig. 3.17). Rainfall intensities ranged from 15 to 40 mm h⁻¹, with the majority of tests falling in the 20 to 25 mm h⁻¹ range. A 1 mm mesh was supported 15 cm below the drop-formers. This mesh broke down the drops to a much finer spray. It also increased the spatial uniformity of the rainfall, as the fine drops falling from the mesh were randomly spread out over a certain area. A



Fig. 3.16 Experimental set-up during rainfall simulation on plot BR3. The sample is taken at the plot outlet, where a funnel made of thin aluminum is installed. The windscreen wrapped around the frame minimizes disturbance of the rainfall by wind.



Fig. 3.17 Detailed view of the rainfall simulator. The plexiglas box is fed from the blue jerrycans acting as constant-head devices. The vertical tubes are open to the atmosphere, and allow expulsion of air from the box during filling. The water level in these tubes provides an indication of the water pressure in the box, and hence of the rainfall intensity. Suspended below the drop-formers in the bottom of the box is a mesh for breaking up the drops into smaller sizes.

transparent plastic windscreen was wrapped around the frame of the simulator to minimize disturbance of the rainfall pattern by wind.

Experimental plots were selected on the basis of surface topography. To eliminate disturbance from the installation of artificial plot boundaries, only plots were used on which the microtopography of the plot provided a natural drainage divide. Because of the absence of plot boundaries, under the wet conditions of the final stages of tests minor lateral subsurface flow losses may have occurred. The disadvantage of such losses is likely more than offset by the elimination of proportionally large edge effects caused by boundary conditions on small plots. Under dry conditions, during the early stages of tests, lateral losses can be expected to be minimal. Thresholds of runoff generation are hence unlikely to be affected.

At the plot outlet a funnel made of thin aluminum was installed to facilitate taking representative samples of the runoff. Because the expulsion of air from the box and the drop-formers caused unpredictable variations in rainfall intensity at the beginning of each test, the plot surface was initially covered by a sheet of plastic. This sheet was removed when the desired rainfall intensity was attained. Frequent intensity measurements were carried out with a hand-held standard rain gauge to establish the variation during each test. Causes of this variation were differences in temperature of the water supply causing variations in viscosity, development of air bubbles in the drop-formers and in the hoses feeding the water into the box, and clogging of the drop-formers by remobilization of deposits which built up inside the rainfall simulator.

During the tests, discharge was estimated by measuring the volume of runoff collected in a sample bottle over a known period of time. The sediment concentration of this sample was subsequently determined in the laboratory. Additional samples were taken to measure the EC of the runoff. The EC was measured in the field, directly after sampling. Sampling intervals generally varied from 3 to 9 minutes.

The water used for the test was from the locally pumped supply at the Dinosaur Provincial Park campsite, and had an EC_0 of 1135 to 1160 $\mu\text{S cm}^{-1}$. Despite its high EC, this water was more suitable for the rainfall simulations than the Red Deer River water used in the direct-runoff tests, as it was feared that the small amount of fine sediment present in the Red Deer River water would clog the drop-formers. As with the direct-runoff tests, EC_0 is subtracted from the EC's measured in the plot runoff, and in the following sections, \underline{EC} , \underline{EC}_p , and \underline{EC}_s represent the corrected EC's and peak and steady value of the EC, respectively, whereas EC , EC_p , and EC_s indicate uncorrected values. This procedure allows comparison between the plots, and between the rainfall simulations and direct-runoff tests.

On sandstone and pediment plots, the test was carried out at least twice. First under dry antecedent moisture conditions ('dry run'), and, usually immediately following the dry run, under wet antecedent moisture conditions ('wet run'). Because of adverse wind conditions, the test on plot BR7 was twice discontinued after the dry run, so that for this plot data from three dry runs and one complete wet run are available. Before the dry run and after the wet run, samples of the crust and the underlying materials were taken on each plot to determine the gravimetric moisture content. Runoff generation on the shale plots required a very long dry run. To save water and time, a wet run was not carried out on the shale plots. Previous rainfall simulations have indicated that under wet conditions runoff generation on the shales is rapid (e.g. Bryan et al., 1978). Table 3.4 gives the characteristics of each plot, and Fig. 3.2 and 3.3 show the locations of the plots within Subbasins A and B. Table 3.5 provides an overview of the test results. On the sandstone and pediment plots, the duration of the test was 3600 to 4800 s for the dry run. During the wet run the duration of the test was decreased to ca. 2400 s because a steady discharge was attained rapidly. On the shale plots the test duration ranged from 6800 to 9700 s for the dry run.

Table 3.4 Characteristics of rainfall simulation plots

plot no.	surface unit†	slope (°)
BR1	ped/sst	7
BR2	ped/sst	9
BR3	ped/sst	5
BR4	ped/sst	2
BR5	sst	32
BR6	sst	32
BR7	sst	31
BR8	sst	32
BR9	sh	8
BR10	sh	23
BR11	sh	20
BR12	sh	9
AR1	ped/sh	5
AR2	ped/sh	6

† sst - sandstone

sh - shale

af - alluvial fill

ped/sst - pediment in sandstone

ped/sh - pediment in shale

Table 3.5 Overview of results of rainfall simulations

plot no.	surface unit †	EC ₀ (μS cm ⁻¹) †		EC _p (μS cm ⁻¹) †		EC _s (μS cm ⁻¹) †		EC _s (μS cm ⁻¹) †		start of runoff (s) †		threshold of runoff (mm) †		RC (%) †	SC _p (gl ⁻¹) †	SC _s (gl ⁻¹) †	SC _m (gl ⁻¹) †
		†	†	†	†	†	†	†	†	†	†	†	†				
BR1	ped/sst	1160/1160	1440/1320	280/160	1256/1320	96/160	226/0	0.6/0	45/56	17.6*/18.4*	--/--	12.1/15.2					
BR2	ped/sst	1140/1140	1280/1260	140/120	1230/1255	90/115	80/0	0.9/0	65/64	18.6*/19.0*	--/--	16.3/14.3					
BR3	ped/sst	1140/1140	1260/1210	120/70	1185/1206	45/66	973/0	3.0/0	31/52	5.4*/3.2*	3.2/2.8	3.5/2.8					
BR4	ped/sst	1120/1120	1270/1240	150/120	1203/1177	83/57	479/0	3.5/0	52/46	4.6/3.8*	3.3/3.3	3.4/3.3					
BR5	sst	1140/1140	1370*/1420	230*/280	--/1333	--/193	293/55	2.2/0.3	74/52	28.0*/27.6*	--/--	21.0/20.1					
BR6	sst	1140/1140	1770/1490	630/350	--/1300	--/160	330/0	1.4/0	56/55	46.6*/31.8*	--/--	36.6/26.8					
BR7	sst	1140/1140	1360/1500	220/360	--/--	--/--	413/56	2.3/0.2	75/--	27.0*/--	--/--	20.4/--					
BR7	sst	1140/--	1420/--	280/--	1342/--	202/--	210/--	1.1/--	78/--	22.4*/--	--/--	17.0/--					
BR7	sst	1140/1140	1380/1300	240/160	--/1250	--/110	347/32	1.5/0.2	88/94	18.8*/23.8*	--/--	14.1/17.1					
BR8	sst	1125/1125	1410/1335	285/210	--/1284	--/159	100/20	0.7/0.1	47/58	25.6*/27.0*	--/--	18.5/18.6					
BR9	sh	1140	1510*	370*	--	--	4433	24.9	20	28.4*	--	25.8					
BR10	sh	1150	1830	680	--	--	2672	17.8	31	71.8*	--	58.6					
BR11	sh	1140	2000	860	1703	563	2510	14.1	30	74.4*	--	65.0					
BR12	sh	1140	1700	560	1583	443	1815	11.0	30	85.0*	--	73.6					
AR1	ped/sh	1135/1135	1340/1320	205/185	1263/1280	128/145	265/0	1.7/0	46/53	11.0*/12.9*	8.2/9.3	8.7/9.7					
AR2	ped/sh	1135/1135	1320/1305	185/170	1249/1260	114/125	614/0	4.2/0	43/60	14.0*/13.0*	12.0/12.5	12.0/12.0					

Table 3.5 Supplementary notes

data are given as: dry run/wet run

— - no data available

† sst - sandstone

sh - shale

af - alluvial fill

ped/sst - pediment in sandstone

ped/sh - pediment in shale

‡ EC of water used for the test

‡ peak value of EC in runoff (* indicates that peak value did not occur during the first stage of flow.)

peak value of EC in runoff minus EC of water used for the test

†† steady value of EC in runoff

††† steady value of EC in runoff minus EC of water used for the test

‡‡ time between beginning of test and the start of runoff

mm of rainfall needed to generate runoff

††† runoff coefficient = total discharge / total rainfall * 100 per cent

†††† peak value of sediment concentration

‡‡‡ steady value of sediment concentration

average sediment concentration

3.3.2 RESULTS

3.3.2.1 PEDIMENT SURFACES

\underline{EC}_p ranged from 120 to 280 $\mu\text{S cm}^{-1}$ for the dry run, and from 70 to 185 $\mu\text{S cm}^{-1}$ for the wet run. In general, \underline{EC}_p was lower for the wet run than for the dry run, indicating a diminishing solute supply. However, in most cases the difference in \underline{EC}_p for the dry and wet run was outside the precision of the EC meter. During all runs the EC decreased linearly or exponentially with time, although not as regularly as during the direct-runoff tests. In some cases, variations in EC appeared to be associated with variations in sediment concentration. This suggests that an increase in EC can be caused by an increasing erosion rate on the plot, causing fresh material with a high solute content to be eroded. In other cases, the EC varied independently of the sediment concentration, and variations in EC were associated with discharge variations in the opposite direction. This behaviour indicates a dilution effect analogous to that often observed in streams when an increased proportion of water possessing a lower solute content than the baseflow causes solute concentrations to decrease with increasing flow (Gregory and Walling, 1973). In the case of the rainfall simulations it appeared that the plot could only release solutes to the runoff at a limited rate. When discharge increased, this rate-limited release caused solute concentrations to decrease.

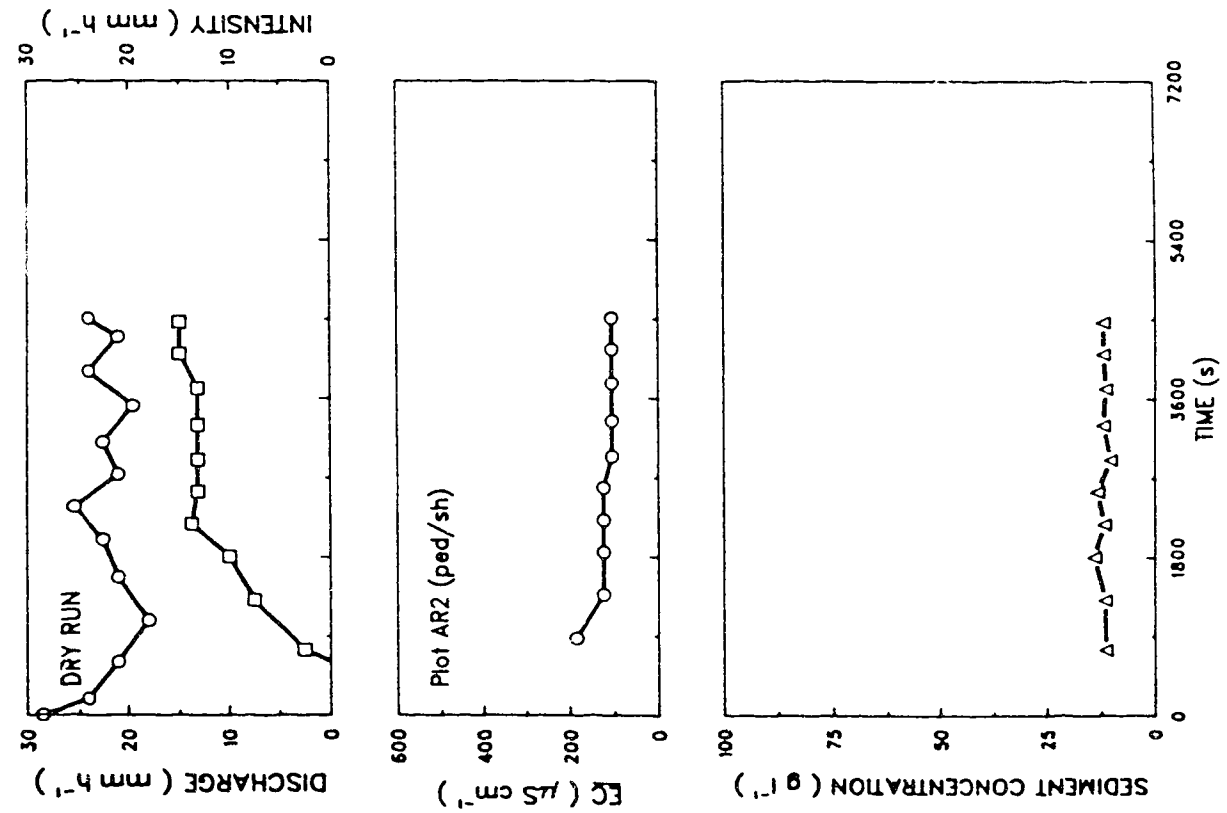
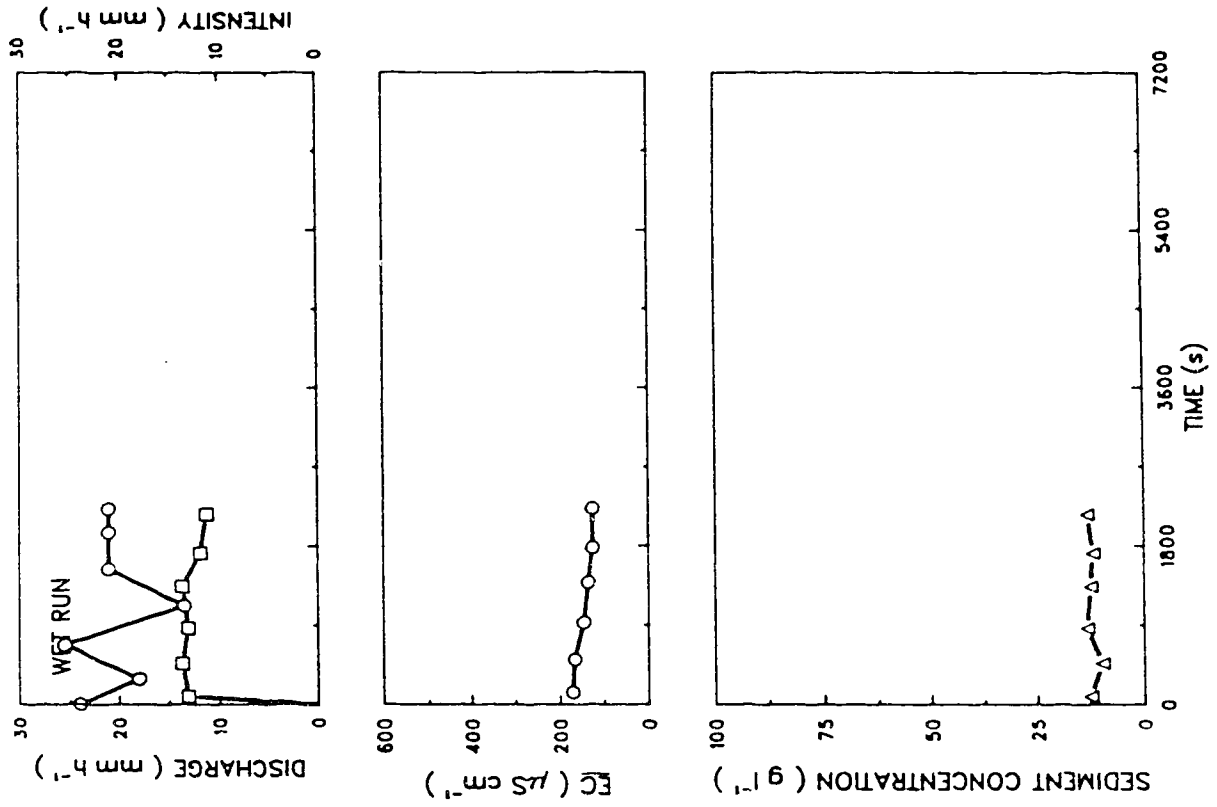
\underline{EC}_s varied from 45 to 128 $\mu\text{S cm}^{-1}$ for the dry run, and from 57 to 160 $\mu\text{S cm}^{-1}$ for the wet run. Generally, \underline{EC}_s increased from the dry to the wet run, although in the majority of cases this increase is outside the range of precision of the EC meter. The most likely cause for the increase in \underline{EC}_s is the dissolution of sediment, which compared to the dry run, can progress to a further stage under the conditions of the wet run. The values of SC_s and SC_m for the dry and the wet run indicate that higher erosion rates and sediment concentrations cannot be a factor here. The time to reach \underline{EC}_s varied from ca. 230 to 1860

s for the dry run, and from 0 to 1800 s for the wet run.

SC_p varied from 4.6 to 18.6 g l⁻¹ for the dry run, and from 3.2 to 19.0 g l⁻¹ for the wet run. Only once did SC_p occur during the initial stages of runoff (Table 3.5). During most tests, sediment concentrations varied, seemingly independent of discharge, around a relatively constant level (Figs. 3.18, 3.19, and Appendix A). In a few cases, however, the variations in sediment concentration followed variations in discharge. On most plots, sediment concentrations during the wet run were similar or slightly higher than during the dry run, probably reflecting the reduced strength of the wet regolith, and the hence increased effectiveness of overland flow and splash detachment. Variations in sediment concentrations precluded calculating SC_s for most plots. Values of SC_s showed considerable variation. On three out of four plots, SC_s remained equal or increased from the dry to the wet run. The exception on plot BR3 may be explained by the lower average rainfall intensity during the wet run on plot BR3, causing discharge and flow capacity to be low.

On the pediments, the underlying bedrock type affected the export of solutes and suspended sediment. Plots on pediment surfaces could be divided into those developed in sandstone (plots BR1 up to BR4), and those developed in shale (plots AR1 and AR2). \underline{EC}_p for both the dry and the wet run were considerably higher on the shale pediments than on the sandstone pediments, with the exception of plot BR1. Similarly, \underline{EC}_s was slightly higher for the dry run on the shale pediments than on the sandstone pediments (with the exception of plot BR1), although in some cases the difference was outside the range of precision of the EC meter. For the wet run, \underline{EC}_s for the sandstone and shale pediments became more similar. SC_p and SC_m appeared not to be influenced by the underlying bedrock.

The four pediment plots on sandstone could be divided into two groups on the basis of solute and sediment export and characteristics of runoff generation. The first group consisted of plots BR1 and BR2. Compared to the second group, consisting of plots



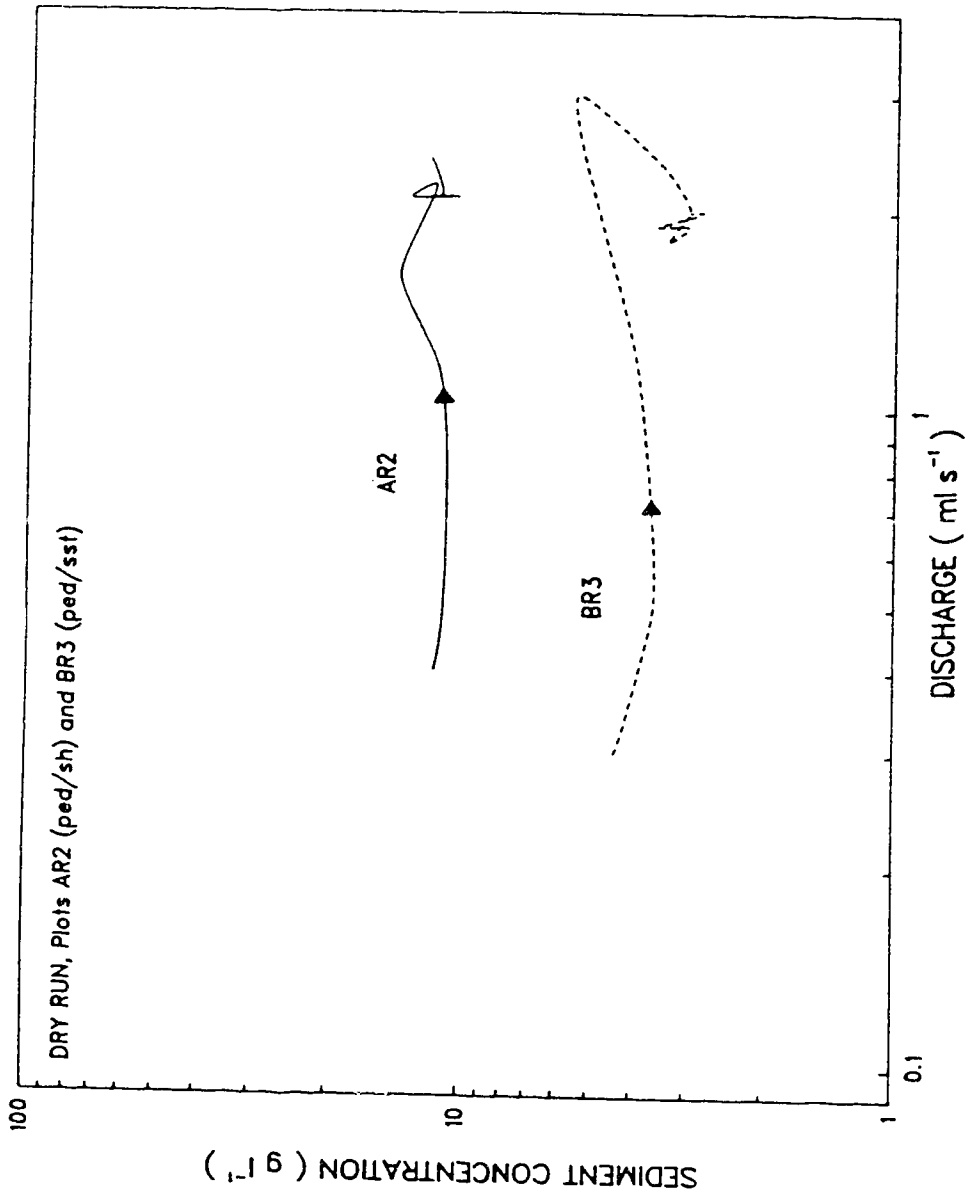


Fig. 3.19 Sediment concentration/discharge relationship for the dry run on plots AR2 and BR3. On plot AR2, sediment concentrations remain relatively constant throughout most of the test, notwithstanding an increase in discharge from 0.4 to 13.7 ml s⁻¹. Plot BR3 shows evidence of initial flushing, followed by a slight increase in sediment concentration as discharge increases. The curve of plot BR3 possesses clockwise hysteresis, indicating a decreasing sediment supply.

BR3 and BR4, these plots showed lower thresholds of runoff generation, higher \underline{EC} , and higher SC_p and SC . In addition, there is some indication that in the first group \underline{EC} increased from the dry to the wet run. The difference between the two groups was most likely caused by the thickness of the sheetwash deposit on the plot. On plots BR1 and BR2 this thickness was only 1 to 2 mm, whereas on plots BR3 and BR4 the sediment thickness reached up to 10 mm. Because the hydraulic conductivity and storage capacity is much higher for the sheetwash deposit than for the sandstone, the increased thickness of the deposit delayed the start of runoff and increased the threshold of runoff generation. The amount of sandstone in contact with runoff was, due to the limited accumulation of sediment on plots BR1 and BR2, much larger there than on plots BR3 and BR4. The sheetwash deposits and the sandstone respond differently when brought into contact with water. The sheetwash deposit has lost most of its clays and solutes during transport, and consists mainly of very fine sand and silt (Hodges, 1982; Bryan et al., 1984). Sutherland and Bryan (1988) report a pediment surface silt layer with an EC of $159 \mu S \text{ cm}^{-1}$, measured on a 1:5 regolith/water paste. Because of its composition, dispersion of the sheetwash deposit is limited. The main mechanism of sediment entrainment and transport is by lift and drag exerted by flowing water. On sandstone plots, dispersion is an important additional mechanism of sediment entrainment due to the presence of highly montmorillonitic clays and large amounts of Na, both adsorbed and as soluble salts, in the regolith. This causes erosion rates to be high so that sediment concentrations in runoff from the sandstone parts of the pediments are much higher than in runoff from the sheetwash deposits.

The subdivision of the pediments in distinctively different areas based on the response to simulated rainfall is at odds with the results from the direct-runoff tests, during which bedrock did not appear to affect response. This contrast likely arises because data from the direct-runoff tests reflect sediment and solute release characteristics in rills and channels, whereas rainfall simulation data also include the response of interrill areas

(Section 3.2.2.1).

The start of runoff on the pediment plots varied from 80 to 973 s for the dry run. During the wet run, the start of runoff was reduced by a significant amount, and runoff was instantaneous on all plots. The threshold rainfall of runoff generation of course behaved similarly, varying from 0.6 to 4.2 mm for the dry run, and becoming 0 mm for the wet run. Runoff coefficients (total discharge/total rainfall X 100 per cent) were high, and ranged from 31 to 65 per cent for the dry run, and from 46 to 64 per cent for the wet run. The steady state infiltration rate f ranged from ca. 8 to 11 mm h⁻¹ on most plots, although values as low as ca. 3 to 4 mm h⁻¹ (plot BK3, wet run) occurred. The surprisingly high value of f_c was caused by lateral subsurface flow from the wet plot to the surrounding dry area. To minimize surface disturbance on the plots, no boundaries to halt lateral subsurface flow were used, resulting in an overestimation of f . During natural rainfall, when the whole surface would be wetted, f would be significantly lower. The moisture profiles (Fig. 3.20) indicate that, on the shale pediments, the depth of moisture penetration was considerably higher than on the sandstone pediments, and comparable to that on shale plots.

3.3.2.2 SANDSTONE SURFACES

The range of \underline{EC}_p was from 220 to 630 $\mu\text{S cm}^{-1}$ for the dry run, and from 160 to 360 $\mu\text{S cm}^{-1}$ for the wet run. During the majority of tests, the EC decreased exponentially with time. Towards the end of the test on some plots the EC increased again. On some plots, this increase could be attributed to a decreasing discharge, as described for the rainfall simulations on the pediment plots (Fig. 3.21, Appendix A). On other plots, the increase of the EC coincided with an increase in sediment concentration. During most of the dry runs and a few wet runs the variation of the EC precluded estimating \underline{EC}_s .

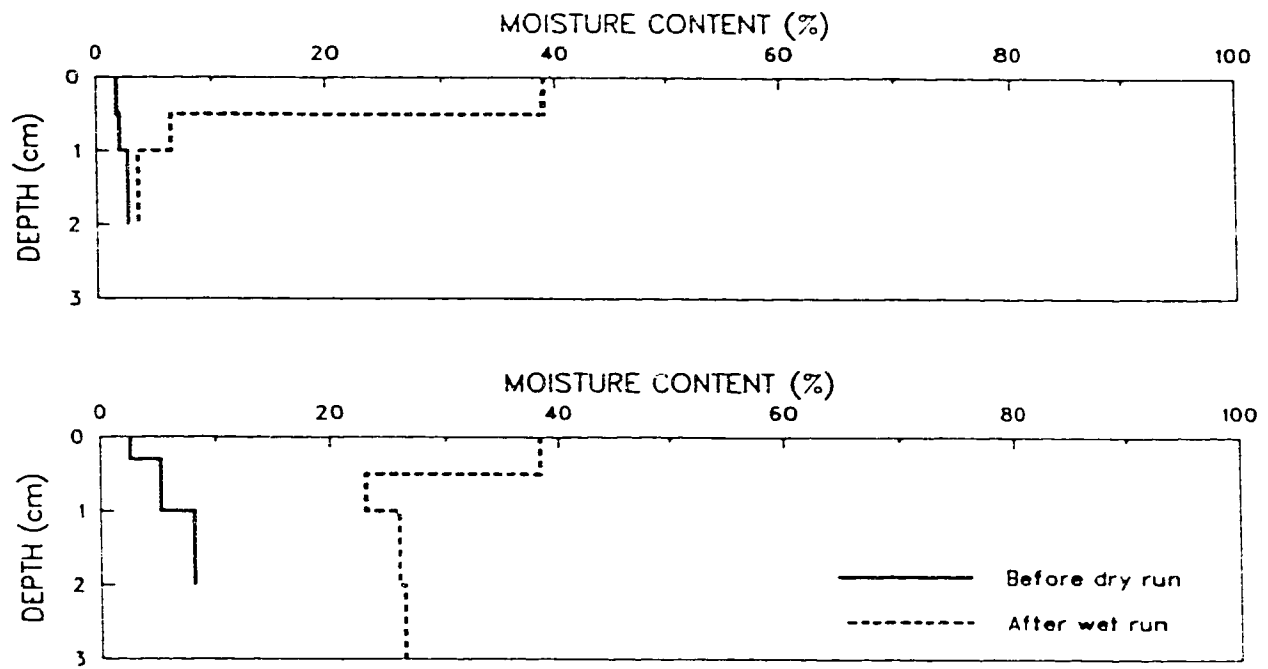
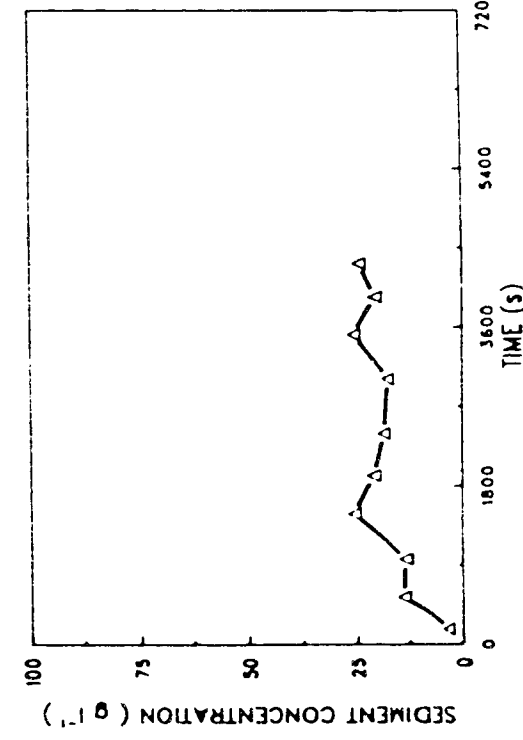
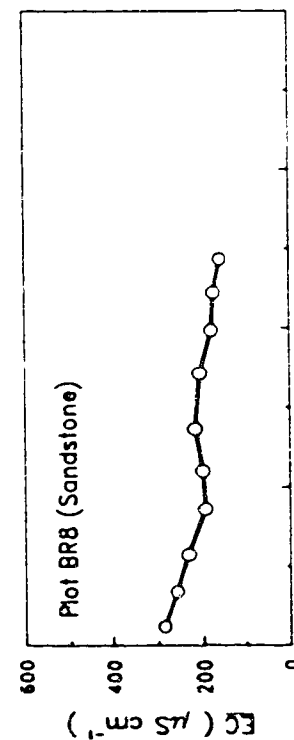
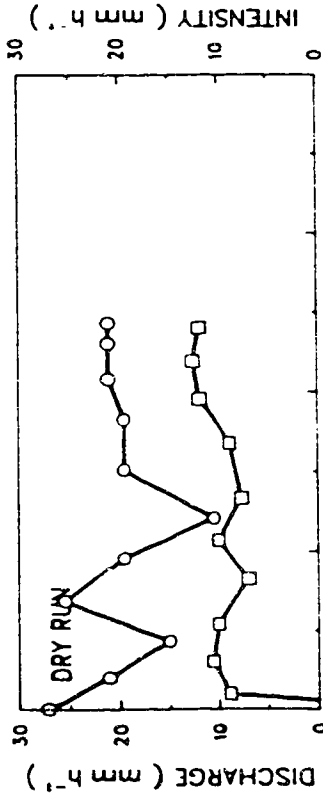
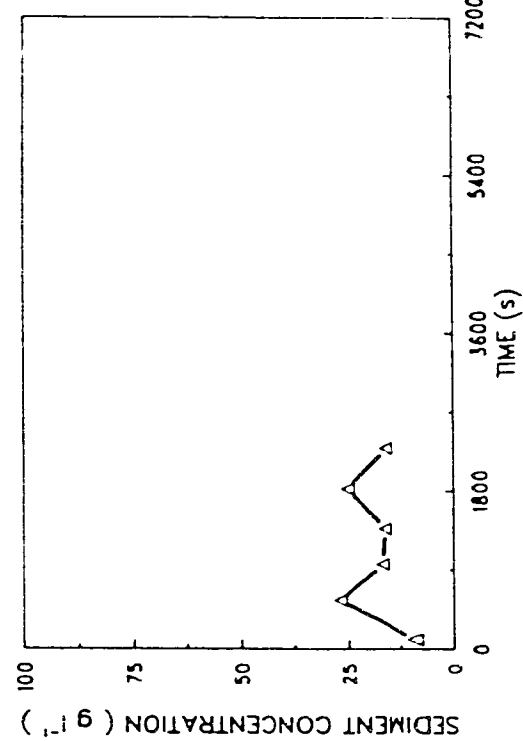
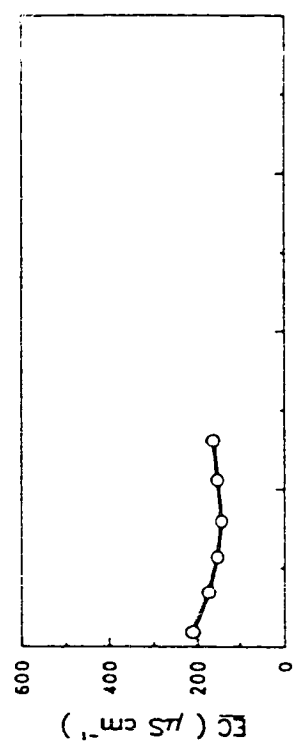
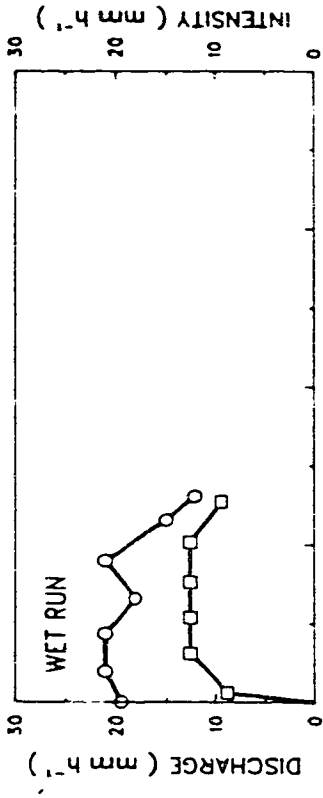


Fig. 3.20 Contrasts between the moisture profiles before the dry, and after the wet run on plots BR2 (top), a sandstone pediment, and AR2 (bottom), a shale pediment.



SC_p ranged from 18.8 to 46.6 g l⁻¹ for the dry run, and from 23.8 to 31.8 g l⁻¹ for the wet run. In all instances, SC_p did not occur during the initial stages of runoff. The sediment concentration varied with discharge (Fig. 3.21, dry run, at ca. 3000 s), but was also affected by small slumps and mudflows occurring independently from the discharge (Fig. 3.21, dry run, at ca. 1500 s). During all tests, variations in sediment concentration precluded calculating SC_s .

The majority of sediment concentration/discharge relationships for the dry runs on sandstone plots indicate exhaustion of the sediment supply (Fig. 3.22). This pattern, however, is complicated by increasing sediment concentrations independently of the discharge, especially during the later stages of tests. As an exception, plot BR8 exhibited an increase in sediment concentrations at a relatively constant discharge during the dry run. This is likely caused by the reduced strength of the wet regolith. During the wet run, this factor also strongly affects the sediment concentration discharge relationship, and most plots show a relatively steep increase in sediment concentrations at slowly rising discharges.

Because of the variability of the sediment concentration, the average value SC_m may provide further insight into the characteristics of sediment export from sandstone plots. SC_m ranged from 14.1 to 36.6 g l⁻¹ for the dry run, and from 17.1 to 26.8 g l⁻¹ for the wet run. The lowest value of SC_m occurred during the third dry run on plot BR7 (Table 3.5). SC_m decreased from the first to the third dry run on plot BR7. This decrease reflects the decrease in average rainfall intensity, rather than exhaustion of the sediment supply. If the data from the second and third dry run on plot BR7 are left out, SC_m is higher for the sandstone plots than for the pediment plots, both during the dry and wet run.

The start of runoff varied from 100 to 413 s for the dry run. For the wet run a considerable decrease occurred, and the start of runoff varied from 0 to 56 s. Similarly, the threshold of runoff varied from 0.7 to 2.3 mm for the dry run, and from 0 to 0.3 mm for the wet run. Runoff coefficients were very high, and ranged from 47 to 88 per cent for the

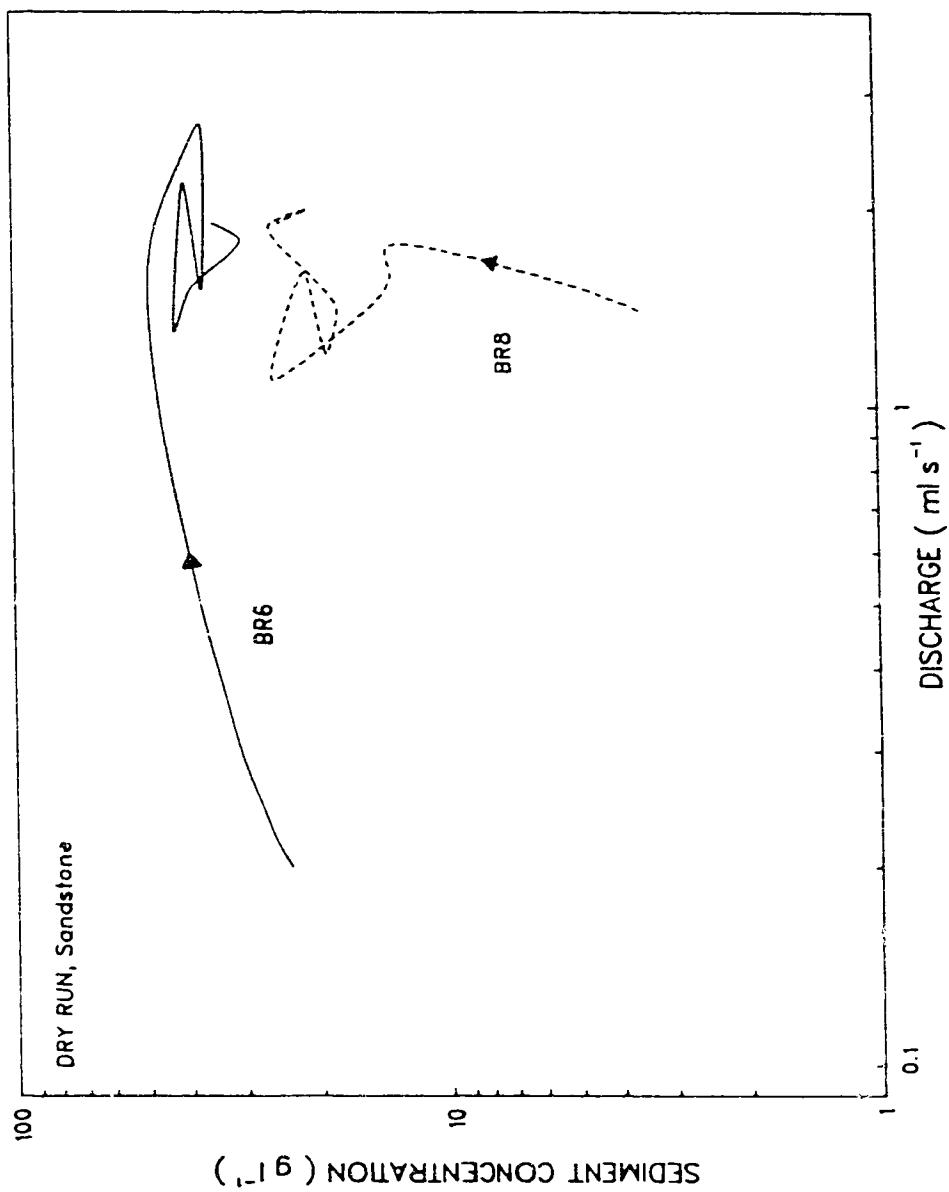


Fig. 3.22 Contrasting sediment concentration/discharge relationships for the dry runs on plots BR6 and BR8. Plot BR6 shows exhaustion of the sediment supply, whereas plot BR8 displays an increase in sediment concentration at a relatively constant discharge.

dry run, and from 52 to 94 per cent for the wet run. The steady state infiltration rate f_c varied from ca. 4 to 9 mm h⁻¹, with most values lying in the range of 8.5 to 9 mm h⁻¹. As stated earlier, the unexpectedly high values of f_c were likely caused by lateral subsurface flow from the wet plot to the surrounding dry area. The moisture profile indicates that wetting occurred to depths in excess of 10 mm (Fig. 3.23). The rise of moisture content at this depth, however, is in the range of only 2 to 4%, and most of the water does not infiltrate more than a few mm.

On the whole, the test results did not indicate significant differences in response between the four sandstone plots.

3.3.2.3 SHALE SURFACES

On the shale plots, EC_p ranged from 370 to 860 $\mu\text{S cm}^{-1}$. EC_p did not occur at the beginning of runoff on plot BR9, but instead at the end of the test. The rise in EC at the end of this test can be attributed to a decreasing discharge. On two plots, the EC decreased exponentially, and reached a relatively steady level of 563 and 443 $\mu\text{S cm}^{-1}$ on plots BR11 and BR12, respectively (Fig. 3.24, Appendix A). On plot BR10, the EC decreased exponentially but did not reach an equilibrium level. On plot BR9, the EC remained relatively steady during the test, except for the slight increase at the end. During all tests the EC showed some variability which could be attributed to variations in discharge and sediment concentration.

Sediment concentration varied considerably during the tests. SC_p ranged from 28.4 to 85.0 g l⁻¹, and did not occur during the initial stages of runoff (Table 3.5). A similar range of values was shown by SC_m , which varied from 25.8 to 73.6 g l⁻¹. During none of the tests did the sediment concentration reach a steady level. Instead, sediment concentrations generally tended to increase towards the end of the tests (Figs. 3.24, 3.25).

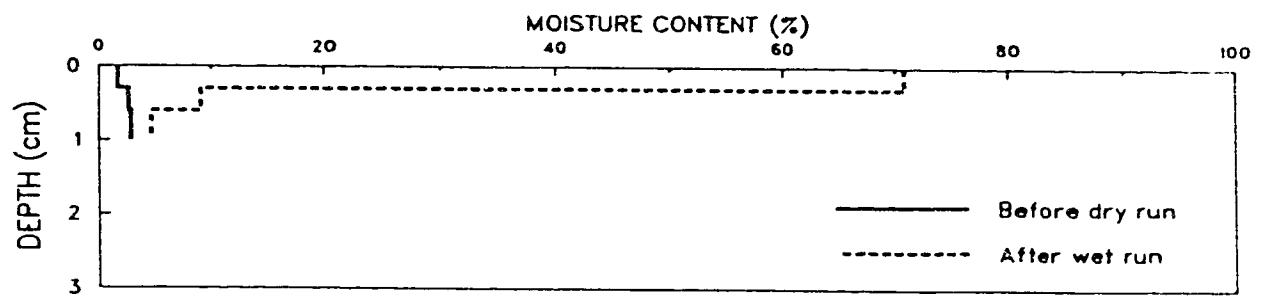


Fig. 3.23 Moisture profiles before the dry, and after the wet run on a representative sandstone plot (BR8).

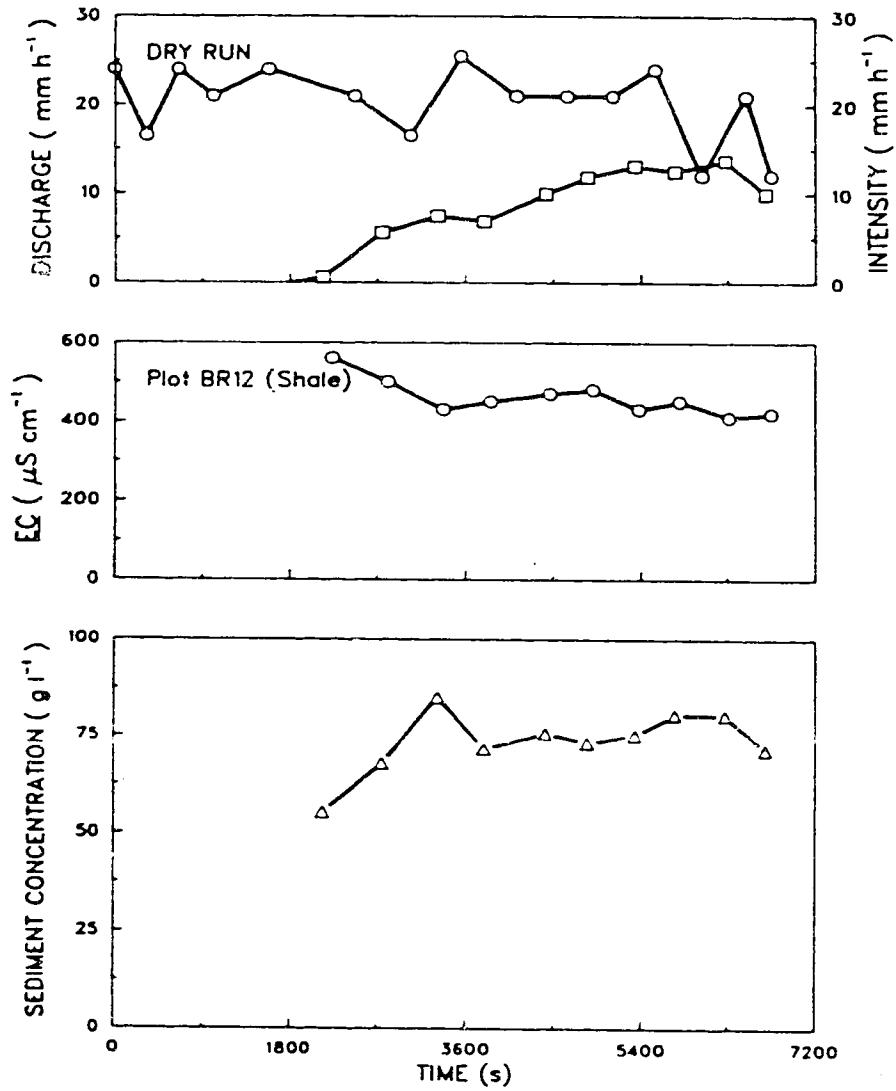


Fig. 3.24 Test results for a representative shale plot (BR12), showing a large lag between the beginning of the test and the start of runoff; high, and exponentially decreasing EC's; and high, and generally increasing sediment concentrations.

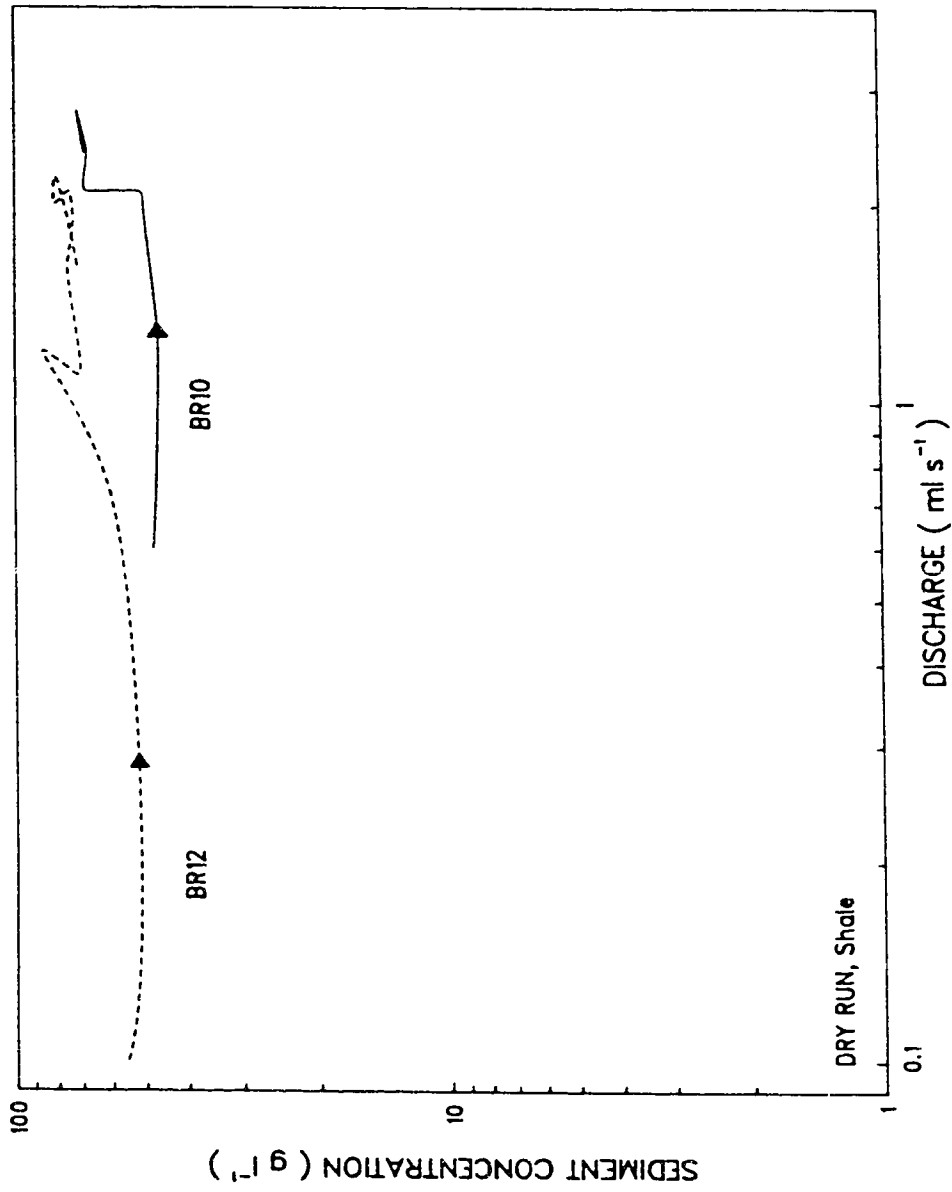


Fig. 3.25 Sediment concentration/discharge relationships for the dry runs on plots BR10 and BR12. Plot BR10 shows increasing sediment concentrations from 50.4 to 68.4 g l⁻¹ at a constant discharge. On plot BR12, microscale slumps and mudflows cause variations in sediment concentration during the later stages of the test.

Because discharge also increased during the tests, part of the increase in sediment concentration may be attributed to increasing flow capacity. Another important factor is the progressively reduced strength of the material during wetting and dispersion of the regolith, causing increased erosion rates on the plot. On plot BR10, for example, a steady increase in sediment concentration from 50.4 to 68.4 g l⁻¹ occurred over a period of 20 min while discharge remained constant at 2.1 ml s⁻¹, ruling out increasing flow capacity as a factor (Fig 3.25). In addition, microscale slumps and mudflows often occurred under the wet conditions of the later stages of tests, causing seemingly random variations in sediment concentration (Fig. 3.25).

The start of runoff on the shale plots varied from 1815 s (ca. 30 min) to 4430 s (ca. 74 min). The threshold of runoff reached similar high values, and varied from 11.0 to 24.9 mm. The steady state infiltration rate f_c was ca. 10 mm h⁻¹. As on the pediment and sandstone plots, the high value of f_c was likely caused by lateral subsurface flow from the wet plot to the surrounding dry area. Both the start of runoff and the threshold of runoff reached their highest value on plot BR9. On this plot the aluminum funnel for sampling the flow was located at the surface of the popcorn crust. During the test a considerable amount of subsurface flow occurred on top of the dense subcrust, and runoff on the dense subcrust preceded runoff on the popcorn crust by ca. 20 minutes. Runoff from the popcorn crust only started after the extensive crack system of this crust was sealed to a considerable extent. Prior to this, flow on the plot surface was intercepted by the cracks, so that flow was limited to localized patches. The penetration into the subsurface of runoff intercepted by the cracks was impeded by the dense subcrust. The crack density of the subcrust was far less than that of the popcorn crust, so that the subcrust acted as a barrier to infiltrating water, which was diverted laterally downslope. The result was that runoff on top of the dense subcrust preceded runoff on top of the popcorn crust by a significant amount of time. Data from plot BR9 therefore pertain to processes of the popcorn crust. On plots BR10, BR11, and BR12 the funnel was located at the top of the dense subcrust,

and data from these plots therefore concern processes occurring both in the popcorn crust and on the subsurface crust. When the start of runoff from plot BR9 is taken as the moment that subsurface flow starts, the start of runoff and the threshold of runoff of this plot become much more similar to those of the other shale plots. The difference between plots BR9 and the other shale plots is also visible in the runoff coefficient, which was only 20 per cent on plot BR9, but ranged from 30 to 31 per cent on the remaining shale plots.

The differences between plot BR9 on one hand, and plots BR10, BR11, and BR12 on the other hand, were also visible in the EC and sediment concentrations. The EC on plot BR9 remained relatively steady during the test, and only rose slightly towards the end, whereas on the other shale plots the EC decreased exponentially. In addition, the EC on plot BR9 was overall significantly lower than on the other plots. Sediment concentrations were also much lower on plot BR9 than on the other shale plots, as the values of SC_p and SC_m indicate. A similar difference between the popcorn and the subsurface crust was found by Sutherland and Bryan (1988), who, on a 1:5 regolith/water paste of yellow shale, measured an EC of 636 and 860 $\mu\text{S cm}^{-1}$ for the popcorn and subsurface crust, respectively. On grey shale, the value of the EC was 743 and 1040 $\mu\text{S cm}^{-1}$ for the popcorn and subsurface crust, respectively (Sutherland and Bryan, 1988).

The moisture profile illustrates the high water-holding capacity of the shale regolith (Fig. 3.26). Samples were taken from rill and interrill areas, and consisted of the popcorn crust for the interrill sample, and of the popcorn crust or silty deposit, and subsurface crust for the rill samples. The moisture content of the surface layer reflects the differences in material between these areas. Interrill areas, where the surface material consists of popcorn crust, showed moisture contents ranging from 97.7 to 173.8 per cent, whereas the moisture content on rill bottoms ranged from 58.8 to 108.6 per cent. The material in the rills usually is more silty because of the deposition of material in the depressions. Prolonged deposition may lead to the formation of silt stringers, acting as zones of rapid runoff generation, and strongly influencing patterns of runoff generation

and erosion on the shale surfaces. Because of the lower clay content, the material in the rills does not absorb as much water as the interrill popcorn crust. The moisture profile also indicates that, compared to the sandstone and pediment plots, water infiltrated to greater depths on the shales. Because of the structure of the popcorn and subsurface crust, large differences over short distances in moisture content will occur on the shale plots. The moisture profile in Fig 3.26 therefore represents an average moisture content for a situation in which dry and saturated zones are closely intermingled.

3.3.3 DISCUSSION

Results from the simulated rainfall tests on the whole support findings from the direct-runoff tests. On pediments, runoff generation was rapid compared to the sandstones and shales, but only minor amounts of solutes and sediment were released (Fig. 3.27, Table 3.6). The response to rainfall of the pediment plots was affected by the underlying bedrock and by the thickness of the sheetwash deposit. Treating the pediment surfaces as homogeneous may therefore not always be justified. Pediments could be divided into three types: (1) underlain by sandstone (plots BR1 and BR2), (2) underlain by shale (plots AR1 and AR2), and (3) covered with a silty sheetwash deposit (plots BR3 and BR4). Runoff generation occurred fastest on the sections of pediment underlain by sandstone, followed by the sections underlain by shale and those covered with a sheetwash deposit. The differences with regard to runoff generation are likely most pronounced during very small storms, and will become less important with increasing storm size. Differences in the characteristics of solute and sediment release of the different parts of the pediment are probably not affected by storm size. On all pediments, the release of solutes followed the same pattern of exponential decrease to a steady value. The initial peak and the steady values of the EC were highest on pediment plots underlain by shale. On pediment plots

Table 3.6 Summary of results of rainfall simulations

surface unit	\overline{EC}_p $\mu\text{S cm}^{-1}$	\overline{EC}_s $\mu\text{S cm}^{-1}$	SC_p (gl^{-1})	SC_m (gl^{-1})
†	‡	P	#	††
ped	180/138	93/111	11.9/11.7	10.2/ 8.6
sst	314/272	—/156	28.1/27.6	20.7/19.9
sh	618	—	64.9	56.5

data are given as: dry run/wet run

† ped - pediment

sh - shale

sst - sandstone

‡ average peak value of EC in runoff minus EC of water used for the test

P average steady value of EC in runoff minus EC of water used for the test

average peak value of sediment concentration

†† average sediment concentration

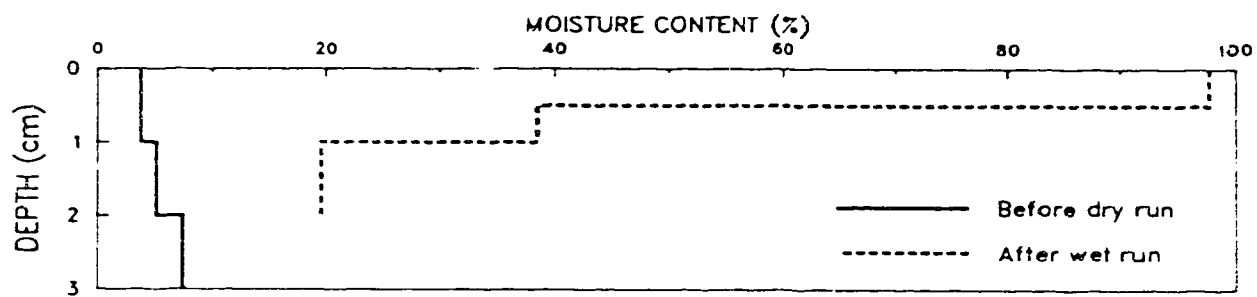


Fig. 3.26 Moisture profiles before the dry, and after the wet run on a representative shale plot (BR12).

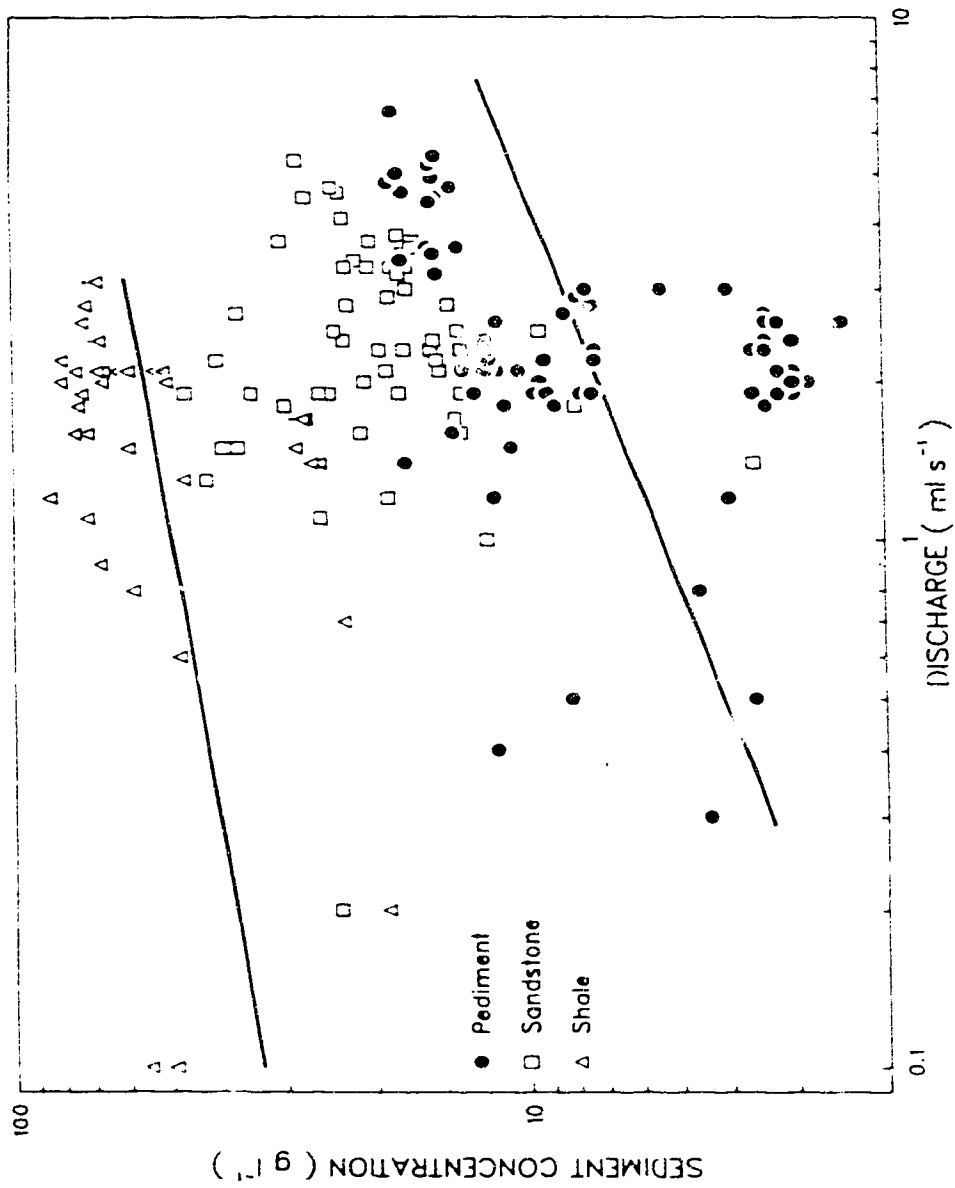


Fig. 3.27 Sediment concentration/discharge data for the dry runs of the rainfall simulations, showing the contrasts in sediment yields between the pediments, sandstones, and shales. Data for the wet runs on the pediments and the sandstones display a similar pattern.

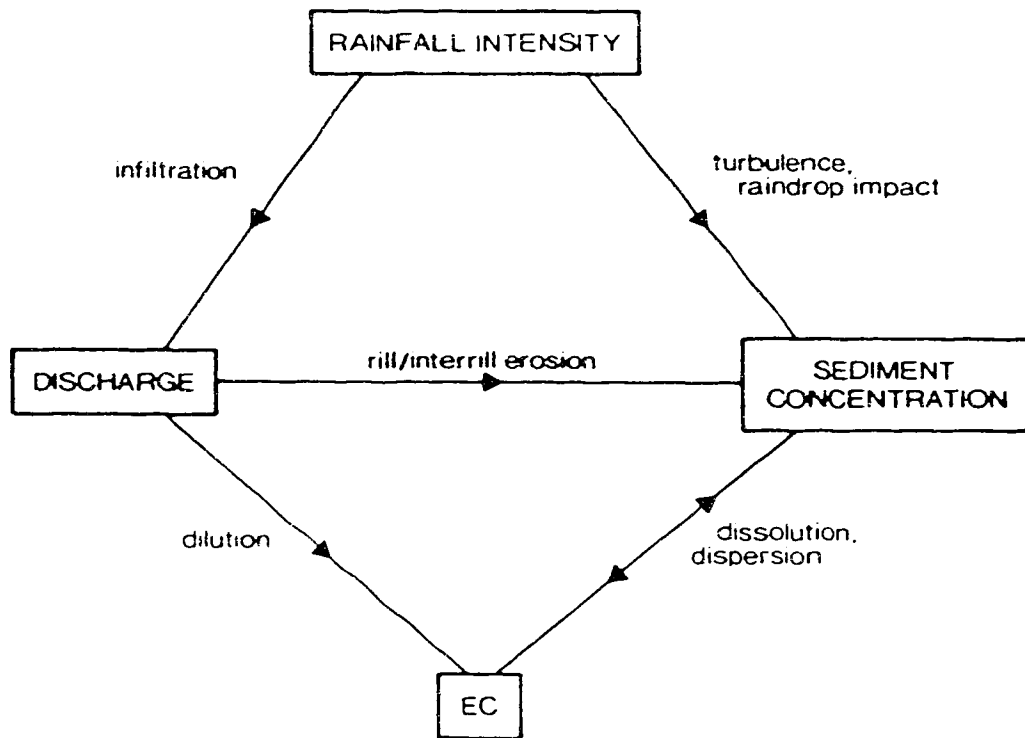


Fig. 3.28 Variables measured during rainfall simulations, and the processes whereby they interact.

underlain by sandstone and on those covered with a sheetwash deposit the initial peak and steady values of the EC were similar, and lower than on the pediment plots underlain by shale. Pediment plots covered with a sheetwash deposit showed very low sediment concentrations. On pediment plots underlain by sandstone and shale, sediment concentrations were similar, and three to four times higher than on the plots covered by sheetwash deposit (Table 3.5).

The sandstone surfaces showed a rapid response to rainfall, and thresholds of runoff generation were similar to those on pediment plots. Solute release followed a similar pattern as on the pediment surfaces, although the initial peak and final steady value of the EC were higher than on the pediments. The average sediment concentration for the sandstone plots was ca. two times that of the pediment plots (Table 3.6). Bryan et al. (1984) found that on the sandstones and pediments, solute and sediment concentrations gradually decreased during simulated rainfall experiments, and concluded that solute and sediment concentrations were supply-controlled. The experimental conditions of Bryan et al. (1984) differ in some important aspects from the present study. The average rainfall intensity during their tests was 29 mm h^{-1} , and plot size ranged from 21.8 to 48.0 m^2 . Consequently, discharges were much higher than during the present study. In addition, the higher rainfall intensity and the different design of the rainfall simulator resulted in a higher rainfall erosivity, and thus, in higher erosion rates. Under the experimental conditions of the present study evidence from the rainfall simulation tests that sediment concentrations are supply-controlled is less clear. In many cases, the decrease in readily available sediment appears to be counterbalanced by the reduced strength of the surface layer under wet conditions. This would suggest that during the low intensity rainstorms often occurring in the area, sediment concentrations in runoff from the sandstones and pediments are likely to be sustained at low, constant levels.

On the shales, runoff generation only occurred after considerable rainfall, so that during most rainstorms the shales will not be a runoff source. Once the threshold of

runoff generation is exceeded, however, the shales become an important source of solutes and sediment. Solute concentrations, as indicated by the EC, generally showed an exponential decrease with time. Peak and equilibrium values of the EC were in excess of those on sandstones and pediments (Table 3.6). Sediment concentrations were high, and tended to increase during the tests, due to the reduced strength of the regolith under wet conditions.

The pattern of runoff generation on the shales emphasizes the importance of changes in characteristics within the regolith profile. It was observed (plot BR9) that runoff on top of the dense subcrust preceded surface runoff on the popcorn crust by ca. 20 minutes. The average rainfall intensity during this period was 20.3 mm h^{-1} . Initially, rainfall is absorbed by the popcorn aggregates. Swelling of the clay-rich material causes the extensive crack system to slowly close. When parts of the surface of the popcorn crust become saturated the excess rainfall will run off into the still open cracks. The pattern of wetting of the underlying material will thus be controlled by the microtopography of the popcorn crust, and especially by the dynamics of the closing crack system. This will lead to the formation of preferential flow paths within the popcorn crust. Because the crack density of the subsurface crust is much lower than that of the popcorn crust, part of the downward flow will be laterally diverted over the top of the subsurface crust, while the remaining part will flow into cracks in the subsurface crust. The latter part of flow may penetrate to the shard layer, and cause the formation of microtunnels at the subsurface crust-shard contact by slaking and dispersion (Hodges and Bryan, 1982). In this model, the concentration of flow along preferential flow paths is an important controlling factor in microtunnel formation.

Figure 3.25 includes rating curves indicating the relationship between sediment concentration and discharge. The equation of the regression line is

$$SC = 5.43 Q^{0.40} \quad [3.3]^{142}$$

(n=71, r²=0.119, P<0.01) for the pediments, and

$$SC = 49.5 Q^{0.17} \quad [3.4]$$

(n=39, r²=0.107, P<0.05) for the shales. For the sandstones, the correlation of sediment concentration and discharge is non-significant. The rating curves are indicative of the differences between the surface units. Nevertheless, the considerable scatter (Fig. 3.27) and the values of r² indicate that factors other than discharge control sediment concentrations to a large extent.

Figure 3.28 shows the variables measured during the rainfall simulations, and indicates the manner of interaction. Rainfall intensity, externally controlled by the rainfall simulator, is the independent variable. Rainfall intensity and infiltration rate determine the discharge, and discharge in turn affects the sediment concentration. However, rainfall intensity also has an effect on sediment concentration, as raindrop impact on the flowing water increases the turbulence and hence erosion rates. In addition, the impacting raindrops may directly disturb the slope surface, which will have the same result. Because on shales most runoff occurs as subsurface flow, rainfall characteristics can be expected to affect sediment concentrations to a lesser extent than on the pediments and sandstones. The interaction between discharge, sediment concentration, and EC is similar to that occurring during the direct-runoff tests, and has been described in Section 3.2.3. Not included in Fig. 3.28 are the two outside factors of: first, supply-limited conditions, limiting solute and sediment concentrations in the later stages of tests; and second, microscale slumps and mudflows occurring independently of discharge.

3.4 RELATING DIRECT-RUNOFF TESTS AND RAINFALL SIMULATIONS

The two experimental techniques used at the microscale differ significantly in the manner of runoff production. Test results should therefore be viewed as complimentary but not directly comparable (Laronne, 1982). Because of the rapid flow concentration, the direct-runoff data mainly concern rill and channel flow. Conversely, the rainfall simulation data incorporate the effects of raindrop impact, albeit of drops which have not reached their terminal velocity.

The water used for the direct-runoff tests came from the Red Deer River, and had an EC_o varying from 465 to 550 $\mu\text{S cm}^{-1}$. The water used for the rainfall simulations, however, was from the locally pumped supply at the Dinosaur Provincial Park campsite with an EC_o of 1135 to 1160 $\mu\text{S cm}^{-1}$. Bryan et al. (1984) investigated the effect of initial water chemistry on solute release using pumped water and distilled water, and found that using distilled water for rainfall simulations resulted in a considerably higher rate of solute release. For instance, during rainfall simulation with distilled water the increase in Na concentrations in runoff from a shale plot was 1.3 times that during simulations using pumped water. Even larger differences were found on the sandstones and pediments. The inverse relationship between solute concentration and rate of solute release has been described in a number of studies (e.g. Kemper et al., 1975; Jurinak et al., 1977; Keren and O'Connor, 1982).

Comparison of Tables 3.3 and 3.6 shows that on the sandstones and pediments, \underline{EC}_p and \underline{EC}_s were higher during the rainfall simulations than during the direct-runoff tests. It appears that the effect of the higher EC_o during the rainfall simulations is more than compensated for by that of raindrop impact and contributions from interrill areas. The effectiveness of rainfall in increasing solute release rates was demonstrated by Ingram and Woolhiser (1980) and Ahuja et al. (1982). On the shales, \underline{EC}_p was similar for the direct-runoff tests and the rainfall simulations, which is to be expected as runoff on the

shales occurs mainly as subsurface flow so that raindrop impact will not greatly affect solute release.

3.5 SUMMARY

The macroscale studies indicate strong contrasts in the response to rainfall of the three major runoff-producing surface units in the badlands. Under dry antecedent moisture conditions, pediments may be expected to produce runoff after 0.6 to 4.2 mm of rainfall, depending on the underlying bedrock and on variations in thickness of the sheetwash-derived deposits of fine sands and silts. Sandstones surfaces will produce runoff after 0.7 to 2.3 mm of rainfall, whereas runoff from shale surfaces will start after a total rainfall varying from 11.0 to 24.9 mm. On average, sediment and solute concentrations on the sandstones were two times, and on the shales up to six times those on the pediments. The following chapter shows how the various surface units control the response of the two subbasins.

CHAPTER 4

4.1 INTERMEDIATE SCALE DRAINAGE BASINS

To investigate drainage basin response at a spatial scale between that of the microscale plots and the mesoscale Rimco Basin and New Basin, two small basins were instrumented. The first of these, Subbasin A, is located in the New Basin and has an area of 1882 m². The second, Subbasin B, with an area of 2104 m², is located in the Rimco Basin (Fig. 4.1).

4.2 GENERAL DESCRIPTION OF SUBBASINS

Subbasins A and B have a similar topography. Gently sloping pediments account for a considerable portion, more than 40 per cent, of the basin surface area (Table 4.1) and are located close to the outlet (Fig. 4.2 and 4.3). The upper part of both basins is formed by steeper slopes, consisting of sandstone and shale (Fig. 3.2 and 3.3). Runoff dominantly occurs as rill flow on the sandstones; as rill flow and microtunnel flow on the shales; and as a combination of sheet flow and braided flow on the pediments.

Table 4.1 shows that Subbasin A has a larger percentage of sandstone and shale, whereas Subbasin B has a larger percentage of vegetated surface. More important than the differences in percentage of area, however, are the differences in how the surface units are arranged within each basin. In Subbasin A the highest portion of the basin consists of shale. The extent of this shale is nevertheless limited, and a considerable portion of the upper slopes consists of sandstone (Fig. 4.4). The lower two-thirds of the slope, between sandstone and pediment, consists of shale again. The arrangement of the sandstones and shales causes runoff generated on the rapidly-yielding sandstones to flow downslope onto

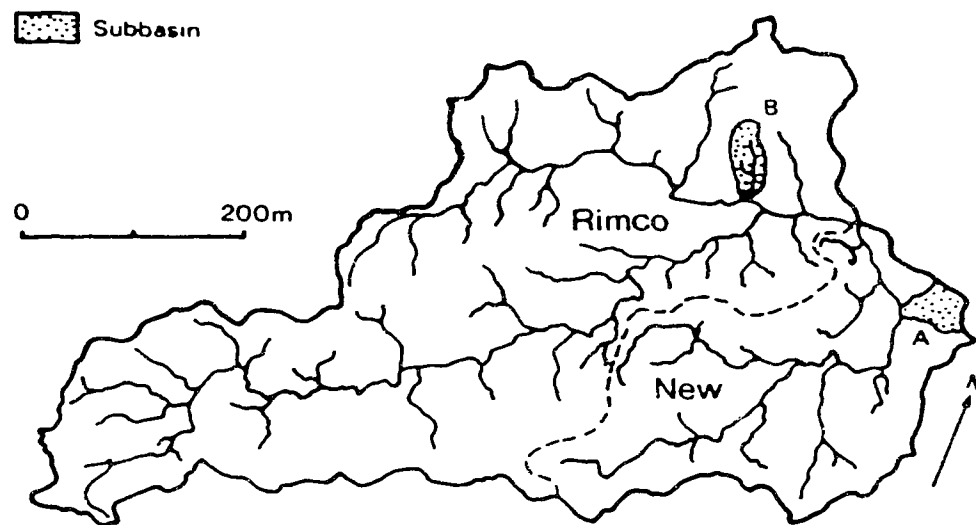


Fig. 4.1 Locations of Subbasins A and B in the Rimco Basin and the New Basin.

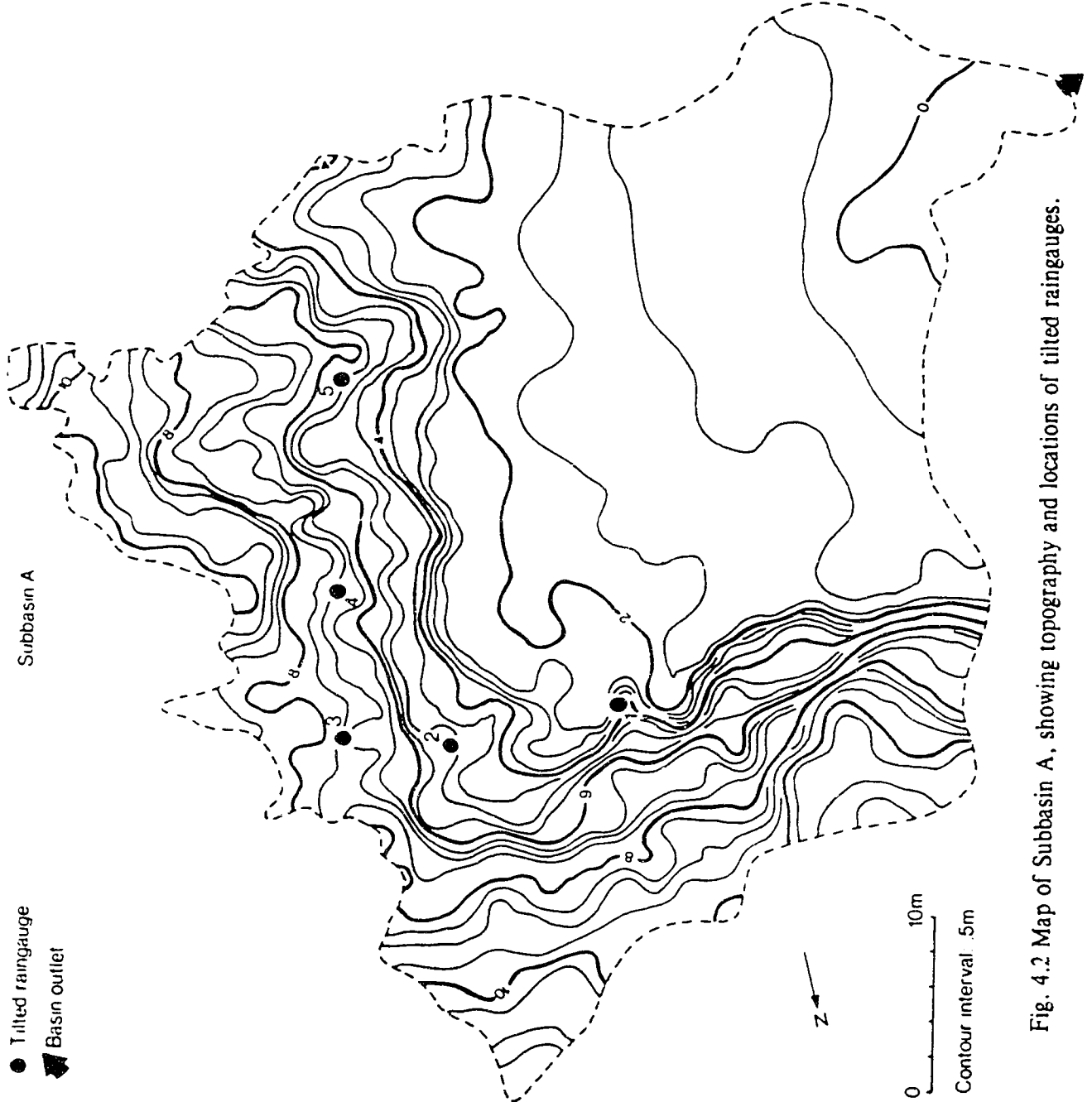


Fig. 4.2 Map of Subbasin A, showing topography and locations of tilted raingauges.

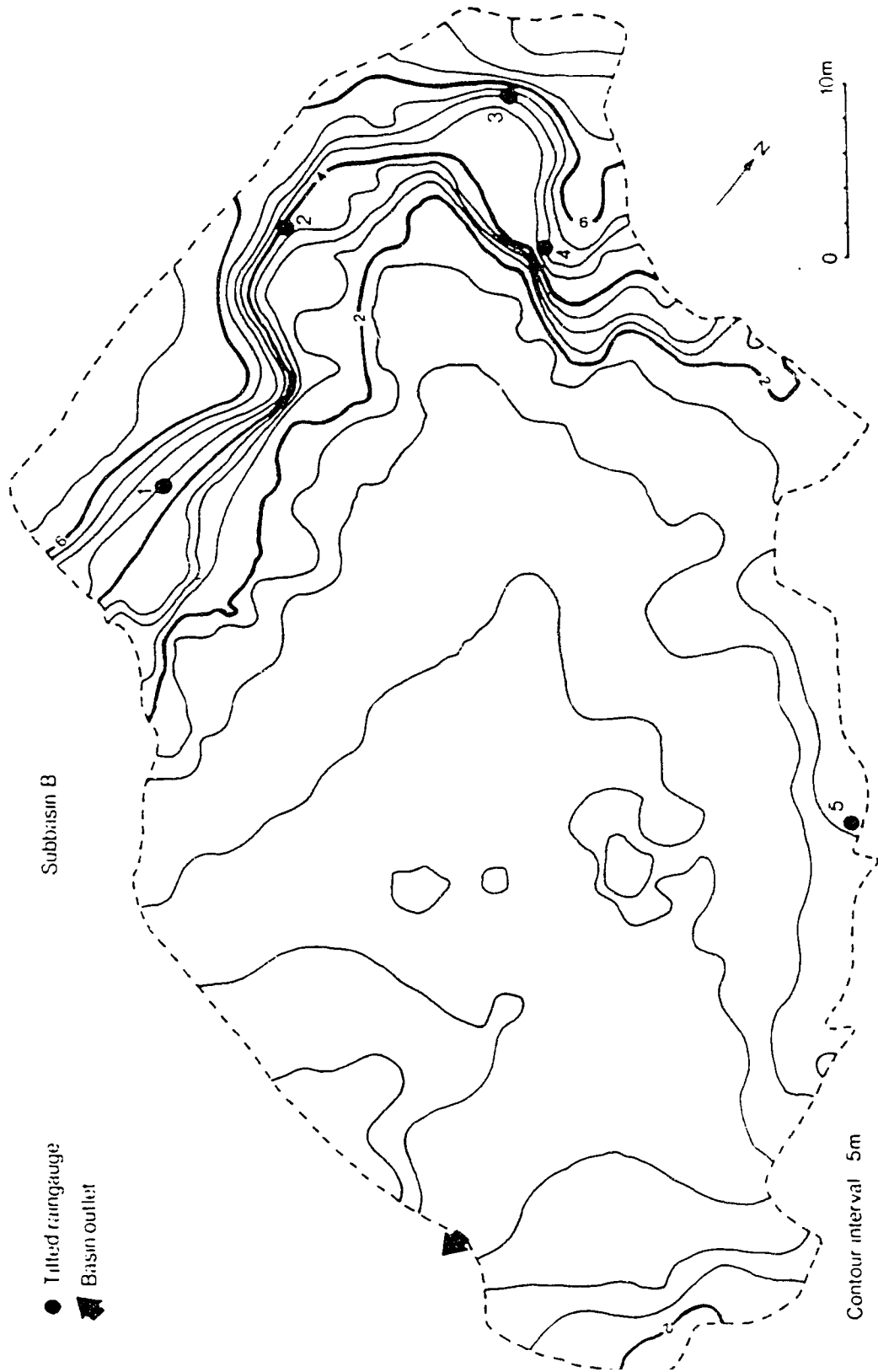


Fig. 4.3 Map of Subbasin B, showing topography and locations of tilted rain gauges.

Table 4.1 Percentage of basin area taken up by different surface units.

surface unit	Subbasin A (%)	Subbasin B (%)
sandstone	15	8
pediment + alluvial	42	49
vegetated	2	22
shale	35	16
ironstone	3	2
disturbed	3	4



Fig. 4.4 Overview of Subbasin A, showing topography and arrangement of surface units. Note that sandstone overlies shale on the steep slope sections, causing the formation of rill and erosion features in shale, transmitting runoff generated on sandstone. Photograph by J.A. Campbell.

the shale. This has resulted in the formation of tunnel erosion features in the shale, transmitting runoff generated on the overlying sandstones.

In Subbasin B the highest portion of the basin also consists of shale, in this case extending downwards for one-third of the slope (Fig. 4.5). The remainder of the slope down to the pediment consists of sandstone. Because of the arrangement of the surface units tunnel erosion in Subbasin B is limited to microscale features on the shale. Sediment export from the basins can be expected to be affected by the surface unit arrangement.

4.3 INSTRUMENTATION

In each of the basins five tilted Tru-Check raingauges were installed with the opening parallel to the local slope. Table 4.2 gives the aspect and tilt of each gauge, and Fig. 4.2 and 4.3 show the locations of the gauges. Information on the temporal characteristics of rainfall could be derived from the Rimco recording raingauge, located just outside Subbasin B.

At the outlet of Subbasin A a metal funnel was installed to enable collecting total runoff for discharge measurements, and to facilitate sampling. During runoff, grab samples were taken manually for determination of EC's and sediment concentrations. Problems arose because occasionally the high stage in the channel to which Subbasin A contributes caused reversal of the flow direction into Subbasin A.

At the outlet of Subbasin B a resistant bank of ironstone caused the formation of a waterfall during runoff. This situation allowed installing a plastic barrel with a total capacity of 65 l (Fig. 4.6). Because this capacity was too small to hold the total runoff from all but the smallest storms, a small 115° V-shaped opening was cut just below the upper rim of the barrel. Stage in the barrel was measured with a type F Stevens stage recorder (Leupold & Stevens, Inc.) with a temporal resolution of ca. 8 min per mm. A



Fig. 4.5 Overview of Subbasin B, showing topography and arrangement of surface units. Because, in contrast to the situation in Subbasin A, shale overlies sandstone on the steep slopes, tunnel erosion features are limited to microscale features on the shale. The basin outlet is located to the left, just outside the picture. Photograph by J.A. Campbell.

Table 4.2 Characteristics of tilted raingauges in Subbasins A and B.

raingauge	aspect (°)	tilt (°)	effective horizontal area †
A1	158	84	0.10
A2	196	58	0.58
A3	209	53	0.60
A4	295	39	0.78
A5	307	37	0.80
B1	93	42	0.74
B2	56	42	0.74
B3	142	56	0.56
B4	189	54	0.59
B5	214	35	0.82

† the vertical rainfall that would be caught by a tilted raingauge, expressed as a fraction of that caught by a similar, horizontally-installed raingauge.



Fig. 4.6 Instrumentation at the outlet of Subbasin B. Runoff is collected in a 65 l barrel into which a V-shaped opening is cut to allow controlled overflow. Stage in the barrel is measured with a Stevens stage recorder. The inlet for the ISCO water sampler is suspended from the length of lumber across the channel.

Table 4.3 Overview of data collected in Subbasin A and B during 1986 and 1987.

date	average rainfall ^B (mm)	Rimco rainfall (mm)	API [‡] (mm)	Subbasin A [†]			Subbasin B [†]		
				Q	SC	EC	Q	SC	EC
<u>1987</u>									
May 26 (I)	6.0	7.6	0.0	X	X	X	X	X	X
May 26 (II)	4.5	4.3	6.0	X					
May 27 (I)	2.5(I+II)	—	8.4	X					
May 27 (II)		—		X					
June 16	3.0	2.0	0.1	X	X	X			
June 19 (I)	4.0	2.8 [#]	1.6	X	X	X	X	X	X
June 19 (II)	12.6	0.5 [#]	5.8	X	X	X	X	X	X
June 20	3.9	—	14.7	X					
June 30	2.0	—	2.0	R					
July 3 (I)	3.9(I+II)	3.6	2.0	X					
July 3 (II)		1.0		X					
July 5	2.6	3.3	3.8	X	X	X			
July 6-7	1.0	1.0	5.1	—					
July 16	2.0	2.3	0.7	X					
July 18 (I)	10.2(I+II)	8.6	1.7	X	X	X	X	X	X
July 18 (II)		1.8		X					
July 25	3.5	3.8	2.5	X					
July 28	1.3	1.3	3.1	—					
August 4	2.1	3.0	0.9	X					
August 10	4.6	5.6	0.8	X	X	X			
August 11	2.8	2.8	4.3	X					
August 13	0.5	0.5	4.6	—					
August 14	17.6	22.4	4.0	X	X	X	X	X	X
August 16-17	4.1	4.3	13.9	X					
August 18-19	6.3	6.9	11.5	X					

† — - no runoff

X - data were collected

R - (only for Subbasin B) runoff occurred, but no data were collected

‡ Antecedent Precipitation Index for the Rimco Basin and the New Basin

^B average total rainfall for the Rimco Basin and the New Basin

incomplete data

stage/ discharge relationship for the V-shaped opening was obtained under controlled conditions. The maximum outflow through the V was found to be 1200 ml s^{-1} . Higher discharges, however, did occur during a number of storms, and caused uncontrolled overflow across the rim of the barrel.

An ISCO Model 1680 water sampler was used to sample runoff at the outlet of Subbasin B. The ISCO sampler was triggered by runoff, and was programmed to take up to 28 separate sequential samples of ca. 350 ml at a sampling interval of 3 min. A 10 s interval elapsed between triggering the ISCO, and the start of sampling. Because the sampler inlet was not totally submerged during very low flow stages, the sample was usually less than the programmed amount during the last phase of a flow event. The sampling interval was programmed to be 3 minutes. After a flow event, the EC of the samples was measured in the field, and the samples were transported to the laboratory to determine sediment concentrations.

Although both basins were located relatively close to the outlets of the Rimco Basin and the New Basin, difficult terrain conditions during rainstorms prevented frequent observations of the basins during runoff events. In addition, direct observations were limited by a shortage of manpower during runoff events so that observations on Basin A were only made on five occasions (Table 4.3). The automatic instrumentation of Subbasin B, however, provided ample discharge, EC, and sediment concentration data. The dataset from Subbasin B suffers somewhat from timing problems during some storms. These problems were caused by the mechanical clock chart recorders in the Rimco raingauge and the Stevens stage recorder which did not allow accurate synchronization, and by uncertainties about the exact time the ISCO was triggered.

4.4 RAINFALL CHARACTERISTICS

As a rule, rainfall is measured with a raingauge having a horizontal orifice. Data obtained with such a raingauge indicate how much rainfall would be received by a horizontal plane. In some drainage basins, however, the terrain has considerable slope angles which, in combination with rain falling at a (usually sizeable) inclination, results in significant differences between rainfall received by a horizontal plane - meteorological rainfall - and that received by an inclined slope - hydrological rainfall (Yair et al., 1978; Sharon, 1980; Yair and Lavee, 1985). From the viewpoint of process geomorphology, hydrological rainfall is the most relevant of the two types, as it concerns the rainfall actually intercepted by the slope surface, and thus pertains to the amount of water involved in infiltration, runoff and erosion. The deviation of hydrological from meteorological rainfall is controlled by terrain slope, wind speed, wind direction, and raindrop size distribution (Sharon, 1980). Over a given topography the last three factors usually vary considerably in time and in space. Models have been developed to derive hydrological rainfall from detailed observations of rainfall and wind, but the easiest method to acquire accurate results, especially in areas with an irregular topography, is by employing tilted raingauges with orifices parallelling the local slope (Sharon, 1980).

In each of the basins five tilted raingauges were installed (Fig. 4.2 and 4.3). Tilt and aspect of the gauges are given in Table 4.2. The rectangular orifice of the raingauges measured 58.5 by 64.0 mm, and the gauges were positioned with the longest dimension of the orifice in a horizontal direction. The location of the raingauges was chosen such that while providing a representative sample of the slopes in the basin, they would be accessible after rainfall without extensive disturbance of the slope surface.

Each tilted raingauge can be characterized by its effective horizontal area, which can be interpreted as the vertical rainfall that would be caught by a tilted raingauge expressed as a fraction of that caught by a similar, horizontally-installed gauge (Table

4.2). Comparison of this characteristic for the raingauges shows that the SW-SSW to NW-facing raingauges receive more rainfall than can be explained by their effective horizontal area (Table 4.4). For instance, during the entire observation period (June 26 - August 8, 1986, and May 26 - August 18, 1987) gauge B5 received 142.2 mm. On the basis of the ratio of their effective horizontal areas, gauge B3 should, when all rainfall would have fallen vertically, have intercepted $0.56/0.82 \cdot 142.2 = 97.1$ mm. Gauge B3 did, however, receive only 75.7 mm, or 22 per cent less than can be explained by the difference in tilt between the two gauges.

The effect of differing tilt of the raingauges may be eliminated by dividing the rainfall for each gauge by the cosine of its tilt. Table 4.4 gives this value expressed as a fraction of the total average rainfall (=146 mm) for the New Basin and the New Basin during the same period. Figure 4.7 clearly shows that raingauges and hence slopes, facing in westerly directions receive 1.2 to 1.3 times more rainfall than horizontal surfaces, whereas east-facing raingauges and slopes receive only ca. 0.95 times the rainfall intercepted by horizontal surfaces.

An exception to this general rule is gauge A1, receiving five times more rainfall than a horizontal plane. This anomaly may be explained by local, small-scale effects of the topography on wind direction and speed. Gauge A1 was in a relatively sheltered position at the base of a high, steep slope (Fig. 4.2). Such locations are conducive to carry-over effects, caused by high wind speeds at the upper portions of slopes promoting the downwind drift of raindrops and higher rainfall in sheltered, leeward locations (Sharon, 1980). The data from gauge B2 also show evidence of the carry-over effect, although not to the extent of gauge A1. All other gauges are either facing in more westerly directions or are located much closer to the slope crest so that carry-over does not occur or is not as pronounced.

During some storms the pattern of hydrological rainfall differed considerably from the general pattern described in the previous paragraphs. For instance, on July 18-19,

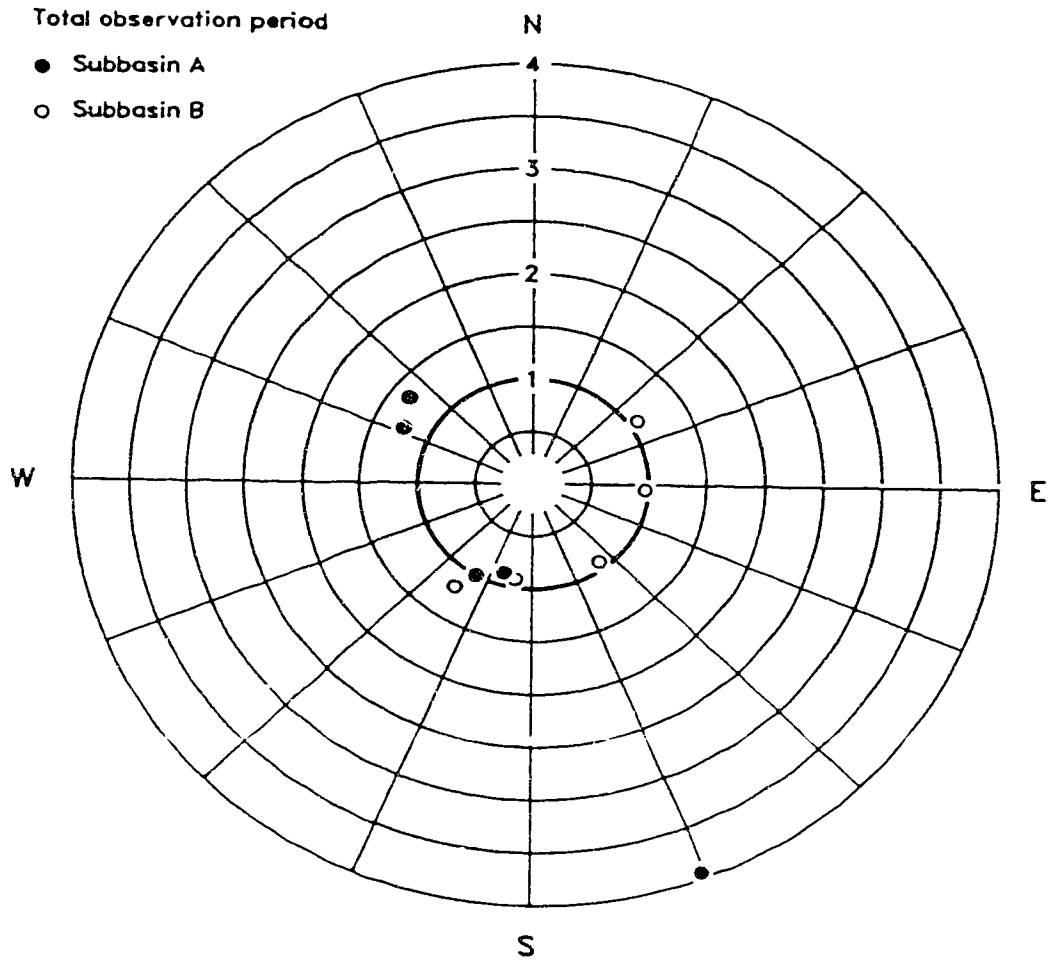


Fig. 4.7 Total hydrological rainfall for tilted raingauges during the entire observation period, corrected for differing tilts, and expressed as a fraction of the total average rainfall for the Rimco Basin and the New Basin during the same period. The thickened circle indicates a fraction of 1.

1987, rainfalls corrected for differing tilts and expressed as a fraction of average total rainfall in the Rimco Basin and the New Basin indicate that gauges B1, B2, and B3 received considerably more rainfall than the data for the entire observation period would suggest, whereas gauges B4 and B5 received considerably less (Table 4.4). In Subbasin A all gauges except A1 received less than their normal fraction of rainfall, emphasizing the high spatial variability of the meteorological conditions controlling hydrological rainfall. Similarly, on June 25, 1987, gauges A4 and A5 received, after correction for tilt and as a fraction of the average total rainfall, considerably less rainfall than all the other raingauges (Table 4.4). The data indicate that the tilted raingauges facing in southeasterly directions (NE to SW) received much more rainfall than would be expected. Raingauge B3, which during the entire observation period received only 0.93 times the average total rainfall, on this date intercepted 1.84 times the average total rainfall in the Rimco Basin and the New Basin. Both examples indicate that large deviations from the long-term average pattern of hydrological rainfall may occur during individual storms.

Because the duration of rainfall is equal for all tilted raingauges within a basin, the differences in hydrological rainfall also imply differences in rainfall intensity. Runoff generation can thus be expected to be non-uniform due to rainfall characteristics alone, even within relatively small areas such as Subbasins A and B. It should be emphasized that due to temporal and spatial variations in wind speed and direction and in raindrop size distribution, rainfall intensity variations may vary in magnitude and direction over very short distances. Yair and Lavee's (1985) method of calculating the spatial variability in rainfall intensity over an arid slope by using the ratio of rainfall intercepted by tilted raingauges to that collected in one horizontally-installed recording raingauge may hence provide inaccurate results, and so defeat the purpose of the exercise.

Table 4.4 Hydrological rainfalls in Subbasins A and B for entire observation period and for selected storms.

raingauge	entire observation period†		July 18-19 1987		July 25, 1987		August 14, 1987	
	mm	‡	mm	‡	mm	‡	mm	‡
A1	57.7	3.95	3.6	3.53	3.2	9.14	6.0	3.41
A2	74.6	0.88	2.2	0.37	3.6	1.77	5.8	0.57
A3	87.7	1.00	4.2	0.69	3.6	1.71	8.4	0.80
A4	139.7	1.23	8.2	1.03	2.4	0.88	17.0	1.24
A5	156.0	1.34	10.0	1.23	2.4	0.86	20.0	1.42
B1	104.3	0.97	12.5	1.66	3.4	1.31	12.0	0.92
B2	116.4	1.08	12.0	1.59	3.0	1.16	14.2	1.09
B3	75.7	0.93	10.0	1.75	3.6	1.84	6.0	0.61
B4	79.2	0.92	1.6	0.27	2.9	1.40	8.2	0.79
B5	142.2	1.19	6.4	0.77	3.8	1.32	15.0	1.04

† June 26 - August 8, 1986, and May 26 - August 18, 1987.

‡ corrected for differing tilts, and expressed as a fraction of the average rainfall in the Rimco Basin and the New Basin.

4.5 SUBBASIN A

Because no automated instrumentation was employed in Subbasin A only limited data are available, and no complete dataset for any storm is available. Hence it was not possible to calculate runoff coefficients and sediment yields. During both storms of June 19, 1987, no discharge measurements were made because due to the high discharge the metal funnel at the outlet was washed out, allowing water to flow around the funnel. Nevertheless, on this date samples were taken for determining sediment concentrations and EC's (Table 4.3).

4.5.1 RUNOFF CHARACTERISTICS

Response to rainfall of Subbasin A was very rapid, and the onset of flow preceded that of the Rimco Basin and New Basin by a substantial period of time. For instance, on May 26, 1987 (I), upon arrival at Subbasin A at 1024 h flow had already started whereas runoff from the Rimco Basin and the New Basin began at 1031 h, so that runoff from Subbasin A preceded that from the mesoscale basins by at least 7 min. Similar leads were observed during other storms.

Because of the data collection problems all available data for Subbasin A are from long-duration, low-intensity, frontal storms. Consequently, measured discharges tended to be very low, and ranged from 20 to 160 ml s⁻¹. The variability of the discharge indicates that the hydrograph was extremely sensitive to the rainfall intensity pattern (Fig. 4.8). The Rimco recording raingauge is located ca. 230 m WNW of Subbasin A so that, in view of the spatial variability of rainfall characteristics, the Rimco raingauge data shown in Fig. 4.8 and in the figures following should be regarded as only an approximation of rainfall characteristics in Subbasin A.

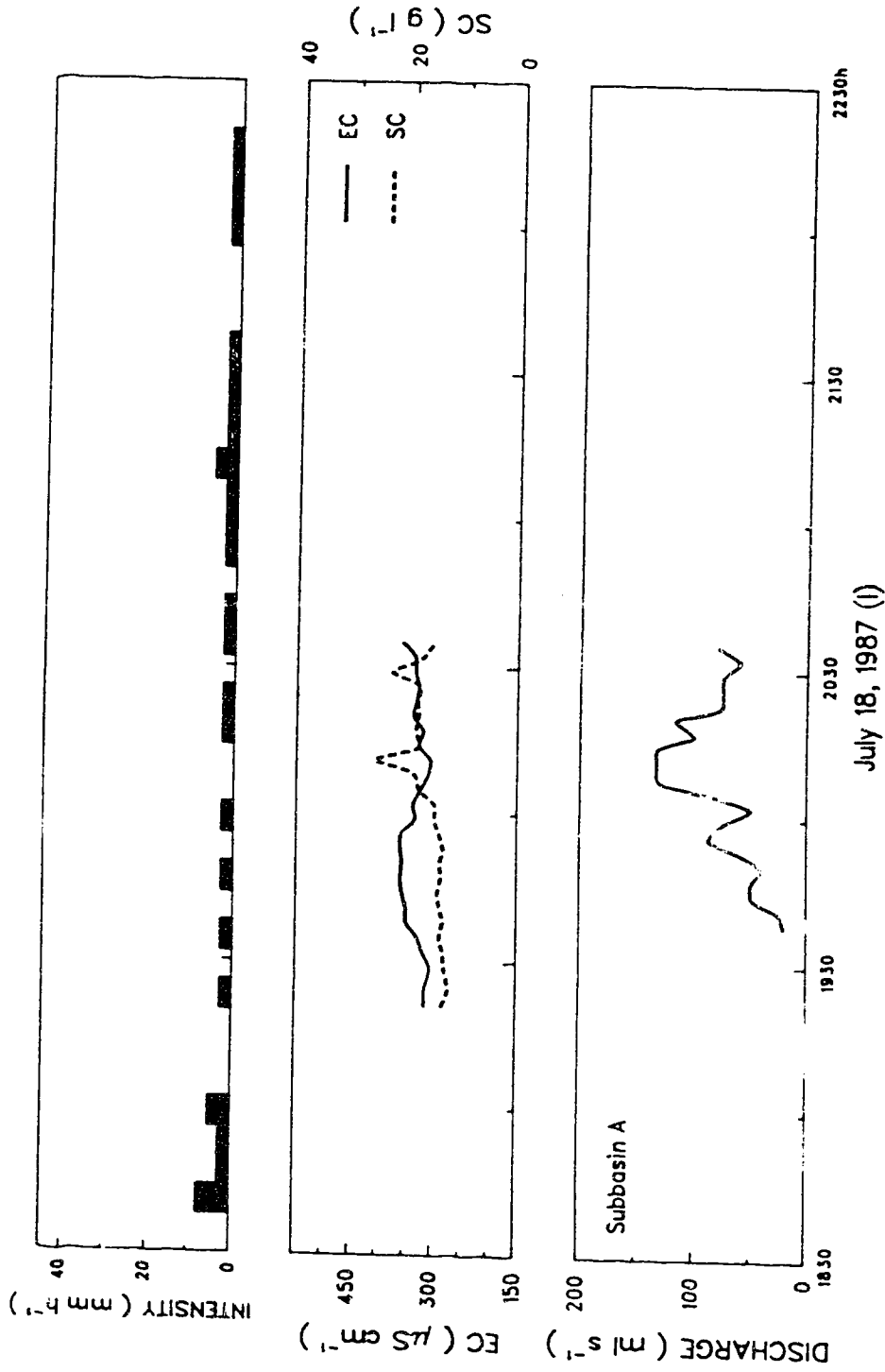


Fig. 4.8 Hydrograph, hyetograph (Rimco recording rain gauge), sediment concentration, and EC of Subbasin A on July 18, 1987 (I). The Rimco recording rain gauge is located ca. 230 m WNW of Subbasin A. Because of the limited basin size the hydrograph of Subbasin A is extremely sensitive to rainfall intensity variations.

4.5.2 SEDIMENT AND SOLUTE DYNAMICS

Sediment concentrations in Subbasin A ranged from 12.2 to 44.6 g l⁻¹. Evidence of initial flushing was shown by sediment concentration data for the runoff event of July 19, 1987 (II). During this event observers were at the site when rainfall and runoff started, and the lack of evidence for initial flushing for other storms must be attributed to missing data for the initial phases of runoff.

In general, sediment concentrations increase with discharge (Fig. 4.8 and 4.9). Figure 4.10 displays the relationship between discharge and sediment concentration in Subbasin A. The equation of the regression line is

$$SC = 5.27 Q^{0.33} \quad [4.1]$$

($n=61$, $r^2=0.301$, $P<0.001$). In Eq. 4.1, SC is the sediment concentration (g l⁻¹) and Q is the discharge (ml s⁻¹). The value of the exponent usually lies between 1 and 2 (Gregory and Walling, 1973; Graf, 1988). The low value found for Subbasin A implies a slow rise in sediment concentration with discharge, indicating that sediment concentration in the basin is almost entirely controlled by supply conditions, i.e. the response of the surface units.

Scatter around the regression line is considerable, and reflects variations in basin response under differing rainfall conditions caused by exhaustion of the sediment supply on the sandstones and pediments, and sediment-rich runoff contributions from tunnel systems and shales. Figure 4.11 shows the contrast between the sediment concentration/discharge relationships of the runoff events of May 26, 1987 (I), and August 14, 1987. On May 26, 1987 (I), average total rainfall for the Rimco Basin and the New Basin was 6.0 mm. This amount is less than the thresholds of both runoff generation on the shales and of tunnel flow initiation (Section 5.5.3). Consequently, sediment sources in Subbasin A were confined to the sandstones and pediments. These surface units act as

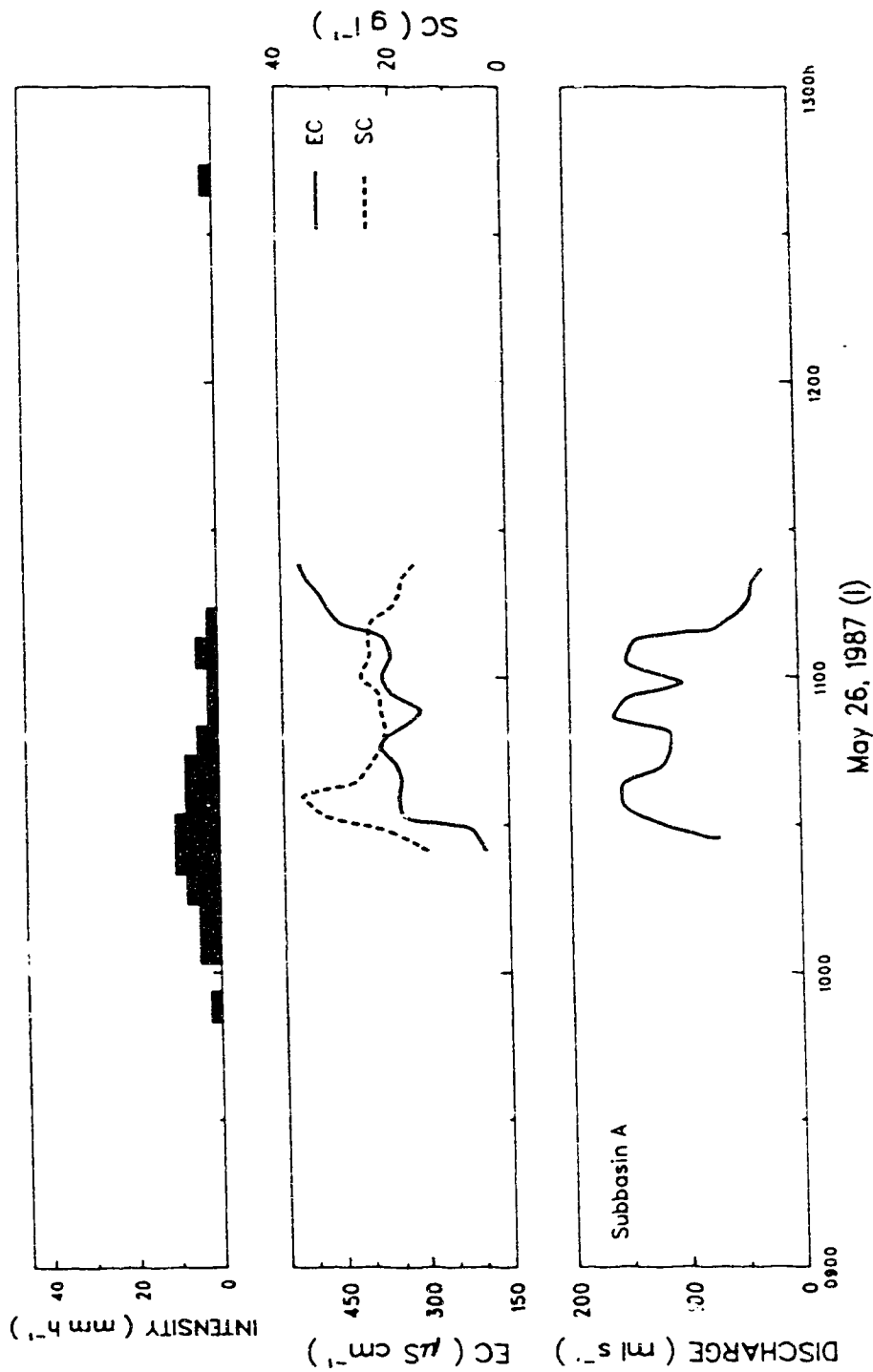


Fig. 4.9 Hydrograph, hycetograph (Rimco recording raingauge), sediment concentration, and EC of Subbasin A on May 26, 1987 (I).

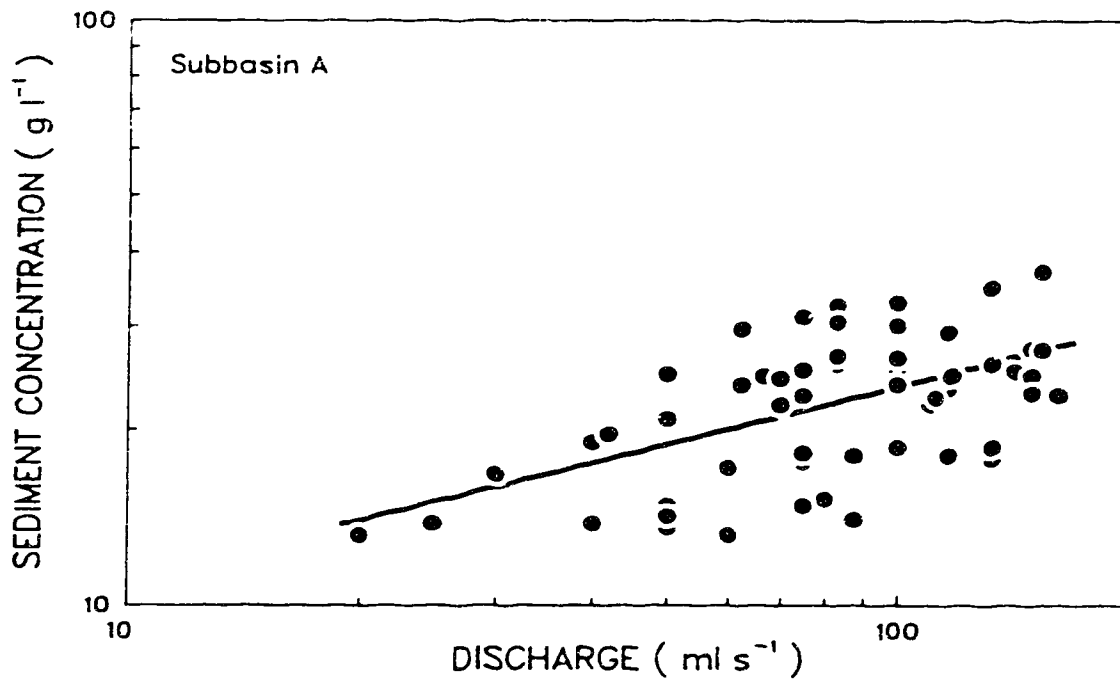
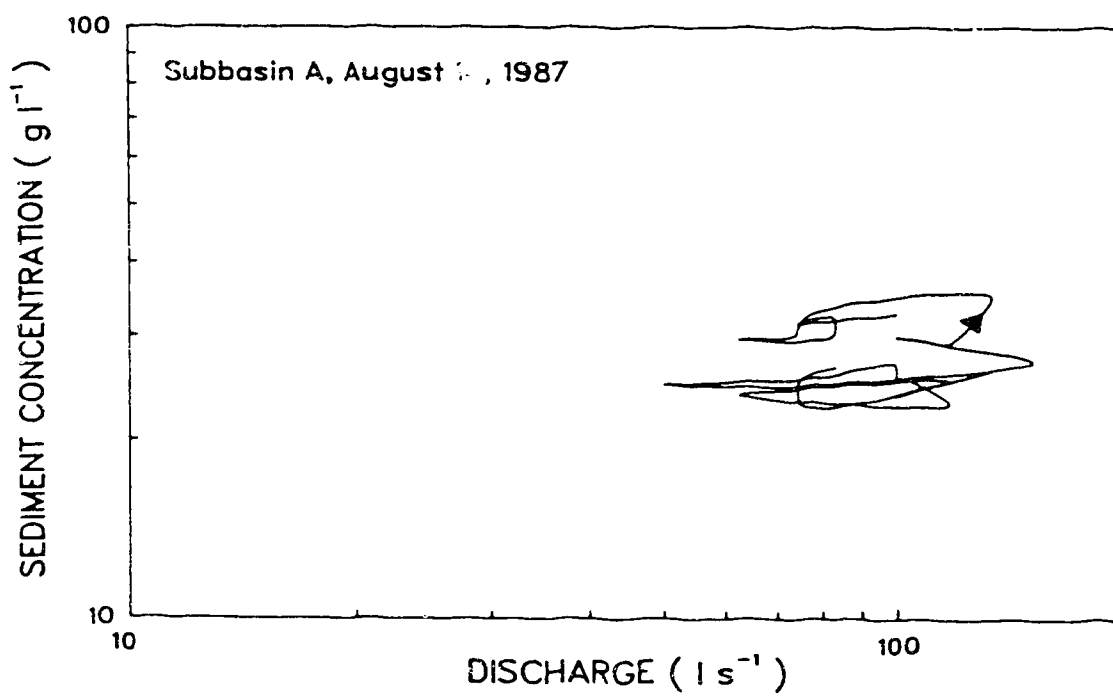
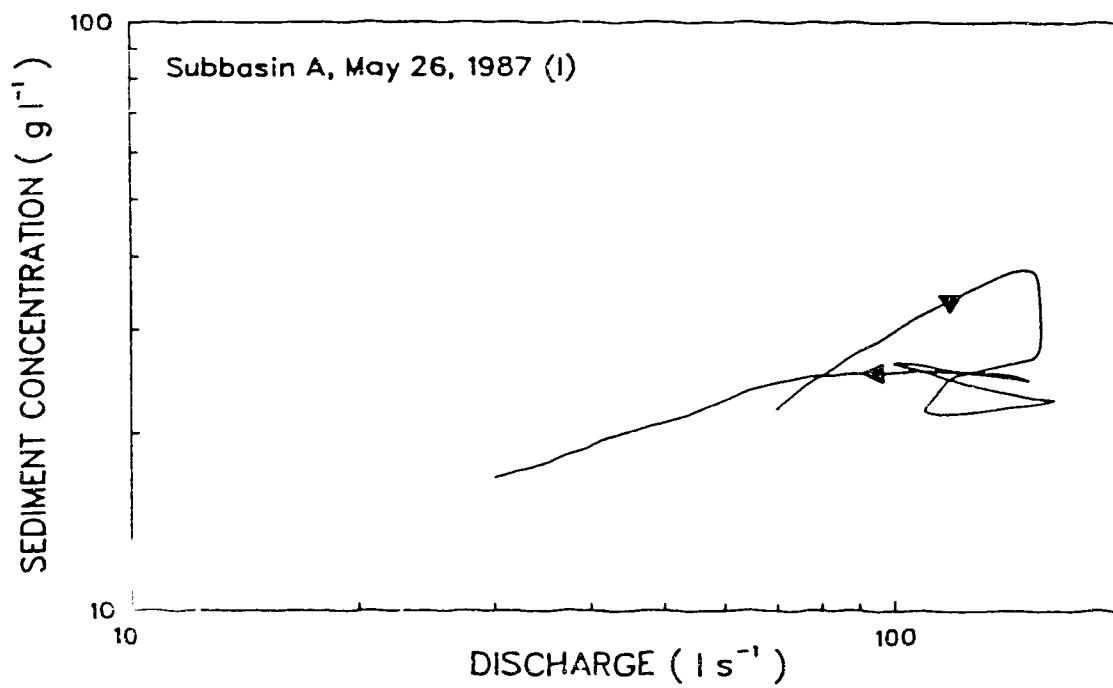


Fig. 4.10 Sediment concentration/discharge relationship for Subbasin A.



supply-limited sediment sources and hence, during the event, exhaustion occurred resulting in clockwise hysteresis of the sediment concentration/discharge relationship. On August 14, 1987, average total rainfall in the Rimco Basin and the New Basin was 17.6 mm, which is in excess of the thresholds of both runoff generation on the shales and initiation of tunnel flow. The sediment concentration/discharge relationship during this runoff event shows that sediment concentrations increased due to the sediment-rich runoff from the shales and the tunnel systems (Fig. 4.11)

Observed EC's ranged from 190 to 750 $\mu\text{S cm}^{-1}$. During none of the runoff events did the EC indicate initial flushing. The EC generally increased with time due to increasing solute release by the surface units under wet conditions, and due to the dissolution of suspended sediment in transit. Superimposed on this rising trend were the effects of dilution, causing the EC to vary inversely with discharge. Figure 4.12 shows the EC/discharge relationship for Subbasin A. The equation of the regression line is

$$\text{EC} = 564.2 Q^{-0.01} \quad [4.2]$$

($n=61$, $r^2=0.111$, $P<0.01$). The negative slope of the regression line is caused by dilution during high discharges.

4.6 SUBBASIN B

4.6.1 RUNOFF CHARACTERISTICS

Figure 4.13 shows the relationship between total rainfall and antecedent moisture condition expressed as the Antecedent Precipitation Index (API). The API is calculated as

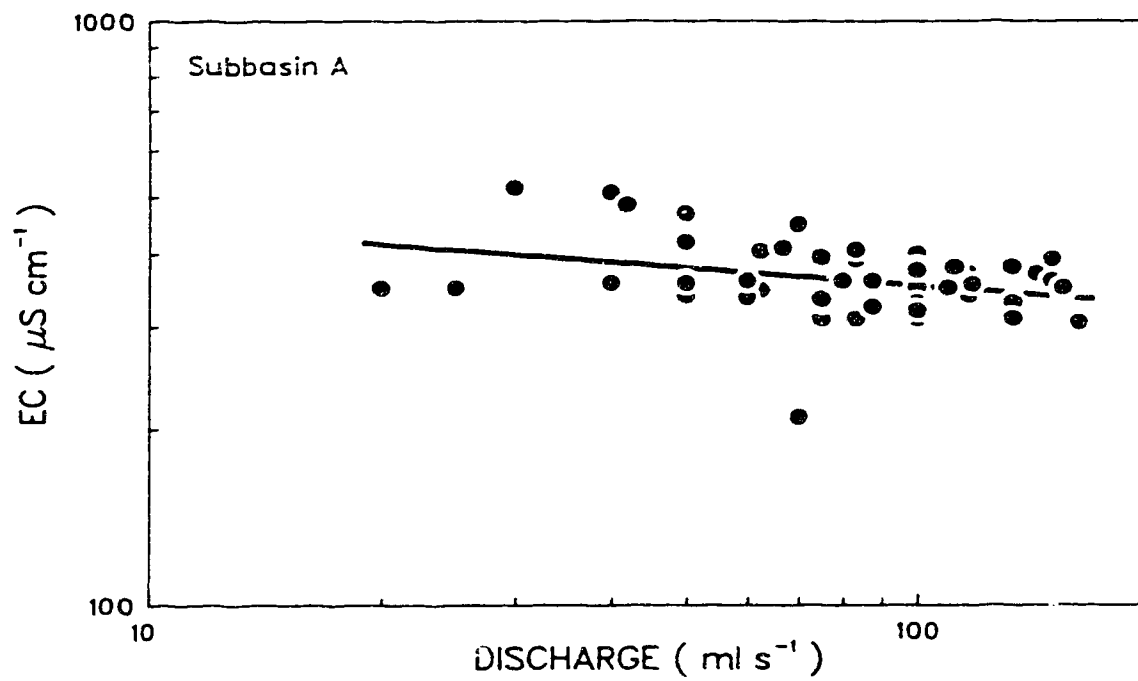


Fig. 4.12 EC/discharge relationship for Subbasin A.

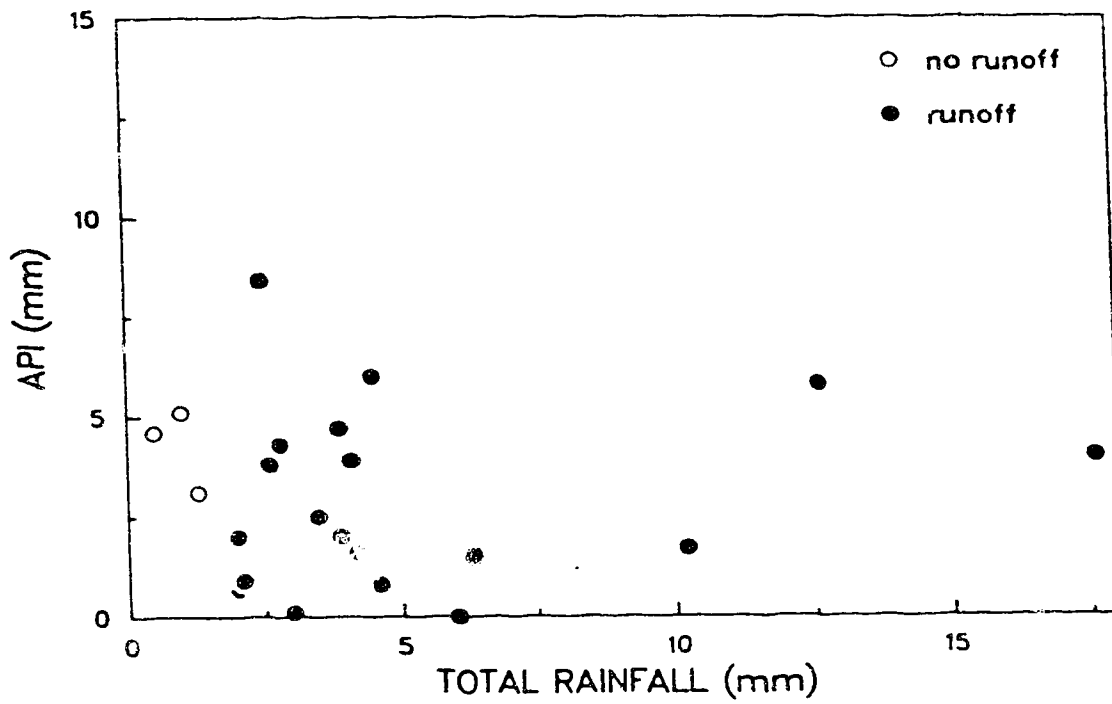


Fig. 4 13 Antecedent Precipitation Index plotted against total rainfall for the Rimco Basin and the New Basin. Indicated is whether or not runoff from Subbasin B occurred.

$$I_t = I_0 k^t \quad [4.3]$$

where I_0 is the initial value of the API; I_t , the reduced value after a period of t days; and k , a recession factor usually ranging from 0.85 to 0.98 (Linsley et al., 1982). In this model, the rate at which the basin loses moisture through evapotranspiration is assumed to be roughly proportional to the amount present, resulting in a logarithmic decline between rainstorms. Since evapotranspiration varies with the meteorological (e.g. wind speed) and surface conditions (e.g. microtopography, stage of plant growth), k should also vary to reflect such changes. Because the API is used here to compare the antecedent moisture conditions for each storm, rather than as a tool to estimate the amount of runoff yielded, a constant value of k for both summers was assumed. To reflect the high evapotranspiration rates in Dinosaur Provincial Park due to the usually high winds and temperatures, k was given a value of 0.8, indicating a rapid loss of soil moisture.

Because data for the Rimco raingauge, the recording raingauge nearest to Subbasin B, were incomplete due to battery problems, the variables refer to the Rimco Basin and the New Basin but are thought to represent the situation in Subbasin B adequately. Figure 4.13 shows whether or not runoff was generated in Subbasin B. The available data indicate that runoff generation occurred whenever rainfall exceeded a threshold value of 1.5 to 2 mm. The data do not suggest a dependence of the threshold of runoff generation on antecedent moisture conditions. This can be explained by the fact that, because transmission losses are slight because of the absence of significant accumulations of alluvial deposits, the onset of runoff from Subbasin B is controlled by runoff generation on the pediments and sandstones. This process is affected by conditions in the upper few mm of material on each surface unit. The usually high winds and temperatures cause antecedent moisture conditions in these upper layers to be dry most of the time. The initial situation of the surface units with regard to runoff generation is hence similar for the majority of storms, and the onset of runoff from Subbasin B is not noticeably affected by antecedent moisture

conditions.

4.6.1.1 RUNOFF COEFFICIENTS

Table 4.5 gives total discharge and runoff coefficients for 21 runoff events in Subbasin B. As mentioned in Section 4.3, during a number of runoff events discharge exceeded the maximum discharge through the V-shaped opening causing uncontrolled overflow over the rim of the barrel. Consequently, for these events total discharge was computed using the maximum discharge of 1200 ml s^{-1} for the unknown, but larger, actual discharge, so that the total discharges and runoff coefficients for these events represent a minimum value. Data from the Rimco recording raingauge, located just north of Subbasin B, were used to calculate runoff coefficients.

Runoff coefficients for storms for which total runoff is not a minimum estimate varied from 0.5 to 34.9 per cent, and were dependent on total rainfall and antecedent moisture conditions (Fig. 4.14). Not surprisingly, runoff coefficients tended to increase with total rainfall and, for similar values of total rainfall, with higher antecedent moisture conditions, as losses account for a smaller portion of the total rainfall.

Figure 4.14 also indicates that rainfall characteristics such as distribution and intensity affected runoff coefficients. For instance, on July 18-19, 1987, the runoff coefficient was 32.7 per cent for the two runoff events combined. On August 14, 1987, when both total rainfall and antecedent moisture conditions were twice as high as on July 18-19, the runoff coefficient reached only 26.3 per cent. Both rainstorms were long-duration, low-intensity, frontal rainstorms. Total rainfall at the Rimco raingauge was 11 mm on July 18-19, and 23 mm on August 14. Rainfall intensities during both storms were quite similar. Intensity for a six-minute period reached a peak value of only 7.6 mm h^{-1} for one six-minute period on July 18-19, and for three periods on August 14. During

Table 4.5 Rainfall and runoff of Subbasin B.

date	total discharge (mm)	total rainfall† (mm)	runoff coefficient (%)
<u>1987</u>			
May 26 (I)	1.8‡	7.6	23.7‡
May 26 (II)	1.2‡	4.3	27.9‡
May 27 (I)	0.5‡	—	—
May 27 (II)	0.5‡	—	—
June 16	0.04	2.0	2.0
June 19 (I)	0.5‡	2.8 ^b	17.9‡
June 19 (II)	2.4‡	0.5 ^b	—
June 20	0.4‡	—	—
July 3 (I)	0.4	3.6	11.1
July 3 (II)	0.2	1.0	20.0
July 5	0.4	3.3	12.1
July 15	0.01	2.0	0.5
July 18 (I)	3.0	8.6	34.9
July 18 (II)	0.4	1.8	22.2
July 25	0.2‡	3.8	5.3‡
August 4	0.2‡	3.0	6.7‡
August 10	2.4‡	5.6	42.9‡
August 11	0.3	2.8	10.7
August 14	5.9	22.4	26.3
August 17	0.8	4.3	18.6
August 18	2.0	6.9	29.0

† Rainfall at the Rimco recording raingauge

‡ indicates a minimum estimate

^b incomplete data

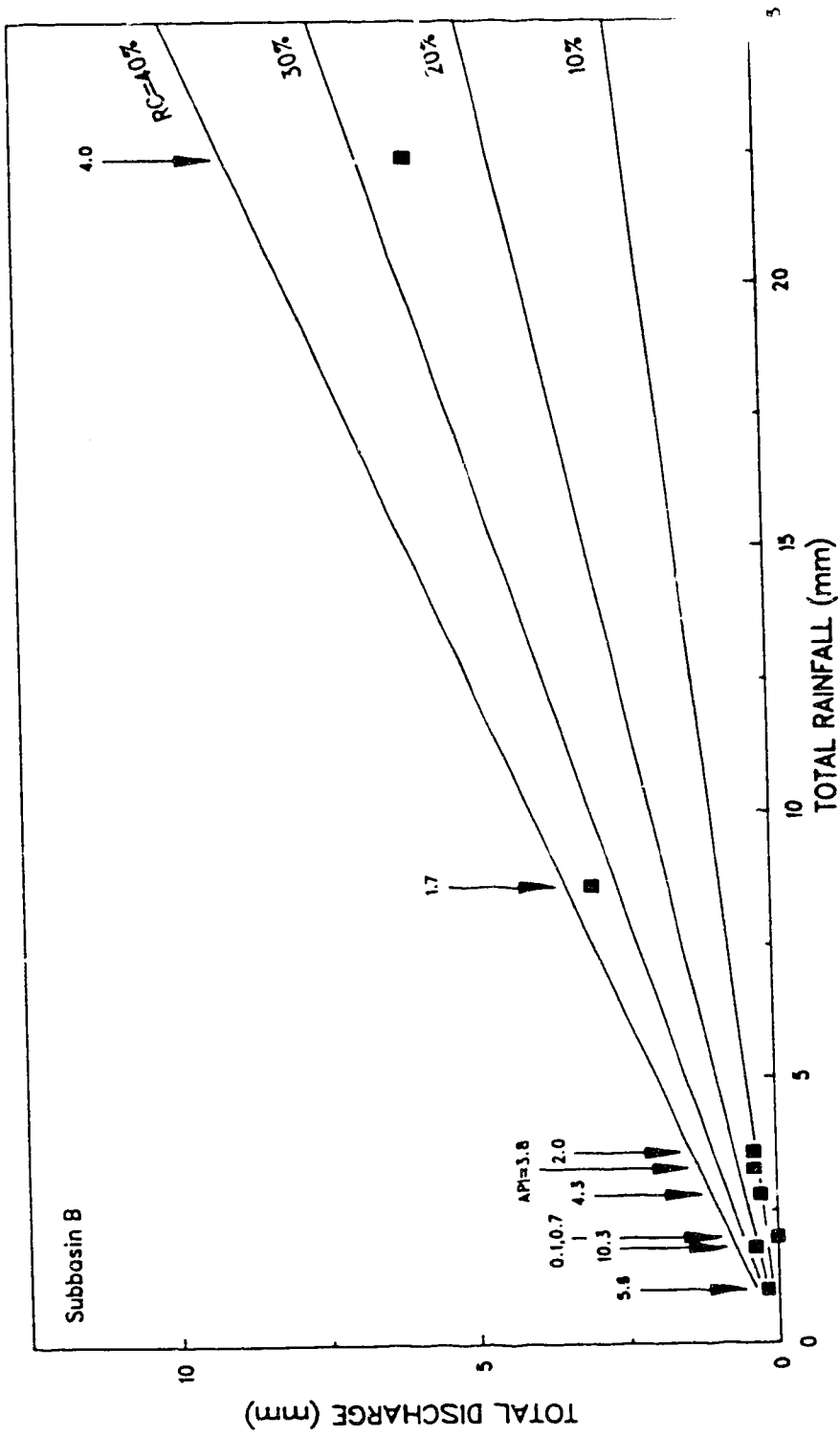


Fig. 4.14 Relationship between total rainfall and total discharge, and the effect of antecedent moisture conditions, in Subbasin B. The lines indicate the value of the runoff coefficient.

the remainder of the storm rainfall intensity generally was only 2.5 mm h^{-1} on both days, with occasional six-minute periods of 5.1 mm h^{-1} .

Important differences, however, occurred between the hydrological rainfalls of the two storms. On July 18-19 gauges B1, B2, and B3 received large amounts of rainfall, whereas gauges B4 and B5 received relatively little (Table 4.4, Fig. 4.15). This indicates that on this date gauges, and hence slopes, facing NE to SE in Subbasin B received much more rainfall than those facing SW. The hydrological rainfalls for Subbasin B also indicate a large angle of incidence (angle between the incoming rainfall and the vertical) of rainfall. On August 14, hydrological rainfall displayed a totally different pattern (Table 4.4, Fig. 4.16). Gauges B2 and B5 received most hydrological rainfall, although in the case of B5 less than the average for the total observation period would indicate, whereas the remaining gauges in Subbasin B received slightly to considerably less rainfall, and always less than the average for the total observation period indicated. The hydrological rainfalls for August 14 imply that raingauges and slopes facing in northwesterly directions (NE to SW) received slightly more rainfall than those facing the opposite side, although the angle of incidence was relatively small on this date. The hydrological rainfalls for Subbasin A on August 14 confirm this pattern (Fig. 4.16). On July 18-19, hydrological rainfalls in Subbasin A are for all gauges slightly to considerably less than their average for the entire observation period would indicate. Nevertheless, gauges A1, A4, and A5 received most hydrological rainfall, whereas gauges A2 and A3 received least (Fig. 4.15). In contrast to Subbasin B, the overall pattern of hydrological rainfall in Subbasin A on July 18-19 does not deviate to any great extent from that for the total observation period, showing that trends in the spatial pattern of hydrological rainfall can differ greatly between nearby locations, and emphasizing that hydrological rainfall is controlled not only by meteorological factors operating at a macroscale (e.g. a prevalent wind direction), but also by smaller-scale effects (e.g. the airflow pattern as affected by topography).

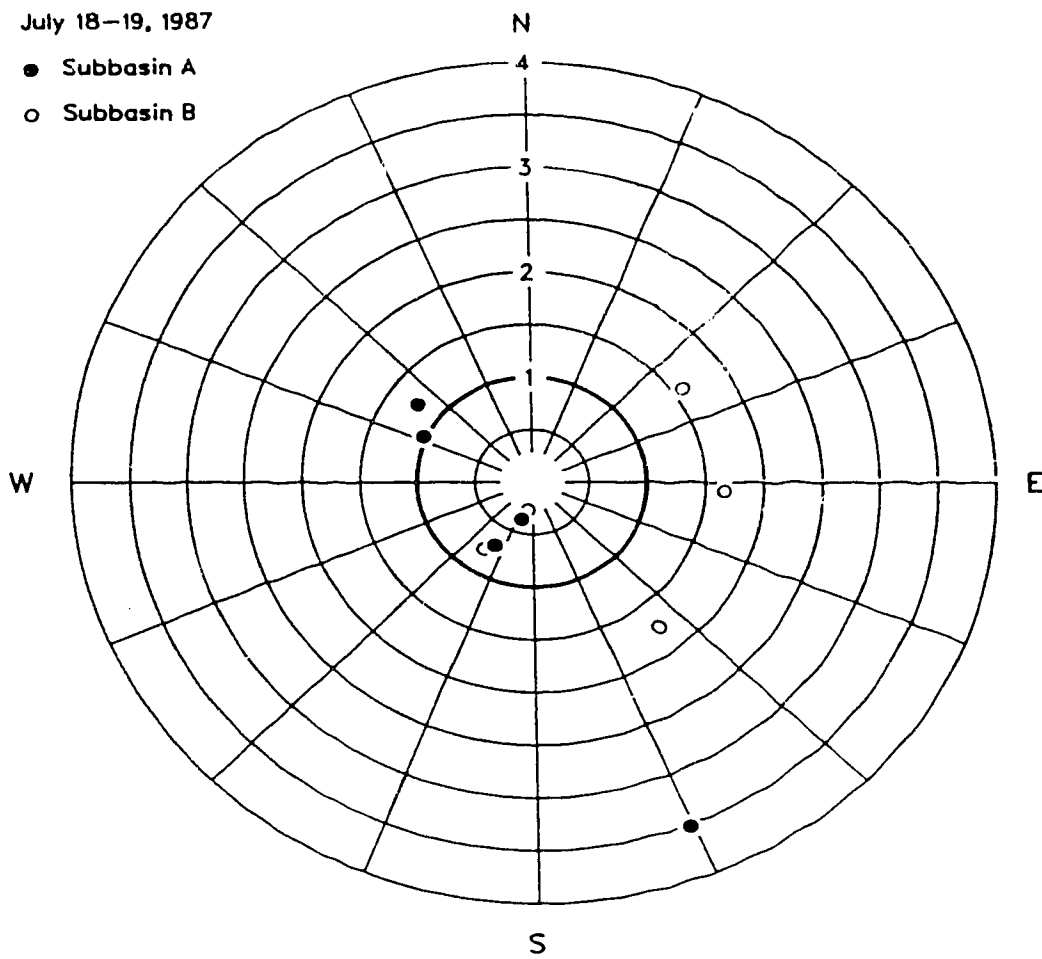


Fig. 4.15 Hydrological rainfall on July 18-19, 1987, corrected for differing tilts, and expressed as a fraction of the average rainfall for the Rimco Basin and the New Basin on the same day.

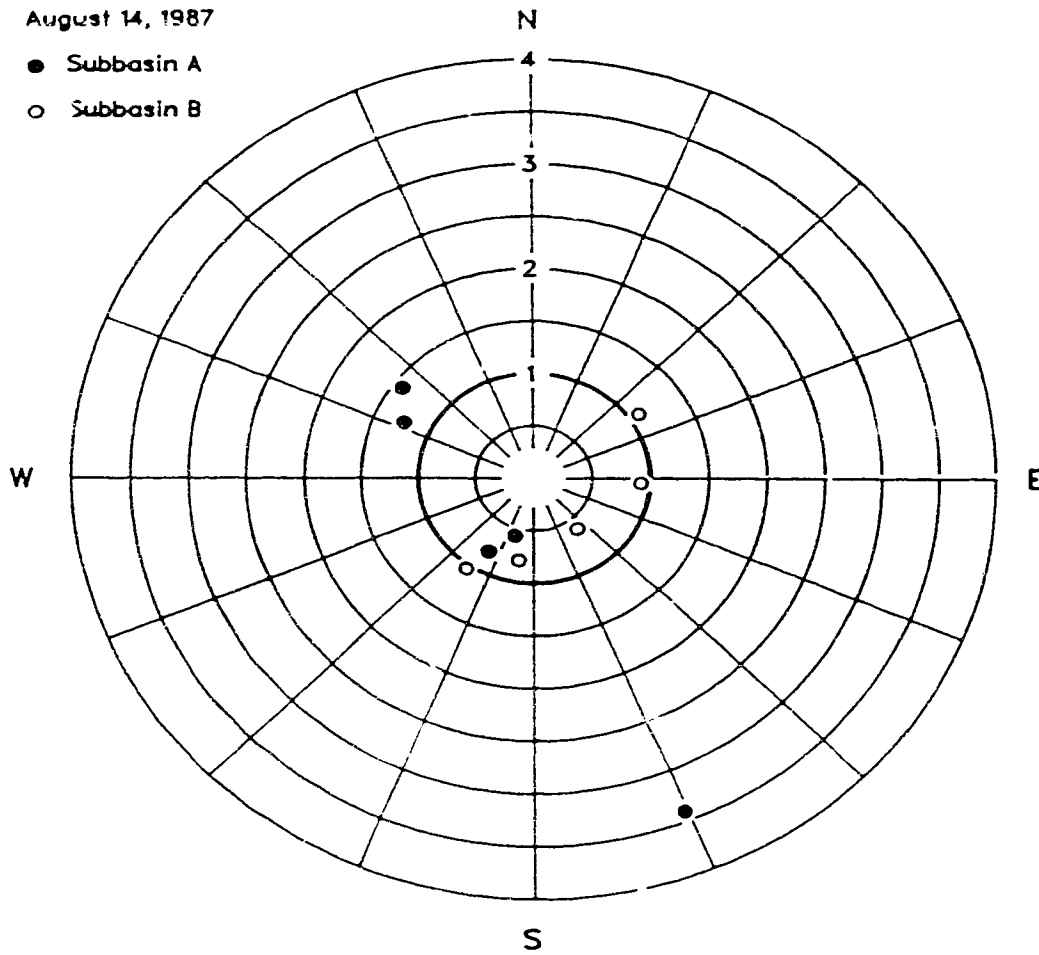


Fig. 4.16 Hydrological rainfall on August 14, 1987, corrected for differing tilts, and expressed as a fraction of the average rainfall for the Rimco Basin and the New Basin on the same day.

Comparison of the rainfall characteristics for both days must lead to the conclusion that the difference in runoff coefficients between July 18-19 and August 14 was caused by differences in hydrological rainfall. On August 14, rainfall came from the NW, and the angle of incidence was slight. On July 18-19, rainfall came from the NE to SE, and the angle of incidence was larger than on August 14. Hence, on July 18-19 the NE to SE-facing steep sandstone slopes in the NW to N portion of Subbasin B contributed a larger portion of the total runoff than on August 14, resulting in a higher runoff coefficient. It would be expected that the higher angle of incidence on July 18-19 would also result in a reduced contribution to the total runoff by the gently sloping pediments, but this effect seems to be counterbalanced by the increased contribution of the sandstones.

4.6.1.2 HYDROGRAPH CHARACTERISTICS

Because of the small basin size, hydrographs of Subbasin B were extremely sensitive to the rainfall pattern. Typically, the hydrograph showed a very steep rise, a sharp, short peak, and a very steep falling stage (Fig. 4.17). Periods of rainfall separated by dry periods frequently result in isolated runoff events, separated by short (a few minutes) periods of no flow (Fig. 4.18). Low-intensity rainfall during the falling stage resulted in a much broader hydrograph shape (Fig. 4.19). Figure 4.20 shows a typical hydrograph during a long-duration, low-intensity, frontal storm. Flow during such a storm was continuous, but discharge varied greatly in response to rainfall intensity.

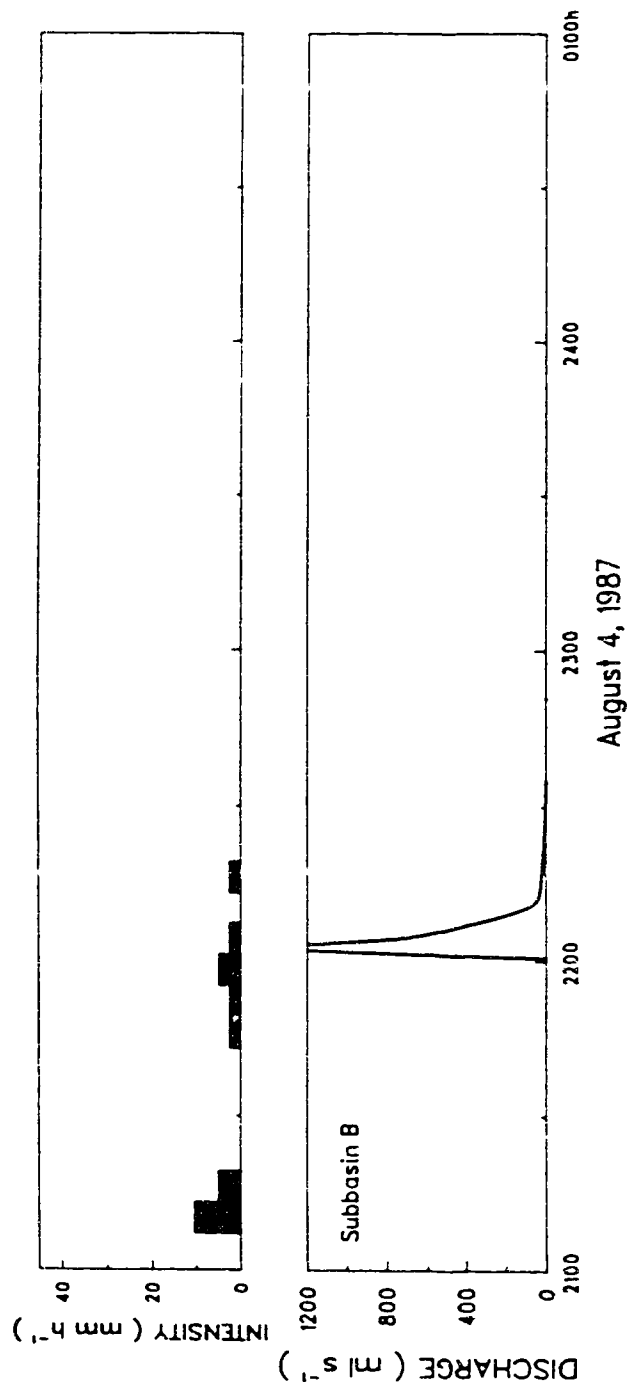


Fig. 4.17 Hydrograph and hietograph (Rimco recording raingauge) for Subbasin B on August 4, 1987, showing a typical hydrograph characterized by a very steep rise, a short, sharp peak, and a steeply declining falling stage.

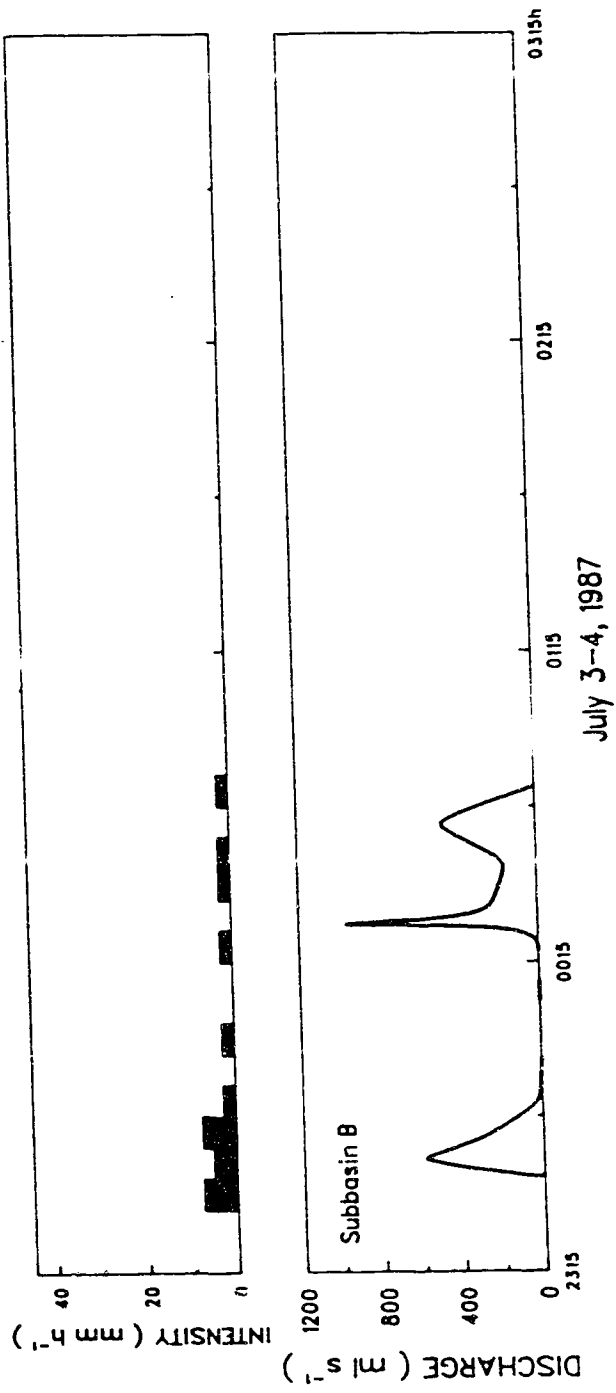


Fig. 4.18 Hydrograph and hyetograph (Rimco recording raingauge) for Subbasin B on July 3-4, 1987, showing isolated periods of flow separated by short, dry intervals.

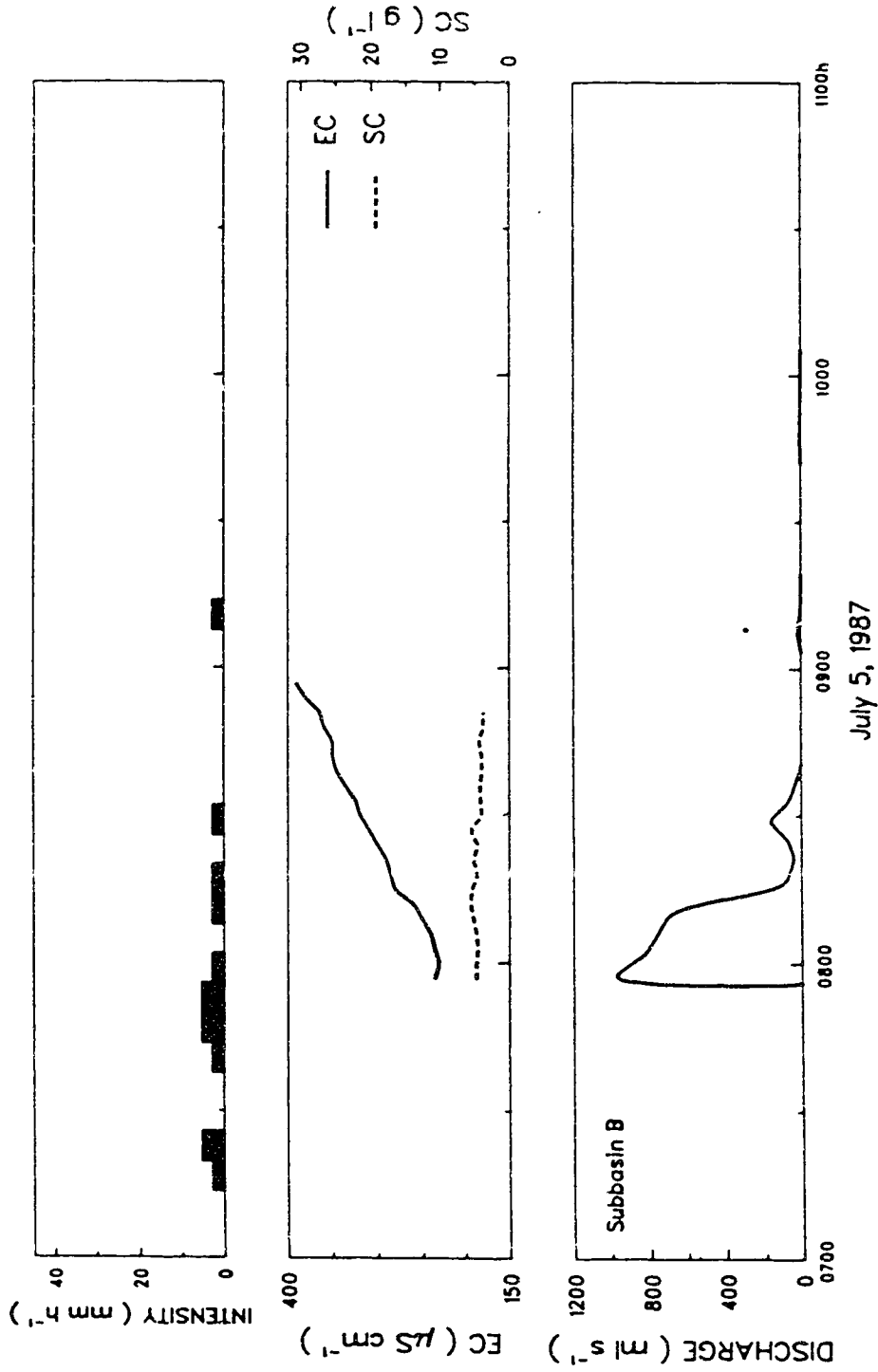
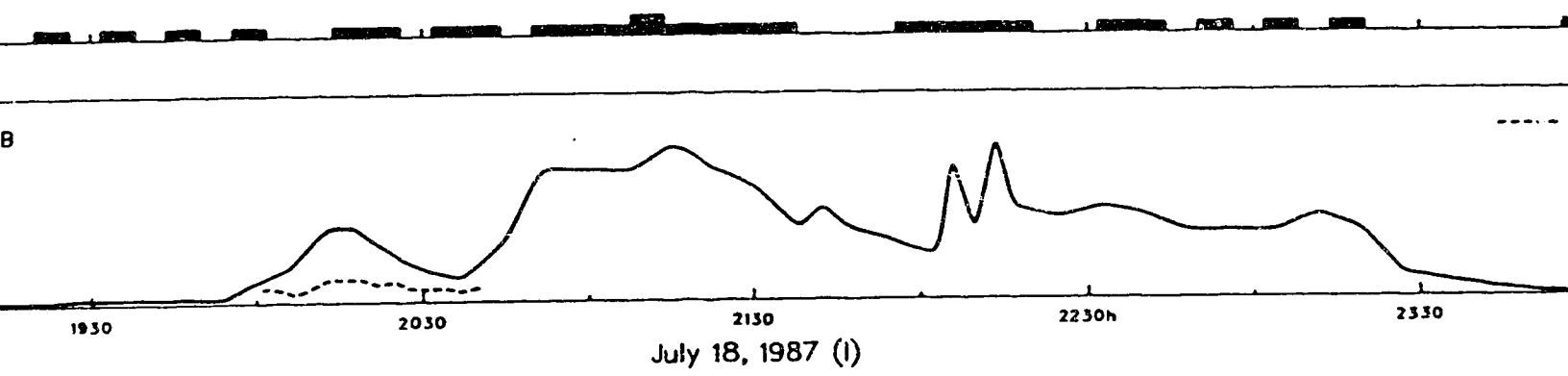


Fig. 4.19 Hydrograph and hietograph (Rimco recording raingauge) for Subbasin B on July 5, 1987, showing the effect of low-intensity rainfall during the falling stage of the hydrograph. The sediment concentration does not show evidence of initial flushing, and is low and fairly constant throughout the runoff event. The EC shows some evidence of initial flushing, reaches a trough during peak flow, and increases sharply during the falling stage.



20 Hydrograph and hyetograph (Rimco recording raingauge) for Subbasin B on July 18, 1987 (I), showing the hydrograph intensity, long-duration, frontal rainstorm. Also shown is the hydrograph of Subbasin A. The smaller discharges in the latter basin are caused by a greater thickness and extent of sheetwash deposits, and by the fact that a portion of the pediment is plain by shale instead of by sandstone as in Subbasin B.

4.6.2 SEDIMENT AND SOLUTE DYNAMICS

As stated in Section 4.2, during runoff 28 samples at most could be taken at 6 min intervals to determine sediment concentrations and EC's. Data are available for eight storms. During most storms less than the maximum of 28 samples were collected due to various problems with the ISCO sampler. A complete EC record is available for only one storm, while there are no storms with a complete sediment concentration record. Thus, it was not possible to calculate sediment yields.

Observed sediment concentrations ranged from 3.4 to 34.4 g l⁻¹. During most runoff events sediment concentrations did not display any evidence of initial flushing, and were relatively constant with time (Fig. 4.19). On July 5, 1987, sediment concentrations were fairly constant and low, ranging from 3.8 to 5.6 g l⁻¹, while peak discharge was only 960 ml s⁻¹. Considerably higher sediment concentrations occurred on May 26, 1987 (I) (Fig. 4.21) and on July 19, 1987 (II). On these dates, the peak discharge exceeded the maximum discharge from the plastic barrel of 1200 ml s⁻¹ (Section 4.2) by a substantial amount, and uncontrolled overflow occurred. Sediment concentrations during peak flow ranged from 30 to 34.4 g l⁻¹. The only event with sediment concentrations showing evidence of initial flushing is that of May 26, 1987 (I) (Fig. 4.21). This event was the first runoff event after a period of a month during which no runoff occurred allowing time for extensive accumulation of readily available sediment. During the second flow peak, sediment concentrations again reached a high value of 30 g l⁻¹. During the third flow peak, however, sediment concentrations did not increase (Fig. 4.21). This may reflect exhaustion of the sediment supply, but may also have been caused by a too large sampling interval causing the peak sediment concentration to be missed. Together with the 10 s lag between triggering the ISCO and the start of sampling this latter cause may also be a factor in explaining the absence of evidence of initial flushing in the sediment concentration data.

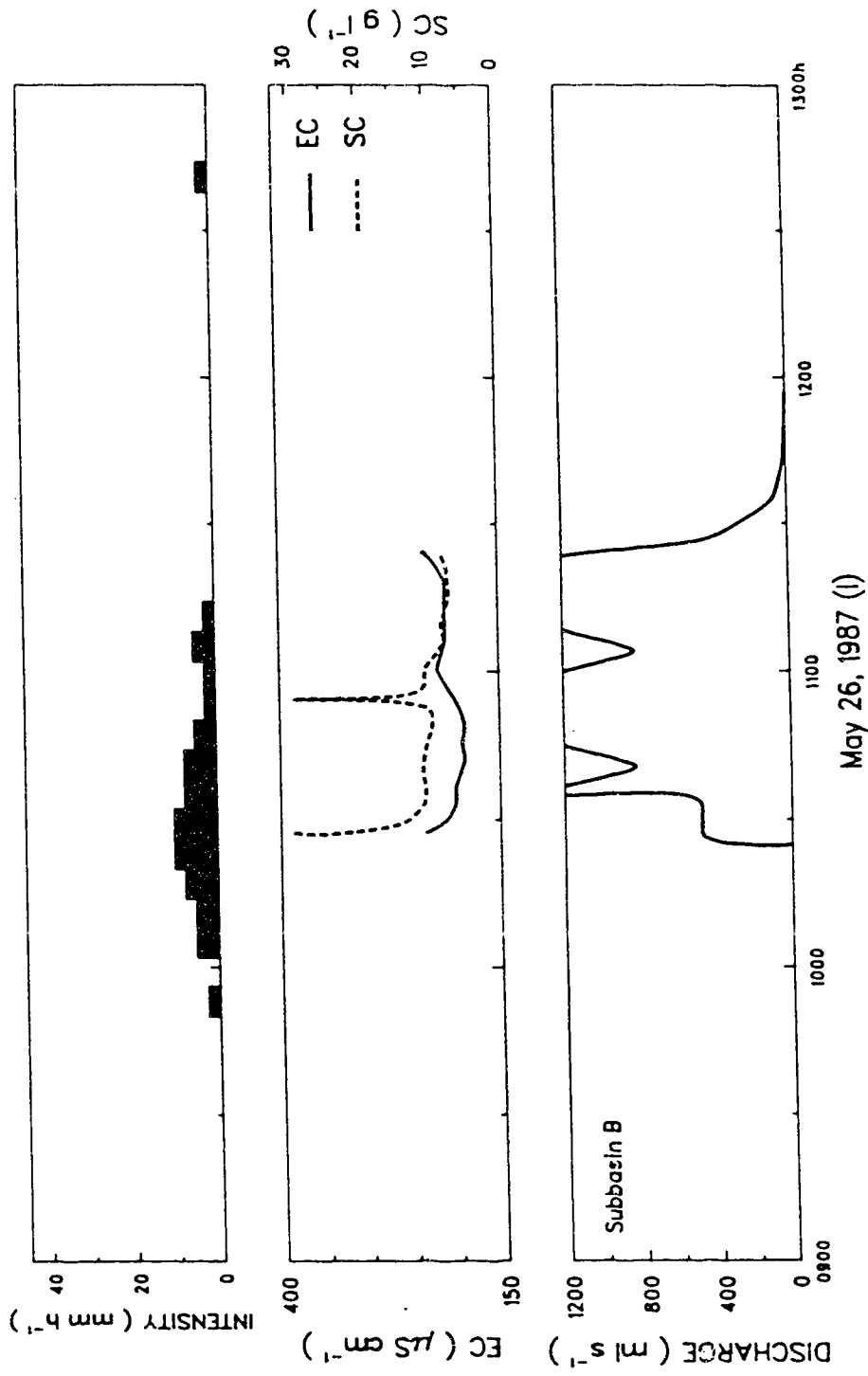


Fig. 4.21 Hydrograph, hycograph (Rimco recording raingauge), sediment concentration, and EC of Subbasin B on May 26, 1987 (I). Peak discharge exceeded the maximum measurable discharge. Sediment concentrations indicate initial flushing, and reach high values during peak flow. EC's show evidence of initial flushing also, reach minimum values during peak flow, and increase again during the falling stage.

Observed EC's ranged from 160 to 390 $\mu\text{S cm}^{-1}$. For three runoff events the EC showed evidence of initial flushing, reached a low during peak flow, and increased again during the falling stage (Fig. 4.19 and 4.21). During other events evidence of initial flushing was absent, likely because the ISCO sampler missed the first runoff from the basin. For August 14, 1987, EC's are available for the entire length of the runoff event. During this long-duration, low-intensity, frontal storm the EC varied inversely with discharge, reaching troughs during peak flows (Fig 4.22). Towards the end of runoff the EC increased steadily to very high values.

4.7 CONTRASTS BETWEEN SUBBASINS A AND B

A comparison of the response of Subbasins A and B shows distinct differences between the two basins. These differences are characterized by the following points:

(1) In Subbasin A, discharges are considerably lower than in Subbasin B (Fig. 4.20). The differences in discharge are considerably larger than can be explained by the differences in area and in the areas of the various surface units between the two basins (Table 4.1). A factor that could possibly explain the differences in discharge is the dissimilar character of the pediment in the basins. In Subbasin A, portions of pediment are underlain by shale, whereas in Subbasin B the entire pediment is underlain by sandstone. The threshold of runoff generation on pediments developed in shale is larger than on those developed in sandstone (Section 3.3.2.1). In addition, the thickness of sheetwash deposit is larger in Subbasin A than in Subbasin B. In the channel at the outlet of Subbasin A a stratified alluvial/sheetwash deposit containing a thin gravel band was present. Thickness of this deposit was in excess of 11 cm. During the microscale plot studies in Subbasin A (Chapter 3) sheetwash deposits with thicknesses of up to 3.5 cm were observed, whereas in Subbasin

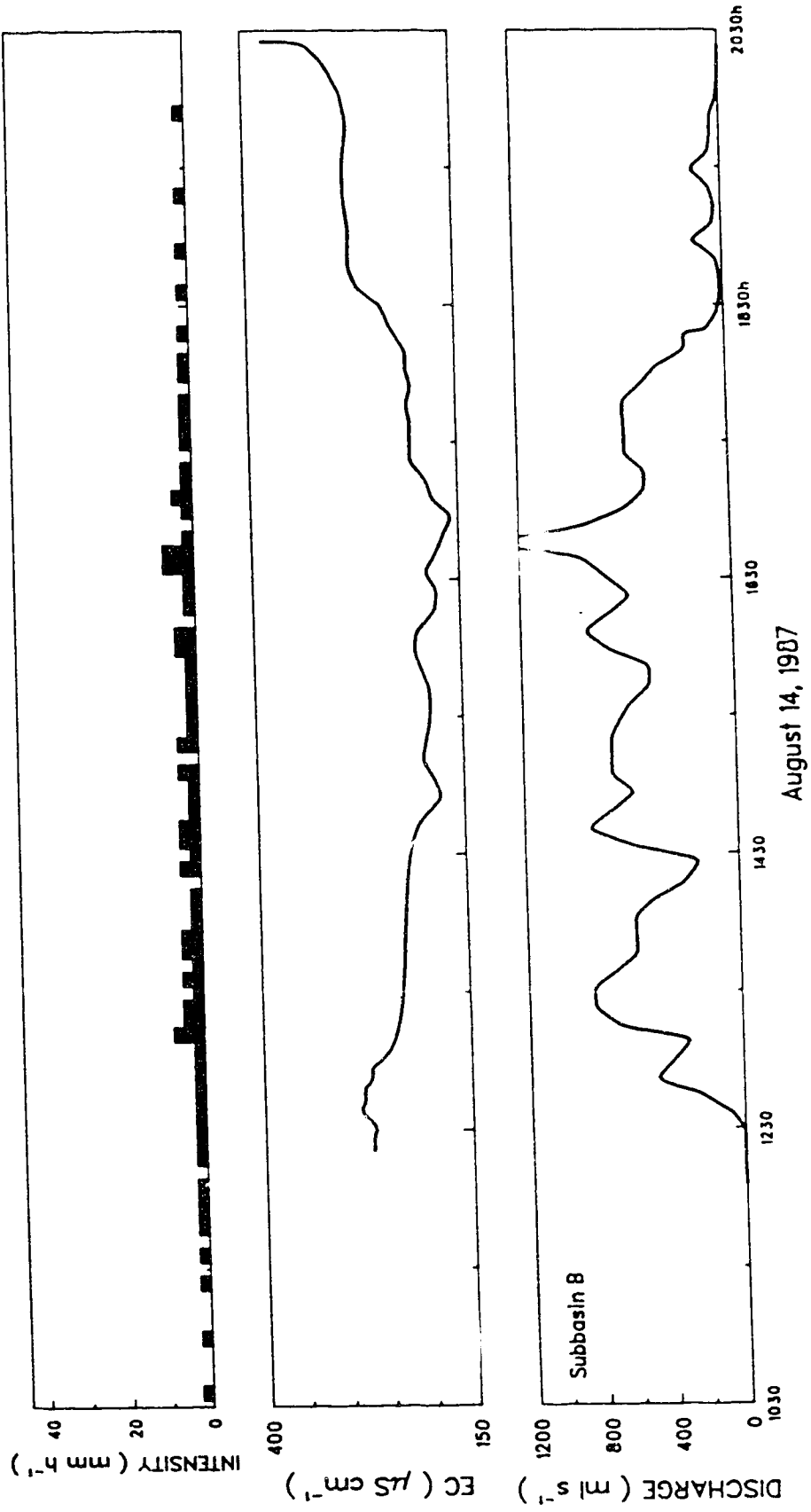


Fig. 4.22 Hydrograph, hyetograph (Rimco recording raingauge), and EC for Subbasin B on August 14, 1987. The EC varies inversely with discharge, and increases to high values towards the end of the runoff event.

B the maximum thickness noted was only 1.0 cm. Both factors, a large portion of the pediment underlain by shale, and a greater thickness of the sheetwash deposit, would serve to delay runoff generation (Section 3.3.2.1) and to increase transmission losses, and hence may explain the lower discharges in Subbasin A.

(2) Sediment concentrations and EC's in runoff from Subbasin A are higher than in runoff from Subbasin B. The high EC's can be explained by the fact that part of the pediment in Subbasin A is underlain by shale. Rainfall simulations showed that runoff from pediments underlain by shale possessed higher EC's than runoff from pediment underlain by sandstone (Section 3.3.2.1). The underlying bedrock, however, did not affect sediment concentrations. A factor that would cause higher EC's and could also explain the higher sediment concentrations in Subbasin A is the arrangement of the surface units within the basin. As stated in Section 4.2, in Subbasin A runoff from sandstones flows downslope onto shales. This has caused tunnel erosion features which can act as important sources of sediment. In Subbasin B such features are absent. This contrast between the two basins has resulted in considerable differences between sediment concentrations in runoff from the basins. For instance, on July 18, 1987 (I), sediment concentrations ranged from 12.2 to 25.8 g l⁻¹ in Subbasin A, and from 5.6 to 6.8 g l⁻¹ in Subbasin B. Similarly large differences were observed during other events.

4.8 SUMMARY

At the subbasin scale, hydrological rainfall (the rainfall received by a tilted raingauge with its orifice parallel to the local slope) and its distribution is more important for explaining the rainfall-runoff relationship than meteorological rainfall (the rainfall received by a standard, horizontally installed raingauge).

The microscale experiments, described in Chapter 3, indicated strong contrasts between the major runoff-producing surface units in the badlands. At the subbasin scale, differences in percentage of the surface units cause contrasts in the magnitudes of discharge, sediment concentration, and EC between Subbasin A and B. Differences in the arrangement of the surface units have resulted in the presence of deep tunnel systems in Subbasin A, and in their absence in Subbasin B, and enhance the contrast between the subbasins. In the following chapter, basin response at the next higher scale level, the mesoscale, will be examined.

CHAPTER 5

5.1 MESOSCALE DRAINAGE BASIN STUDIES

Two drainage basins, the 202,260 m² Rimco Basin and the 79,230 m² New Basin, were instrumented to establish the relationship between rainfall characteristics and the output of water, solutes, and suspended sediment at the mesoscale. Both basins are part of the 336,810 m² Aquatot Basin. The Rimco Basin and the Aquatot Basin have been monitored since 1981 (Bryan and Campbell, 1982, 1986), whereas observation of the New Basin was commenced in 1986. Figure 5.1 shows the configuration and instrumentation of the Rimco Basin and the New Basin. The surface units in both basins are shown in Fig. 5.2. Table 5.1 gives the percentage of the area of each basin taken up by each different surface unit. The percentage of the basin area consisting of rapidly responding surface units (sandstones and pediments) is about equal in both basins (43 per cent in the New Basin, 42 per cent in the Rimco Basin). Differences in area, however, occur in the other surface units. Compared to the New Basin, the Rimco Basin has a larger percentage of vegetated surfaces, whereas shales form a smaller percentage. These differences between the basins are reflected in their response.

5.2 BASIN INSTRUMENTATION

Rainfall was measured by two Belfort weighing rainfall recorders; a Lambrecht automatic siphoning, Hellman-type, recording rain gauge; a CSIRO Rimco tipping bucket rain gauge with a rainfall resolution of 0.01 inch (0.25 mm) and a temporal resolution of 6 min; and nine Taylor Clear-Vu standard rain gauges (Fig. 5.1). Two bulk rainfall collectors were installed near the basin outlets to obtain rainfall samples for chemical analysis. The

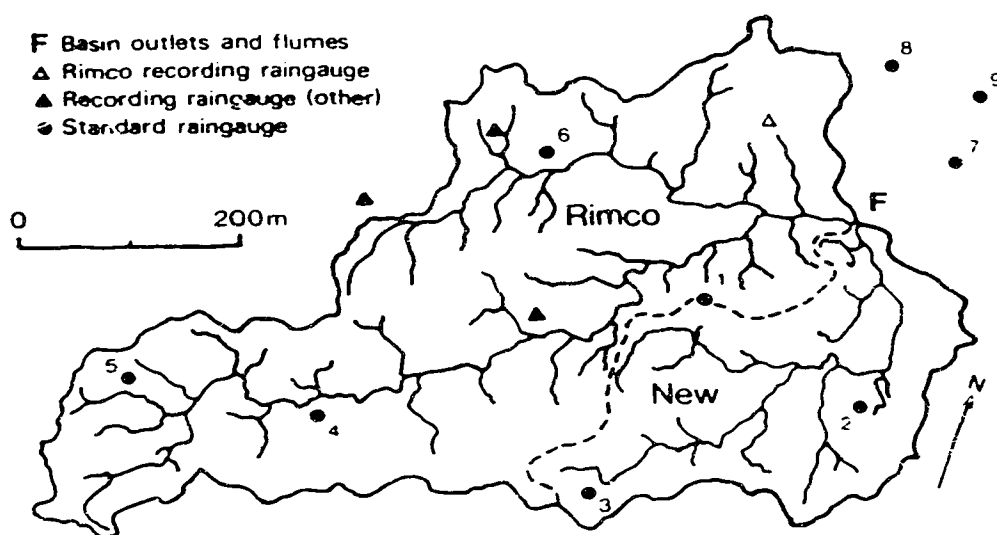


Fig. 5.1 Mesoscale basin configuration and instrumentation.

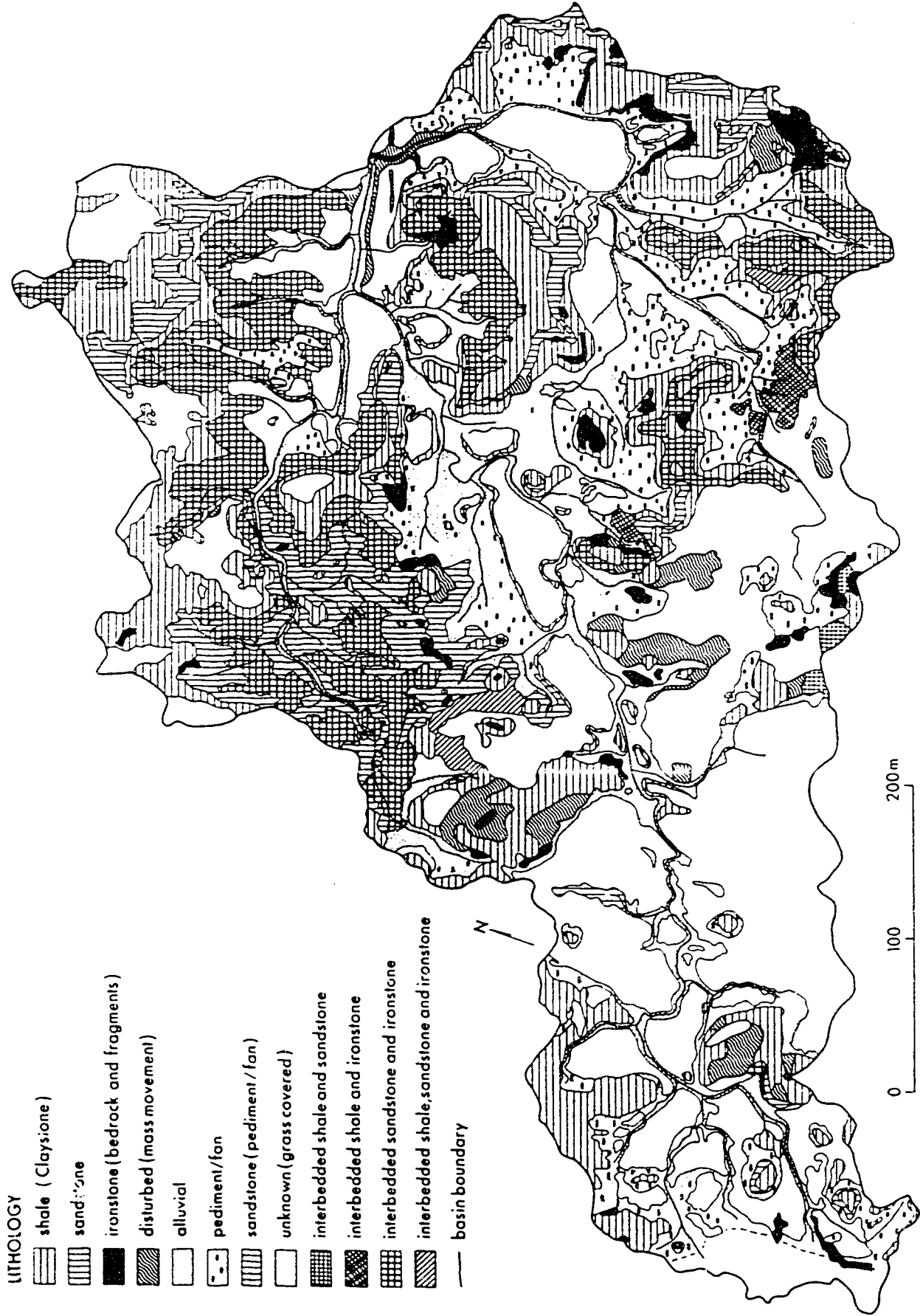


Fig. 5.2 Surface units of the Rimco Basin and the New Basin (Modified after Bryan and Campbell, 1986)

Table 5.1 Percentage of basin area taken up by different surface units.

surface unit	New Basin (%)	Rimco Basin (%)
sandstone†	13	18
pediment‡	30	24
vegetated	24	35
shaleⒹ	25	18
miscellaneous#	7	5

Each group consists of the following units (Fig. 5.2):

† sandstone; interbedded sandstone and ironstone.

‡ alluvial; pediment/fan; sandstone (pediment/fan).

Ⓓ shale; interbedded shale and ironstone.

ironstone; disturbed; interbedded shale and sandstone; interbedded shale, sandstone, and ironstone.

collectors were only opened during rainfall, and extreme care was taken to avoid contamination of the sample. Because the collector had to be opened manually, the first part of rainfall was usually not sampled.

Discharge from the New Basin was measured using a 1.5 feet Parshall flume, combined with a runoff-triggered Aquatot FMS 2280 sonic-echo flow gauge (Fig. 5.3). Discharge from the Rimco Basin was measured using a CSIRO MK.III Rimco streamgauge and a rated flume. Visual stage recordings supplemented the charts of the automatic stage recorders.

During flow, runoff samples were taken manually a few meters upstream from the flumes. The sampling interval was 3 to 4 minutes during the rising stages and the hydrograph peak and was increased, in some cases up to 20 minutes, during the falling stage. Samples for determining solute and sediment concentrations were transported to the laboratory. In 1987, EC data were collected. EC's were measured in the field, directly after sampling.

5.3 LABORATORY PROCEDURES

As with the direct-runoff tests and the rainfall simulations, weakly crystalline gels in the runoff samples (Bryan et al., 1984) precluded separating solutes and suspended sediment by filtration. The sediment concentration was therefore determined by pipetting a known volume of sample into a cup, and measuring the weight of the residue remaining after evaporation of the water. The sediment concentration thus obtained refers to the concentrations of solutes and suspended sediment combined. An analysis of data for twelve storms by Sutherland and Bryan (1988) indicates that solutes accounted for only 1.4 per cent of the total load of solutes and suspended sediment. Sediment concentrations found by the evaporation method will therefore closely approximate suspended sediment

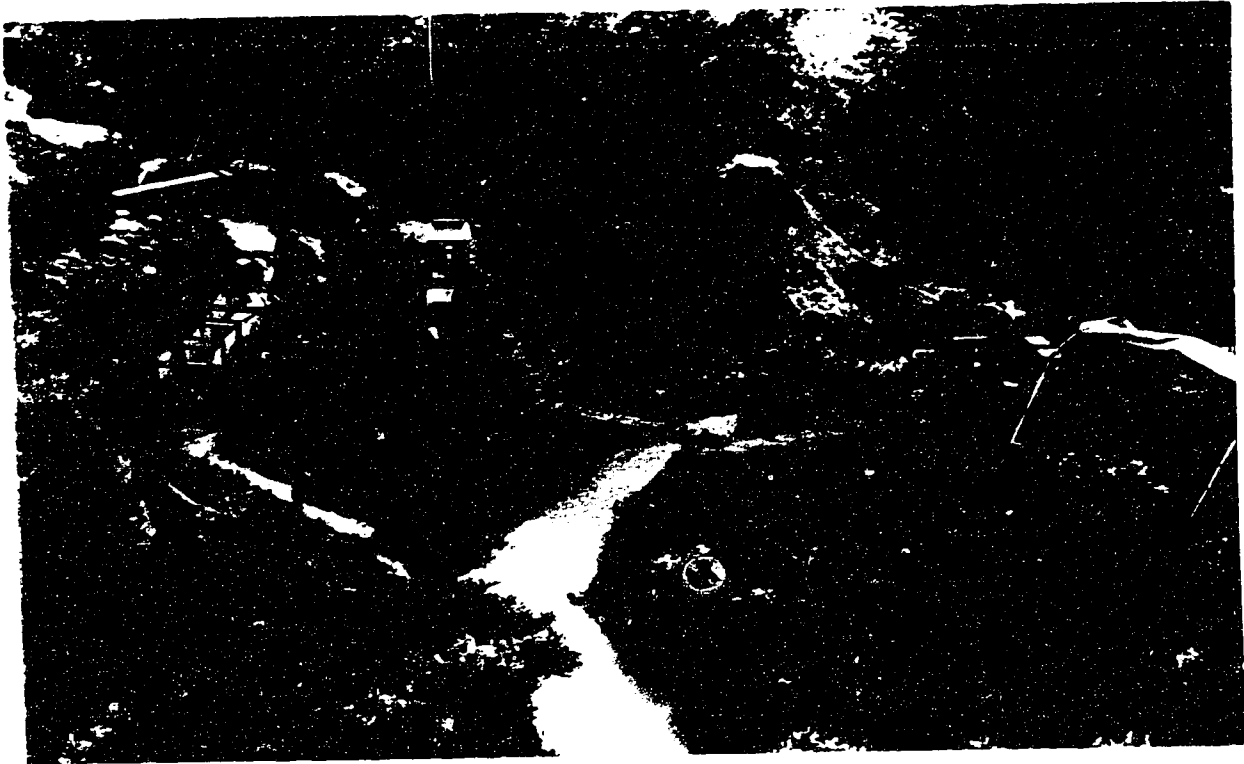


Fig. 5.3 Upstream view of the outlets of the New Basin (left) and the Rimco Basin (right) with the associated instrumentation. The Aquatot sonic-echo flow gauge can be seen suspended above the 1.5 foot wide Parshall flume of the New Basin. The instrument stand between the channels contains batteries, a solar panel for recharging, and the chart recorder for the Aquatot flow gauge. Note the typical light brown colour of the runoff, indicative of the high sediment concentrations.

concentrations.

Because of the problems with filtration, solutes and suspended sediment were separated by centrifuging part of selected samples. About 120 ml of the supernatant liquid was poured into 125 ml polyethylene bottles and stored in a refrigerator for further analysis of the major cations and SO_4 . Concentrations of Na, K, Ca, Mg, and Al were determined by atomic absorption spectrometry on a Perkin-Elmer spectrometer. Sulphate concentrations were determined with a Technicon Autoanalyzer II.

5.4 THE RAINFALL-RUNOFF RELATIONSHIP

During the summers of 1986 and 1987 data for the falling and rising stage of 15 runoff events were collected in the Rimco Basin and the New Basin (Table 5.2). Data were collected for an additional 4 minor runoff events, but because the rising stage was missed, these data are incomplete, and are not used. No runoff data were collected for 7 minor runoff events, either because rainfall was so localized that rainfall characteristics at the campsite did not suggest runoff would occur in the research basins, or because all sample bottles were full. In Table 5.2, rainfall for each storm is calculated by taking the average of the rainfall for each raingauge. The density of the gauge network in relation to the spatial variability of the rainfall does not warrant applying more sophisticated methods of calculating total rainfall over the basin. Certain standard raingauges (no.'s 3 and 7) consistently received less rainfall than the others. These deviations are caused by the local topography in relation to the prevailing wind directions during a storm. Extrapolation of the rainfall data to obtain accurate areal values would need to take these two factors into account, and is beyond the scope of this study.

Table 5.2 also shows the API (Antecedent Precipitation Index) for each storm (Section 4.6.1). A plot of the API against total rainfall for each storm shows that the

Table 5.2 Overview of rainfall and runoff data collected during 1986 and 1987.

date	average rainfall (mm)	API†	Rimco Basin‡	New Basin‡
<u>1986</u>				
June 8	3.8	0.0	—	—
June 14	3.0	1.0	—	—
June 18	1.0	1.6	—	—
June 29	2.6	0.2	F	F
June 30	4.9	2.3	F	F
July 5 (I)	7.3	2.3	X	X
July 5 (II)	3.4	9.6	X	R
July 9	7.0	5.3	X	X
July 11	3.1	7.9	F	F
July 19	2.4	1.8	R	R
July 26	8.0	0.9	X	X
August 5	4.3	1.0	X	X
August 8	1.8	2.7	X	X
<u>1987</u>				
May 26 (I)	6.0	0.0	X	X
May 26 (II)	4.5	6.0	X	X
May 27	2.5	8.4	X	R
June 16	3.0	0.1	—	—
June 19 (I)	4.2	1.6	X	X
June 19 (II)	12.6	5.8	X	X
June 20	3.9	14.7	X	X
June 30	2.0	2.0	—	—
July 3-4	3.9	2.0	R	R
July 5	2.6	3.8	F	F
July 6-7	1.0	5.1	—	—
July 16	2.0	0.7	—	—
July 18-19	10.2	1.7	X	X
July 25	3.5	2.5	R	R
July 28	1.3	3.1	—	—
August 4	2.1	0.9	R	R
August 10	4.6	0.8	X	X
August 11	2.8	4.3	R	R
August 13	0.5	4.6	—	—
August 14	17.6	4.0	X	X
August 16-17	4.1	13.9	R	R
August 18-19	6.3	11.5	R	R

† Antecedent Precipitation Index

‡ — - no runoff

X - complete data (rising and falling stage)

F - data for falling stage only

R - runoff occurred, but no data were collected

rainfall necessary to cause runoff tends to increase under drier antecedent moisture conditions (Fig. 5.4). However, this tendency does not always occur. A few storms indicate that runoff generation is also controlled by factors other than total rainfall and antecedent moisture conditions, such as rainfall intensity and spatial distribution of rainfall. Although the larger Aquatot Basin shows a larger response time (Bryan and Campbell, 1986), in the size range of the Rimco Basin and the New Basin this effect of increasing size is not evident, and is overshadowed by the effect of the rainfall distribution. The effect of basin size on response times would probably be more apparent if the New Basin and the Rimco Basin were nested.

5.4.1 RUNOFF COEFFICIENTS

Data on the total rainfall, total discharge, runoff coefficients, and antecedent moisture conditions are presented in Tables 5.3 and 5.4, for the Rimco Basin and the New Basin, respectively. Table 5.5 contains previously published data for the Rimco Basin for 1981 from Sutherland (1983), and for 1982 from Bryan and Campbell (1986).

Part of the total discharge data for 1986 and 1987 are minimum estimates because the start of the flow was missed so that reliable estimates of discharge in the early stages of runoff could not be made. Consequently, runoff coefficients calculated for these events are minimum estimates also. Runoff coefficients and total discharges for 1981 and 1982 in Table 5.5 may suffer from the same problem, and should be interpreted with caution.

The relationship between total rainfall (mm) and total discharge (mm) for the Rimco Basin and the New Basin in 1986 and 1987 is shown in Fig. 5.5 for those storms for which total discharge is not a minimum estimate. Also shown in Fig. 5.5 are the antecedent moisture conditions for each storm, and lines indicating the value of the runoff coefficient. As expected, runoff coefficients tended to increase with higher antecedent

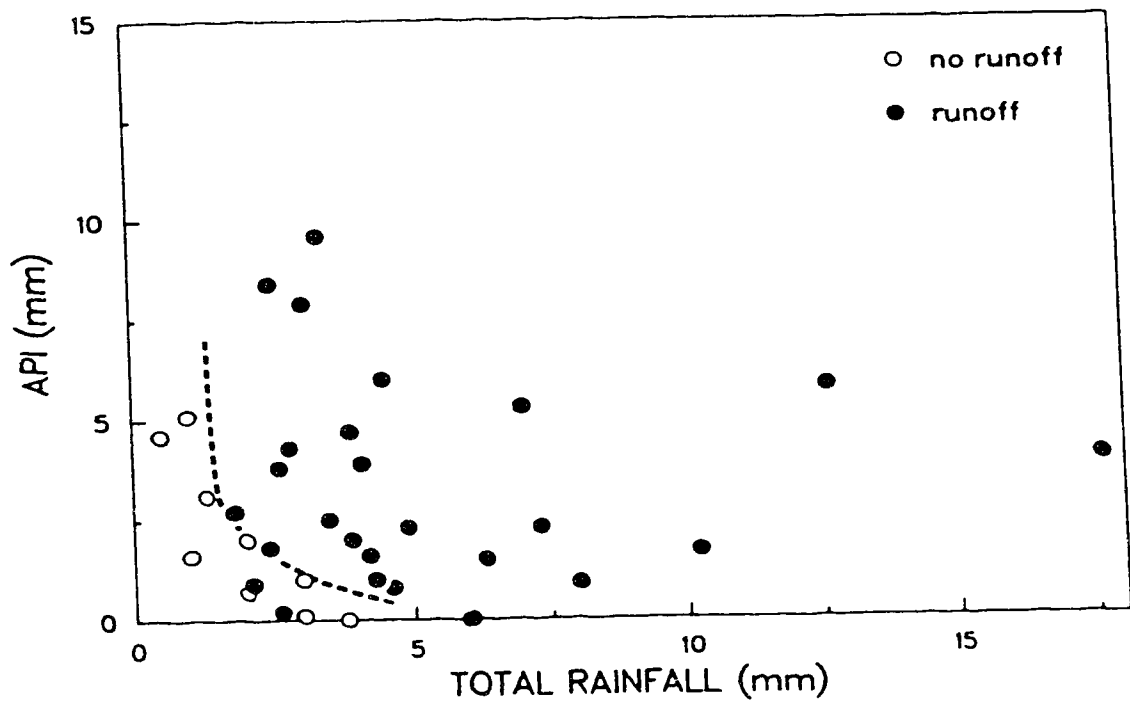


Fig. 5.4 Antecedent Precipitation Index plotted against total rainfall for each storm for the Rimco Basin and the New Basin.

Table 5.3 Rainfall, runoff, and sediment yields of the Rimco Basin for 1986 and 1987.

date	total rainfall (mm)	total discharge (mm)	runoff coefficient (%)	sediment yield per unit area (kg ha ⁻¹)
<u>1986</u>				
July 5 (I)	7.3	0.3†	4†	46†
July 5 (II)	3.4	0.5	14	144
July 9	7.0	1.3†	19†	495†
July 26	8.1	1.5†	18†	546†
August 5	4.3	0.4†	9†	92†
August 8	1.8	0.1	4	10
<u>1987</u>				
May 26 (I)	6.0	0.5	8	84
May 26 (II)	4.5	0.3†	8†	65†
May 27	2.5	0.2†	9†	61†
June 19 (I)	4.2	0.2	4	26
June 19 (II)	12.6	3.1	25	1042†
June 20	3.9	0.6	15	149
July 18	10.2	0.6	6	58
August 10	4.6	0.3†	7†	53†
August 14	17.6	2.5†	14†	592†

† indicates a minimum estimate

Table 5.4 Rainfall, runoff, and sediment yields of the New Basin for 1986 and 1987.

date	total rainfall (mm)	total discharge (mm)	runoff coefficient (%)	sediment yield per unit area (kg ha ⁻¹)
<u>1986</u>				
July 5 (I)	7.3	0.4†	5†	80†
July 9	7.0	1.1†	16†	454†
July 26	5.2	1.7†	32†	728†
August 5	4.3	0.6†	14†	198†
August 8	1.8	0.04	2	7
<u>1987</u>				
May 26 (I)	6.0	0.4	7	109
May 26 (II)	4.5	0.3†	6†	60†
June 19 (I)	4.2	0.1	3	14
June 19 (II)	12.6	4.4	35	1719†
June 20	3.9	0.9	22	299
July 18	10.2	1.0	10	134
August 10	4.6	0.5†	11†	107†
August 14	17.6	6.4†	36†	2296†

† indicates a minimum estimate

Table 5.5 Rainfall, runoff, and sediment yields of the Rimco Basin for 1981 and 1982.

date	total rainfall (mm)	total discharge (mm)	runoff coefficient (%)	sediment yield per unit area (kg ha ⁻¹)
<u>1981</u>				
May 6	11.0	2.1	20	—
May 7	8.5	4.5	54	—
May 15-16	25.1	10.6	43	—
May 22	3.5	1.0	29	—
June 3	4.2	1.3	32	—
June 10	7.4	1.7	23	—
June 13	20.5	6.7	33	—
June 23	2.5	0.7	29	—
June 27	3.6	0.9	26	—
June 28	5.0	2.2	45	—
July 1	30.2	5.0	17	—
July 13	7.6	2.0	27	—
<u>1982</u>				
June 5	24.1	10.1	42	—
June 27	21.0	5.2	25†	1340
July 1	10.0	3.9	39	1040
July 9	17.9	8.4	47	1870
July 25	8.0	2.0	24	190

† indicates a minimum estimate

(Source: Sutherland, 1983; Bryan and Campbell, 1986)

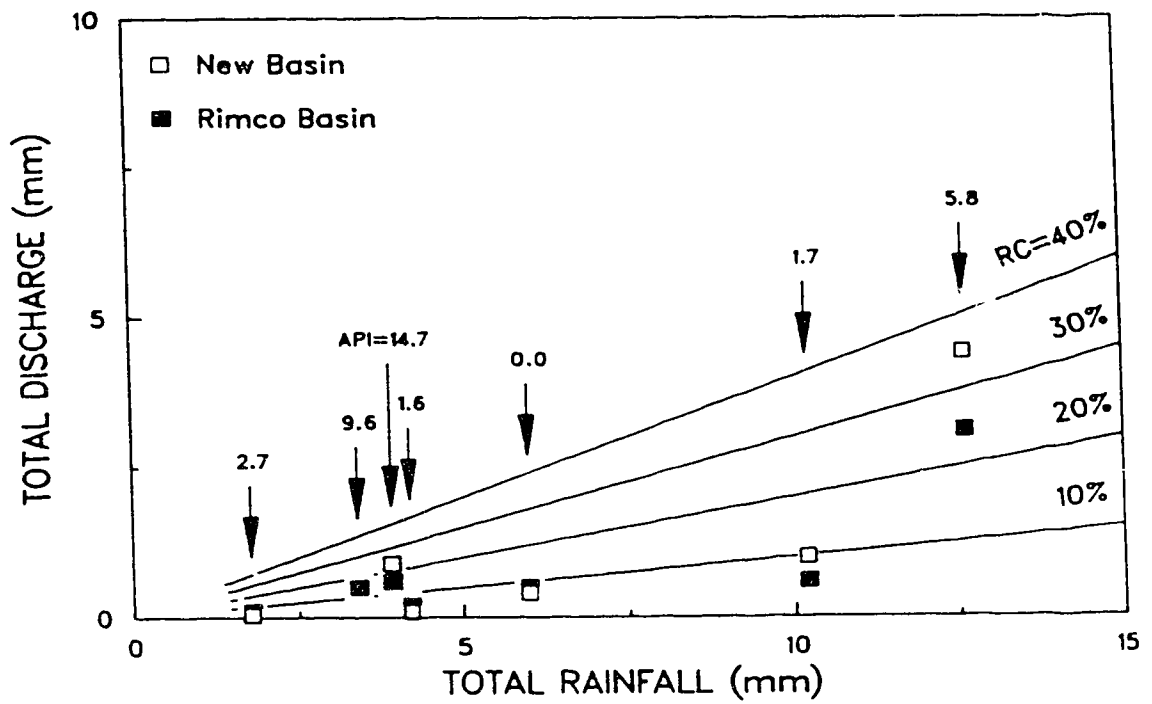


Fig. 5.5 Relationship between total rainfall and total discharge for the Rimco Basin and the New Basin.

moisture conditions. Equally expected, for similar moisture conditions, runoff coefficients increased with rainfall, as losses constituted a smaller percentage of the total rainfall.

Compared to the runoff coefficients for the Rimco Basin reported by Sutherland (1983) and Bryan and Campbell (1986) (Table 5.5), runoff coefficients found during the present study are generally lower. This may partly be explained by antecedent moisture conditions. Overall, 1981 and 1982 were much wetter. For instance, total rainfall for June and July combined was 81.0 mm in 1981 (Sutherland, 1983), 115.3 mm in 1982 (Bryan and Campbell, 1986), but only 45.2 mm and 50.2 mm in 1986 and 1987, respectively. The Rimco Basin was generally much drier in 1986 and 1987, and infiltration and transmission losses were higher than during 1981 and 1982.

Runoff coefficients of the Rimco Basin and the New Basin were generally similar (Tables 5.3 and 5.4). Figure 5.6 shows the ratio of the runoff coefficients of both basins (runoff coefficient Rimco Basin divided by runoff coefficient New Basin) plotted against total rainfall. For those events for which the runoff coefficient is a minimum estimate, it has been assumed that the true value of the runoff coefficient has been underestimated by the same percentage for both basins, so that the ratio of the true runoff coefficients is equal to that of the minimum estimates. Figure 5.6 suggests that with increasing total rainfall, the runoff coefficient of the New Basin increases more rapidly than that of the Rimco Basin. This can be explained by the higher proportion of vegetated, aeolian surfaces in the Rimco Basin (Table 5.1). Infiltration capacities on these surfaces are very high. Bryan and Hodges (1984) found that no runoff was generated during rainfall simulations in which ca. 16 mm of rainfall were delivered to a vegetated plot at intensities of ca. 40 mm h⁻¹. Thus, except possibly during exceptionally prolonged, severe storms, vegetated surfaces will not produce runoff. The presence of vegetated surfaces will limit the runoff coefficient to a greater extent in the Rimco Basin than in the New Basin. This effect will be most pronounced under conditions of high antecedent rainfall and, possibly, of high antecedent moisture. The influence of the latter factor, however, was not evident from the

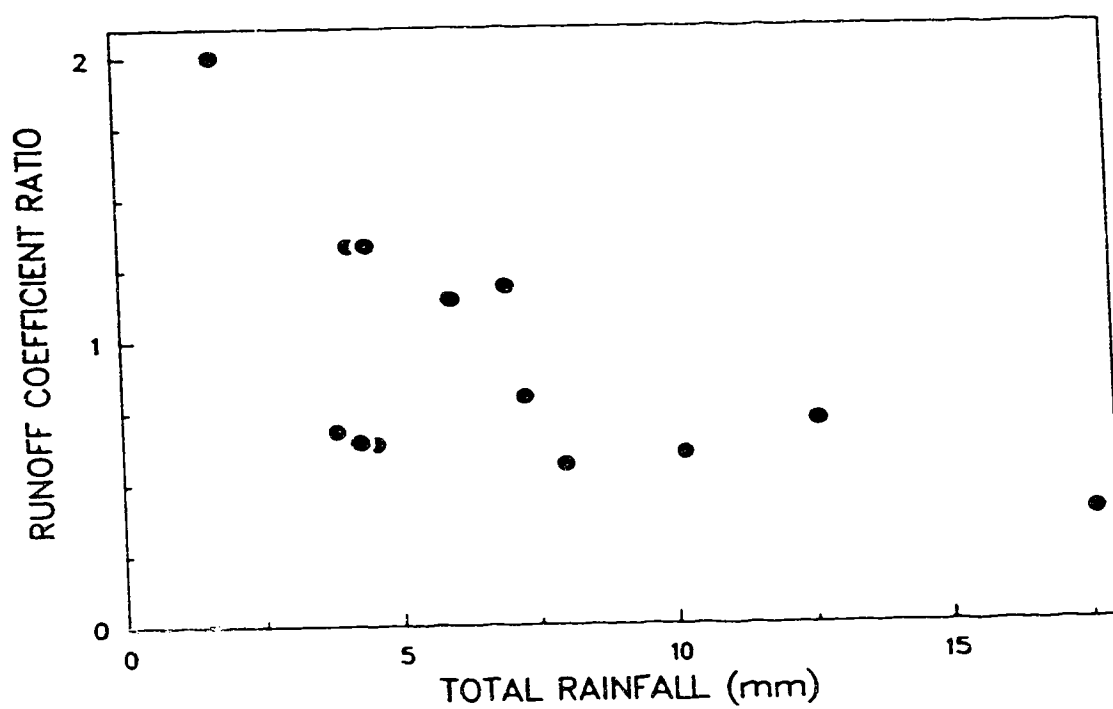


Fig. 5.6 Ratio of runoff coefficients of the Rimco Basin and the New Basin (runoff coefficient Rimco Basin divided by runoff coefficient New Basin) plotted against total rainfall.

data, probably because the spatial distribution of the rainfall in relation to the location of the runoff sources also affects runoff coefficients. For five runoff events the ratio of the runoff coefficients of the two basins is greater than one, indicating a higher runoff coefficient for the Rimco Basin than for the New basin. For certain storms (e.g. July 9, 1986) this is attributed to the spatial distribution of rainfall (Fig. 5.7). For other storms, evidence of the effect of rainfall distribution is less clear. Nevertheless, for all storms during which the ratio of the runoff coefficients is larger than one, rainfall intensities reach moderate to high values characteristic of spotty, convective rainfall.

An example of a storm of reasonably high total rainfall and high antecedent moisture conditions, but with a higher runoff coefficient for the Rimco Basin than for the New Basin, occurred on July 9, 1986. The standard raingauges show a total rainfall of 10 to 13.5 mm in the upper part of the Rimco Basin, which was considerably more than in the New Basin and the remainder of the Rimco Basin (Fig. 5.7). This extra rainfall caused a second peak in the hydrograph of the Rimco Basin, while hardly affecting the hydrograph at the Rimco rain gauge and the hydrograph of the New Basin (Fig. 5.8). If the average rainfall in the Rimco Basin is calculated on the basis of only the raingauges in the basin, the total rainfall becomes 8.9 mm, the runoff coefficient decreases to 16 per cent (a minimum estimate), and the ratio of the runoff coefficients becomes 1. This example shows that in addition to antecedent moisture and total rainfall, the spatial distribution of rainfall strongly affect runoff generation in the badlands.

5.4.2 HYDROGRAPH CHARACTERISTICS

The shape of the hydrograph is controlled by the spatial and temporal distribution of rainfall, and by drainage basin characteristics such as the drainage network pattern and the location of partial areas (Gregory and Walling, 1973). Variations in these factors cause

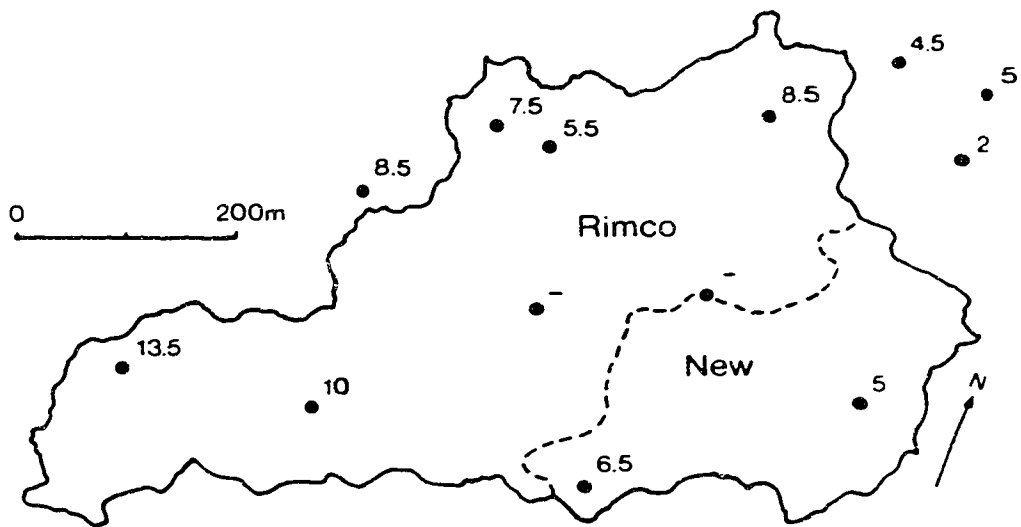


Fig. 5.7 Total rainfall distribution on July 9, 1986.

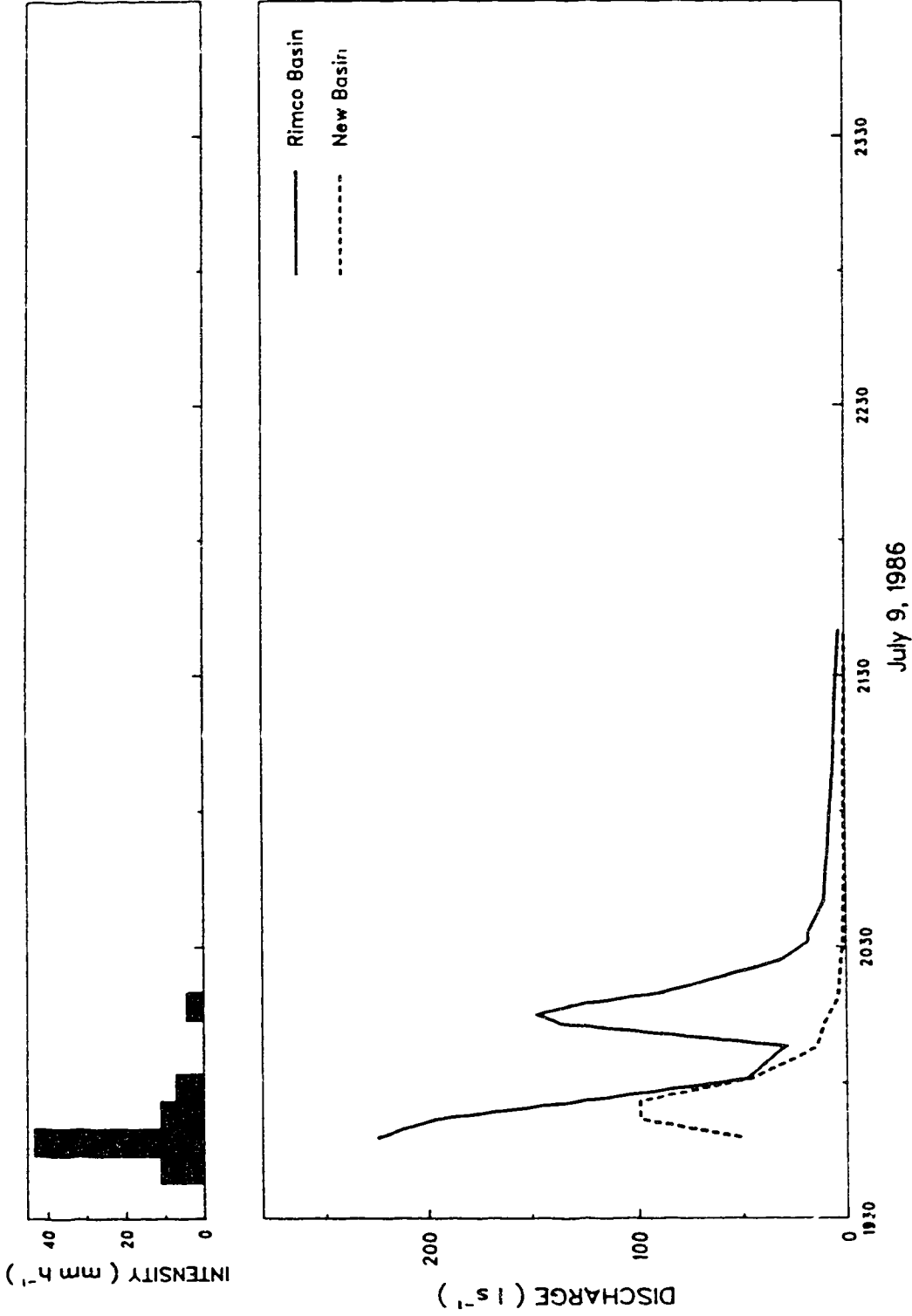


Fig. 5.8 Hydrographs and hyetograph (Rimco recording raingauge) for July 9, 1986. The second peak in the hydrograph of the Rimco Basin is caused by localized rainfall in the upstream parts of the basin. This rainfall, however, has no significant effect on the hydrograph of the New Basin.

a large variety in hydrograph shapes for the Rimco Basin and the New Basin. Rainfall and runoff data from two storms, on July 26, 1986, and July 18, 1987, of similar total rainfall and antecedent moisture conditions show the effect of rainfall characteristics on hydrograph shape.

The storm of July 26, 1986, was a typical early evening, convectional thunderstorm. Total rainfall on this day was 23.7 mm for Brooks AHRC, 6.8 mm for Brooks North, 11.0 mm for Brooks One Tree, 4.4 mm for Cessford, and 7.8 mm for Iddesleigh (Figs. 2.1 and 2.3). Average total rainfalls for the Rimco Basin and the New Basin were 8.1 and 5.2 mm, respectively. Total rainfall for the Rimco tipping bucket rain gauge was 8.3 mm, and peak intensity for a six minute period was 26 mm h^{-1} so that 31 per cent of the total rainfall occurred during this period (Fig. 5.9). The large differences in total rainfall, both between the stations on the prairie surface and between the Rimco and the New Basin, and the relatively high peak intensity, are characteristic of a convectional thunderstorm. The hydrographs of both basins are characterized by a steep rise, a high, narrow peak, and a sharp decline (Fig. 5.10). Peak discharge for the Rimco Basin was 270 l s^{-1} , which occurred at 2122 h, ca. 7 min after the rainfall intensity peak. For the New Basin, the peak discharge of 125 l s^{-1} occurred at 2126 h, ca. 11 min after the peak of the rainfall intensity. Because the Rimco tipping bucket rain gauge is located in the Rimco Basin, ca. 170 m outside the New Basin, the temporal pattern of the rainfall intensity for the Rimco rain gauge may not be representative of rainfall characteristics in the New Basin. When compared to the Rimco Basin, the larger lagtime between peak discharge and peak rainfall intensity for the New Basin is most likely caused by this effect.

In contrast to the previously described event, the storm of July 18, 1987, exemplifies a rainstorm associated with the passage of a frontal disturbance. The daily rainfall was 18.8 mm for Brooks AHRC, 20.4 mm for Brooks North, 19.4 mm for Brooks One Tree, 0 mm for Cessford, and 13.4 mm for Iddesleigh (Figs. 2.1 and 2.4). Average total rainfall for the Rimco and the New Basin was 10.2 mm. Total rainfall for the Rimco

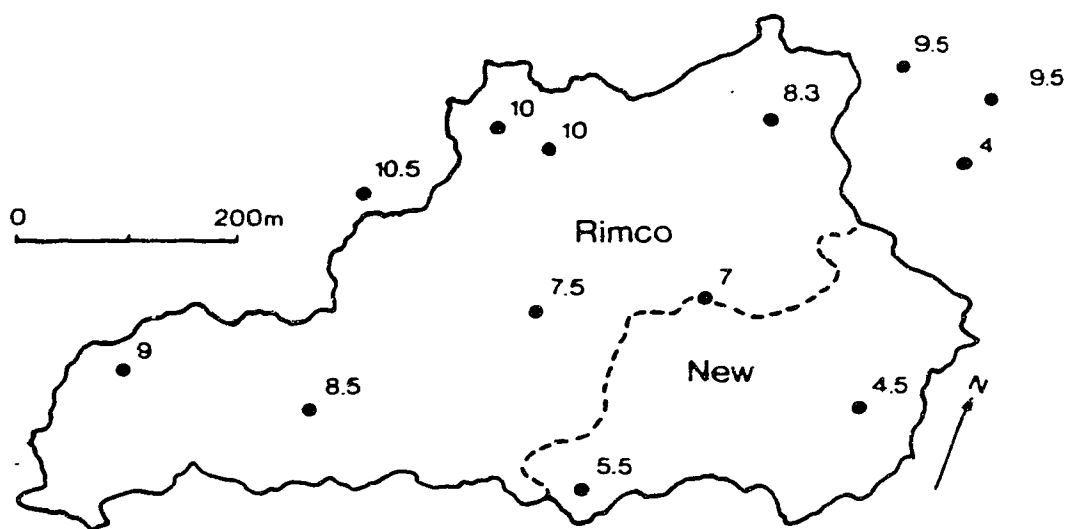


Fig. 5.9 Total rainfall distribution on July 26, 1986.

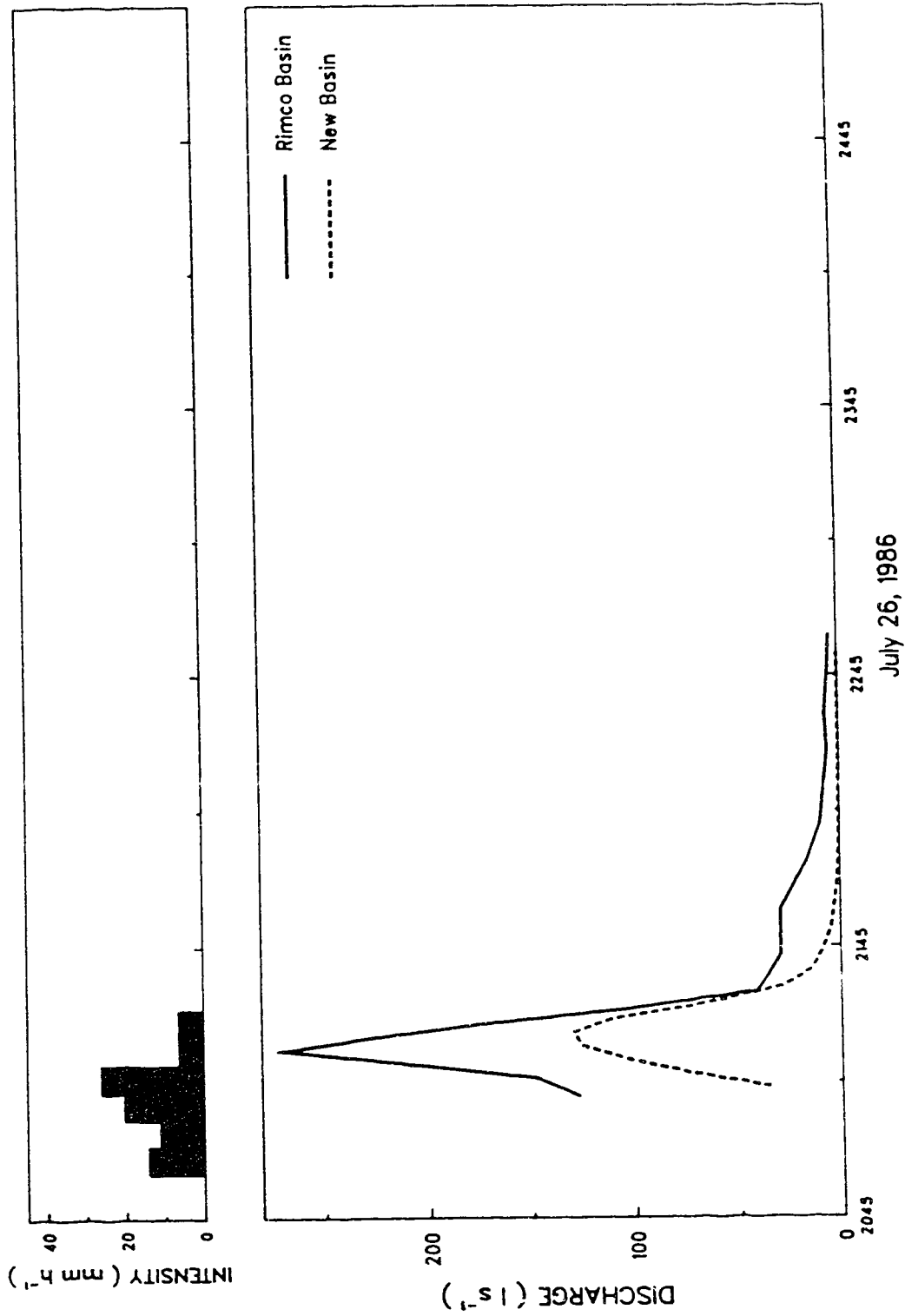


Fig. 5.10 Hydrographs and hietograph (Rimco recording raingauge) for July 26, 1986, showing typical basin response to a convectonal thunderstorm.

tipping bucket raingauge was 9.1 mm, and peak intensity for a six minute period was 7.6 mm h⁻¹ so that only 8 per cent of the total rainfall occurred during this period (Fig. 5.11). The total rainfalls for the three stations in Brooks were very similar. In contrast to this, on July 26, 1986, Brooks North received only 29 per cent of the total rainfall at Brooks AHRC. This indicates that even though differences in total rainfall between the three stations in Brooks and those in Cessford and Iddesleigh are sizeable, the variability of rainfall was considerably less on July 18, 1987, than on July 26, 1986. Combined with the long duration and the low intensity of the rainfall, this points to a frontal storm.

Because of the temporal pattern of rainfall, the hydrograph differs strongly from the hydrograph caused by a convectional storm. The hydrograph of July 18, 1987, is characterized by a very slow and gradual rise, a flat, rounded peak, and a gradual fall sustained by low intensity (less than 2.5 mm h⁻¹) rainfall (Fig. 5.12). Peak discharge for the Rimco Basin was 21 l s⁻¹, which occurred at 2124 h, ca. 7 min after the peak rainfall intensity. For the New Basin, peak discharge was 23 l s⁻¹, and occurred between 2123 and 2127 h. The similarity of the peak discharges of the two greatly different in size basins, illustrates the differences in rainfall and drainage basin characteristics between the Rimco and the New Basin.

The differences in rainstorm characteristics between the storms of July 26, 1986, and July 18, 1987, are also reflected in the runoff coefficients of the basins. On July 26, 1986, the runoff coefficient of the Rimco basin was minimally 18.4 per cent, whereas on July 18, 1987, the runoff coefficient was 5.9 per cent. Similarly, the runoff coefficient of the New Basin was minimally 31.8 per cent on July 26, 1986, and 9.5 per cent on July 18, 1987. A small portion of the difference between the runoff coefficients for both storms may be explained by the long duration of rainfall on July 18, 1987, allowing increased evaporation during the event. More importantly, however, the low rainfall intensities on July 18, 1987, allowed a considerable portion of rainfall to infiltrate, even though two of the three major surface units in the basins (pediments and sandstones) have limited

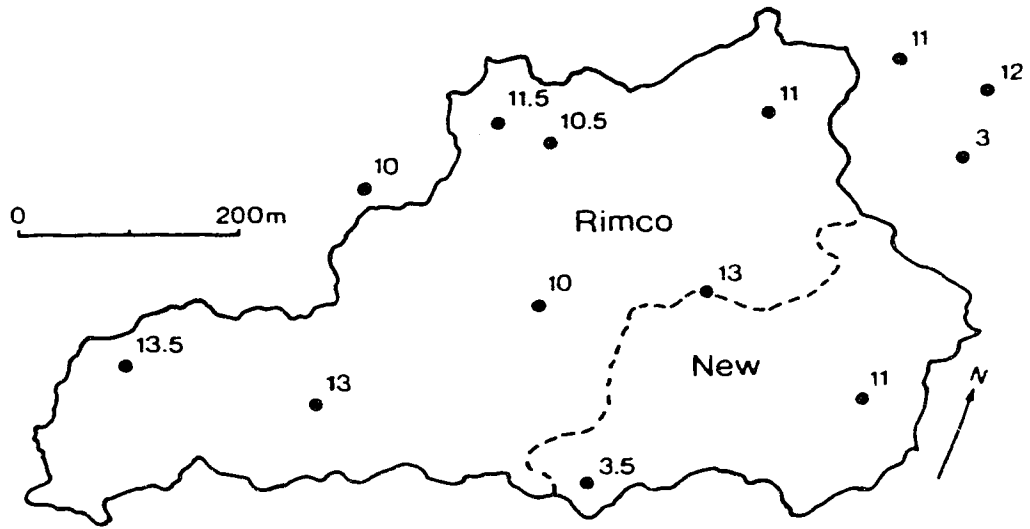


Fig. 5.11 Total rainfall distribution on July 18, 1987.

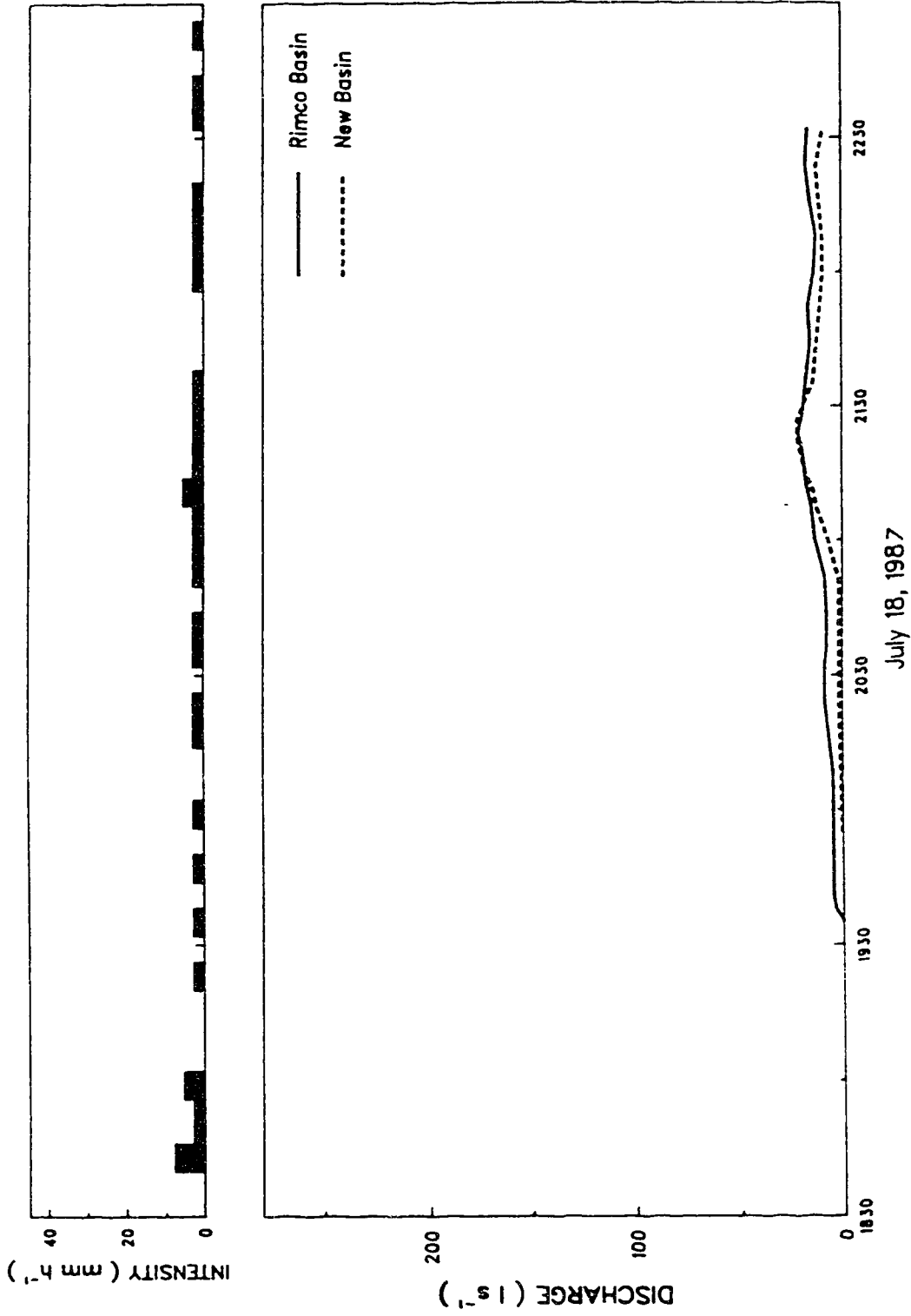


Fig. 5.12 Hydrographs and hyetograph (Rimco recording rain gauge) for July 18, 1987, showing typical basin response to frontal rainfall.

infiltration capacities. The higher rainfall rates on July 26, 1986, exceeded the infiltration capacity of most surface units, resulting in a considerably higher runoff coefficient.

5.5 SEDIMENT DYNAMICS

5.5.1 SEDIMENT YIELDS

Included in Tables 5.3 and 5.4 are the sediment yields per unit area for the Rimco and the New Basin. As with the runoff coefficients, certain sediment yields represent a minimum estimate because of missing data for the rising limb of the hydrograph. On one occasion, the runoff event of June 19, 1987 (II), the sediment yields represent a minimum estimate because of missing sediment concentration data during the event.

A plot of total rainfall against sediment yield shows that for those events for which the sediment yield is not a minimum estimate, sediment yield in general sharply increases with total rainfall (Fig. 5.13). Also shown in Fig. 5.13 is the effect of antecedent moisture conditions on the sediment yield. As expected, higher antecedent moisture conditions are accompanied by higher sediment yields. This pattern is not disturbed by adding the minimum estimates (Tables 5.3 and 5.4). Because of the difference in size between the Rimco Basin and the New Basin, runoff coefficients and sediment yields would be expected to be lower in the Rimco Basin than in the New Basin due to larger transmission losses and increased possibilities for storage of sediment. Both Fig. 5.6 and 5.14, however, show that additional factors have to be taken into account. Figure 5.14 shows the ratio of the sediment yields per unit area for the Rimco Basin and the New Basin (sediment yield Rimco Basin divided by sediment yield New Basin) plotted against total rainfall. For those events for which the sediment yield is a minimum estimate, it has been assumed that the true value of the sediment yield has been underestimated by the

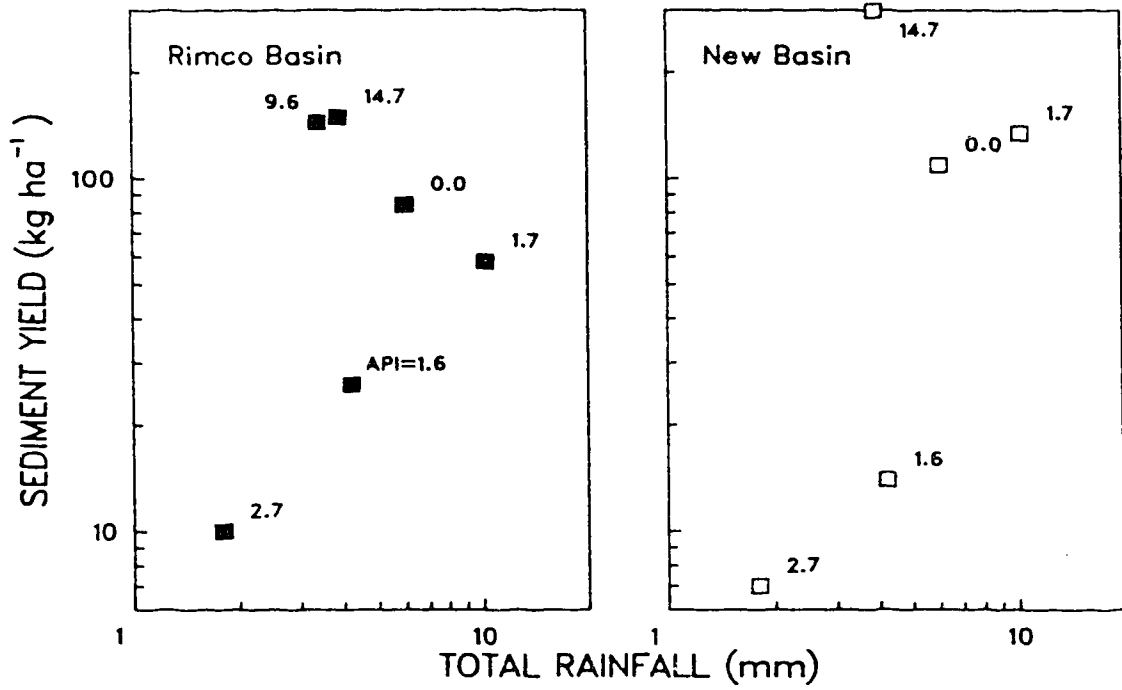


Fig. 5.13 Relationship between total rainfall and sediment yield per unit area, and the effect of antecedent moisture conditions (API).

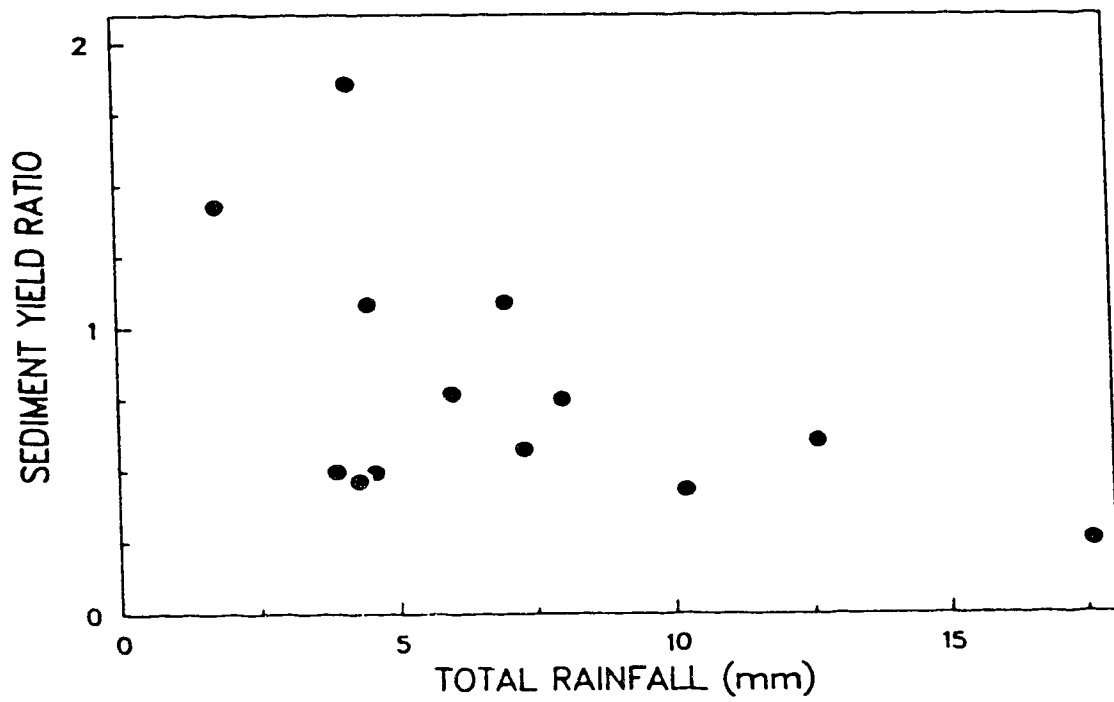


Fig. 5.14 Ratio of sediment yield per unit area of the Rimco Basin and the New Basin (sediment yield Rimco Basin divided by sediment yield New Basin) plotted against total rainfall.

same percentage for both basins, so that the ratio of the true sediment yields is equal to that of the minimum estimates. The pattern displayed in Fig. 5.14 is similar to that of Fig. 5.6, so that with increasing total rainfall, the sediment yield of the New Basin increases more rapidly than that of the Rimco Basin, resulting in a lower ratio of the sediment yields. As in the case of the runoff coefficients, this may be explained by the higher proportion of vegetated surfaces in the Rimco Basin, yielding neither runoff nor sediment, which thus limits the sediment yield under conditions of high total rainfall.

There is no clear effect of antecedent moisture conditions on the relationship between the ratio of the sediment yields and the total rainfall in Fig. 5.14. It would be expected that under high antecedent moisture conditions, the sediment yield of the New Basin would exceed that of the Rimco Basin but, like the runoff coefficients, sediment yields are strongly affected by the additional factor of rainfall characteristics. Furthermore, under high total rainfall the shales become an additional source of runoff and sediment. Because shales account for a larger portion of the New Basin than of the Rimco Basin (Table 5.1), under such conditions the ratio of the sediment yields of the two basins may be expected to decrease (Fig. 5.14). For four runoff events the ratio of the sediment yields of the two basins is larger than one, indicating that sediment yield is higher in the Rimco Basin than in the New Basin. For all of these events the ratio of the runoff coefficients is also larger than one. The connection between runoff coefficients and sediment yields indicates that the higher sediment yields in the Rimco Basin are caused by the same factor, spatial distribution of rainfall, as the higher runoff coefficients.

The sediment yields per unit area from Tables 5.3 and 5.4 were converted into erosion rates using an average bulk density of 1826 kg m^{-3} (Campbell, 1977a). For the Rimco basin, the erosion during the fieldwork period was 0.07 mm in 1986, and 0.12 mm in 1987, whereas in the New Basin, the values were 0.08 mm in 1986, and 0.26 mm in 1987. The differences in erosion rates between the two basins, although small in 1986, again reflect the different percentages of vegetated surfaces and shales in the basins, in

addition to differences in rainfall characteristics between the basins.

If it were assumed that the average annual rainfall in Dinosaur Provincial Park was 250 mm (Bryan and Campbell, 1986), erosion rates based on the data from 1986 and 1987 would for these two years be only 0.6 and 0.5 mm for the Rimco Basin, and 0.8 and 1 mm for the New Basin. Even when taking into account the effect of missing data causing underestimation, erosion rates in 1986 and 1987 are very much lower than the value of 3 mmyr^{-1} reported by Bryan and Campbell (1986). The low values likely reflect the small rainstorms of 1986 and 1987, which mainly generated runoff and sediment on the rapidly yielding sandstones and pediments, whereas on the shales, which are important contributors of sediment under high rainfalls, runoff generation and sediment entrainment was limited to a few high-magnitude storms.

5.5.2 EFFECT OF STORM TYPE

The sediment yield patterns of the basins also reflect the contrast between the convective storm of July 26, 1986, and the frontal storm of July 18, 1987. For the Rimco Basin, the sediment yield per unit area (solutes and suspended sediment combined) was minimally 546 kgha^{-1} on July 26, 1986, and 58 kgha^{-1} on July 18, 1987. For the New Basin, the sediment yield was minimally 728 kgha^{-1} on July 26, 1986, and 134 kgha^{-1} on July 18, 1987. On July 26, 1986, therefore, the sediment yield was more than 9.4 times larger than on July 18, 1987, in the Rimco Basin, whereas in the New Basin the sediment yield on July 26, 1986, was more than 5.4 times the sediment yield on July 18, 1987.

Only part of the difference between the sediment yields can be explained by the difference in the total discharge for the two storms. On July 26, 1986, the total discharge was more than 2.5 times, and more than 1.7 times the total discharge of July 18, 1987, for the Rimco and the New Basin, respectively. Another factor causing higher sediment yields

on July 26, 1986, is that discharges, and hence flow velocities, were significantly higher than on July 18, 1987. The increased transport capacity of the runoff on July 26, 1986, caused a higher sediment yield than on July 18, 1987. Sediment yields for both days also differ because of differences in the response of runoff and sediment sources, and because of differences in rainfall erosivity. Although no direct measurements of the energy characteristics of the rainfall were made, rainfall intensities allow a comparison between the erosivities of the storms. On July 26, 1986, the average intensity for the 36 min storm was 13.8 mm h^{-1} , with a peak intensity of 26 mm h^{-1} for a six minute period. On July 18, 1987, the average intensity for the 6 h 18 min storm was only 1.4 mm h^{-1} , with a peak intensity of 7.6 mm h^{-1} for a six minute period. Generally, a higher rainfall intensity will cause an increase in the detachment and transport rates of sediment on hillslopes (Meyer and Wischmeier, 1969; Foster and Meyer, 1975; Kirkby, 1980). However, the effect of the increased rainfall intensity on the sediment yield and sediment concentrations is hard to separate from the effects of higher flow competence and the response variations of the sediment sources. Differences between the sediment concentrations for the two storms would be most evident during the rising stage of the hydrograph, when the effect of rainfall intensity on the sediment concentrations would be most pronounced. Discharges on the rising stage of both events, however, differ greatly in magnitude, precluding separation of the effects of rainfall intensity and flow competence on sediment concentrations.

5.5.3 THE SEDIMENT CONCENTRATION/DISCHARGE RELATIONSHIP

The relationship between sediment concentration and discharge is usually established by combining data for several runoff events and fitting a straight regression line on logarithmic coordinates to the data. For the Rimco Basin the equation of the regression line is

$$SC = 10.9 Q^{0.26} \quad [5.1]^{221}$$

($n=105$, $r^2=0.504$, $P<0.001$) (Fig. 5.15), whereas for the New Basin it is

$$SC = 14.5 Q^{0.27} \quad [5.2]$$

($n=140$, $r^2=0.576$, $P<0.001$) (Fig. 5.16). In both equations, SC is the sediment concentration (g l^{-1}), and Q is the discharge (l s^{-1}). The value of the exponent usually lies between 1 and 2 (Gregory and Walling, 1973; Graf, 1988), although values as low as 0.159 have been found in arid, ephemeral streams (see Reid and Frostick, 1987, for a review). The low values found in the present study imply a slow rise of sediment concentration with discharge. This indicates that sediment concentrations in the Rimco basin and the New Basin are almost entirely controlled by the supply conditions, i.e. the response of the surface units. Flow capacity, the other variable controlling sediment concentration, appears to be of lesser importance. Most of the sediment exported from the two basins has the grain size of silt/fine sand and finer. This material can be transported even at very low flows so that sediment concentrations remain high ($>10 \text{ g l}^{-1}$) even during the final stages of flow.

A rating curve as given by Eq. [5.1] and [5.2] conceals an often considerable scatter of the data points. This scatter is caused by variations in the response of sediment and runoff source areas and in flow conditions on the rising and falling stages (Gregory and Walling, 1973). The scatter may be eliminated by using data from individual runoff events.

A plot of the sediment concentration/discharge relationship for an individual runoff event generally displays hysteresis, which may be either clockwise or counterclockwise. Clockwise hysteresis has been associated with a decrease in the availability of suspended sediment during the runoff event, and with an increase in the proportion of baseflow during the falling stage (Walling, 1974; Walling and Webb, 1982).

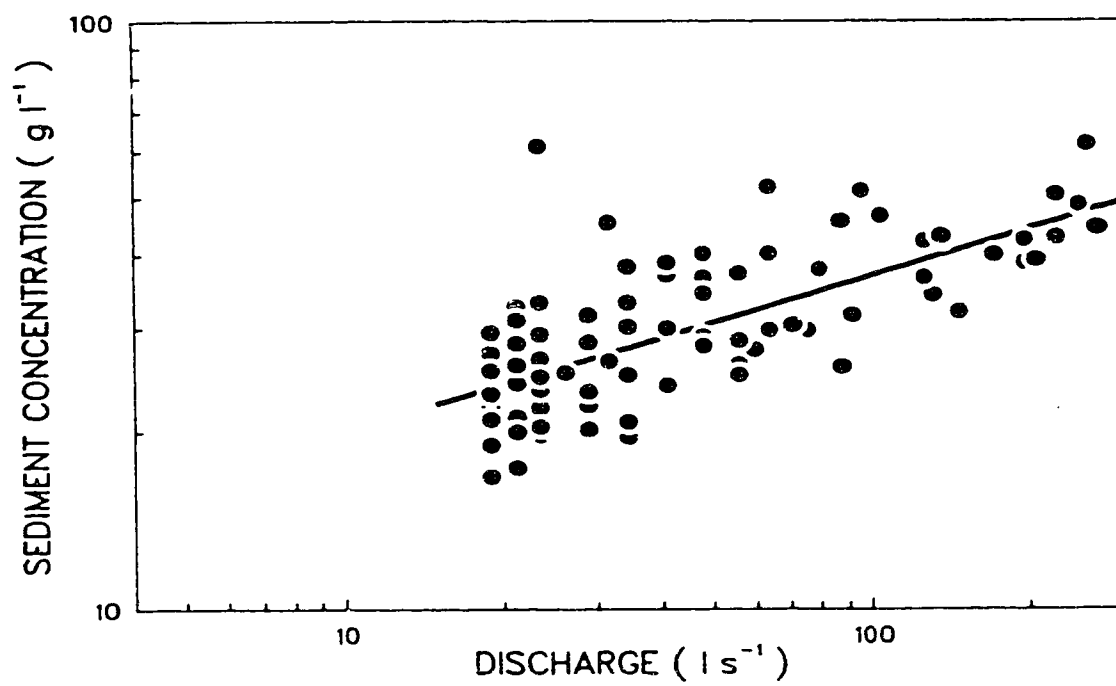


Fig. 5.15 Sediment concentration/discharge relationship for the Rimco Basin.

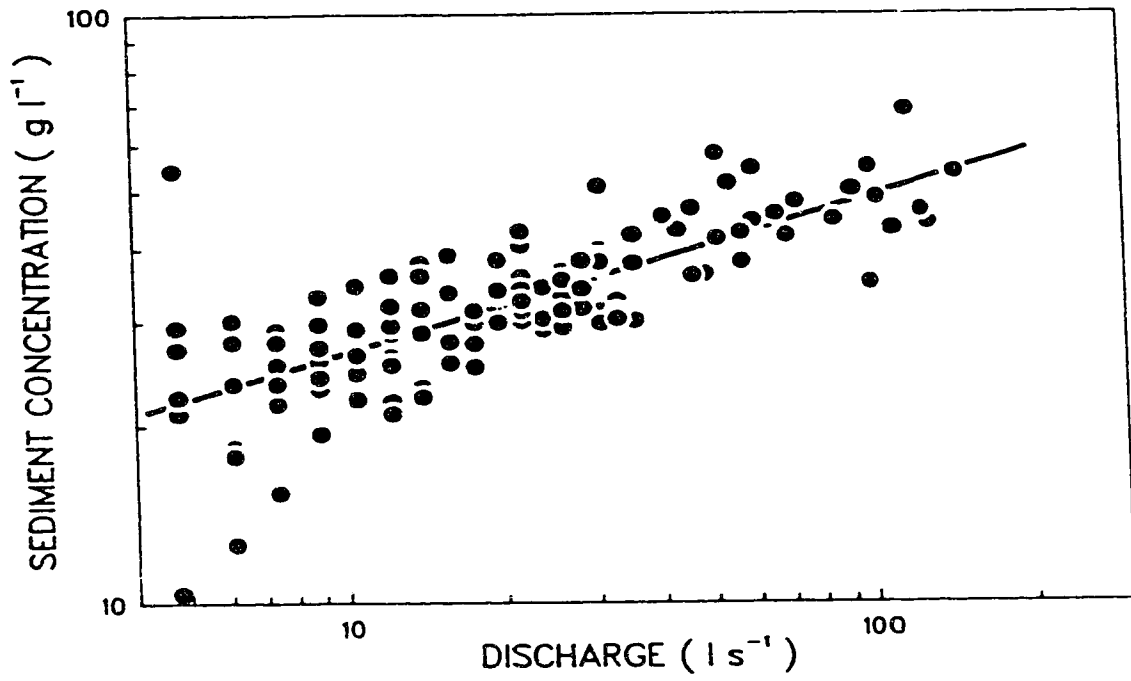


Fig. 5.16 Sediment concentration/discharge relationship for the New Basin.

Clockwise hysteresis has also been attributed to a reduction in rainfall erosivity during the falling stage (Gregory and Walling, 1973). In two small basins in England, Klein (1984) found that hysteresis type varied with sediment source location. In the case of clockwise hysteresis the sediment source was the channel area, whereas counterclockwise hysteresis occurred when the sediment source was located on the upper part of the slopes (Klein, 1984). Counterclockwise hysteresis has also been related to a sustained or increased sediment supply (Burt et al. 1983), and to the downstream increase in lag between the sediment and flood peaks (Gregory and Walling, 1973). Analysis of sediment concentration/ discharge relationships for individual events can be of assistance in clarifying the response and spatial distribution of sediment sources, and in this manner aids in the explanation of drainage basin behaviour (Grimshaw and Lewin, 1980; Loughran et al., 1986).

The sediment concentration/discharge relationship for individual runoff events for the Rimco Basin and the New Basin displays both clockwise and counterclockwise hysteresis (Table 5.6). Within each of these categories a distinction may be made as to whether the relationship shows a single loop or a more complex pattern of loops. Single loops occur during events for which the temporal distribution of rainfall is relatively simple and does not lead to multiple discharge peaks at the basin outlet. Complex patterns of loops are associated with storms during which the temporal distribution of rainfall causes multiple discharge peaks. Combined with variations in the sediment concentration this results in a more complex pattern of the sediment concentration/discharge relationship. This pattern, however, is still indicative of increases or decreases in sediment availability, and in all aspects drainage basin response during these events is similar to that during events which display a single loop. All observed complex loop patterns are from frontal storms with a relatively low intensity, long duration, and uniform rainfall. Variations in the spatial pattern of rainfall, which may also result in complex loop patterns, are therefore unlikely to be a factor here.

Table 5.6 Effect of average total rainfall on the sediment concentration/discharge relationship

date †	Rimco Basin ‡	New Basin ‡	average total rainfall p	average total rainfall #	antecedent moisture conditions ††
<u>1986</u>					
July 5 (I)	CC	CC	7.3	4.4	7.5
July 5 (II)	C	—	3.4	—	4.8
July 9	C	C	7.0	—	7.6
July 26	CC	C	8.1 (Rimco), 5.2 (New)	7.1	0.0
August 5	C	C	4.3	—	0.0
August 8	C	C	1.8	—	4.3
<u>1987</u>					
May 26 (I)	*	*	6.0	—	0.0
May 26 (II)	C	—	4.5	—	6.0
May 27	C	—	2.5	—	10.5
June 19 (I)	C	C	4.2	—	3.0
June 19 (II)	+	+	12.6	—	7.2
June 20	C	C	3.9	—	19.8
July 18	CC	CC	10.2	6.0	2.0
August 10	—	+	4.6	5.0	2.1
August 14	+	+	17.6	4.0	7.9

†(I) and (II) indicate multiple runoff events

‡ CC - counterclockwise hysteresis

C - clockwise hysteresis

* - complex pattern of loops indicating decrease in sediment supply

+ - complex pattern of loops indicating increase in sediment supply

— - no data available

p average total rainfall during event (mm)

average total rainfall at time of increasing sediment concentration (mm)

†† average total rainfall in week prior to event (mm)

For those events showing an increase in sediment supply, Table 5.6 gives the total rainfall at the time when the sediment concentration/discharge relationship indicates a rise in sediment concentration which cannot be attributed to increasing transport capacity of the flow. Figure 5.17 shows the relationship between this value of total rainfall and antecedent moisture conditions expressed as total rainfall in the week prior to the runoff event. This definition of antecedent moisture condition was chosen as a first approximation of the conditions in the tunnel systems. An alternative choice would be an API calculated with a value of close to 1 (Section 5.4) to reflect the slow drying rates in the tunnels, which are sheltered from sun and wind.

The total rainfall associated with the increase in sediment concentration (Fig. 5.17) is evidently well below the threshold rainfall for runoff generation and sediment entrainment on the shale surfaces, ruling out these surfaces as the source of the additional sediment. Another possible source of the additional sediment is the deep tunnel systems. Bryan and Harvey (1985) showed that solute and sediment concentrations of tunnel flow are typically three to four times higher than normally found in channel flow, as runoff passing through the tunnel systems picks up solutes and sediment. Initiation of tunnel flow would therefore cause an increase in sediment concentrations during the runoff event, resulting in counterclockwise hysteresis (Fig. 5.18). Accordingly the total rainfall at the time of rising sediment concentrations is interpreted as the threshold rainfall necessary to overcome initial transmission losses within the tunnel system, and to initiate spatially continuous flow in the tunnels.

Two factors serve to limit initial transmission losses within the tunnel system. First, because of repeated flow through the tunnels the tunnel bottom may in places be lined with a silty deposit analogous to the silt stringers described by Hodges and Bryan (1982). Second, tunnels are shielded from wind and sun so that antecedent moisture conditions are generally higher than at the surface.

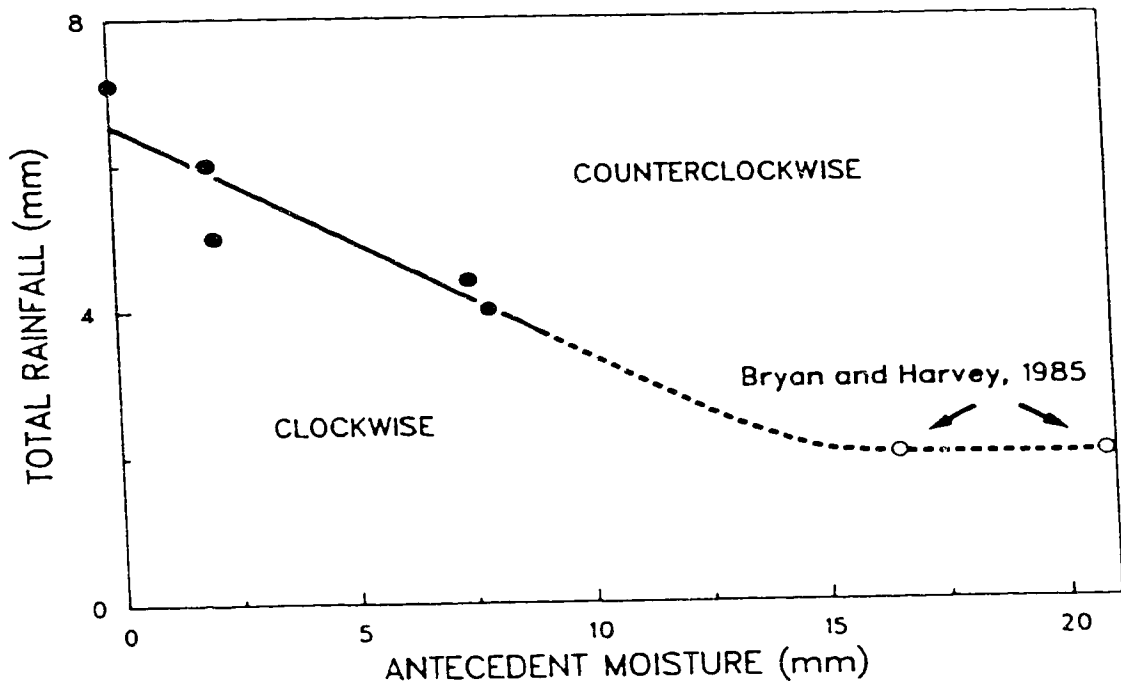


Fig. 5.17 Relationship between antecedent moisture conditions and total rainfall at the time of increasing sediment concentration. The latter variable is interpreted as the threshold of tunnel flow initiation, exceedance of which causes a change from clockwise to counterclockwise hysteresis.

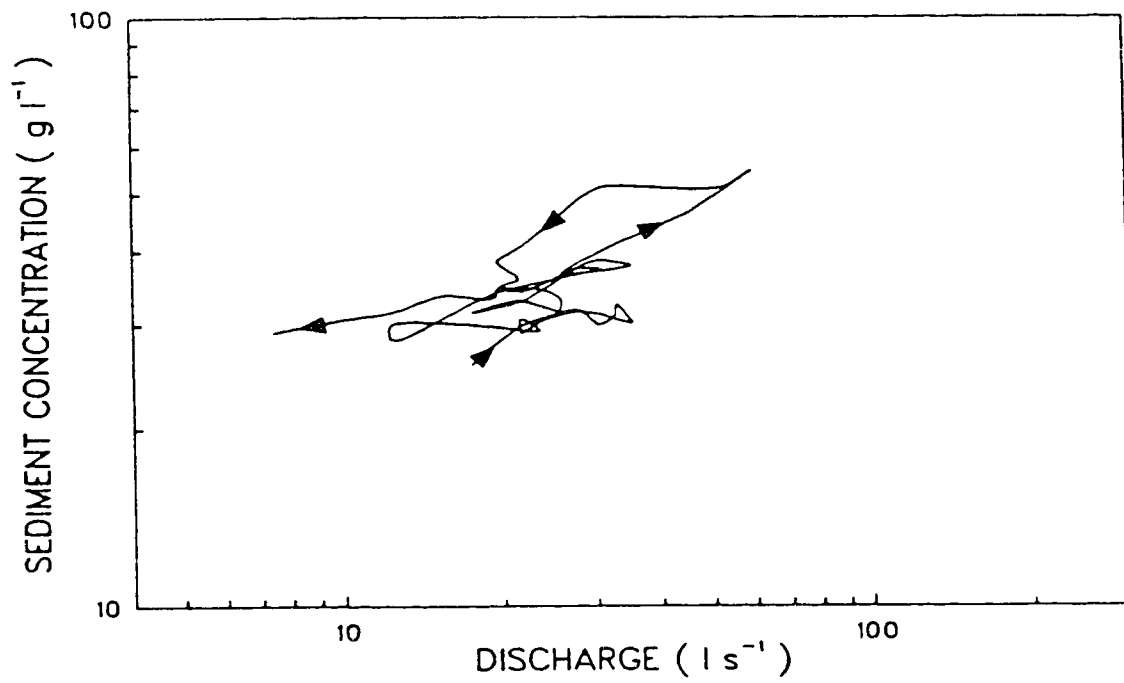


Fig. 5.18 Sediment concentration/discharge relationship for the New Basin on August 14, 1987, showing an increasing sediment supply as deep tunnel systems and shale surfaces contribute sediment.

Figure 5.17 also contains two data points on the initiation of tunnel flow from Bryan and Harvey (1985). Under the antecedent moisture conditions of these two points transmission losses within the tunnel system are assumed to be negligible, as the tunnel system is still wet from the previous runoff event. Tunnel flow therefore starts when total rainfall exceeds the threshold of runoff generation on the sandstone and pediment surfaces feeding into the tunnel system. This causes the curve of the threshold of tunnel flow initiation to level off under wet antecedent moisture conditions.

Data collected by Bryan and Harvey (1985) indicate that, depending on antecedent moisture conditions, tunnel flow starts between 0 and 30 minutes after the start of flow from the Rimco Basin. Because of this delay, tunnel flow generally does not contribute to the first part of runoff from the Rimco Basin. During these larger storms total rainfall may also exceed the 8 to 25 mm threshold of runoff generation on the shale surfaces. The high sediment concentrations in the runoff from the shale surfaces (Bryan et al. 1984) will reinforce the counterclockwise hysteresis in the sediment concentration/ discharge relationship. In addition, microtunnel collapse and small slumps and mudflows on the shale surfaces may contribute to increased sediment concentrations during the later stages of the storm (Bryan et al. 1978, Bryan and Campbell 1980).

Clockwise hysteresis generally occurs during storms for which the total rainfall does not exceed the threshold of tunnel flow initiation, with three exceptions to be discussed later. During these relatively small rainstorms runoff is generated only on the rapidly responding sandstone and pediment surfaces. This restricts the sediment sources within the basin to these two units and to the channel system. Sediment available in the channel system is, except possibly under extreme circumstances, not supply-limited. It consists, however, of the coarser fractions of the material moving through the system, so that transport is more closely controlled by flow competence. On the pediments, Hodges (1982) describes the development of chutes or ephemeral rills triggered by flow instability, which would suggest that sediment is not supply-limited on these surfaces. It is important

to note, however, that rainfall intensity during Hodges' (1982) experiments averaged 29 mm h^{-1} over 30 min. The actual intensity in the center of the plot may have been considerably higher due to the spray pattern of the rainfall simulator (Bryan et al. 1978). Flow instability hence occurs under conditions of prolonged rainfall of fairly high intensity. During storms of a lower intensity flow instability and chute development will not occur, and sediment concentrations on both the pediment surfaces and the sandstones will be supply-controlled. Thus, sediment and solutes produced and accumulated on these surfaces during dry periods are flushed away during the initial stages of runoff (Fig. 5.19). In Table 5.6, the total rainfall for July 26, 1986, has been separately calculated for the Rimco Basin and the New Basin because the basins showed a different kind of hysteresis.

When the average total rainfall during each event is plotted against antecedent moisture conditions (Fig. 5.17), the data points for the events exhibiting clockwise hysteresis plot below the curve of the threshold of tunnel flow initiation, with the exception of the runoff events which occurred on July 5 (II) and July 9, 1986, and on June 20, 1987. The event of July 9, 1986, shows the effect of rainfall intensity on drainage basin response. Although the sediment concentration/discharge relationship displayed clockwise hysteresis, total rainfall averaged 7.0 mm. This is in excess of the threshold rainfall for tunnel flow and counterclockwise hysteresis. During this event rainfall intensity reached 43 mm h^{-1} for a six minute period at the beginning of the storm. This short burst accounts for a total rainfall of more than 4 mm, most of which, however, is rapidly lost through cracks within the tunnel system. Only after the sealing of such cracks by swelling of the material on wetting can the tunnel system contribute to drainage basin discharge. There appears to be a maximum rate at which cracks within the tunnel system can be sealed. When water is applied to the tunnel system at high rates at the beginning of a rainstorm this water does not contribute to the sealing of cracks in the tunnel system, but instead flows into these cracks. It does then not contribute to basin discharge, but instead

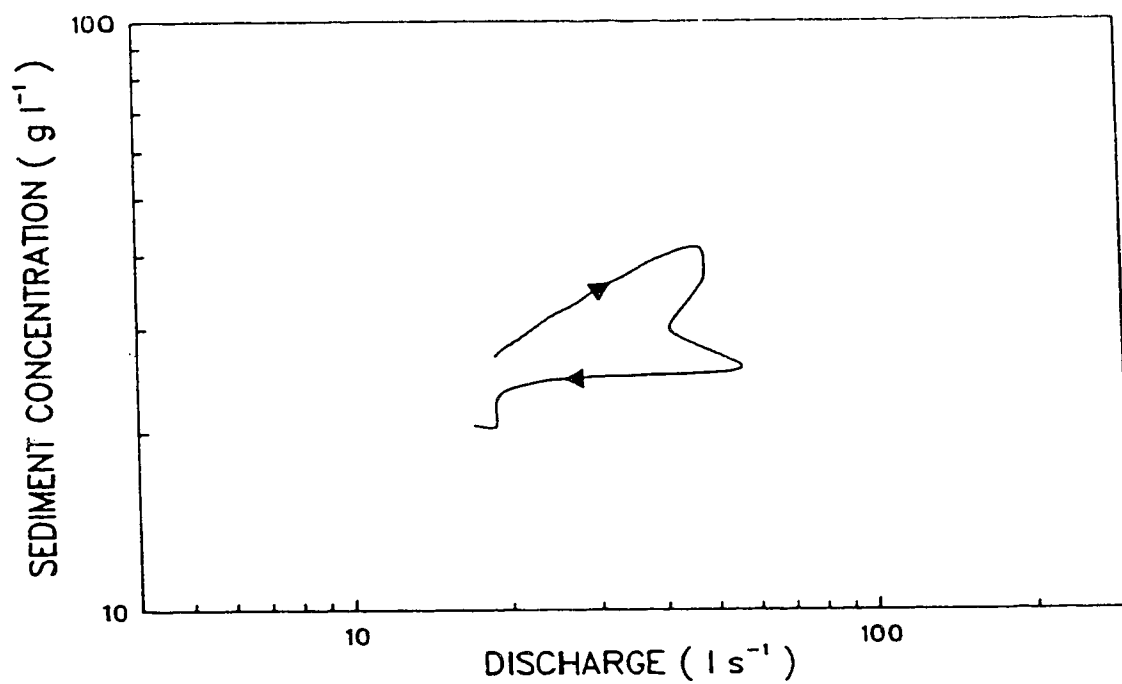


Fig. 5.19 Sediment concentration/discharge relationship for the Rimco Basin on May 27, 1987, showing exhaustion of the sediment supply as sediment accumulated on the sandstone and pediment surfaces is flushed away during the rising stage.

contributes to deep infiltration. The relationship between antecedent moisture conditions and the threshold of tunnel flow initiation in Fig. 5.17 was determined for rainstorms which occurred during the 1986 and 1987 summer seasons. Peak intensity for a six minute period for these rainstorms did not exceed 11 mm h^{-1} in the majority of cases.

The runoff events of July 5, 1986 (II), and June 20, 1987, both followed runoff events during which tunnel flow and, in the case of June 20, 1987, runoff generation on the shale surfaces occurred. During the falling stage of these preceding events a considerable amount of sediment derived from the shale surfaces and the tunnel systems was deposited in the form of thin clay skins on the pediment surfaces and in shallow ponds in the channel. This sediment was flushed away during the early stages of the runoff events of July 5, 1986 (II) and June 20, 1987 (Fig. 5.20). The exceptionally high sediment concentrations, which reached values in excess of 60 g l^{-1} during the first phase of runoff, caused clockwise hysteresis and effectively concealed the counterclockwise hysteresis expected during these events.

At the beginning of the majority of storms, the channel alluvium is still moist from the previous runoff event. This reduces transmission losses, so that runoff from both basins occurs when total rainfall exceeds the threshold of runoff generation on the sandstone and pediment surfaces. When total rainfall is increased and exceeds the threshold of tunnel flow initiation the tunnel system starts to function as an additional sediment source and sediment concentrations increase significantly, as is evidenced by the sediment concentration/discharge relationship. A further increase of total rainfall resulting in runoff generation on the shale surfaces will raise sediment concentrations even more. The effect of the sediment-rich runoff from the shale surfaces is similar to that of tunnel flow, and is therefore not separately discernible in the sediment concentration/discharge relationship of the Rimco Basin and the New Basin.

In this model, the change from clockwise to counterclockwise hysteresis occurs because the start of flow from the basin precedes the initiation of tunnel flow. Comparison

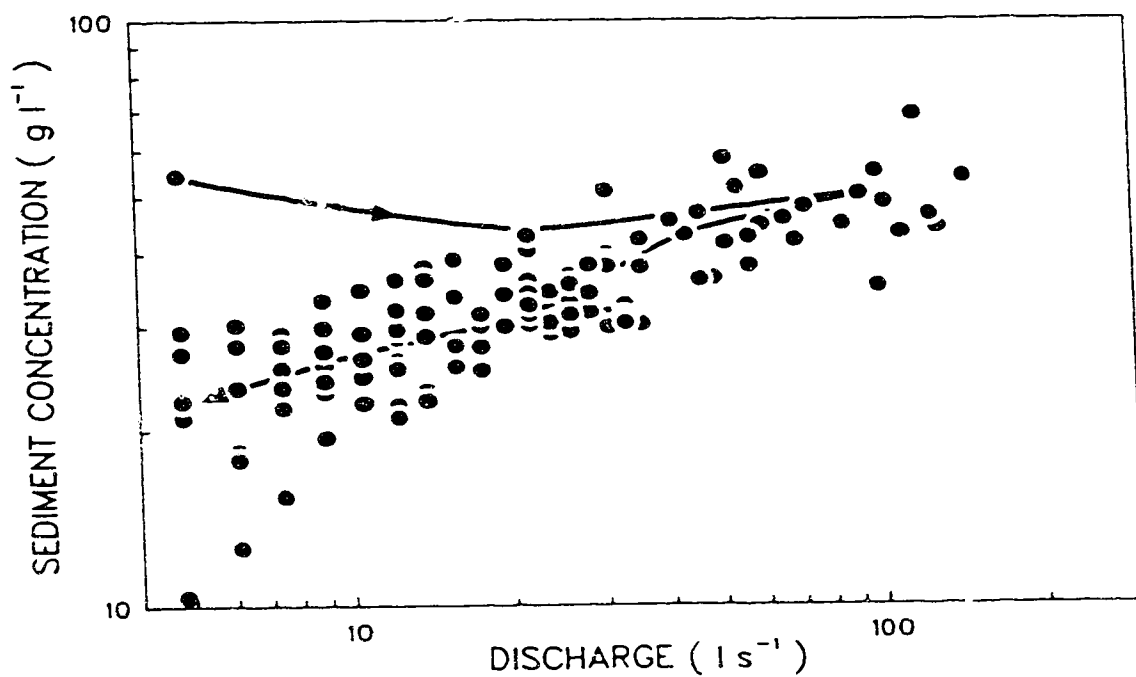


Fig. 5.20 Sediment concentration/discharge relationship on June 20, 1987, compared to other data for the New Basin. The flushing away of sediment accumulated on the sandstone and pediment surfaces causes exceptionally high sediment concentrations on the rising stage, disguising the counterclockwise hysteresis expected during this event.

of the starting times of flow for the Rimco Basin, the New Basin, and the 336,810 m² Aquatot Basin (Bryan and Campbell, 1986) indicates that the start of flow is delayed as basin area increases. Since the tunnels discharge directly into the channel system, for a sufficiently large basin the start of flow from the basin will coincide with the initiation of tunnel flow. Thus, sediment concentrations will be high from the beginning of runoff and tunnel flow initiation will not cause a change in hysteresis. The ratio of the response times of the deep tunnel systems to that of the basin will control this scale dependent aspect of the sediment dynamics.

5.6 SOLUTE DYNAMICS

Although solutes account for a mere 1.4 per cent of the total stream load (Sutherland, 1983; Sutherland and Bryan, 1988), an analysis of the solute dynamics of the Rimco Basin and the New Basin was undertaken to clarify drainage basin response.

5.6.1 ELECTRICAL CONDUCTIVITY

Both the Rimco Basin and the New Basin showed the same general pattern of EC variation with time and discharge. Initially, the EC decreased sharply to reach a low value around the time of peak flow. During the subsequent falling stage, the EC gradually increased to high levels in the final phases of flow. The steep decline in EC during the rising stage represents flushing of solute-rich runoff, whereas the gradual increase during the falling stage is caused by the dissolution of suspended sediment and, in some cases, by the delayed contributions of solute-rich runoff from tunnel systems and shales (Fig. 5.21).

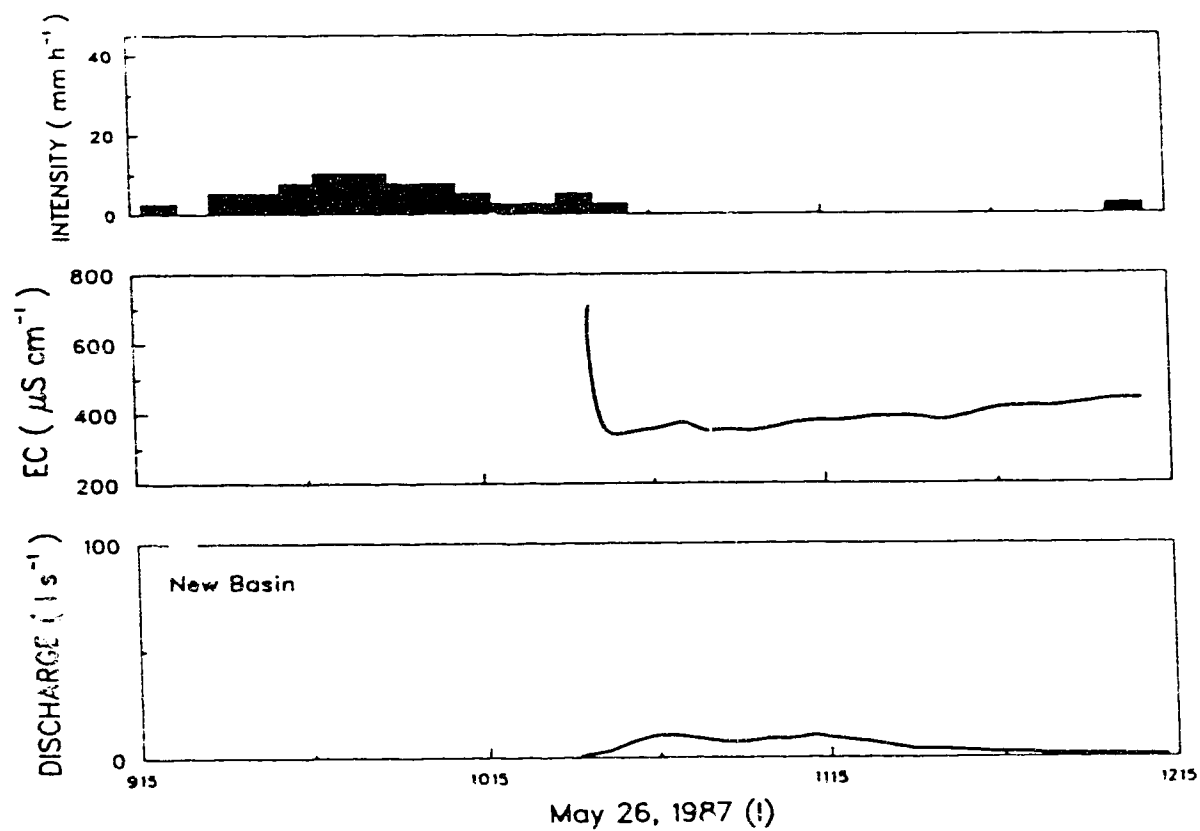


Fig. 5.21 Hydrograph, hyetograph (Rimco recording raingauge), and EC for the New Basin on May 26, 1987 (I), showing step decrease in EC during initial flushing, followed by a gradual increase during the falling stage.

Because of this mechanism, an inverse relationship between EC and discharge would be expected. In the New Basin, the EC/discharge relationship follows this pattern (Fig. 5.22), and is described by

$$EC = 502.2 Q^{-0.08} \quad [5.3]$$

($n=134$, $r^2=0.116$, $P<0.001$). In the Rimco Basin, however, the regression equation is

$$EC = 275.2 Q^{0.05} \quad [5.4]$$

($n=82$, $r^2=0.061$, $P<0.05$), indicating an increase, albeit slow, of EC with discharge (Fig. 5.23). This is caused by the higher cut-off point for the Rimco Basin; the stage below which no reliable estimates of the discharge are available. The cut-off point for the Rimco Basin lies at a stage of 10 cm, corresponding to a discharge of 19 l s^{-1} , whereas for the New Basin it lies at a stage of 3 cm and a discharge of 3 l s^{-1} . The positive slope of the EC/discharge relationship for the Rimco Basin is caused by the exclusion of the low discharges with high EC's, not by some fundamental difference between the two basins. Comparison of Figs. 5.22 and 5.23 shows that EC's are generally higher in the New Basin. EC's in the New Basin ranged from 260 to $800 \mu\text{S cm}^{-1}$, whereas in the Rimco basin, EC's ranged from 255 to $685 \mu\text{S cm}^{-1}$. In both basins the highest EC values occurred late during the falling stage.

During the majority of storms, the initiation of tunnel flow is not discernable from the EC/discharge relationship, and a counterclockwise loop of the sediment concentration/discharge curve can be accompanied by a clockwise loop of the EC/discharge curve. This discrepancy is caused by two opposite effects found during tunnel flow initiation. Tunnel flow initiation generally occurs during periods of higher rainfall intensity and peak (channel) flow. This results in a lowering of the EC due to the increased input

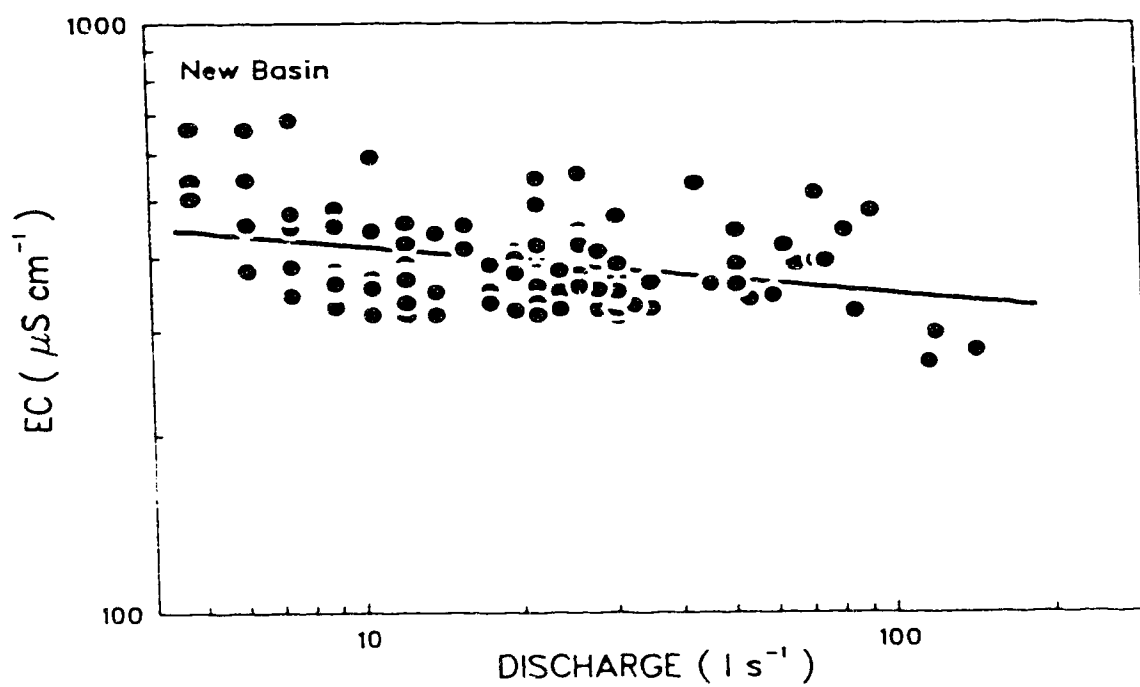


Fig. 5.22 EC/discharge relationship for the New Basin.

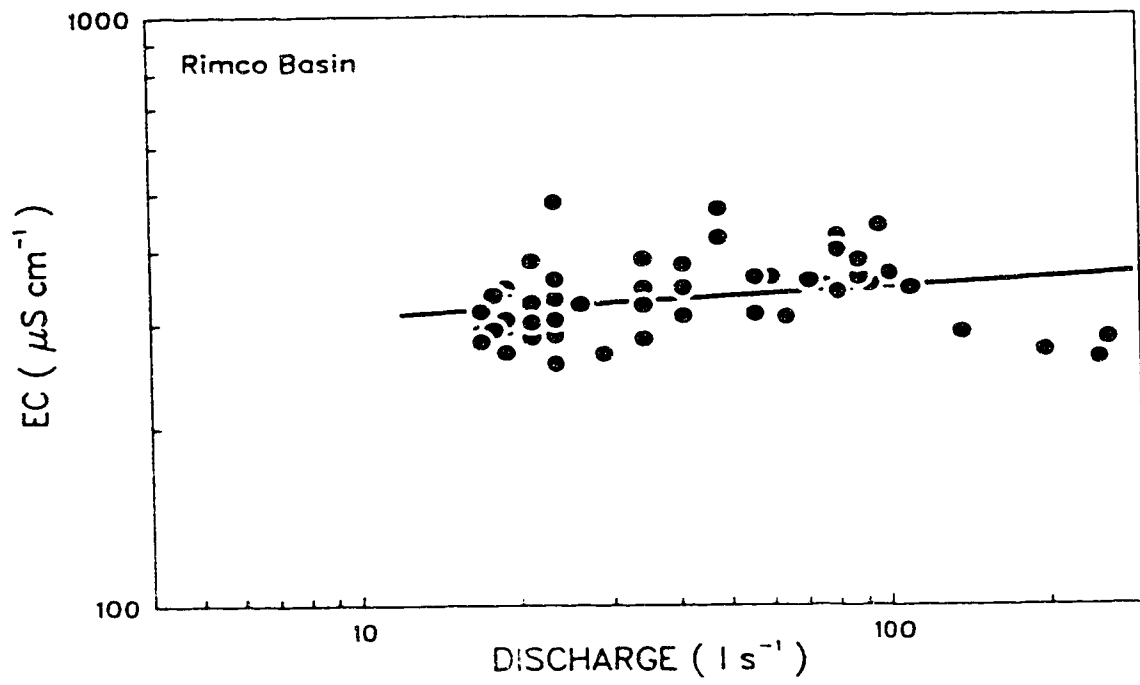


Fig. 5.23 EC/discharge relationship for the Rimco Basin.

of water with a low solute concentration. Conversely, tunnel flow initiation causes an inflow of solute-rich water into the channel system. The amount of solutes thus added to the channel flow is not sufficient to prevent the occurrence of an EC trough, but does result in a reduction of its depth.

The time of occurrence of the EC trough and its actual value (or depth) are controlled by three factors:

- (1) the amount of readily available solutes that can be flushed away during the first stages of flow;
- (2) the dissolution rate of components of the suspended sediment;
- (3) the contribution of solute-rich runoff by tunnel systems and shales.

All three factors are affected by rainfall characteristics and drainage basin conditions so that, although both basins showed the same general pattern of a steep decrease in EC, followed by a gradual increase during the falling stage, details of this pattern differed between the two basins. In the Rimco Basin, peak discharge always preceded, or coincided with, the EC trough. In the New Basin, however, during three runoff events (May 26, 1987 (I), June 19, 1987 (II), and June 20, 1987) peak discharge lagged after the EC trough, whereas during the remaining runoff events peak discharge preceded, or coincided with, the EC trough (Fig. 5.24). When secondary discharge peaks occurred they preceded, or coincided with, the EC trough in both basins. During storms with multiple discharge peaks there generally was an inverse relationship between the magnitude of the peak discharge and that of the EC trough.

The differences in behaviour between the basins can be explained by a more rapid flushing of solute-rich water, causing higher EC's on the rising stage and, more

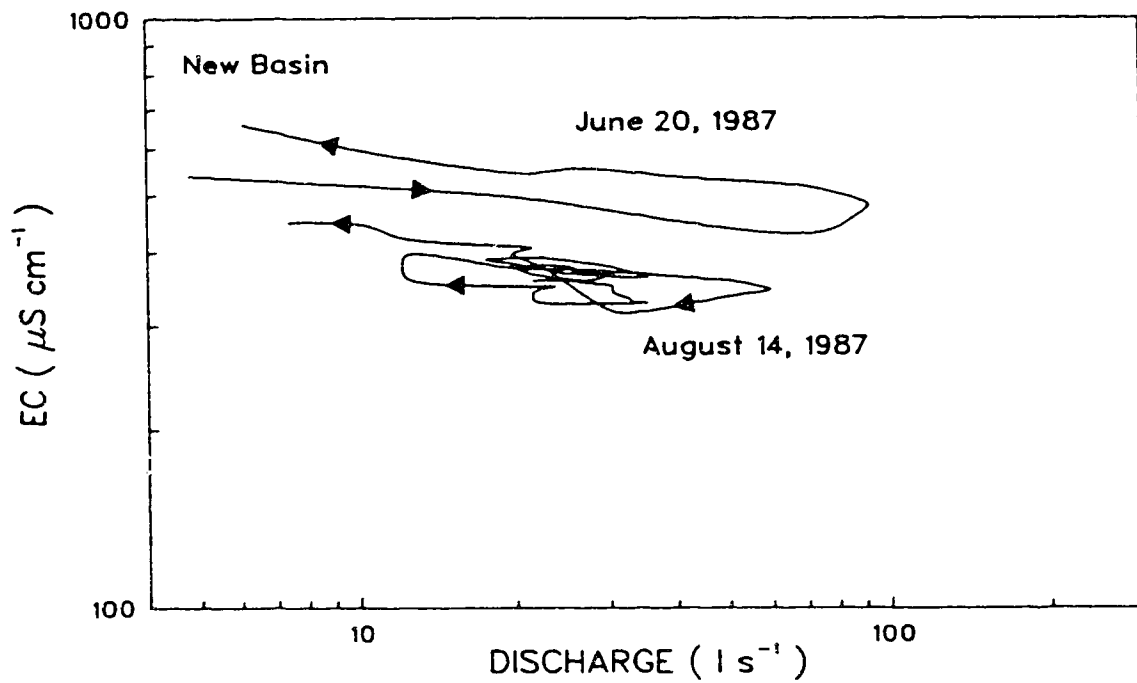


Fig. 5.24 Contrasting EC/discharge relationships for the New Basin. On June 20, 1987, the peak discharge lagged after the EC trough, resulting in counterclockwise hysteresis. On August 14, 1987, the peak discharge preceded the EC trough a number of times, resulting in a series of clockwise loops. On both days, however, the highest EC's occurred during the final stages of flow.

importantly, by a more rapid solution of suspended sediment in the New Basin (Fig. 5.25). The latter factor can be attributed to the higher sediment concentrations in the New Basin.

The change in the EC/discharge relationship for the New Basin, from a leading to a lagging EC trough, may be attributed to increased solute concentrations on the rising stage. This effect was most pronounced during the lengthy, low-intensity rainstorms of July 18 and August 10 and 14, 1987. The low-intensity rainfall allowed considerable wetting of the sandstones and pediments prior to the start of runoff, reducing the strength of the upper layers and causing higher EC's during the rising stage and the flow peak (Fig. 5.26). The same process also caused the EC trough to lag after the peak discharge during secondary and later peaks. In the Rimco Basin, the latter process also operated but had no effect on the relative timing of the discharge peak and the EC trough.

5.6.2 RUNOFF CHEMISTRY

As stated in Section 5.3, a number of samples was centrifuged to separate dissolved and suspended sediment. The time elapsed between sampling and centrifuging enabled additional dissolution and hydrolysis of suspended sediment and a further completion of exchange reactions, so that the runoff chemistry at the time of analysis may differ from that at the time of sampling. It may be expected that the change in chemistry during storage is mainly due to dissolution and hydrolysis of suspended sediment in the sample, as exchange reactions on kaolinite, montmorillonite, and illite are usually quite rapid, and can be expected to be close to or at equilibrium at the time of sampling (Sparks, 1985). It was noted in the field that the EC of samples increased rapidly with time. It should be emphasized, however, that the EC's reported in Section 5.6.1 were measured directly after sampling. Figure 5.27 compares the EC at the time of sampling (EC) to that after

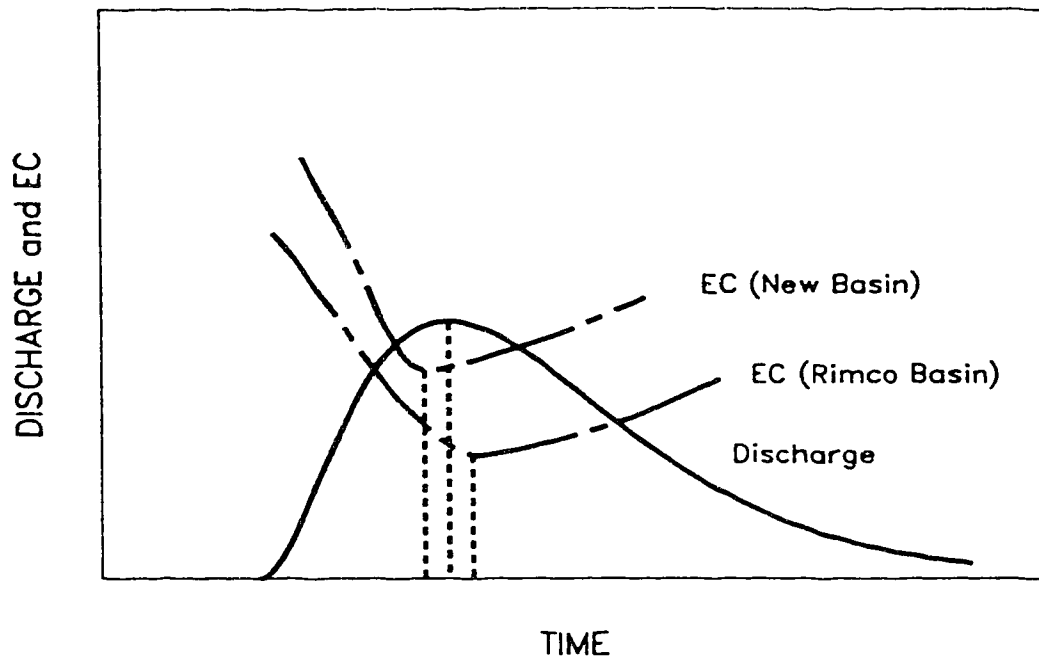


Fig. 5.25 Contrast between EC/discharge relationship of the Rimco Basin and the New Basin. In the Rimco Basin, the discharge peak precedes (or coincides with) the EC trough, whereas in the New Basin it lags after the EC trough on two occasions. The difference is possibly caused by more rapid flushing of solute-rich water and, more importantly, by an earlier contribution to the EC by dissolving suspended sediment in the New Basin.

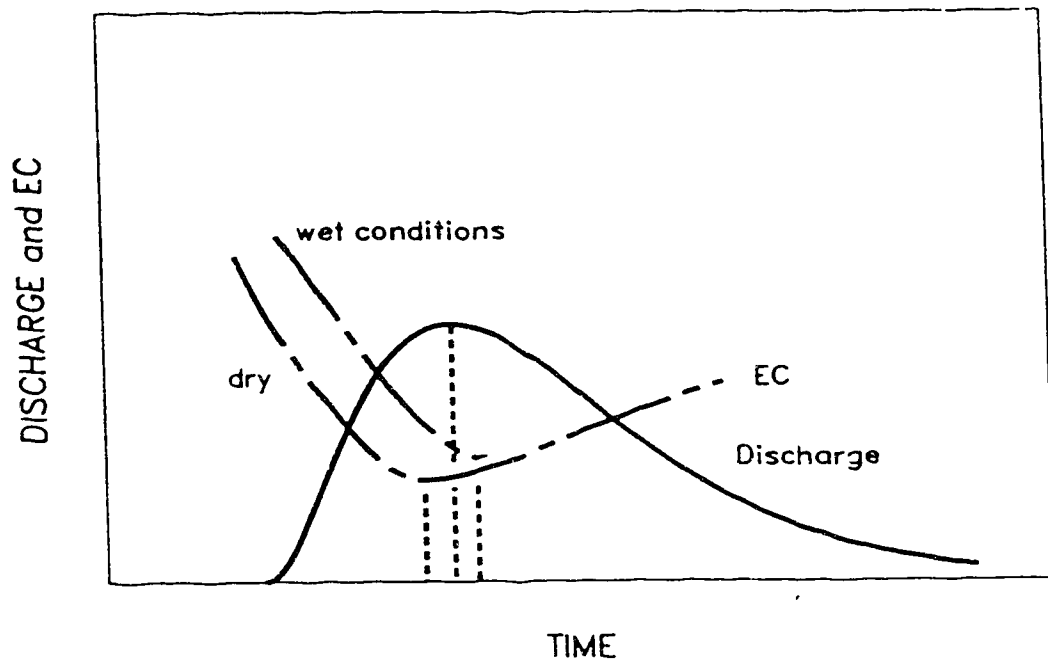


Fig. 5.26 Change in EC/discharge relationship of the New Basin during low-intensity rainstorms. The wetness of the basin at the time of runoff generation causes higher solute export and increases the EC during the rising stage and the flow peak, causing the EC trough to lag after the peak discharge. The same mechanism also operates during secondary and later flow peaks.

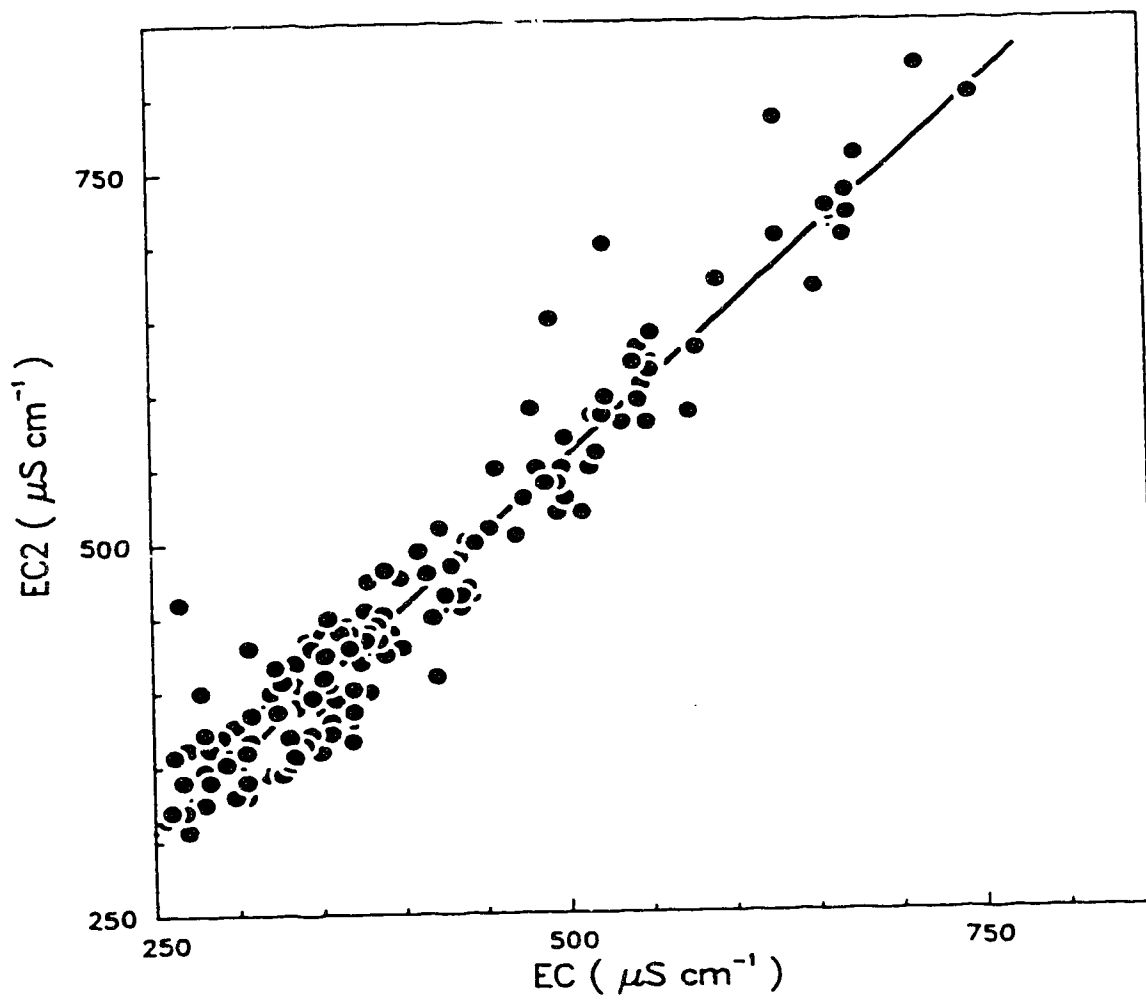


Fig. 5.27 Comparison of the EC at the time of sampling (EC) and after centrifuging (EC2).

centrifuging (EC2). The former was obtained by interpolation of EC data; the latter, by measuring the EC of centrifuged samples. The regression line is given by

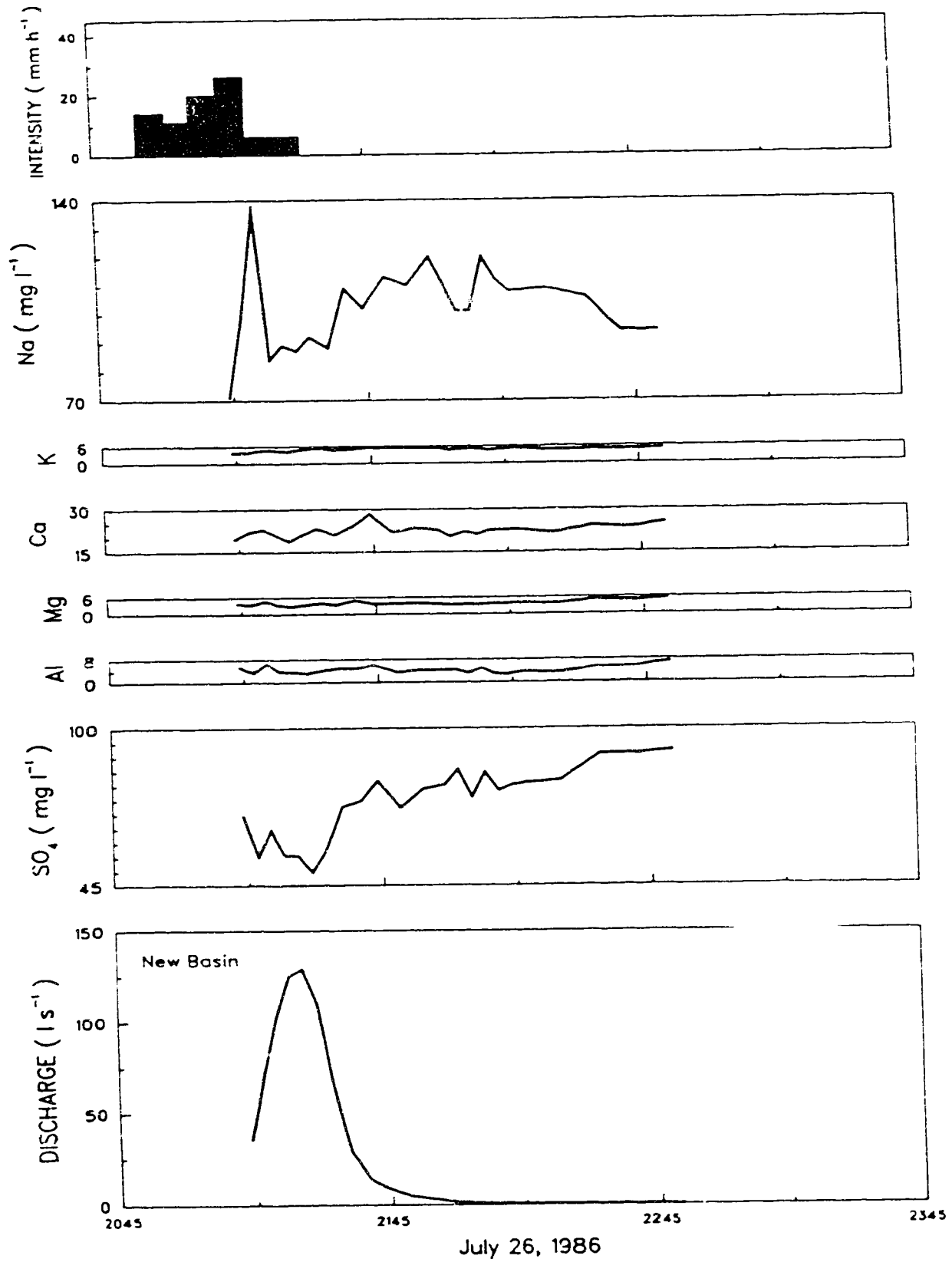
$$EC2 = 56.69 + 1.00 EC \quad [5.5]$$

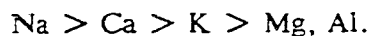
($n=182$, $r^2=0.935$, $P<0.001$). This equation indicates that over the range of EC's measured, the EC increased by $57 \mu S \text{ cm}^{-1}$ between sampling and centrifuging. It is somewhat surprising that the increase in EC would be this constant, considering that the time interval between sampling and centrifuging varied from a few hours to about a week for different samples. Sutherland (1983) found considerable variation of EC increase during a period of several hours. Using Sutherland's (1983) relation of EC and TDS (Section 2.8), Eq. [5.5] would indicate an increase in TDS of 58 mg l^{-1} between sampling and centrifuging. The chemical analyses should be interpreted with this in mind.

5.6.2.1 CATIONS

Runoff chemistry confirms the position of Na as the dominant cation. Concentrations of Na varied rather irregularly with time, which is likely due to analytical error (Fig. 5.28). Because of the dominance of Na, EC and Na concentrations may be expected to be closely correlated, as has been shown for tunnel flow by Bryan and Harvey (1985). This suggests that Na concentrations should vary as smoothly as the EC generally does. Unfortunately, in 1986 the EC meter was not available so that a direct comparison of EC's and Na concentrations is not possible.

The remaining major cations (K, Ca, Mg, and Al) in the runoff show little variation with time (Fig. 5.28). In general, concentrations of the major cations rank as follows:





Potential sources for the cations are gypsum, calcite, and dolomite for Ca and Mg; the cation exchange complex for Na and K; and the clay mineral lattice for Al. Evangelou et al. (1984), working with the Mancos shale in the Upper Colorado River Basin, propose that when water comes into contact with the regolith, gypsum dissolves and releases Ca and SO_4 . Because it is divalent, Ca^{2+} displaces Na^+ from the cation exchange complex, resulting in high Na concentrations of the runoff. The preferential adsorption of Ca^{2+} causes Ca concentrations to remain relatively constant, despite the dissolution of gypsum. The same process will affect Ca released by the dissolution of calcite and dolomite. In Dinosaur Provincial Park, the same processes can be expected to control cation concentrations of runoff.

5.6.2.2 ANIONS

A check of the chemical balance of the samples (sum of the equivalent concentrations of cations minus the sum of the anions) indicates a large deficit of anions, suggesting a large error in one or more of the determinations or the presence of undetermined anions. Regarding the first possibility, the irregular variations of Na suggest an inaccuracy in the determination of Na, as variations in Na concentration should follow the smooth variations in EC. Regarding the second possibility, determination of NO_3 was attempted but experimental difficulties, possibly caused by interference by SO_4 , caused spurious results. The pH values of saturated extracts, water-regolith suspensions, and microplot runoff indicate that CO_3 and HCO_3 are also present. Bryan et al. (1984) found Cl in very low concentrations in saturated extracts. It can therefore be expected that HCO_3 and NO_3 , with smaller amounts of CO_3 and Cl, account for the missing equivalent

concentrations of anions. It is, however, somewhat surprising that SO_4 does not appear to be the dominant anion. This is a contradiction of the findings of Bryan et al. (1984) who analyzed saturated extracts derived from regolith samples. During runoff events, however, water comes into contact with the upper few mm of sandstones and pediment only, so that saturated extracts of bulk samples of regolith from these units may give a misleading impression of the runoff chemistry. Runoff from shales, however, can be expected to possess high SO_4 concentrations as runoff on these surfaces usually occurs as subsurface flow.

In rainfall, SO_4 concentrations are low. A rainfall sample taken on May 26, 1987, had an SO_4 concentration of 20.10 mg l^{-1} and an EC of $12.4 \text{ } \mu\text{S cm}^{-1}$, and a sample taken on July 18, 1987, had an SO_4 concentration of 15.34 mg l^{-1} and an EC of $7.0 \text{ } \mu\text{S cm}^{-1}$.

Sulphate concentrations are strongly correlated with EC's (Fig. 5.29). The equation of the regression line is

$$\text{SO}_4 = -79.27 + 0.42 \text{ EC} \quad [5.6]$$

($n=184$, $r^2=0.879$, $P<0.001$). The pattern of the data in Fig. 5.24 suggests that an exponential regression of the form $\text{SO}_4 = \exp(a + b \text{ EC})$ might be applicable, but it was found that this model did only slightly increase the correlation coefficient, from 0.938 for the linear model, to 0.943 for the exponential model. Despite the strong correlation, consistent deviations from the regression line do occur. For both basins the data of June 20, 1987, plot above the regression line (Fig. 5.30). This small (3.9 mm) rainstorm occurred under high antecedent moisture conditions, and followed the two runoff events of June 19, 1987. As stated in Section 5.5.3, during the second of these two preceding events sediment derived from the shales and the tunnel systems was deposited in the form of thin clay skins on the pediment surfaces and in shallow ponds in the channel. Remobilization of this material during the

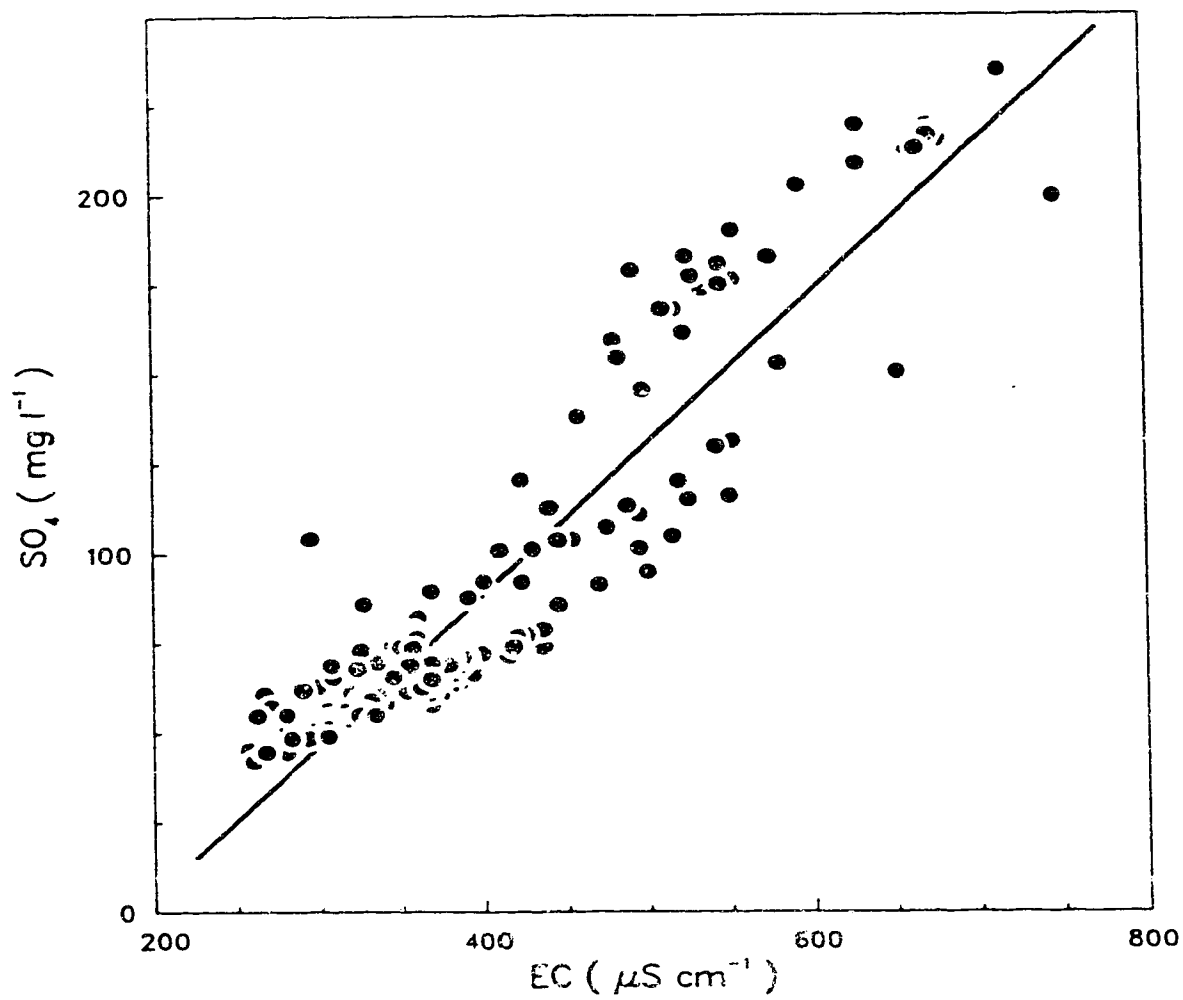


Fig. 5.29 Relationship between EC and SO_4 concentration.

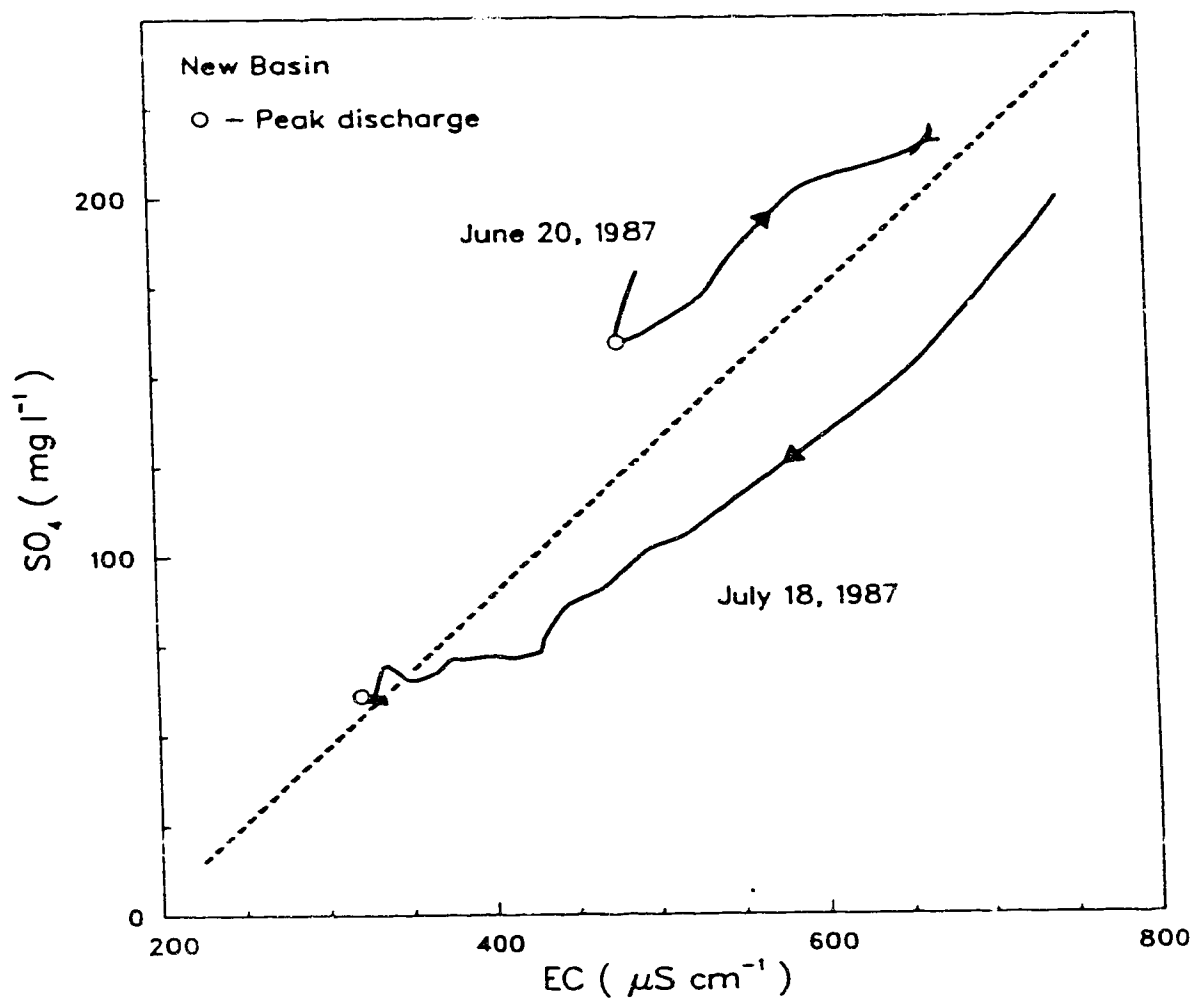


Fig. 5.30 SO_4/EC relationship for the New Basin on June 20, 1987, and July 18, 1987. See text for explanation.

runoff event of June 20, 1987, caused high SO_4 concentrations at the beginning of runoff. The high antecedent moisture conditions promoted tunnel flow and runoff generations on the shales, causing SO_4 concentrations to remain high during the rest of the runoff event.

The SO_4/EC relationship for the runoff event of July 18, 1987, caused by a long-duration, low-intensity, frontal rainstorm, displays a quite different behaviour (Fig. 5.30). For both basins the curve starts below the regression line. Near the time of peak discharge, coinciding with the initiation of tunnel flow as determined from the sediment concentration/discharge relationship, the SO_4/EC curve starts to approach, and ultimately crosses, the regression line.

The SO_4/EC curves of both basins on June 19, 1987 (I), show a start well above the regression line, followed by a steep drop to levels at and below the regression line (Fig. 5.31). The shape of the SO_4/EC curve indicates that the solute chemistry during initial flushing differs from that later during the runoff event, the difference being a higher concentration of SO_4 during initial flushing. This difference reflects the processes controlling accumulation of solutes on the sandstones and pediments during dry periods. The storm of June 19, 1987 (I), occurred within a few days after a small rainstorm which did not generate runoff (Table 5.2). The infiltration and subsequent evaporation of the small amount of rainfall may have caused the translocation of SO_4 derived from gypsum to the surface, resulting in an efflorescence of SO_4 salts ready to be flushed away during the next runoff event. It should be noted that in such an efflorescence, SO_4 need not be exclusively associated with Ca as gypsum, but instead can form highly soluble salts with Na, K, and Mg (Evangelou et al., 1984).

Data for the runoff event of June 19, 1987 (II), for both basins are unfortunately only available for the period before the initiation of tunnel flow. As expected, these data plot close to the regression line. Thus, while not providing support, at least the data do not contradict the theory that SO_4 concentrations in tunnel flow and in runoff from the shales are higher than in runoff from other sources.

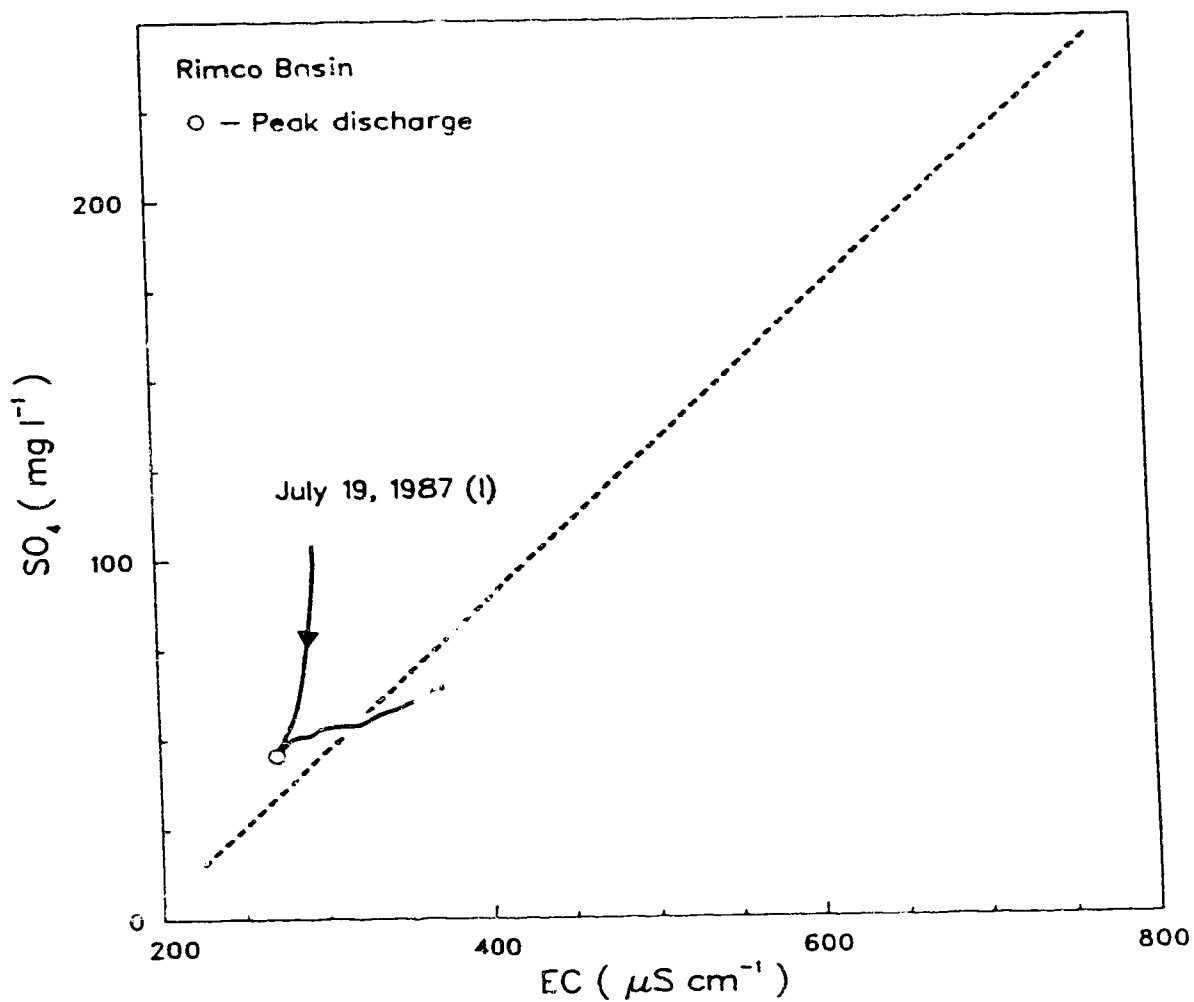


Fig. 5.31 SO_4 /EC relationship for the Rimco Basin on July 19, 1987 (I). See text for explanation.

The SO_4/EC data for May 26, 1987 (I), a medium-sized (6.0 mm) storm with no tunnel flow or runoff from shales, show initial flushing, analogous to that occurring on June 19, 1987 (II), followed by a steep decline to levels near the regression line.

The relationship between SO_4 concentration and EC described also holds for that between SO_4 concentration and EC2. The pattern of deviations from the regression line generally indicates that SO_4 concentrations are proportionally higher in runoff from shales and tunnels than from sandstones and pediments. The combination of SO_4 concentration and EC can therefore be used to distinguish runoff sources and pathways, even though each variable may have little value when used separately.

The SO_4/EC relationship is likely to be a more sensitive indicator of runoff sources and pathways than sediment concentrations because increases in sediment concentration can be caused by increasing discharge, as well as by tunnel flow initiation and runoff from shales, but also by increasing discharge. The inability to separate these two effects necessitates estimating the time of tunnel flow initiation from the sediment concentration/discharge relationship as the time of an increase in sediment concentration which cannot be attributed to increasing discharge (Section 5.5.3). Tunnel flow initiation, however, may actually occur earlier. For example, the SO_4/EC relationship of July 18, 1987 (Fig. 5.30) indicates that following a decrease in SO_4 concentration and EC, after 2035h SO_4 concentrations remained constant whereas EC's continued to decrease. Analysis of the sediment concentration/discharge relationship led to an estimate of the time of tunnel flow initiation of 2124h (around peak discharge), which is ca. 50 min later. Unfortunately, the runoff event of July 18, 1987, is the only event for which SO_4/EC data are available for a sufficiently long period, so that additional comparisons of times of tunnel flow initiation are not possible.

CHAPTER 6

6.1 SPATIAL SCALE TRANSFERENCE IN SEMI-ARID DRAINAGE BASINS

The previous three chapters reported results of investigating the rainfall-runoff relationship and sediment and solute dynamics at three levels of spatial scale: (1) the microscale of experimental plots (0.6 m²); (2) the spatial scale of Subbasins A and B (1882 - 2104 m²), in the following sections referred to as the 'subbasin scale'; and (3) the mesoscale of the Rimco Basin and the New Basin (79,230 - 202,260 m²). This chapter will analyze the relationship between the results obtained at the different spatial scales, and will discuss what information can be transferred between basins of dissimilar scale. Of key interest will be the range of scale over which spatial scale transference may take place. Within this range, transference does not necessitate extensive revision of the concepts involved. Characterization of the boundaries across which spatial scale transference cannot take place without such extensive revision is an essential part of spatial scale research in geomorphology.

6.2 RAINFALL-RUNOFF RELATIONSHIP

6.2.1 HYDROLOGICAL RAINFALL AND COMPLEXITY OF BASIN TOPOGRAPHY

Variations in the inclination and direction of rainfall in relation to the aspect and angle of slopes can cause large variations in hydrological rainfall (Section 4.4). In Subbasins A and B, such variations may affect the rainfall-runoff relationship to a considerable extent. Differences between runoff coefficients of storms in Subbasins A and B could be explained by variations in hydrological rainfall (Section 4.6.1.1). The

hydrological rainfalls in Subbasins A and B also indicated that carry-over occurred (Section 4.4), which adds to the effect of inclination and direction of incoming rainfall.

Basin topography in Subbasins A and B is relatively simple. Both basins have a basic amphitheatrical shape in which a pediment forming a large portion of the basin borders on a half-circle of steep sandstone and shale slopes. Because of this shape, variations in inclination and direction of rainfall will affect the total input to the basin, and hence runoff coefficients, to a considerable extent. This effect is even more pronounced at the microscale. The topography of the Rimco Basin and the New Basin, however, is much more complex so that variations in inclination and direction of rainfall result in reduced rainfall in certain areas, but simultaneously, in increased rainfall in others. The total input to the Rimco Basin and the New Basin is therefore not noticeably affected by the inclination and direction of the incoming rainfall.

Complexity of basin topography is a function of the resolution with which it is measured (Mandelbrot, 1967, 1983). To adequately compare topographical complexity at different scales, topography should therefore be examined with the same spatial resolution at all scales of interest. If the resolution were allowed to increase with decreasing spatial scale, topography would be very complex even at the microscale of the experimental plot. The complexity of basin topography may be quantified using techniques for describing surface roughness such as, for example, a comparison of the distribution and orientation of a set of triangular planes fitted to the topography (Hobson, 1972).

In Dinosaur Provincial Park, complexity of basin topography increases with spatial scale. At the microscale of the experimental plot, a basin consists of a small part of a slope, and topography can be characterized as a straight, convex, or concave slope. At the subbasin scale of Subbasins A and B, basin topography becomes amphitheater-shaped. When spatial scale is increased further, basin topography becomes increasingly complex because of the presence of ridges, hills, and other landforms inside the drainage basin. Because sensitivity to inclination and direction of rainfall is a function of the complexity

of basin topography, and this latter variable is in its turn a function of drainage basin scale, there exists a direct relationship between the sensitivity to inclination and direction of rainfall of a basin and the basin's spatial scale.

6.2.2 HYDROLOGICAL VERSUS METEOROLOGICAL RAINFALL

The rainfall-runoff relationship at the mesoscale was controlled by the distribution of meteorological rainfall (Fig. 5.7 and 5.8). The variability of meteorological rainfall is caused by non-uniform synoptic conditions independent of topography. It can reasonably be assumed that at the microscale, variability of meteorological rainfall is absent to negligible so that when spatial scale is increased from the micro- to the mesoscale, meteorological rainfall replaces hydrological rainfall as a factor controlling basin response. This situation exemplifies proposition VIII which states that there is a close similarity, or balance, between the spatial and temporal dimensions of a geomorphic system, and the characteristic dimensions of the dominant processes controlling its morphology, functioning, and evolution (Section 1.3.3).

For hydrological rainfall, the characteristic dimension of interest is the drainage basin size (up to ca. 2000 m²) for which differences in inclination and direction of incoming rainfall will affect basin response. With increasing scale, the distribution of hydrological rainfall seemingly becomes more and more random, and hydrological rainfall loses its prominence in controlling basin response. For meteorological rainfall, the characteristic dimension in this context is the basin scale at which variations in meteorological rainfall modify basin response. In Dinosaur Provincial Park this is the case at the mesoscale. At smaller spatial scales, i.e. at the micro- and subbasin scale, variability of meteorological rainfall is much smaller, and its importance is overshadowed by that of hydrological rainfall.

The matter of hydrological in contradistinction to meteorological rainfall also concerns proposition VII which says that differences in morphology, functioning, and evolution between geomorphic systems at the same level in a hierarchy are controlled by variables showing systematic variations over distances equal to, or shorter than, the distance between the geomorphic systems, but equal to, or longer than, the spatial dimensions of the geomorphic systems (Section 1.3.3). Hydrological rainfall shows a variability over distances much shorter than the dimensions of the Rimco Basin and the New Basin, and viewed at the mesoscale the distribution of hydrological rainfall seems random. Consequently, differences in response between the two mesoscale basins can never be explained by hydrological rainfall, but instead may be attributed to variability in meteorological rainfall. On the other hand, differences in response between Subbasins A and B may be caused by differences in meteorological rainfall as well as by differences in hydrological rainfall.

Although hydrological rainfall shows variability within Subbasins A and B, in each basin hydrological rainfall can be characterized by a dominant inclination and direction of rainfall, which may then aid in explaining differences in basin response. In this manner, a transformed variable accounting for the differences in basin response is obtained (Section 1.3.3). Differences in hydrological rainfall between the two subbasins occur because the effects of basin topography on wind direction and speed cause the dominant inclination and direction of hydrological rainfall to differ between Subbasins A and B. For instance, on July 18-19, 1987, the pattern of hydrological rainfall differed from the pattern for the entire observation period by a substantial amount in Subbasin B, whereas in Subbasin A the deviation was minor (Section 4.4).

6.2.3 THRESHOLDS OF RUNOFF GENERATION AND THRESHOLDS OF FLOW

To distinguish between the rainfall necessary to generate runoff on a surface unit, and the rainfall necessary to cause runoff from a basin, the term 'threshold of flow' will be introduced to refer to the latter. The threshold of flow may exceed the threshold of runoff generation, as runoff generation in a drainage basin may not lead to basin outflow because of transmission losses.

At the microscale, thresholds of flow equal the thresholds of runoff generation which are controlled by surface unit properties. Runoff is generated after 0.7 to 2.3 mm of rainfall on the sandstones, and after 11.0 to 24.9 mm of rainfall on the shales (Table 3.5). On the pediments, thresholds of runoff generation vary with the underlying bedrock and with sheetwash deposit thickness. During rainfall simulations, runoff occurred after 1.7 to 4.2 mm of rainfall on shale pediments, after 0.6 to 0.9 mm on sandstone pediments, and after 3.0 to 3.5 mm on pediments with a sheetwash deposit of up to 10 mm (Table 3.5, Section 3.3.2.1).

At the subbasin scale, flow from Subbasin B occurred after 1.5 to 2 mm of rainfall (Section 4.6.1). The magnitude of this threshold implies that flow from Subbasin B starts when runoff is generated on sandstones and rapidly-yielding portions of the pediment. The data indicate that the threshold of flow of Subbasin B is not sensitive to antecedent moisture conditions (Fig. 4.13). This is explained by the absence of significant accumulations of alluvial deposits, causing transmission losses to be minimal even under dry conditions, so that the onset of flow from Subbasin B is controlled by runoff generation on pediments and sandstones. This latter process is controlled by conditions in the upper few mm of material on both surface units. Because these upper layers dry rapidly and hence are dry most of the time, runoff generation is not noticeably affected by antecedent moisture conditions (Section 4.6.1).

At the mesoscale, the threshold of flow was found to be affected by antecedent moisture (Fig. 5.4). It was observed that under dry conditions (API=0 mm) 3.8 mm of rainfall caused flow from neither the Rimco Basin nor the New Basin. Under wetter conditions, flow from the mesoscale basins occurred after much smaller rainfall. For instance, on August 8, 1986, (API=2.7 mm), flow from the mesoscale basins occurred during a rainfall of only 1.8 mm.

An increase in basin scale is thus accompanied by an increase in the threshold of flow due to the larger volume of alluvial deposits augmenting transmission losses. Up to the mesoscale, however, this mechanism only operates under dry antecedent moisture conditions. Under wet conditions transmission losses appear to be negligible at the basin scales studied, as indicated by the example of the storm of August 8, 1986, quoted in the previous paragraph. Hence, under wet antecedent moisture conditions an increase in basin scale will not result in an increase in transmission losses, so that the threshold of flow will not be affected by basin scale.

6.2.4 RUNOFF COEFFICIENTS

Table 6.1 allows a storm-by-storm comparison of the runoff coefficients of Subbasin B (Table 4.5) and of the Rimco Basin and the New Basin (Tables 5.3 and 5.4). The data indicate that runoff coefficients are higher in Subbasin B than in the Rimco Basin and the New Basin. Storms for which the runoff coefficient is a minimum estimate show the same result (Table 6.1), as differences between the minimum estimates for Subbasin B and the mesoscale basins are too large to be caused by missing values on the rising stage of the hydrographs of the mesoscale basins. A Mann-Whitney Test showed that the difference in runoff coefficients between Subbasin B and the mesoscale basins was significant at $P < 0.01$, whereas the difference between the runoff coefficients of the Rimco

Table 6.1 Runoff coefficients of Subbasin B, the Rimco Basin, and the New Basin

date	runoff coefficient		
	Subbasin B (%)	Rimco Basin (%)	New Basin (%)
<u>1987</u>			
May 26 (I)	24†	8	7
May 26 (II)	28†	8†	6†
June 19 (I)	18†	4	3
July 18	33	6	10
August 10	43†	7†	11†
August 14	26	14†	36†

† indicates a minimum estimate

Basin and the New Basin was non-significant.

Two factors serve to explain this difference in runoff coefficients between Subbasin B and the mesoscale basins. The first is the smaller streamlength and volume of alluvial/sheerwash deposits in Subbasin B, causing transmission losses to be lower than in the mesoscale basins. The second factor is the difference in percentage of basin area taken up by the various surface units.

With regard to the first factor, field observations of the channelbeds indicate a considerably larger volume of alluvial deposits in the mesoscale basins, so that the difference in streamlength between Subbasins A and B and the mesoscale basins must result in lower runoff coefficients due to higher transmission losses in the latter, especially under dry antecedent moisture conditions when the alluvial deposits will be driest.

Regarding the second factor, the effect of differences in properties and percentages of surface units on runoff coefficients may overshadow that of transmission losses when basins of dissimilar scale are compared. Although runoff coefficients are not available for Subbasin A, the low magnitude of the discharge indicates that runoff coefficients in this basin will be significantly lower than in Subbasin B. Subbasin A may thus have a runoff coefficient comparable in magnitude to, or even smaller than, that of the mesoscale basins, solely due to the nature of its surface units and their relative proportions. The effect of surface unit properties becomes even more pronounced at the microscale. On shale plots, runoff only started after at least 30 min of rainfall at intensities ranging from 20 to 25 mm h^{-1} . Hence, for many, smaller storms the runoff coefficient of a microscale shale plot will be 0 per cent. Conversely, on pediment and sandstone plots runoff started after 0.6 to 4.2 mm of rainfall of similar intensity. Runoff coefficients on pediments and sandstones ranged from 31 to 88 per cent for the dry run with a duration of 60 to 80 min. Because in general discharge rapidly reached equilibrium, runoff coefficients for shorter storms will be of the same order of magnitude. Since microscale plots may consist entirely of shale, sandstone, or pediment, the effect of any single surface unit on the runoff coefficient will

be largest at the microscale. With increasing basin size, it becomes more likely that all surface units will be present in the basin, so that the influence of a specific surface unit will decrease. Thus, when runoff coefficients of basins of differing scale are compared, the possibility of the surface units controlling runoff coefficients should be taken into account, in addition to the effects of differences in streamlength and transmission losses under dry antecedent moisture conditions.

Differences in properties and percentages of the surface units also give rise to differences in runoff coefficients between basins of similar scale. The contrast between Subbasins A and B was attributed to differences in sheetwash deposit thickness and in bedrock type underlying the pediment (Section 4.7). Similarly, differences in runoff coefficients between the Rimco Basin and the New Basin could be explained by the higher proportion of vegetated, aeolian surfaces in the former (Section 5.4.1). As stated earlier, differences in runoff coefficients are most pronounced at the microscale so that the effect of differing properties and percentages of surface units causes differences in runoff coefficients between basins of similar scale over the full range of spatial scales examined in this study.

In addition to the effect of the percentages of the surface units on runoff coefficients, the spatial arrangement of the surface units should be taken into account. An important distinction between Subbasins A and B is the relative position of the shales and the sandstones (Section 4.7). In Subbasin A, a sizeable portion of the upper slopes consists of sandstone. Runoff from this rapidly-yielding surface unit flows downslope onto shale, and has caused the formation of a number of tunnel erosion features in the shale, transmitting runoff from the higher sandstone slopes. In Subbasin B, only the lower two-thirds of the steeper slopes consist of sandstone, whereas shale forms the upper slopes. The shales hence do not receive runoff from sandstones, and tunnel erosion features other than the microtunnels on shale are absent in Subbasin B. Although the main effect of this distinction between Subbasins A and B is that sediment concentrations differ

considerably between the two basins, runoff coefficients should be affected also. The presence of tunnel systems in the drainage network will increase transmission losses due to the presence of cracks in the shales in which the tunnels have formed.

In Dinosaur Provincial Park, the distribution pattern of the surface units can be characterized by the shape, location, and lateral and vertical extent of each unit. When basin size is increased it becomes more likely that the pattern of surface units within that basin approaches that of the whole area, so that basin response is less likely to deviate from the average due to a certain, dominating unit, or controlled by a specific arrangement of its surface units. Larger basins are therefore less likely to differ in response due to differing percentages of surface units or due to a certain arrangement of the surface units. In smaller basins, deviations from the pattern of the whole area are more likely, and basin response can vary considerably with changes in percentage of area consisting of a certain surface unit, or with a special arrangement of the surface units.

The inverse relationship between spatial scale and effectiveness in controlling basin response of a single surface unit or of a certain arrangement of surface units, forms another illustration of proposition VII. Even at the mesoscale, differences in basin response may be caused by differences in percentages of the surface units, although not to the extent found at the microscale. The upper scale limit of the influence of the surface units on basin response, assuming it exists, was hence not reached in the basins studied. This example also indicates that the boundaries separating basins of dissimilar scale are gradational rather than abrupt, so that transference of knowledge between basins of dissimilar scale becomes less appropriate as the scale difference increases.

The dominance of surface unit characteristics over transmission losses in controlling runoff coefficients reflects the range of spatial scales (0.6 - 202,260 m²) investigated here. Studies reporting a decrease in runoff coefficients with increasing basin area are all concerned with much larger basins (up to 10¹⁰ m²) in which the larger volume of alluvial deposits considerably increases transmission losses (Renard and Keppel, 1966;

Pilgrim et al., 1982; Pilgrim et al., 1988).

6.2.5 HYDROGRAPH CHARACTERISTICS

Figure 6.1 shows the dimensionless hydrographs of Subbasin B and the Rimco Basin on July 18, 1987 (1). The dimensionless hydrograph is obtained by dividing basin discharge by the peak discharge from the basin during that storm, so that the dimensionless discharge ranges from 0 (no flow) to 1 (peak flow). Figure 6.1 indicates that runoff started 30 min earlier in Subbasin B than in the Rimco Basin. This lead is caused by the time it takes runoff to travel downstream to the outlet of the Rimco Basin, and is strongly controlled by transmission losses occurring in the channel. A few times it was observed that during small storms under dry antecedent moisture conditions, runoff from Subbasin B and similar basins travelled down the main channel for a short distance only with considerable losses occurring due to infiltration into the channel bed and the filling of pools. Such losses under dry antecedent moisture conditions prevent runoff from the Rimco Basin during small storms, and delay it during larger ones.

The shapes of the dimensionless hydrographs of Subbasin B and the Rimco Basin are broadly similar (Fig. 6.1). Nevertheless, the hydrograph of Subbasin B is extremely sensitive to rainfall intensity variations, and displays multiple sharp discharge peaks, whereas the dimensionless hydrograph of the Rimco Basin is much smoother and although multiple discharge peaks do occur they are not as steep as in Subbasin B. In addition, the timing of discharge peaks in Subbasin B is closely related to the rainfall intensity pattern. In the Rimco Basin, discharge peaks generally occur later so that the hydrograph and the heteorgraph are sometimes out of phase. The differences in dimensionless hydrographs described for Subbasin B and the Rimco Basin are also present in the dimensionless hydrographs of Subbasin A and the New Basin (Fig. 6.2).

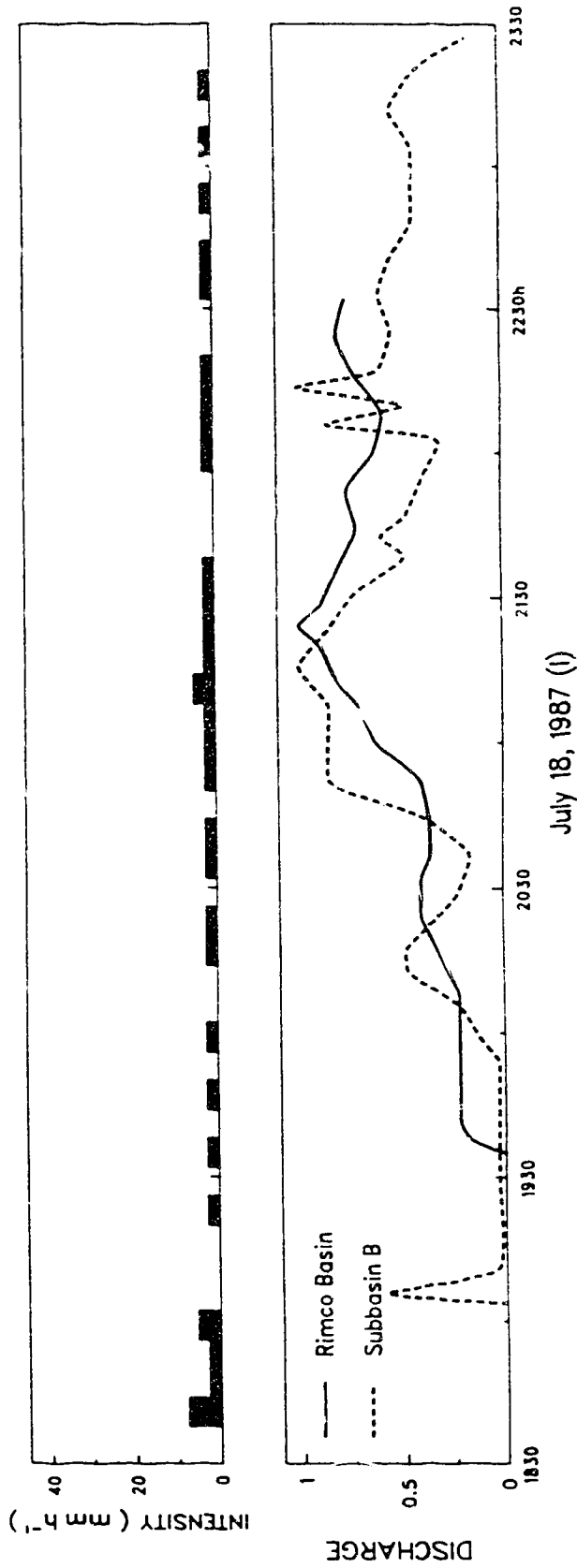


Fig. 6.1 Hectograph (Rimco recording raingauge) and dimensionless hydrographs of Subbasin B and Rimco Basin on July 18, 1987 (I). See text for explanation.

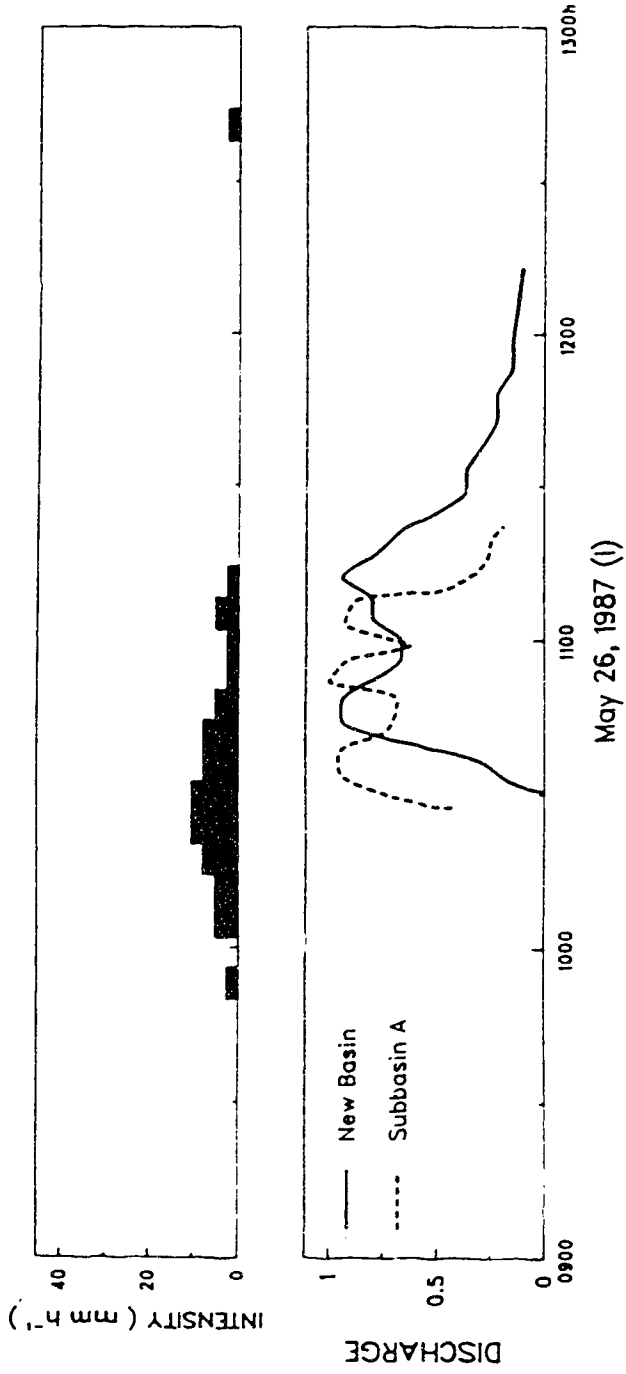


Fig. 6.2 Hycograph (Rimco recording range) and dimensionless hydrographs of Subbasin A and the New Basin on May 26, 1987 (1). See text for explanation.

Differences between the dimensionless hydrographs of the subbasins and the mesoscale basins arise in part because the Rimco raingauge record is not representative of the rainfall intensities over the entire area of the mesoscale basins. More important, however, is the larger scale of the Rimco Basin and the New Basin, allowing temporary storage of runoff in the drainage system. This storage and the subsequent release cause a discrepancy between the pattern of input as seen from the hyetograph, and the pattern of output or the hydrograph, and this discrepancy will increase with spatial scale. It should be noted that storage as used here refers to in-channel storage of water en route to the basin outlet, such as for example wedge storage and prism storage used in hydrologic routing (Linsley et al., 1982). In terms of overland flow, storage as used here represents surface detention rather than depression storage (Chorley, 1978).

Because of storage and the subsequent release of runoff, flow from the Rimco Basin continues for a considerable period after flow from Subbasin B has stopped. Rainfall resulting in periods of flow separated by dry periods in Subbasin B may in the Rimco Basin cause continuous, low flow.

Comparison of the hydrographs of Subbasins A and B and the Rimco Basin and the New Basin hence shows that with increasing spatial scale the hydrograph becomes less sensitive to the hyetograph. At the microscale of the experimental plots this sensitivity was most pronounced because of the extremely limited potential for storage of runoff. The falling stage after cessation of simulated rainfall generally lasted less than 15 s. These results hence support and illustrate proposition X, according to which differences between the temporal patterns of input and output of a geomorphic system increase with spatial scale due to the increased possibilities for temporary, internal storage of matter and energy (Section 1.3.5).

6.3 SEDIMENT DYNAMICS

6.3.1 SEDIMENT CONCENTRATION/DISCHARGE RELATIONSHIPS AND SEDIMENT YIELDS

Rating curves were derived to describe the relationship between sediment concentration and discharge. The equation describing the rating curve is

$$SC = 10.9 Q^{0.26} \quad [5.1]$$

for the Rimco Basin,

$$SC = 14.5 Q^{0.27} \quad [5.2]$$

for the New Basin, and

$$SC = 5.27 Q^{0.33} \quad [4.1]$$

for Subbasin A. In Eq. [4.1], Q is given in ml s^{-1} . Expressing Q in l s^{-1} transforms Eq. [4.1] into

$$SC = 51.5 Q^{0.33} \quad [6.1]$$

Comparison of the coefficients of Eq. [5.1], [5.2], and [6.1] indicates that sediment concentrations tend to decrease with increasing basin size. Furthermore, the exponents of the equations imply a faster increase of sediment concentration with discharge in smaller basins. Several factors, however, should be taken into account in evaluating these results.

In Subbasin A, the presence of tunnel systems transmitting runoff generated on the overlying sandstones strongly affected sediment concentrations. In Subbasin B, where such tunnel systems are absent, sediment concentrations were considerably lower, even though discharges in Subbasin B exceeded those in Subbasin A by a sizeable margin (Section 4.7).

At the mesoscale level, differences in sediment concentrations and yields between the Rimco Basin and the New Basin were explained by differing proportions of shales and vegetated surfaces between the basins. In addition, rainfall characteristics played an important role in determining sediment yields, and in fact could cause sediment export from the Rimco Basin to exceed that from the New Basin (Section 5.5.1).

Thus, over the range of spatial scales examined in this study the effect of basin size on sediment yield is overshadowed by the effects of differing percentages of the various surface units, and by that of the arrangement of the surface units within the basin.

Comparison of the average sediment concentrations at the micro-, subbasin, and mesoscale may give an indication of the magnitude of sediment storage at different scales. Average sediment concentrations for the dry run of the microscale rainfall simulations were 10.2 g l^{-1} for the pediments, 20.7 g l^{-1} for the sandstones, and 56.5 g l^{-1} for the shales. At the mesoscale, the lowest observed sediment concentration was 5.2 g l^{-1} in the Rimco Basin and 6.6 g l^{-1} in the New Basin. Both of these values occurred during the final stages of flow, and the average sediment concentration in the mesoscale basins exceeded these minimum values by a considerable margin, reaching 20.0 g l^{-1} ($n=317$, $SD=10.1$) in the Rimco Basin and 24.5 g l^{-1} ($n=299$, $SD=12.1$) in the New Basin. In Subbasin A, the average sediment concentration was 22.0 g l^{-1} ($n=126$, $SD=7.2$), and in Subbasin B it was 9.4 g l^{-1} ($n=168$, $SD=6.6$). The differences between the average sediment concentrations in basins of similar scale reflect the influence of the various surface units and their arrangement.

It is assumed that the average sediment concentrations are representative of the magnitude of sediment export from the basins, which is reasonable since samples for

determining sediment concentrations were taken under differing rainfall conditions during a variety of discharges. The magnitudes of the average sediment concentrations at the different scales indicate that over a period of several months during the summer, sediment storage in both the subbasins and the mesoscale basins is negligible. This implies that the sediment delivery ratios of these basins are high. The similarity of annual denudation rates observed at the micro- and mesoscale confirms this (Bryan and Campbell, 1986; Campbell, 1981). Thus, over the range of spatial scales examined in this study, basin size was not found to be a factor determining sediment dynamics through the increased potential for sediment storage in larger basins.

A factor that should be taken into account when evaluating sediment storage in drainage basins is complex response (Schumm, 1977). At the outlet of the Aquatot Basin considerable deposition of sediment had occurred, causing the Parshall flume at that site to be filled in with a ca. 50 cm thick sediment deposit. This recent fill extends a distance of tens of meters downstream and a few meters upstream, and is thought to represent temporary deposition of sediment due to complex response of the basin rather than being caused by the presence of the flume in the channel (Bryan and Campbell, 1986). At present none of the instrumented basins is undergoing a similar phase of sediment deposition, as the average sediment concentrations and the absence of aggrading channel sections indicate. Nevertheless, in these basins, where complex response is a potential factor controlling sediment dynamics, system behaviour may change considerably without external disturbance, and the effects of complex response could easily be mistaken for a spatial scale effect.

6.3.2 TUNNEL SYSTEMS

In the Dinosaur Provincial Park badlands two types of tunnel systems have been distinguished: the first of these are microtunnels on the shale; the second, deep tunnel systems which may transmit runoff generated on sandstones and pediments (Section 2.5). The presence of deep tunnel systems has been shown to affect sediment dynamics at the subbasin and mesoscale. Deep tunnel systems in Subbasin A have been linked to higher sediment concentrations, compared to Subbasin B where tunnel systems are limited to microtunnels on the shales (Section 4.7). At the mesoscale, the initiation of tunnel flow was shown to cause a change from clockwise to counterclockwise hysteresis of the sediment concentration/discharge relationship, due to the delayed increase in sediment concentration caused by the sediment-rich tunnel flow (Section 5.5.3).

The presence of deep tunnel systems leads to a contrast in sediment dynamics between the microscale, and the subbasin and mesoscale. At the microscale of the rainfall simulations, response is determined by the threshold rainfall of runoff generation. Sediment entrainment and transport occur when total rainfall exceeds this threshold. Further increases in total rainfall do not signify changes in the characteristics of the processes of sediment transport, except under supply-limited conditions.

At the mesoscale of the Rimco Basin and the New Basin, however, the thresholds of runoff generation as obtained at the microscale are not in every case associated with significant changes in basin behaviour. At the beginning of many storms the channel alluvium is still moist from previous runoff events. This causes transmission losses to be relatively small, so that runoff from both basins occurs when total rainfall exceeds the threshold of runoff generation on the sandstones and pediments. When total rainfall is increased and exceeds the threshold of tunnel flow initiation the tunnel systems start to function as an additional sediment source, as is evidenced by the sediment concentration/discharge relationship. A further increase of total rainfall resulting in runoff

generation on the shales will raise sediment concentrations even more. The effect of the sediment-rich runoff from the shales, however, is similar to that of tunnel flow, and is therefore not separately discernible in the sediment concentration/discharge relationship of the Rimco Basin and the New Basin.

Comparison of micro- and mesoscale sediment dynamics hence indicates two effects of an increase in spatial scale. First, thresholds defined at the microscale are not by necessity associated with mesoscale thresholds, so that extrapolation from the microscale to the mesoscale is not a straightforward process. Second, at the mesoscale, elements exist which are non-existent at the microscale, e.g. a deep tunnel system. The behaviour of the mesoscale basin is under certain circumstances controlled by such elements, rather than by the microscale components the basin contains.

Tunnel flow initiation leads to a change from clockwise to counterclockwise hysteresis because the start of flow from the basin precedes the initiation of tunnel flow. Under uniform rainfall conditions, the start of flow is generally delayed as basin area increases (Section 5.5.3). Thus, for a sufficiently large basin the start of flow from the basin will coincide with the initiation of tunnel flow, since the tunnel systems are not limited to the upper reaches of the basins but discharge directly into the channel system. Sediment concentrations will thus be high from the beginning of runoff, and tunnel flow initiation will not cause a change in hysteresis. The ratio of the response times of the deep tunnel systems to that of the basin will control this aspect of the sediment dynamics, and imposes an upper limit on the size of basins in which tunnel flow initiation causes a change in hysteresis. At the same time, the absence of deep tunnel systems in small drainage basins imposes a lower limit upon the basin scale for which tunnel flow initiation causes a change in hysteresis.

Deep tunnel systems are found in both the Rimco Basin and the New Basin. At the subbasin scale, however, deep tunnel systems may or may not be present, depending on the arrangement of the surface units. Thus, at the subbasin scale, contrasts in sediment

dynamics may exist between basins due to the presence of deep tunnel systems. When the percentage of basins having a deep tunnel system is plotted against spatial scale, that percentage will range from 0 per cent at the microscale, to 100 per cent at the mesoscale. (Fig. 6.3). The exact shape of the curve between the micro- and mesoscale is unknown, but the curve sketched in Fig. 6.3 serves for the purpose of this discussion. Because none of the microscale basins has a deep tunnel system, contrasts in sediment dynamics at the microscale cannot be caused by tunnel systems. Similarly, every mesoscale basin possesses deep tunnel systems so that at the mesoscale, contrast in sediment dynamics between basins cannot be caused by tunnel systems. At the subbasin scale, however, the possibility of the presence of tunnel systems in one basin and of their absence in another may lead to strong contrasts between basins, as the example of Subbasins A and B illustrates. Because the presence of deep tunnel systems is caused by the arrangement of the surface units this latter factor is the basic cause for contrasts at the subbasin scale.

Differences in sediment dynamics between basins of similar scale thus are from the microscale to the mesoscale controlled by the proportions and arrangements of the surface units. In addition, over a range of scales in between the microscale and the mesoscale, differences in sediment dynamics may occur due to the presence or absence of tunnel systems. At neither the microscale nor the mesoscale can this be a factor, since none of the microscale basins possesses a tunnel system, and all of the mesoscale basins do.

Differences in sediment dynamics between basins of dissimilar scale may also be caused by varying proportions and arrangements of the surface units. In addition, the possible presence of deep tunnel systems in larger basins causes dissimilarity between the microscale, and the subbasin and mesoscale basins.

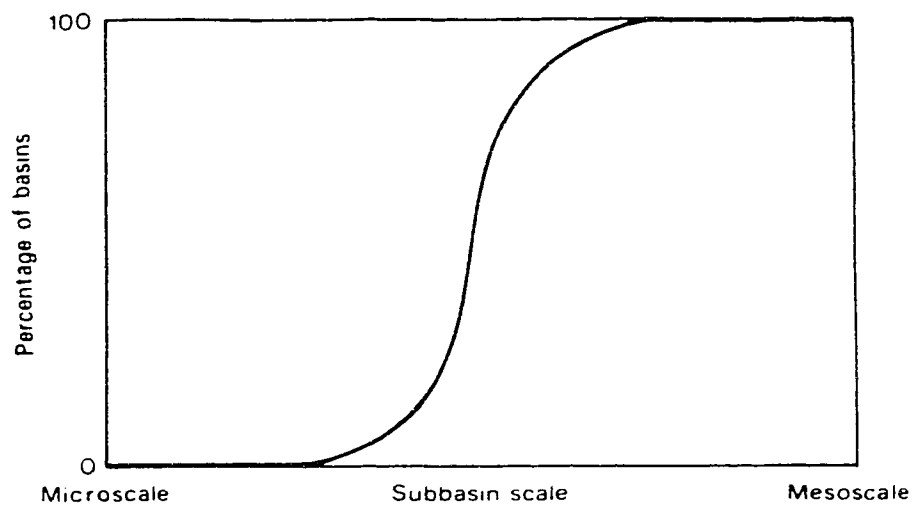


Fig. 6.3 Percentage of basins having a deep tunnel system plotted against spatial scale. See text for explanation.

6.4 MORPHOLOGICAL AND FUNCTIONAL CONSTRAINTS ON SPATIAL SCALE TRANSFERENCE

Spatial scale transference in geomorphic systems may be limited by morphological as well as functional constraints. Morphological constraints concern morphological elements present in large-scale systems, but absent in small-scale ones. Functional constraints relate to limitations imposed by the characteristics of the matter and energy flows in the systems of interest.

The deep tunnel systems in Dinosaur Provincial Park are an example of a morphological element which is present in larger-scale systems only. Another example of such an element is alluvium present along gently sloping, downstream channel reaches, which affects baseflow characteristics and hinders transferring results between small and large basins (Klaassen and Pilgrim, 1975; Pilgrim, 1983).

An example of a functional constraint is the upper limit of basins for which tunnel flow initiation causes a change in hysteresis (Section 6.3.2). This limit is determined by the ratio of response times of the deep tunnel systems to that of the basin, and is hence independent of the presence or absence of scale-dependent morphological elements. Another example may be found in the hydrograph characteristics of basins of differing scales (Section 6.2.5). Differences between the hydrograph and the hyetograph increase with spatial scale, solely due to the increased possibilities for temporary storage.

The distinction between morphological and functional constraints parallels that between morphological and cascading systems (Chorley and Kennedy, 1971). In ecology, O'Neill et al. (1986) distinguish hierarchies of species and hierarchies of processes, indicating that the separation of form and process has also proved fruitful for the analysis of systems outside of geomorphology.

Neither morphological nor functional constraints impose what could be called 'sharp' boundaries upon spatial scale transference. In the case of deep tunnel systems,

whether or not a change in hysteresis will be found depends on the presence of deep tunnel systems rather than on the actual size of the basin. If the discrepancy in spatial scale is large enough, as it is between the micro- and mesoscale, the absence of deep tunnel systems in the former and their presence in the latter hinders transferring information between the two, and the basins can be distinguished purely by their size. Within the smaller range of the subbasin scale, however, deep tunnel systems may or may not be present, and basins of similar size may display contrasting behaviour whereas basins of dissimilar size may respond alike.

The fuzziness of the boundaries of spatial scale transference is also illustrated by the inverse relationship between spatial scale and the effect of individual surface units on basin response. The smaller the basin, the greater the chance that its response is controlled by a certain surface unit and deviates from that of the larger basins having average percentages of each surface unit. Thus, a subbasin may or may not be representative of a mesoscale basin, depending on its (the subbasin's) percentages of surface units and their arrangement. A microscale basin, however, can never be representative of a mesoscale basin because response at the microscale is dominated by a single surface unit, whereas at the mesoscale this is never the case. Thus, as in the previous example, transference between two widely differing scales is not possible, but transference over a smaller scale range may succeed, depending on the compatibility of the characteristics of the basins between which transference is undertaken.

An extremely fuzzy boundary arising from a functional constraint is that created by dispersion. The deviation of the hydrograph from the hyetograph increases with increasing spatial scale, but this decrease is gradual over the whole range of scale, and dispersion does not cause a sharp boundary across which spatial scale transference cannot take place.

CHAPTER 7

7.1 CONCLUSIONS

The effect of spatial scale on the rainfall-runoff relationship and solute and sediment dynamics was investigated in semi-arid badland basins drained by ephemeral streams. The field study was carried out at three scale levels: (1) the microscale of the experimental plot, typically concerned with an area of less than 1 m²; (2) the subbasin scale, concerned with two subbasins of ca. 2000 m²; and (3) the mesoscale, concerned with two basins of 79,230 and 202,260 m², respectively. The basins were nested, so that each mesoscale basin contained one subbasin which, in turn, contained a number of microscale basins. The timescale of interest concerned basin response to a single rainstorm.

The following points characterize the results of the field study:

- (1) When spatial scale increases from the micro- to the mesoscale, meteorological rainfall replaces hydrological rainfall as the input factor controlling the rainfall-runoff relationship.
- (2) Under wet antecedent moisture conditions, the thresholds of flow for the subbasin and mesoscale basins equal the microscale thresholds of runoff generation on the rapidly-yielding sandstones and pediments, as transmission losses are negligible. Transmission losses under dry antecedent moisture conditions increase the thresholds of flow for the mesoscale basins, but do not affect thresholds of runoff generation at the microscale and thresholds of flow at the subbasin scale.
- (3) When spatial scale increases from the subbasin scale to the mesoscale, the start of runoff is delayed.
- (4) Over the range of spatial scales examined in this study, the effect of differing percentages of surface units and their arrangement on the runoff coefficient, on the start

of runoff, and on the threshold of flow, may overshadow that of spatial scale.

(5) Comparison of the average sediment concentrations at the microscale, subbasin scale, and mesoscale indicates that over a period of several months during a summer, sediment storage in both the subbasins and the mesoscale basins is negligible.

(6) Tunnel flow initiation causes a change from clockwise to counterclockwise hysteresis in the sediment concentration/discharge relationships of the mesoscale basins.

(7) Microscale thresholds may not be in evidence at the mesoscale. The threshold of runoff generation on the shales, for instance, does not lead to a distinguishable mesoscale threshold, but instead is masked by the effects of tunnel flow initiation.

(8) At the mesoscale, elements may exist which are non-existent at the microscale, e.g. a deep tunnel system. Under certain conditions, aspects of mesoscale basin response are controlled by such elements rather than by the microscale components the basin contains.

(9) At the subbasin scale, contrasts in the response of basins of similar scales may be caused by the presence or absence of deep tunnel systems. Deep tunnel systems are absent in all microscale basins and present in all mesoscale basins, so that at these two scales they do not lead to contrasts between basins of similar scale.

(10) The response of basins of differing scales may be similar in some aspects, but dissimilar in others. An example is the similarity of the thresholds of runoff generation on sandstones and pediments at the microscale, and the thresholds of flow under wet antecedent moisture conditions at the mesoscale. As far as this aspect is concerned, response at the mesoscale can be derived from microscale experiments. Other facets of mesoscale basin response, however, cannot be examined at the microscale, e.g. tunnel flow initiation.

(11) In some instances the success of spatial scale transference between two basins depends on the presence of a morphological element in both basins, rather than on the actual sizes of the basins. For example, the initiation of tunnel flow observed at the mesoscale helps to explain the behaviour of Subbasin A, but contributes very little to the understanding of the

response of Subbasin B, similar in size to Subbasin A but lacking deep tunnel systems. Another example may be found in the similarity in behaviour of the Rimco Basin and the New Basin. Despite a large discrepancy in size, differences in response between the basins are minimal and are caused by differing percentages of surface units rather than by spatial scale effects. The reason for this similarity is that the difference in scale between the two basins is not large enough for either morphological or functional constraints to cause significant differences in basin response.

The following propositions generalize the findings summarized in the points given above, and identify general aspects concerning spatial scale transference in process geomorphology. Although these propositions are the result of investigations under a very specific set of environmental conditions, it is likely that they have a general application.

(1) Morphological and functional constraints. Spatial scale transference between geomorphic systems of differing scales is restricted by morphological and functional constraints. Morphological constraints are caused by morphological elements existing in larger-scale systems while being non-existent at smaller scales. Functional constraints follow from the characteristics of the matter and energy flows in the systems of interest.

(2) Fuzzy Boundaries. The boundaries imposed upon spatial scale transference by morphological and functional constraints are fuzzy rather than sharp in character. Thus, the more two geomorphic systems differ in spatial scale, the smaller the amount of information that can be extrapolated from the one to the other. From the viewpoint of a geomorphic system, when a systems 'looks' at systems of smaller and larger scales, the amount of detail and information the system 'sees' decreases with distance. Nevertheless, certain prominent features may continue to stand out even at a considerable distance.

(3) Alike but different. Geomorphic systems of differing scales may be similar in some aspects while being dissimilar in others. Certain facets of large-scale geomorphic systems

may hence be studied at a smaller scale, but others must be investigated at the scale of the geomorphic system of interest.

Combined with the propositions given in Fig. 1.11, the last three propositions contribute to a further understanding of spatial scale transference in process geomorphology. The propositions have been deduced from information on many, diverse geomorphic systems. It is hoped that the framework for investigating the hierarchical structure of geomorphic systems outlined here will invite application to geomorphic systems other than the ones from which it was originally derived.

BIBLIOGRAPHY

- Ahuja, L.R., A.N. Sharpley, and O.R. Lehman, 1982. Effect of soil slope and rainfall characteristics on phosphorus in runoff. *J. Environ. Qual.*, 11, 9-13.
- Allen, T.F.H., and T.B. Starr, 1982. *Hierarchy: Perspectives for Ecological Complexity*. University of Chicago Press, Chicago.
- Anderson, P.W., 1972. More is different. *Science*, 177, 393-396.
- Arnett, R.R., 1979. The use of differing scales to indentify factors controlling denudation rates. p. 127-147. In: A.F. Pitty (ed.), *Geographical Approaches to Fluvial Processes*. Geo Abstracts, Norwich.
- Atmospheric Environment Service, 1982. *Canadian Climate Normals, Temperature and Precipitation, 1951-1980. Vol. 3, Prairie Provinces*. Atmospheric Environment Service, Environment Canada, Downsview, Ontario.
- Atmospheric Environment Service, 1986. *Monthly Record, Meteorological Observations in Canada*. Atmospheric Environment Service, Environment Canada, Downsview, Ontario [microfiche].
- Atmospheric Environment Service, 1987. *Monthly Record, Meteorological Observations in Canada*. Atmospheric Environment Service, Environment Canada, Downsview, Ontario [microfiche].
- Barendregt, R.W , and E.D. Ongley, 1977. Piping in the Milk River Canyon, southeastern Alberta - a contemporary dryland geomorphic process. *Int. Assoc. Hydrol. Sci. Publ.* 122, 233-243.
- Beer, T., and P.C. Young, 1983. Longitudinal dispersion in natural streams. *J. Environ. Eng.*, 109, 1049-1067.
- Bennett, R.J., and R.J. Chorley, 1978. *Environmental Systems: Philosophy, Analysis, and Control*. Princeton University Press, Princeton.
- Berndtsson, R., and J. Niemczynowicz, 1986. Spatial and temporal characteristics of

- high-intensity rainfall in northern Tunisia. *J. Hydrol.*, 87, 285-298.
- Bowyer-Bower, T.A.S., and R.B. Bryan, 1986. Rill initiation: concepts and experimental evaluation on badlands slopes. *Z. Geomorph. N.F., Suppl. Bd. 60*, 161-175.
- Brady, J.A., and P. Johnson, 1981. Predicting times of travel, dispersion, and peak concentrations of pollution incidents in streams. *J. Hydrol.*, 53, 135-150.
- Bresler, E., B.L. McNeal, and D.L. Carter, 1982. *Saline and Sodic Soils*. Springer-Verlag, Berlin.
- Brunsdon, D., and D.K.C. Jones, 1980. Relative timescales and formative events in coastal landslide systems. *Z. Geomorph. N.F., Suppl.-Bd. 34*, 1-19.
- Brunsdon, D., and J.B. Thornes, 1979. Landscape sensitivity and change. *Trans. Inst. Br. Geogr., N.S.*, 4, 463-484.
- Bryan, R.B., and I.A. Campbell, 1980. Sediment entrainment and transport during local rainstorms in the Steeveville badlands, Alberta. *Catena*, 7, 51-65.
- Bryan, R.B., and I.A. Campbell, 1982. Surface flow and erosional processes in semiarid mesoscale channels and drainage basins. *Int. Assoc. Hydrol. Sci. Publ. 137*, 123-133.
- Bryan, R.B., and I.A. Campbell, 1986. Runoff and sediment discharge in a semi-arid ephemeral drainage basin. *Z. Geomorph. N.F., Suppl.-Bd. 58*, 121-143.
- Bryan, R.B., and L.E. Harvey, 1985. Observations on the geomorphic significance of tunnel erosion in a semi-arid ephemeral drainage system. *Geografiska Annaler*, 67A, 257-272.
- Bryan, R.B., and W.K. Hodges, 1984. Runoff and sediment transport dynamics in Canadian badland microcatchments. p. 115-131. In: T.P. Burt and D.E. Walling (eds.), *Catchment Experiments in Fluvial Geomorphology*. GeoBooks, Norwich.
- Bryan, R.B., I.A. Campbell, and A. Yair, 1987. Postglacial geomorphic development of the Dinosaur Provincial Park badlands, Alberta. *Can. J. Earth Sci.*, 24, 135-146.
- Bryan, R.B., A.C. Imeson, and I.A. Campbell, 1984. Solute release and sediment entrainment on microcatchments in the Dinosaur Park badlands, Alberta, Canada. *J.*

- Hydrol., 71, 79-106.
- Bryan, R.B., A. Yair, and W.K. Hodges, 1978. Factors controlling the initiation of runoff and piping in Dinosaur Provincial Park badlands, Alberta, Canada. *Z. Geomorph. N.F., Suppl.-Bd. 29*, 151-168.
- Burt, T.P., M.A. Donohoe, and A.R. Vann, 1983. The effect of forestry drainage operations on upland sediment yields: the results of a storm based study. *Earth Surface Processes*, 8, 339-346.
- Cambers, G., 1976. Temporal scales in coastal erosion systems. *Trans. Inst. Br. Geogr., N.S.*, 1, 246-256.
- Campbell, I.A., 1977a. Stream discharge, suspended sediment and erosion rates in the Red Deer River basin, Alberta, Canada. *Int. Assoc. Hydrol. Sci. Pub. 122*, 244-259.
- Campbell, I.A., 1977b. Sediment origin and sediment load in a semi-arid drainage basin. p. 165-185. In: D.O. Doehring (ed.), *Geomorphology in Arid Regions*. State University of New York, Binghamton.
- Campbell, I.A., 1981. Spatial and temporal variations in erosion measurements. *Int. Assoc. Hydrol. Sci. Pub. 133*, 447-456.
- Campbell, I.A., 1982. Surface morphology and rates of change during a ten-year period in the Alberta badlands. p. 221-237. In: R.B. Bryan and A. Yair (eds.), *Badland Geomorphology and Piping*. Geo Books, Norwich.
- Campbell, I.A., 1987. Infiltration characteristics of badland surfaces and storm runoff. p. 251-261. In: Y.-S. Fok (ed.), *Infiltration Development and Application*. Water Resources Center, University of Hawaii at Manoa.
- Chorley, R.J., 1978. The hillslope hydrological cycle. p. 1-42. In: M.J. Kirkby (ed.), *Hillslope Hydrology*. John Wiley, Chichester.
- Chorley, R.J., and B.A. Kennedy, 1971. *Physical Geography: A Systems Approach*. Prentice Hall International, London.
- Chorley, R.J., S.A. Schumm, and D.E. Sugden, 1984. *Geomorphology*. Methuen, London.

- Church, M., 1980. Records of recent geomorphological events. p. 13-29. In: R.A. Cullingford, D.A. Davidson, and J. Lewin (eds.), *Timescales in Geomorphology*. John Wiley, Chichester.
- Corradini, C., and V.P. Singh, 1985. Effect of spatial variability of effective rainfall on direct runoff by a geomorphologic approach. *Journal of Hydrology*, 81, 27-43.
- Cullingford, R.A., D.A. Davidson, and J. Lewin, 1980. *Timescales in Geomorphology*. John Wiley, Chichester.
- Dawson, M., 1982. Sediment variation in a braided reach of the Sunwapta River, Alberta. Unpublished M.Sc. Thesis, Department of Geography, University of Alberta.
- Day, T.J., 1975. Longitudinal dispersion in natural channels. *Water Resour. Res.*, 11, 909-918.
- Dickinson, W.T., and G.J. Wall, 1977. The relationship between source area erosion and sediment yield. *Hydrol. Sci. Bull.*, 22, 527-530.
- Dietrich, W.E., and T. Dunne, 1978. Sediment budget for a small catchment in mountainous terrain. *Z. Geomorph. N.F., Suppl.-Bd.* 29, 191-206.
- Douglas, I., 1976. Lithology, landforms and climate. p. 345-366. In: E. Derbyshire (ed.), *Geomorphology and Climate*. John Wiley and Sons, London.
- Drew, D.P., 1982. Piping in the Big Muddy badlands, southern Saskatchewan, Canada. p. 293-304. In: R.B. Bryan and A. Yair (eds.), *Badland Geomorphology and Piping*. Geo Books, Norwich.
- Evangelou, V.P., L.D. Whittig, and K.K. Tanji, 1984. Dissolved mineral salts derived from Mancos shale. *J. Environ. Qual.*, 13, 146-150.
- Evenari, M., D.H. Yaalon, and Y. Gutterman, 1974. Note on soils with vesicular structure in deserts. *Z. Geomorph. N.F.*, 18, 162-172.
- Foster, G.R., and L.D. Meyer, 1975. Mathematical simulation of upland erosion by fundamental erosion mechanics. p. 190-207. In: *Present and Prospective Technology for Predicting Sediment Yields and Sources*. USDA-ARS Rep. ARS-S-40.

- Gerson, R., 1974. Karst Processes of the eastern Upper Galilee, northern Israel. *J. Hydrol.*, 21, 131-152.
- Graf, W.L., 1988. *Fluvial Processes in Dryland Rivers*. Springer-Verlag, Berlin.
- Gregory, K.J., and D.E Walling, 1973. *Drainage Basin Form and Process*. Edward Arnold, London.
- Greene, M., 1969. Hierarchy: one word, how many concepts? p. 56-58. In: L.L. Whyte, A.G. Wilson, and D. Wilson (eds.), *Hierarchical Structures*. Elsevier, New York.
- Grimshaw, D.L., and J. Lewin, 1980. Source identification for suspended sediments. *J. Hydrol.*, 47, 151-162.
- Haggett, P., R.J. Chorley, and D.R. Stoddart, 1965. Scale standards in geographical research: a new measure of areal magnitude. *Nature*, 205, 844-847.
- Haigh, M.J., 1985. Geography and general system theory, philosophical homologies and current practice. *Geoforum*, 16, 191-203.
- Haigh, M.J., 1987. The holon: hierarchy theory and landscape research. p. 181-192. In: F. Ahnert (ed.), *Geomorphological Models: Theoretical and Empirical Aspects*. Catena Supplement 10. Catena-Verlag, Cremlingen.
- Hamlin, M.J., 1983. The significance of rainfall in the study of hydrological processes at basin scale. *Journal of Hydrology*, 65, 73-94.
- Harty, K.M., 1984. *The geomorphic role of snow in a badland watershed*. Unpublished M.Sc. Thesis, Department of Geography, University of Alberta.
- Harvey, A., 1982. The role of piping in the development of badlands and gully systems in south-east Spain. p. 317-335. In: R.B. Bryan and A. Yair (eds.), *Badland Geomorphology and Piping*. Geo Books, Norwich.
- Harvey, D.W., 1968. Pattern, process, and the scale problem in geographical research. *Trans. Inst. Br. Geogr.*, 45, 71-78.
- Hobson, R.D., 1972. Surface roughness in topography: quantitative approach. p. 221-245. In: R.J. Chorley (ed.), *Spatial Analysis in Geomorphology*. Harper & Row, New

York.

- Jodges, W.K., 1982. Hydraulic characteristics of a badland pseudo pediment slope system during simulated rainstorm experiments. p. 127-151. In: R.B. Bryan and A. Yair (eds.), *Badland Geomorphology and Piping*. Geo Books, Norwich.
- Jodges, W.K., and R.B. Bryan, 1982. The influence of material behavior on runoff initiation in the Dinosaur Badlands, Canada. p. 13-46. In: R.B. Bryan and A. Yair (eds.), *Badland Geomorphology and Piping*. Geo Books, Norwich.
- Jonsaker, J.L., I.A. Campbell, and R.B. Bryan, 1984. Remote semiautomatic instrumentation for intermittent streamflow measurement and suspended sediment sampling. *Can.J. Civ. Eng.*, 11,993-996.
- Korton, R.E., 1945. Erosional development of streams and their drainage basins: hydrophysical approach to quantitative morphology. *Geol. Soc. Am. Bull.*, 56, 275-370.
- Koyt, W.G., and W.B. Langbein, 1955. *Floods*. Princeton University Press, Princeton.
- Krueger, J.J., and D.A. Woolhiser, 1980. Chemical transfer into overland flow. p. 40-53. In: *Proc. ASCE Watershed Management Symposium*, Boise, Idaho, 21-23 July, 1980. ASCE, New York.
- Kuznetsov, A.G., 1973. *Principles of landscape science and physical geographic regionalisation*. Melbourne University Press, Carlton.
- Lackey, R.G., II, 1975. Hierarchical attributes and a unifying model of bedforms composed of cohesionless material and produced by shearing flow. *Geol. Soc. Am. Bull.*, 86, 1523-1533.
- Langbein, R.S., 1977. Drainage network analysis. *Progress in Physical Geography*, 1, 271-295.
- Langbein, J.A.A., 1981. *The Nature of Soil Piping - A Review of Research*. Geo Books, Norwich.
- Langbein, J.J., J.C. Whitmore, and R.J. Wagenet, 1977. Kinetics of salt release from a saline soil. *Soil Sci. Soc. Am. J.*, 41, 721-724.

- Kemper, W.D., J. Olsen, and C.J. DeMooy, 1975. Dissolution rate of gypsum in flowing water. *Soil Sci. Soc. Am. Proc.*, 39, 458-463.
- Kennedy, B.A., 1977. A question of scale. *Progress in Physical Geography*, 1, 154-157.
- Keren, R., and G.A. O'Connor, 1982. Gypsum dissolution and sodic soil reclamation as affected by water flow velocity. *Soil Sci. Soc. Am. J.*, 46, 726-732.
- Kirkby, M.J., 1980. Modelling water erosion processes. p. 183-216. In: M.J. Kirkby and R.P.C. Morgan (eds.), *Soil Erosion*. John Wiley and Sons.
- Klaassen, B, and D.H. Pilgrim, 1975. Hydrograph recession constants for New South Wales streams. *Civ. Eng. Trans. Inst. Eng. Aust.*, CE17, 43-49.
- Klemes, V., 1978. Physically based stochastic hydrologic analysis. *Adv. Hydrosci.*, 11, 285-356.
- Klemes, V., 1983. Conceptualization and scale in hydrology. *J. Hydrol.*, 65, 1-23.
- Klein, M., 1984. Anti clockwise hysteresis in suspended sediment concentration during individual storms. *Catena*, 11, 251-257.
- Koestler, A., 1967. *The Ghost in the Machine*. Hutchinson and Co., London.
- Koestler, A., 1978. *Janus: A Summing Up*. Hutchinson and Co., London.
- Koster, E.H., 1983. *Sedimentology of the Upper Cretaceous Judith River (Belly River) Formation, Dinosaur Provincial Park, Alberta*. Alberta Geological Survey, Edmonton, Alberta, field trip guidebook.
- Laronne, J.B., 1982. Sediment and solute yield from Mancos Shale hillslopes, Colorado and Utah. p. 181-207. In: R.B. Bryan and A. Yair (eds.), *Badland Geomorphology and Piping*. Geo Books, Norwich.
- Laronne, J.B., and H.W. Shen, 1982. The effect of erosion on solute pickup from Mancos Shale hillslopes, Colorado, U.S.A. *J. Hydrol.*, 59, 189-207.
- Leopold, L.B., and T. Maddock, Jr., 1954. *The Flood Control Controversy*. The Ronald Press Company, New York.
- Lewin, J., 1980. Available and appropriate timescales in geomorphology. p. 3-10. In: R.A.

- Cullingford, D.A. Davidson, and J. Lewin (eds.), *Timescales in Geomorphology*. John Wiley, Chichester.
- Linsley, R.K., Jr., M.A. Kohler, and J.L.H. Paulhus, 1982. *Hydrology for Engineers* (3rd edition). McGraw Hill, New York.
- Longley, R.W., 1972a. The climate of the prairie provinces. *Climatological Studies No. 13*, Atmospheric Environment Service, Environment Canada.
- Longley, R.W., 1972b. Precipitation on the Canadian prairies. *Climate Circ. 2-72*, Atmospheric Environment Service, Environment Canada.
- Longley, R.W., 1973. Note on the effects of valleys on precipitation. *Climate Circ. 3-73*, Atmospheric Environment Service, Environment Canada.
- Longley, R.W., 1975. Precipitation in valleys. *Weather*, 30, 294-300.
- Loughran, R.J., B.L. Campbell, and G.L. Elliott, 1986. Sediment dynamics in a partially cultivated catchment in New South Wales, Australia. *J. Hydrol.*, 83, 285-297.
- McFadden, L.D., S.G. Wells, and J.C. Dohrenwend, 1986. Influences of Quaternary climatic changes on processes of soil development on desert loess deposits of the Cima Volcanic field, California. *Catena* 13, 361-389.
- McGuinness, J.L., L.L. Harold, and W.M. Edwards, 1971. Relation of rainfall energy and streamflow to sediment yield from small and large watersheds. *J. Soil Water Conserv.*, 26, 233-235.
- Mackin, J.H., 1948. Concept of the graded river. *Geol. Soc. Am. Bull.*, 59, 463-512.
- Mandelbrot, B.B., 1967. How long is the coast of Britain. *Science*, 156, 636-638.
- Mandelbrot, B.B., 1983. *The Fractal Geometry of Nature*. W.H. Freeman and Company, San Francisco.
- Mark, D.M., 1980. On scales of investigation in geomorphology. *Canadian Geographer*, 24, 81-82.
- Meyer, L.D., and W.H. Wischmeier, 1969. Mathematical simulation of the process of soil erosion by water. *Trans. ASAE* 12 (6) 751-758 760

- Miller, D.E., 1971. Formation of vesicular structure in soil. *Soil Sci. Soc. Amer. Proc.*, 35, 635-637.
- Morgan, R.P.C., 1973. The influence of scale in climatic geomorphology: a case study of drainage density in West Malaysia. *Geografiska Annaler*, 55A, 107-115.
- O'Neill, R.V., 1988. Hierarchy theory and global change. p. 29-45. In: T. Roswall, R.G. Woodmansee, and P.G. Risser (eds.), *Scales and Global Change - Spatial and Temporal Variability in Biospheric and Geospheric Processes*. John Wiley and Sons, Chichester
- O'Neill, R.V., D.L. DeAngelis, J.B. Waide, and T.F.H. Allen, 1986. *A Hierarchical Concept of Ecosystems*. Princeton University Press, Princeton.
- Paletskaya, L.N., A.P. Lavrov, and Sh. I. Kogan, 1958. Pore formation in takyrs crust. *Soviet Soil Sci.*, 3, 245-250.
- Pattee, H.H., 1973. The physical basis and origin of hierarchical control. p. 71-108. In: H.H. Pattee (ed.), *Hierarchy Theory: The Challenge of Complex Systems*. George Braziller, New York.
- Penning-Rowsell, E.C., and J.R.G. Townshend, 1978. The influence of scale on the factors affecting stream channel slope. *Trans. Inst. Br. Geogr. N.S.*, 3, 395-415.
- Pilgrim, D.H., 1983. Some problems in transferring hydrological relationships between small and large drainage basins and between regions. *J. Hydrol.*, 65, 49-72.
- Pilgrim, D.H., T.G. Chapman, and D.G. Doran, 1988. Problems of rainfall runoff modelling in arid and semi-arid regions. *Hydrol. Sci. J.*, 33, 379-400.
- Pilgrim, D.H., I. Cordery, and B.C. Baron, 1982. Effects of catchment size on runoff relationships. *J. Hydrol.*, 58, 205-221.
- Pittman, E.D., and A.T. Ovenshine, 1968. Pebble morphology in the Merced River. *Sed. Geol.*, 2, 125-140.
- Platt, J.R., 1969. Theorems on boundaries in hierarchical systems. p. 201-213. In: L.L. Whyte, A.G. Wilson, and D. Wilson (eds.), *Hierarchical Structures*. Elsevier, New

York.

- Potter, P.E., J.B. Maynard, and W.A. Pryor, 1980. *Sedimentology of Shale*. Springer-Verlag, New York.
- Reid, I., and L.E. Frostick, 1987. Discussion. p. 410-411. In: C.R. Thorn, J.C. Bathurst, and R.D. Hey (eds.), *Sediment Transport in Gravel-Bed Rivers*. John Wiley, Chichester.
- Renard, K.G., and R.V. Keppel, 1966. Hydrographs of ephemeral streams in the Southwest. *J. Hydraul. Div. ASCE*, 92 (HY2), 33-52.
- Riezebos, H.T., and E. Seyhan, 1977. Essential conditions of rainfall simulation for laboratory water erosion experiments. *Earth Surface Processes*, 2, 185-190.
- Risser, P.G., 1987. Landscape ecology: state of the art. p. 3-14. In: M.G. Turner (ed.), *Landscape Heterogeneity and Disturbance*. Springer-Verlag, New York.
- Roswall, T., R.G. Woodmansee, and P.G. Risser, 1988. Preface. p. xi-xii. In: T. Roswall, R.G. Woodmansee, and P.G. Risser (eds.), *Scales and Global Change - Spatial and Temporal Variability in Biospheric and Geospheric Processes*. John Wiley and Sons, Chichester
- Schumm, S.A., 1977. *The Fluvial System*. John Wiley, New York.
- Schumm, S.A., and R.W. Lichty, 1965. Time, space, and causality in geomorphology. *Am. J. Sci.*, 263, 110-119.
- Schwartz, M.L., 1968. The scale of shore erosion. *J. Geol.*, 76, 508-517.
- Sharon, D., 1980. The distribution of hydrologically effective rainfall incident on sloping ground. *J. Hydrol.*, 46, 165-188.
- Shen, H.W., J.B. Laronne, E.D. Enck, G. Sunday, K.K. Tanji, L.D. Whittig, and J.W. Biggar, 1981. Role of sediment in non-point source salt loading within the Upper Colorado River Basin. Colorado Water Resources Research Institute, Colorado State University, Fort Collins, CO, Completion Report 107, 213pp.
- Simon, H.A., 1962. The architecture of complexity. *Proc. Amer. Phil. Soc.*, 106, 467-482.

Reprinted in: *General Systems*, 10, 63-76 (1965).

- Sklash, M.G., M.K. Stewart, and A.J. Pearce, 1986. Storm runoff generation in humid headwater catchments. 2. A case study of hillslope and low-order stream response. *Water Resour. Res.*, 22, 1273-1282.
- Slaymaker, H.O., 1972. Patterns of present sub-aerial erosion and landforms in mid-Wales. *Trans. Inst. Br. Geogr.*, 55, 47-68.
- Slaymaker, H.O., and H.J. McPherson, 1973. Effects of land use on sediment production. p. 159-183. In: *Fluvial Processes and Sedimentation*, Proc. Hydrol. Symp., May 1973. National Research Council of Canada, Ottawa.
- Smettem, K.R.J., and N. Collis-George, 1985. Prediction of steady-state ponded infiltration distributions in a soil with vertical macropores. *J. Hydrol.*, 79, 115-122.
- Sparks, D.L., 1985. Kinetics of ionic reactions in clay minerals and soils. *Advances in Agronomy*, 38, 231-266.
- Springer, M.E., 1958. Desert pavement and vesicular layer of some soils of the desert of the Lahontan Basin, Nevada. *Soil Sci. Soc. Amer. Proc.*, 22, 63-66.
- Stoddart, D.R., 1969. Climatic geomorphology: review and re-assessment. *Progress in Geography*, 1, 159-222.
- Strahler, A.N., *Physical Geography* (4th edition). John Wiley and sons, New York.
- Sugden, D., and P. Hamilton, 1971. Scale, systems, and regional geography. *Area*, 3, 139-144.
- Sutherland, R.A., 1983. Mechanical and chemical denudation in a semi-arid badland environment, Dinosaur World Heritage Park, Alberta, Canada. M.Sc. thesis, University of Toronto, Toronto, Ontario.
- Sutherland, R.A., and R.B. Bryan, 1988. Solute sources and transport in an ephemeral catchment, southeastern Alberta, Canada. *Can. J. Earth Sci.*, 25, 167-181.
- Tricart, J., and A. Cailleux, 1972. *Introduction to Climatic Geomorphology*. Longman, London.

- Trimble, S.W., 1981. Changes in sediment storage in the Coon Creek Basin, Driftless Area, Wisconsin, 1853 to 1975. *Science*, 214, 181-183.
- Trimble, S.W., 1983. A sediment budget for Coon Creek Basin in the Driftless Area, Wisconsin, 1853-1977. *Am. J. Sci.* 283, 454-474.
- Trudgill, S.T., 1976. Rock weathering and climate: quantitative and experimental aspects. p. 59-99. In: E. Derbyshire (ed.), *Geomorphology and Climate*. John Wiley and Sons, London.
- U.S. Salinity Laboratory Staff, 1954. L.A. Richards (ed.), *Diagnosis and improvement of saline and alkali soils*. U.S. Dep. of Agriculture Handbook no. 60.
- Walling, D.E., 1974. Suspended sediment and solute yields from a small catchment prior to urbanization. In: K.J Gregory and D.E. Walling (eds.), *Fluvial Processes in Instrumented Watersheds*, Inst. Br. Geog. Special Publication, 6, 169-192.
- Walling, D.E., and B.W. Webb, 1982. Sediment availability and the prediction of storm-period sediment yields. *Int. Assoc. Hydrol. Sci. Pub.*, 137, 327-337.
- Weinberg, G.M., 1975. *An Introduction to General Systems Thinking*. John Wiley and Sons, New York.
- Wilson, E.M., 1974. *Engineering Hydrology* (2nd edition). John Wiley and Sons, New York.
- Wolman, M.G., and R. Gerson, 1978. Relative scales of time and effectiveness of climate in watershed geomorphology. *Earth Surface Processes*, 3, 189-208.
- Wolman, M.G., and J.P. Miller, 1960. Magnitude and frequency of forces in geomorphic processes. *J. Geol.*, 68, 54-74.
- Yair, A., and H. Lavee, 1985. Runoff generation in arid and semi-arid zones. p. 183-220. In: M.G. Anderson and T.P. Burt (eds.), *Hydrological Forecasting*. John Wiley & Sons, New York.
- Yair, A., H. Lavee, R.B. Bryan, and E. Adar, 1980. Runoff and erosion processes and rates in the Zin Valley badlands, northern Negev, Israel. *Earth Surface Processes*. 5.

205-225.

294

Yair, A., D. Sharon, and H. Lavee, 1978. An instrumented watershed for the study of partial area contribution of runoff in the arid zone. *Z. Geomorph. N.F., Suppl.-Bd.* 29, 71-82.

APPENDIX A

DATA FOR REPRESENTATIVE MICROSCALE PLOTS

All times in Mountain Standard Time (Daylight Saving Time), using the 24 h system (hh.mm.ss).

Table A1. Plot A4, pediment, dry run

time	discharge (ml s ⁻¹)	sediment concentration (g l ⁻¹)
10.33.23	8.6	14.8
10.35.15	15.0	19.2
10.37.14	16.8	8.8
10.39.14	16.9	9.8
10.41.29	18.3	4.0
10.43.24	19.1	8.2
10.45.44	18.7	6.6
10.48.44	18.0	7.4
10.50.14	17.5	4.0

time	EC ($\mu\text{S cm}^{-1}$)
10.32.45	630.
10.34.10	580.
10.36.10	560.
10.38.10	555.
10.40.10	550.
10.42.20	545.
10.44.40	530.
10.47.00	540.
10.49.50	540.

Start of test: 10.28.03
 Start of flow: 10.32.45
 EC₀: 520 $\mu\text{S cm}^{-1}$

Table A1. Plot A4, pediment, wet run

time	discharge (ml s ⁻¹)	sediment concentration (g l ⁻¹)
11.01.04	16.0	5.4
11.03.04	17.9	4.4
11.05.04	15.9	4.4
11.07.39	17.1	3.0
11.09.49	17.9	7.6
11.13.04	16.1	4.2
11.17.44	18.6	4.8
11.21.44	18.7	6.2

time	EC ($\mu\text{S cm}^{-1}$)
11.00.44	570.
11.02.00	535.
11.04.00	540.
11.06.10	540.
11.08.20	540.
11.11.00	540.
11.15.00	540.
11.20.00	540.
11.23.00	550.

Start of test: 11.00.22
 Start of flow: 11.00.44
 EC_0 : 530 $\mu\text{S cm}^{-1}$

Table A2. Plot A10, sandstone, dry run

time	discharge (ml s ⁻¹)	sediment concentration (g l ⁻¹)
13.54.06	3.3	23.0
13.56.00	6.8	29.8
13.58.09	7.5	20.2
14.01.00	6.7	11.4
14.04.09	7.6	9.0
14.06.55	7.1	5.4
14.09.58	8.4	7.2
14.12.39	7.6	3.2
14.16.15	7.1	4.0
14.23.33	9.0	3.2
14.27.30	6.7	2.8
14.30.38	8.1	3.0

time	EC ($\mu\text{S cm}^{-1}$)
13.53.18	725.
13.55.00	635.
13.57.00	610.
13.59.40	590.
14.02.10	565.
14.05.10	550.
14.08.00	540.
14.11.00	540.
14.14.05	535.
14.17.40	535.
14.20.40	540.
14.24.20	525.
14.28.40	525.
14.31.20	525.

Start of test: 13.51.33

Start of flow: 13.53.18

EC₀: 465 $\mu\text{S cm}^{-1}$

Table A2. Plot A10, sandstone, wet run

time	discharge (ml s ⁻¹)	sediment concentration (g l ⁻¹)
14.45.55	5.4	3.6
14.48.00	6.4	2.2
14.50.57	10.5	4.6
14.55.10	6.7	4.0
14.58.40	6.4	2.4
15.01.41	5.7	4.4
15.05.00	6.5	1.2
15.08.13	5.4	1.6

time	EC ($\mu\text{S cm}^{-1}$)
14.45.12	630.
14.46.30	530.
14.49.05	535.
14.52.30	520.
14.56.50	520.
14.59.50	510.
15.03.00	540.
15.06.30	540.
15.09.20	540.

Start of test: 14.44.52
 Start of flow: 14.45.12
 EC₀: 460 $\mu\text{S cm}^{-1}$

Table A3. Plot B7, shale, dry run

time	discharge (ml s ⁻¹)	sediment concentration (g l ⁻¹)
12.59.05	12.9	136.8
16.01.34	17.2	72.6
16.03.34	18.3	55.0
16.05.44	16.1	43.6
16.07.54	16.9	36.4
16.10.26	10.7	13.6
16.13.04	18.3	28.4
16.14.34	16.9	29.6

time	EC ($\mu\text{S cm}^{-1}$)
15.58.20	1310.
16.00.30	910.
16.02.30	770.
16.04.30	740.
16.06.40	715.
16.09.05	695.
16.11.20	680.
16.13.40	655.
16.15.15	660.

Start of test: 15.52.20
 Start of flow: 15.58.20
 EC_0 : 530 $\mu\text{S cm}^{-1}$

Table A3. Plot B7, shale, wet run

time	discharge (ml s ⁻¹)	sediment concentration (g l ⁻¹)
16.29.44	16.4	17.8
16.32.09	16.6	15.0
16.34.29	16.1	20.0
16.36.43	21.7	21.4
16.38.58	26.0	22.6
16.41.34	15.8	21.4
16.44.34	19.3	15.6
16.47.24	16.8	22.0
16.50.06	10.7	21.6

time	EC ($\mu\text{S cm}^{-1}$)
16.29.20	850.
16.31.09	620.
16.33.10	620.
16.35.40	640.
16.37.40	655.
16.40.15	655.
16.43.00	630.
16.45.55	670.
16.48.35	650.
16.51.30	650.

Start of test: 16.28.58
 Start of flow: 16.29.20
 EC₀: 530 $\mu\text{S cm}^{-1}$

Table A4. Plot AR2, pediment, dry run

time	discharge (ml s ⁻¹)	sediment concentration (g l ⁻¹)
16.32.13	0.4	11.5
16.41.40	1.2	11.6
16.49.50	1.6	14.0
16.56.00	2.2	11.8
17.02.10	2.1	13.3
17.08.13	2.1	10.3
17.14.45	2.1	12.0
17.21.40	2.1	11.4
17.28.13	2.4	12.0
17.34.13	2.4	12.0

time	EC ($\mu\text{S cm}^{-1}$)
16.34.25	1320.
16.42.40	1260.
16.50.40	1260.
16.56.45	1260.
17.02.55	1260.
17.08.50	1240.
17.15.35	1240.
17.22.40	1240.
17.29.05	1240.
17.35.00	1240.

time	rainfall intensity (mm h ⁻¹)
16.19.50	28.5
16.23.00	24.0
16.30.00	21.0
16.34.25	18.0
16.42.40	21.0
16.50.40	22.5
16.56.45	25.5
17.02.55	21.0
17.08.50	22.5
17.15.35	19.5
17.22.10	24.0
17.29.05	21.0
17.35.00	24.0

Table A4. Plot AR2, pediment, dry run, cont.

Start of test: 16.19.50
Start of flow: 16.30.04
 EC_0 : 1135 $\mu S\ cm^{-1}$

Table A4. Plot AR2, pediment, wet run

time	discharge (ml s ⁻¹)	sediment concentration (g l ⁻¹)
17.54.58	2.1	12.3
18.01.10	2.2	9.7
18.07.53	2.1	13.0
18.15.45	2.2	12.2
18.22.03	1.9	11.7
18.29.25	1.8	12.9

time	EC ($\mu\text{S cm}^{-1}$)
17.55.40	1305.
18.01.55	1300.
18.08.55	1280.
18.16.30	1270.
18.23.05	1260.
18.30.30	1260.

time	rainfall intensity (mm h ⁻¹)
17.53.25	24.0
17.55.40	18.0
18.01.55	25.5
18.08.55	13.5
18.16.30	21.0
18.23.05	21.0
18.30.30	21.0

Start of test: 17.53.25

Start of flow: 17.53.25

EC₀: 1135 $\mu\text{S cm}^{-1}$

Table A5. Plot BR8, sandstone, dry run

time	discharge (ml s ⁻¹)	sediment concentration (g l ⁻¹)
16.33.03	1.4	3.6
16.39.10	1.7	13.8
16.46.20	1.6	13.4
16.54.53	1.1	25.6
17.02.10	1.6	21.2
17.10.05	1.2	18.8
17.20.23	1.4	17.8
17.28.45	1.9	25.6
17.35.55	2.0	20.8
17.42.13	1.9	24.4

time	EC ($\mu\text{S cm}^{-1}$)
16.33.40	1410.
16.40.20	1380.
16.47.20	1355.
16.56.00	1320.
17.03.10	1325.
17.11.05	1340.
17.21.35	1330.
17.29.40	1305.
17.36.50	1300.
17.43.10	1285.

time	rainfall intensity (mm h ⁻¹)
16.30.10	27.0
16.33.40	21.0
16.40.20	15.0
16.47.20	25.5
16.56.00	19.5
17.03.10	10.5
17.11.05	19.5
17.21.35	19.5
17.29.40	21.0
17.36.50	21.0
17.43.10	21.0

Start of test: 16.30.10

Start of flow: 16.31.50

EC₀: 1125 $\mu\text{S cm}^{-1}$

Table A5. Plot BR8, sandstone, wet run

time	discharge (ml s ⁻¹)	sediment concentration (g l ⁻¹)
18.10.27	1.4	9.4
18.17.55	2.0	27.0
18.24.45		17.2
18.31.30	2.0	16.6
18.39.05	2.0	25.2
18.46.50	1.5	16.4

time	EC ($\mu\text{S cm}^{-1}$)
18.11.25	1335.
18.19.00	1300.
18.25.40	1280.
18.32.30	1270.
18.40.20	1280.
18.47.50	1290.

time	rainfall intensity (mm h ⁻¹)
18.08.40	19.5
18.11.25	21.0
18.19.00	21.0
18.25.40	18.0
18.32.30	21.0
18.40.20	15.0
18.47.50	12.0

Start of test: 18.08.40

Start of flow: 18.09.00

EC₀: 1125 $\mu\text{S cm}^{-1}$

Table A6. Plot BR12, shale, dry run

time	discharge (ml s ⁻¹)	sediment concentration (g l ⁻¹)
16.27.25	0.1	55.2
16.37.20	0.9	67.8
16.46.43	1.2	85.0
16.54.38	1.1	71.6
17.05.13	1.6	75.6
17.12.15	1.9	73.2
17.20.30	2.1	75.2
17.27.20	2.0	80.6
17.36.05	2.2	80.4
17.43.00	1.6	71.4

time	EC ($\mu\text{S cm}^{-1}$)
16.29.00	1700.
16.38.20	1640.
16.47.40	1570.
16.55.45	1590.
17.06.00	1610.
17.13.10	1620.
17.21.10	1570.
17.28.10	1590.
17.36.45	1550.
17.44.00	1560.

time	rainfall intensity (mm h ⁻¹)
15.51.33	24.0
15.57.00	16.5
16.02.30	24.0
16.08.30	21.0
16.18.00	24.0
16.29.00	21.0
16.38.20	16.5
16.47.40	25.5
16.55.45	21.0
17.06.00	21.0
17.13.10	21.0
17.21.10	24.0
17.28.10	12.0
17.36.45	21.0
17.44.00	12.0

Table A6. Plot BR12, shale, dry run, cont.

307

Start of test: 15.51.33
Start of flow: 16.21.48
EC₀: 1140 $\mu\text{S cm}^{-1}$